Title
Coupling fine particle and bedload transport in gravel-bedded streams

Author
Park, Jungsu

Publication Date
2015

Peer reviewed|Thesis/dissertation

Coupling fine particle and bedload transport in gravel-bedded streams

by

Jungsu Park

A dissertation submitted in partial satisfaction of the
requirements for the degree of
Doctor of Philosophy

in

Engineering – Civil and Environmental Engineering

in the

Graduate Division

of the

University of California, Berkeley

Committee in charge

Professor James R. Hunt, Co-chair
Professor Mark T. Stacey, Co-chair
Professor Evan A. Variano
Professor Stephanie M. Carlson

Spring 2015

Abstract

Coupling fine particle and bedload transport in gravel-bedded streams

by

Jungsu Park

Doctor of Philosophy in Engineering – Civil and Environmental Engineering

University of California, Berkeley

Professor James R. Hunt, Co-chair
Professor Mark T. Stacey, Co-chair

Fine sediments or particles are important determinants of water quality and ecosystem health. Various contaminants such as nutrients and heavy metals are transported by fine particles and the deposition of fine particles at the surface of stream beds often causes serious impairments of benthic ecosystems. For these reasons understanding fine particle transport within watersheds and interaction with the stream bed are important for assessing impairment of water quality and aquatic ecosystems. Besides a qualitative understanding, restoration and remediation efforts would benefit from quantitative models that predict fine particle dynamics. This thesis adopted an approach that first explored the patterns of fine particle transport within California watersheds, from those patterns processes were investigated that dominated particle transport, and then finally, developing a quantitative model with the goal being able to predict particle dynamics that replicated observed patterns and represented dominant processes.

The rich data base of US Geological Survey stream monitoring data within California provided opportunities for recognizing common patterns in fine sediment loading rates as a function of flow rate. The majority of 38 minimally developed watersheds with extensive flow and particle transport data illustrated a common dependence of particle loading rate on flow rate. Physical surveys of watersheds, collection of stage-discharge data from historical gauging records, and sediment bed analysis revealed that gravel-bedded streams underwent a transition to accelerated rates of fine particle transport above a flow rate sufficient to initiate mobilization of bed sediments. Additionally, continuous flow and turbidity data had hysteresis loops when fine particle concentration is plotted against flow rate that demonstrated stream bed release of fine particles and a limited supply of those particles. These patterns were in qualitative agreement with observations by others over the last 75 years.

The transition from pattern recognition to process analysis required incorporation of the dominant processes controlling fine particle dynamics within gravel-bedded streams into a model.

The process analysis was guided by the use of continuous flow and turbidity data at two locations on the Russian River in California to test process descriptions and then calibrate a quantitative model to represent those processes. The resulting process model coupled fine particle retention within the sediment bed by filtration and sedimentation with the release of accumulated fine particles in response to flood events. Model parameters such as a critical flow rate required to initiate sediment bed fluidization, the maximum fine particle storage capacity within the watershed, and background particle concentration for the watershed were identified directly from monitoring data. Model calibration consisted of optimizing the filtration parameter and the sediment bed fluidization parameter over two or three years of data. Overall the modeled fine particle release was within 5% of what was measured during flood events.

The successful process modeling for two sites formed the basis for partially validating the model for data not used in calibration within the Russian River of California and testing its applicability to other watersheds. The calibrated model parameters combined with over a year of 15-minute flow data was able to replicate within 35% the observed fine particle release by flood events. Six other watersheds were utilized in testing the calibration of the model and providing a preliminary analysis of the sensitivity of the two model parameters representing filtration and fluidization. The model could be successfully calibrated to these watersheds, and there was a limited range observed for the fluidization parameter and a possible watershed area dependency on the filtration parameter. As a further test of the model, particle loading rates were generated from measured flow data and these loading rates were similar to those observed. This agreement provided a demonstration that the model was able to quantitatively replicate the shape and scatter of particle loading observations, both under current and historical conditions.

To my wife, Hyunjung Yang

Contents

List of Figures

List of Table

Acknowledgments

There are so many people who I would like to thank for supporting and guiding to make this dissertation possible.

Firstly, I would like to thank my advisor, Professor James R. Hunt for all the advice and encouragement throughout my graduate study. This research would not have been possible without his thoughtful guidance. I also would like to thank Professor Mark T. Stacey for providing great inspiration and advice throughout all years of my study at Cal.

I would like to thank the other members of my dissertation committee. Professor Evan A. Variano always gives great answers for my questions about research and study. Professor Stephanie M. Carlson shows me what should be the final goal and application of this research. I would like to thank Professor Laurel Larsen for helping me to have better thinking about my research. Thanks to Professor Sally Thompson. I learned lots of precious knowledge need for my research from her.

I would like to thank Berkeley Water Center and Microsoft. My research was initiated by utilizing data from their previous efforts. Thanks to Carolyn Remick for technical supporting for my research. I also would like to acknowledge Deborah Agrwal in Lawrence Berkeley National Laboratory for helping my data search. I would like to thank Shelley Okimoto for all the support and guide of my study in graduate school.

I would like to thank Rebecca Leonardson for sharing her experience and helping me to have better understanding about sediment study. I would like to thank friends in my lab, Thomas Moran and his family, Nathaniel Butler, and Arthur Wiedmer for listening and helping me to have better ideas about my research. The life in Berkeley become enjoyable for me thanks to you. Thanks to my classmates for sharing the precious experience of graduate school.

Thanks to Dr. Seongeun Jeong and Dr. Hjin Choi for all the supporting of the life in Berkeley from the beginning. Thanks to Dr. Chanhyuk Park and his family to make life of my family at Berkeley much more enjoyable.

I would like to thank K-water (Korea Water Resources Corporation) for giving this opportunity and funding my study at the UC, Berkeley.

This study utilized flow rate and fine particle concentration data measured during previous researches. I would like to extend my appreciation to the authors for kindly sharing their data. Thanks to Dr. Francois Birgand at the North Carolina State University and Dr. C. Grimaldi (INRA, UMR Sol-Agronomie-Spatialisation, Rennes cedex, France) for kindly provided their data in two French watersheds. Thanks to Dr. Joe Harrington at Cork Institute of technology, Ireland for providing the data in two Ireland watersheds. Thanks to Dr. Jacques L. Langlois at McGill University for providing the data at Incline Creek in Lake Tahoe basin. I would like to thank Dr. Hans Middelkoop at Utrecht University in the Netherlands for kindly providing the link to daily sediment data at Meuse River, reported by Dutch Institute for Inland Water Management and Waste Water Treatment (RIZA). I also would like to thank U.S. Geological Survey California Water Science Center for kindly providing historical channel cross section measurements data.

Finally, I would like to thank my family for their never ending support. My Father, and Mother always support and encourage me to continue study. Thanks to my brother for the emotional support. I also would like to thank all my family for the unending support. Thanks to Hyunjung Yang, my wife, for all the sacrifice and support during my graduate study.

Chapter 1. Motivation of Research

Sediments smaller than 0.063 mm (silt and clay) are often considered as fine sediments [*Farnsworth and Warrick*, 2007] and are a source of suspended particles which have various effects on water quality [*Rowe*, 2003]. Human activities alter the natural sediment transport system and excess fine particles are introduction into receiving waters which is one of the major causes of impairment to aquatic environments [*USEPA*, 2009]. This study focuses on the mechanisms of fine particle transport in streams and exchange with sediment beds.

Contaminants such as nutrients and pathogens are transported by fine particles [*Leonard et al.*, 1979; *Droppo et al.*, 2009]. The total phosphorous load is predominately transported with fine particles and phosphorous can be released from bed sediments causing algal blooms that degrade water quality. Elevated suspended sediment concentrations in streams also increase the cost for drinking water treatment [*USEPA*, 2000]. High turbidity water has a greater possibility of carrying pathogenic microorganisms such as viruses and bacteria (National Primary Drinking Water Regulations, EPA, http://www.epa.gov. safewater/consumer/pdf/mcl.pdf). Additionally, turbidity is relatively easy to monitor and is often used as an indicator of contamination in drinking water systems. Contaminated fine particles from various industrial activities such as mining are also long lasting sources of toxic substances in watersheds [*Singer et al.*, 2013].

Fine particles are also one of many important factors that determine the health of benthic communities. The deposition of fine particles, referred to as siltation, is considered as one of most important and commonly observed aquatic pollutants. Siltation causes about 38% of the impaired streams and this represents about 13% of the total assessed river miles in the US [*USEPA*, 2000]. Fishes feed on or near the sediment bed and utilize the bed for protection from predators during the juvenile life stages. Siltation can clog the stream bed, which not only directly reduces available habitats for spawning by several stream fishes including Pacific salmon and trout but also limits oxygen exchange into the bed which causes suffocation of eggs [*Chapman*, 1988; *Greig et al.*, 2005; *Jensen et al.*, 2009]. As a result, increased mortality of salmonids caused by excess fine particles is frequently observed in natural streams [*Kemp et al.*, 2011]. Particles smaller than

0.85 mm are often considered as the cause of suffocation of salmon eggs [*Tappel*, 1983; *Chapman*, 1988]. Moreover, increased deposition of fine particles in streams shifts invertebrates toward burrowing taxa which are less available as prey for salmonids. As food and available habitats are restricted by excess fine particles, salmon become more aggressive with each other, and consequently the mortality of salmonids is increased [*Suttle et al.*, 2004]. Siltation also reduces available habitats for invertebrates through suffocation [*Berry et al.*, 2003] and lowers filtration rates of freshwater mollusks [Aldridge et al., 1987].

Fine particles suspended in the water column have various effects on the aquatic ecosystem. The increased turbidity limits light penetration and consequently reduces photosynthesis and primary production which alters the food web of stream ecosystems [*Wood and Armitage*, 1997]. Additionally high turbidity water may cause damage to leaves and stems of macrophytes by abrasion [*Lewis*, 1973]. Turbid water is associated with clogging of fish gill rakers with increased mortality, and turbid water can reduce the efficiency of hunting by visual feeders [*Bruton*, 1985; *Wood and Armitage*, 1997]. Fine particles also have effects on the environment of estuarial mudflats and wetlands where the fine particles are supplied from terrestrial sources [*Syvitski et al.*, 2005; *Farnsworth and Warrick*, 2007]. The marine sediment bed is an important reservoir of organic matter [*Syvitski et al.*, 2003]. *Welsh* [1980] suggested that the flood tide in estuaries cause the entrainment of mudflat surface sediments and associated high nutrient pore water, and consequently the nutrient concentration in the water column is increased. Turbid water might also have positive effects on aquatic biota within limited circumstances. For example, highly turbid water may provide visual protection to the fish from wild birds [*Stevens et al.*, 1997; *Berry et al.*, 2003].

Water resource management systems are essential for water supply, flood control, power production, and ecosystem maintenance, but these systems are coupled with fine particle dynamics. Fine and coarse particle sedimentation reduces the life time of reservoirs [*García*, 2008]. The average annual loss of reservoir storage capacity by sedimentation is estimated at about 0.2% in the U.S [*Crowder*, 1987] and 1% worldwide [*White*, 2001]. Sedimentation in reservoirs not only causes local economic losses [*Palmieri et al.*, 2001] but also alters the downstream channel geomorphology and ecosystem [*Kondolf*, 1997; *García*, 2008]. Besides the ecological consequences of sediment bed clogging, water resource systems can be impacted as well. River bank filtration utilizes the alluvial materials beneath a river to filter out particles and associated contaminants and can provide high quality water at low cost [*Jaramillo*, 2012]. However fine particle clogging of the river bed significantly reduces the advantages of river bank filtration for drinking water treatment [*Tufenkji et al.*, 2002; *Schubert*, 2006]. *Zhang et al.* [2011] observed considerable decrease of river bed permeability in the Russian River, California, during the dry season which reduced the water production rate. Restoration of filtration capacity requires the removal of clogging particles either by higher flow events or mechanical scrapping. There is also a special concern in managing agricultural and forestry lands to minimize soil loss caused by various human activities [*Renard et al.*, 1997].

With these numerous effects of fine particles on watersheds, there is an ongoing effort in monitoring and developing management plans for fine particles. One approach dictated by the Clean Water Act is the assessment of a total maximum daily load (TMDL) of fine particles for a watershed which represents the maximum amount that a waterbody can tolerate without compromising water quality standards. USEPA has been monitoring the environmental conditions

and determining load allocations in multiple watersheds in US. Sediments are ranked as 5th highest pollutant group in US which cause impairment of water quality with about 4500 cases out of a total of about 72,000 reported cases (http://iaspub.epa.gov/waters10/attains_nation_cy.control?p_report_type=T#tmdl_by_pollutant). Thus, estimation of fine particle sources, transport, and storage is important in managing water quality, however, the mechanisms controlling fine particle dynamics within watersheds are poorly understood. Consequently most of theories and management plans about fine particles are based on an empirical analysis of limited monitoring data.

This dissertation presents a systematic analysis of the dependence of fine particle loading rate on flow rate in streams and rivers. The analysis starts with a synthesis of channel cross section measurements in multiple watersheds in Chapter 2 that suggests the relationship between loading rate and flow rate is closely coupled with the movement of gravel sediment beds. A selective review of the literature in Chapter 3 shows support for the observations that fine particle transport is coupled with sediment bed movement, but quantitative models were not available. In Chapter 4 a model which can estimate fine particle accumulation and release in stream bed sediments was suggested by the analysis of high resolution flow and suspended particle concentrations data. The model was developed and calibrated using two gauging station records on the Russian River in California. Chapter 5 presents the analysis of four additional datasets that allowed additional model testing from watersheds in Ireland, France, the Meuse River in Europe, and in the Lake Tahoe basin of Nevada. A summary of the modeling effort is provided in Chapter 6 along with suggestions for further advancements in the model development and application.

Chapter 2. Data Analysis and Conceptual Model

Fine particles transported in streams and stored in stream beds have detrimental effects on water quality and aquatic ecosystems. The relationship between suspended particle load (Q_s) and flow rate (Q) has orders of magnitude scatter which limits its utility in predictive relationships. Even though fine particle transport in streams and particle storage in the sediment bed have been actively studied for nearly 100 years, a quantitative understanding is not available. This lack of knowledge is hindering water resources management and efforts at ecosystem restoration. A preliminary analysis is provided in this chapter of data available in California for stream flow, suspended particle concentration, bed material size distributions, channel cross section data, and on-site observations. Data from over 30 minimally developed watersheds lead to the development of a conceptual model that couples fine particle accumulation within bed sediments with particle release by the scouring or fluidization of the bed sediments during flood events. This conceptual model guided a summary of the relevant literature in Chapter 3 which provided the basis for the development and testing of a quantitative model in Chapters 4 and 5.

2.1 Data Analysis

Coastal California watersheds are a rich source of flow and suspended particle concentration data over many years. Fine particle concentration and flow rate data are often utilized to construct plots of suspended particle loading rate ($Q_s = CQ$) and flow rate (Q) that are called sediment loading curves, even if a curve is a poor representation of the data. To avoid confusion on the meaning of the phase sediment transport, fine particle concentration and fine particle transport refer to the silt and clay size fractions carried as suspended load, and sediment refers to bed materials that are only transported by bedload. In general, the focus of this analysis is on gravel-bedded streams, and while sand-sized particles exist, they were not explicitly considered.

One example of a particle loading relationship is shown in Figure 2.1 for Redwood Creek at Orick, California. The data utilized for the plot were collected over the period of 1970 to 2001 which shows the considerable scatter encountered in particle loading rate at a given flow rate. Besides the vertical scatter in the data, the plot suggests there is a different relationship at flows less than 20 m^3/s which has a shallow slope in this log-log plot compared to higher flows. This shift is called a slope break and is commonly observed. This section describes the data sources for minimally developed watersheds in California that had sufficient data to examine particle loading relationships and identify conditions that led to the presence and absence of slope breaks. These data suggested the mobility of the sediment bed during flooding events was the reason for increased particle loading above the slope break. Additionally, bed geomorphological measurements documented the movement of the sediment bed, and the hysteresis loops encountered between turbidity and flow rate demonstrated fine particle erosion was dependent upon prior flood events. These observations led to the development of a conceptual model on the coupling of particle transport with sediment bed dynamics covered in Section 2.2.

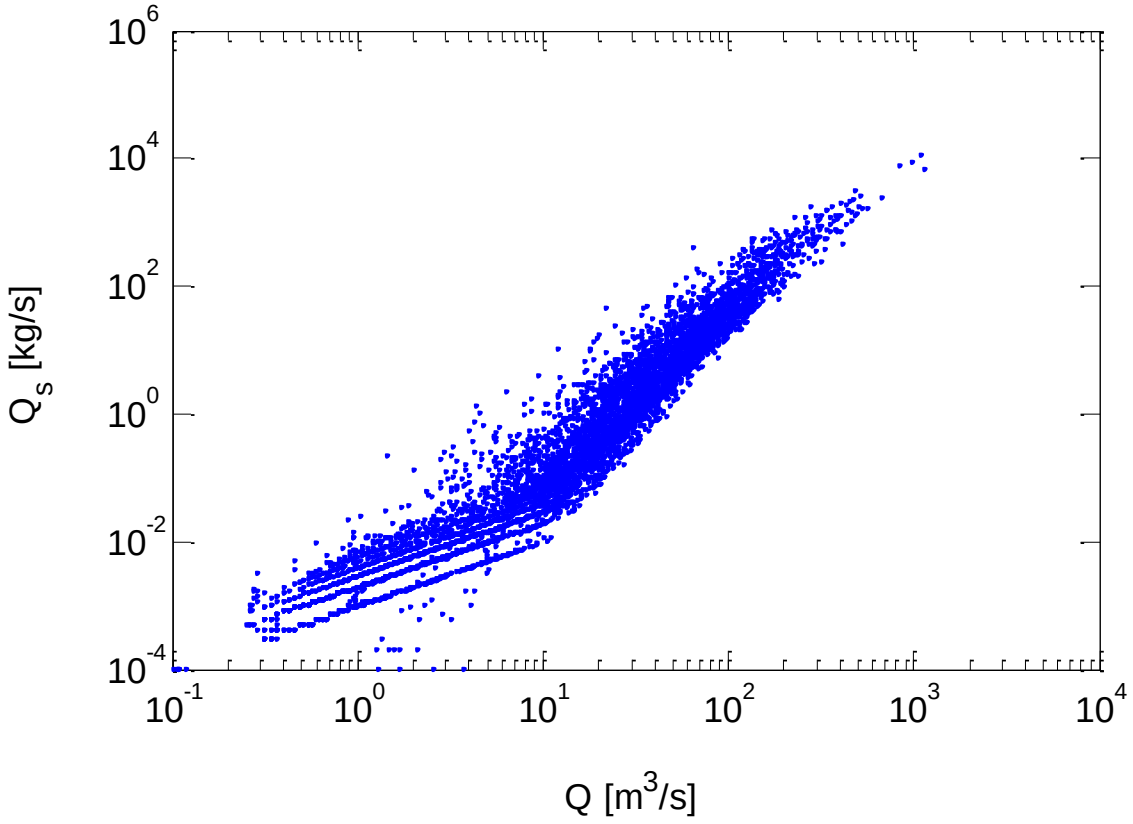

Figure 2.1. Particle loading relationship for Redwood Creek at Orick, California (11482500).

2.1.1 Data Sources

California is relatively rich in hydrologic data with long-term records collected by the USGS (National Water Information System). The original focus on California watersheds was prompted by the easy accessibility to the USGS data in the "California datacube" developed by the UC Berkeley Water Center in collaboration with the Lawrence Berkeley National Laboratory and Microsoft Research (http://bwc.berkeley.edu/DataServerdefault.htm). With multiple watersheds and nested gauging locations within a watershed, there was a broad geographical coverage as well as opportunities to explore scaling relationships related to watershed size.

Daily stream flow records readily exist for approximately 2000 sites and about 200 of those sites have daily estimates of suspended sediment concentration [mg/L] and/or suspended load [Mg/day]. Given the need to select data sets that spanned at least three years to represent local hydrologic variability, 79 sites were identified with flow and suspended sediment data. The USGS also publishes within their gauging station websites near monthly measurements of channel wetted area and width that they used for calibration of stage-discharge relationships. The locations of these 79 sites within California are indicated in Figure 2.2, including 38 sites that were relatively unaffected by human activities such as dam construction or urbanization.

The 38 unaffected sites are referred to as "minimally developed sites" and were utilized for this analysis. Table 2.1 lists these monitoring locations and separated them by the presence or absence of a slope break in the dependence of particle loading rate on flow rate. The table includes the 1.5-year recurrence interval flow rate that is commonly referred to as bank-full discharge [*García,* 2008]. For each of the sites, annual peak flow rates were ordered from highest to lowest. The recurrence interval was calculated for each flood by

$$\text{Recurrence Interval} = \frac{n+1}{m} \tag{2.1}$$

where n is number of years and m is relative rank of each year. The flow rate when there is a slope break, Q_c, is substantially below the 1.5-year return period flood. Table 2.1 also includes an average value of D_{50} for the 18 sites that had five or more sets of sediment bed size distributions (data were obtained at: http://co.water.usgs.gov/sediment/ancillary.cfm).

Additional information on selected watersheds was obtained from the USGS. Channel cross section measurements collected by USGS personnel in Redwood Creek at Orick (USGS site number 11482500) were obtained at the USGS California Water Science Center in Sacramento. High frequency 15-minute flow rate and turbidity data in Russian River at Guerneville are reported by USGS. These high frequency data are used for hysteresis analysis in the relationship of turbidity to flow rate.

Table 2.1. The 38 minimally developed sites within California with long-term data for particle loading analysis.

Slope Break	USGS Site No.	Site Name	Water shed Area [km^2]	Bank-full Discharge [m^3/s]	Flow rate at a slope break [m^3/s]	D_{50}* [mm]	1950s	1960s	1970s	1980s	1990s	2000s	10s
Yes	10336610	Upper Truckee Rv at South Lake Tahoe, CA.	142	10	2	2.0							
	10336645	General C near Meeks Bay,CA	19	3	1.5	-							
	10336660	Blackwood C near Tahoe City, CA.	29	5	2	-							
	10336676	Ward C at HWY 89 near Tahoe Pines, CA.	25	4	2	-							
	10336780	Trout Ck near Tahoe Valley, CA.	95	2	1	1.6							
	11113000	Sespe C near Fillmore, CA.	653	76	5	-							
	11148900	Nacimiento R below Sapaque Creek, near Bryson	420	100	15	6.9							
	11151870	Arroyo Seco near Greenfield, CA.	293	57	20	-							
	11169800	Coyote C near Gilroy, CA.	282	30	10	11.5							
	11335000	Cosumnes R at Michigan Bar, CA.	1,388	90	30	-							
	11382000	Thomes C at Paskenta, CA.	526	80	10	6.4							
	11465150	Pena C near Geyserville, CA.	58	15	5	11.2							
	11465200	Dry C near Geyserville, CA.	420	75	10	11.7							
	11468000	Navarro R near Navarro, CA.	785	240	10	-							
	11472150	Eel R near Dos Rios, CA.	1,368	220	60	18.2							
	11472200	Outlet C near Longvale, CA.	417	170	20	-							
	11472800	MF Eel R ab Black Butte R near Covelo, CA.	528	390	20	-							
	11472900	Black Butte R near Covelo, CA.	420	125	10	7.7							
	11473900	MF Eel R near Dos Rios, CA.	1,930	440	20	11.9							
	11474500	NF Eel R near Mina, CA.	642	310	10	-							

Table 2.1. The 38 minimally developed sites within California with long-term data for particle loading analysis. (continued).

Slope Break	USGS Site No.	Site Name	Water shed Area [km^2]	Bank-full Discharge [m^3/s]	Flow rate at a slope break [m^3/s]	D_{50} * [mm]	1950s	1960s	1970s	1980s	1990s	2000s	10s
Yes	11475000	Eel R at Fort Seward, CA.	5,457	1500	50	5.9							
	11476600	Bull C near Weott, CA.	73	37	2	-							
	11477000	Eel R at Scotia, CA.	8,063	2680	100	8.1							
	11481500	Redwood C near Blue Lake, CA.	175	64	8	-							
	11482500	Redwood C at Orick, CA.	717	320	20	6.7							
	11528700	SF Trinity R below Hyampom, CA.	1,979	330	60	-							
	11529000	SF Trinity R near Salyer, CA.	2,326	575	60	-							
	11530020	Supply C at Hoopa, CA.	41	17	3	-							
	11532500	Smith R near Cresent City, CA.	1,590	1310	200	-							
	14361600	Elliott C near Copper, OREG.	134	17	5	-							
No	11141280	Lopez C near Arroyo Grande, CA.	54	2		9.3							
	11147070	Santa Rita C near Templeton, CA.	47	8		-							
	11149900	San Antonio R near Lockwood, CA.	562	30		2.0							
	11160300	Zayante C at Zayante, CA.	29	4		2.0							
	11176400	Arroyo Valle below Lang Cyn near Livermore, CA.	337	16		-							
	11180960	Cull C ab C Res near Castro Valley, CA.	15	2		3.6							
	11461000	Russian R near Ukiah, CA.	259	85		-							
	11525600	Grass Valley C at Fawn Lodge near Lewiston, CA.	80	9		7.7							

Daily suspended load Near monthly field calibrations

* D_{50} is estimated from the mean sediment bed size distribution when there are 5 or more sets of measurements reported by USGS

The USGS estimates daily suspended particle data from regular field sampling, and from these measurements the USGS defines a relationship between instantaneous flow rate and suspended particle concentration. This relationship is used to estimate 15-minute suspended particle concentrations from 15-minute flow rate by interpolation. To avoid a consistent bias in the power law rating curve method, the USGS prefers a linear interpolation method for the estimation of the suspended particle concentration by using graphical program such as GCLAS (Graphical Constituent Loading Analysis System) [*Koltun et al.*, 2006]. The daily mean of these 15-minute suspended particle data is reported as daily suspended particle data. The rounding convention of USGS is summarized in Table 2.2.

Table 2.2. USGS data rounding conventions

Parameter	0 to < 1	1≤ to < 10	10≤ to <100	100≤ to <1000	>=1000
Discharge [ft^3/s]	0.XX	X.X	XX	XXX	XXX0
Concentration [mg/L]	*	X	XX	XXX	XXX0

* <0.5 mg/L, reported as 0.5 mg/L; 0.5mg/L to 1 mg/L report as 1 mg/L

The sediment bed material characteristics of 33 sites within the 38 minimally developed sites were visually assessed during field investigations from June 2 to July 8, 2014 where 25 of the 33 visited sites show a clear slope break in the relationship of Q_s to Q. The five watersheds draining into Lake Tahoe basin were not visited. The Nacimiento River below Sapaque Creek, near Bryson (USGS 11148900) site was not accessible so bed material measurement data reported by USGS and photo images provided from the USGS Santa Cruz field office were obtained. The stage – discharge relationships downloaded from USGS gauging station websites were also compiled to assess the dynamics of the channel bed in response to moderate and high flow events. Plots of the particle loading relationship, photos of the channel bed, and the stage – discharge relationship over time of all 38 sites are included in Appendix A.

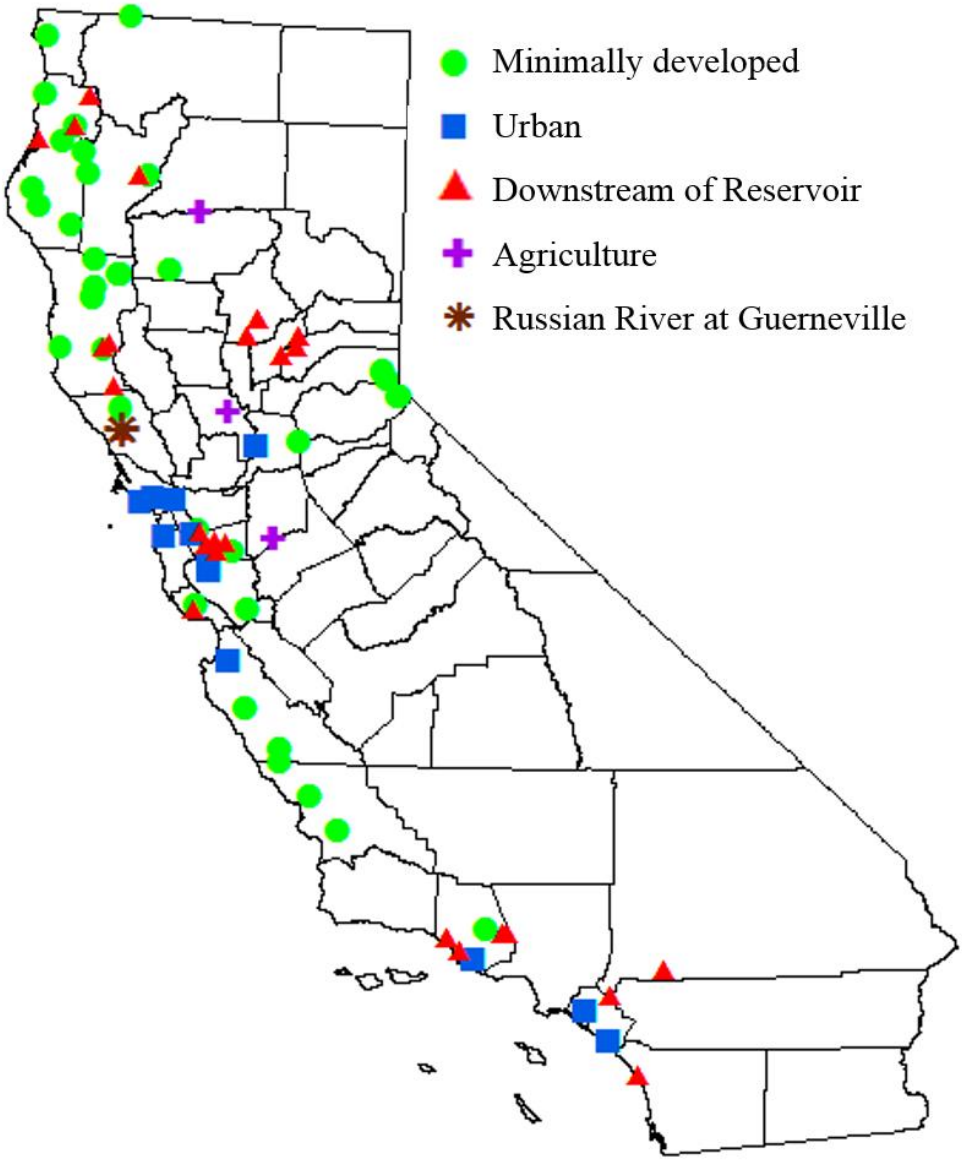

Figure 2.2. Seventy-nine USGS gauging sites having suspended sediment data in California with 38 minimally developed sites indicated in green. Also included is the Russian River site at Guerneville which has 15-minute flow rate and turbidity data.

2.1.2 Sites with a Slope Break

Of the 38 minimally developed sites, 30 sites clearly show a slope break in the log – log plot of the particle loading rate versus flow rate. The particle loading plots of all 38 sites are included in Appendix A. The relationship between flow rate and channel wetted width and mean water depth were compared for all sites with a slope break. Mean water depth is estimated by dividing reported channel cross sectional area by the reported channel wetted width. An example of this channel cross section analysis is shown in Figure 2.3 for Redwood Creek at Orick. Figure 2.3 (a) has Q_s plotted against Q with a slope break at about 20 m^3/s. Figure 2.3 (b) is a plot of mean water depth versus flow rate and Figure 2.3 (c) considers channel wetted width versus flow rate. The channel width data better illustrate the transition from a shallow, wide stream to flow constrained by steep stream channel banks at the slope break compared to the mean water depth data. For the 30 minimally developed sites with slope breaks, flow rates at slope breaks vary from 3% to 50% of the 1.5-year recurrence interval flow rates which are often referred to as bank-full discharge [*García*, 2008]. This suggests there are frequent flood events with flows greater than the flow at the slope break.

The stage-discharge relationships determined at gauging stations show that alluvial channels are actively reworked during moderate and high flow events. This is illustrated in Figure 2.4 where the wetted channel cross section at a gauging station is plotted before and after a flood when flow rates were comparable. There is evidence of a changing sediment bed profile from one measurement to the next indicating sediment bed rearrangement by moderate flow events around 140 m^3/s which is much smaller than bank-full discharge of 320 m^3/s at this watershed where a slope break in the relationship of Q_s to Q is observed at 20 m^3/s.

Of the 30 sites with a slope break in the particle loading relationship, 25 sites were visited during field investigations and all were gravel-bedded streams. At most of these sites there are changes in the stage-discharge relationship every few years in response to large flow events that result in stream bed aggradation followed by multiple years when erosion of the sediment bed causes decreasing stage readings for comparable flow rates. This is illustrated in the stage-discharge relationship for Sespe Creek near Fillmore California in Figure 2.5 where the stage at a given flow rate during the period 2001 – 2005 increases substantially in the 2005 – 2006 period in response to sediment accumulation in the stream bed. Stage-discharge data collected after 2006 show bed erosion with a decreasing stage at a given flow rate until the 2008 – 2011 period where the stage-discharge relationship appears similar to the 2001 − 2005 period relationship. Visual observations, gauging site cross sections, and stage-discharge relationships all support the contention that there is active sediment bed rearrangement intra-annually by moderate flow events and at 5 to 10-year intervals by higher flow events.

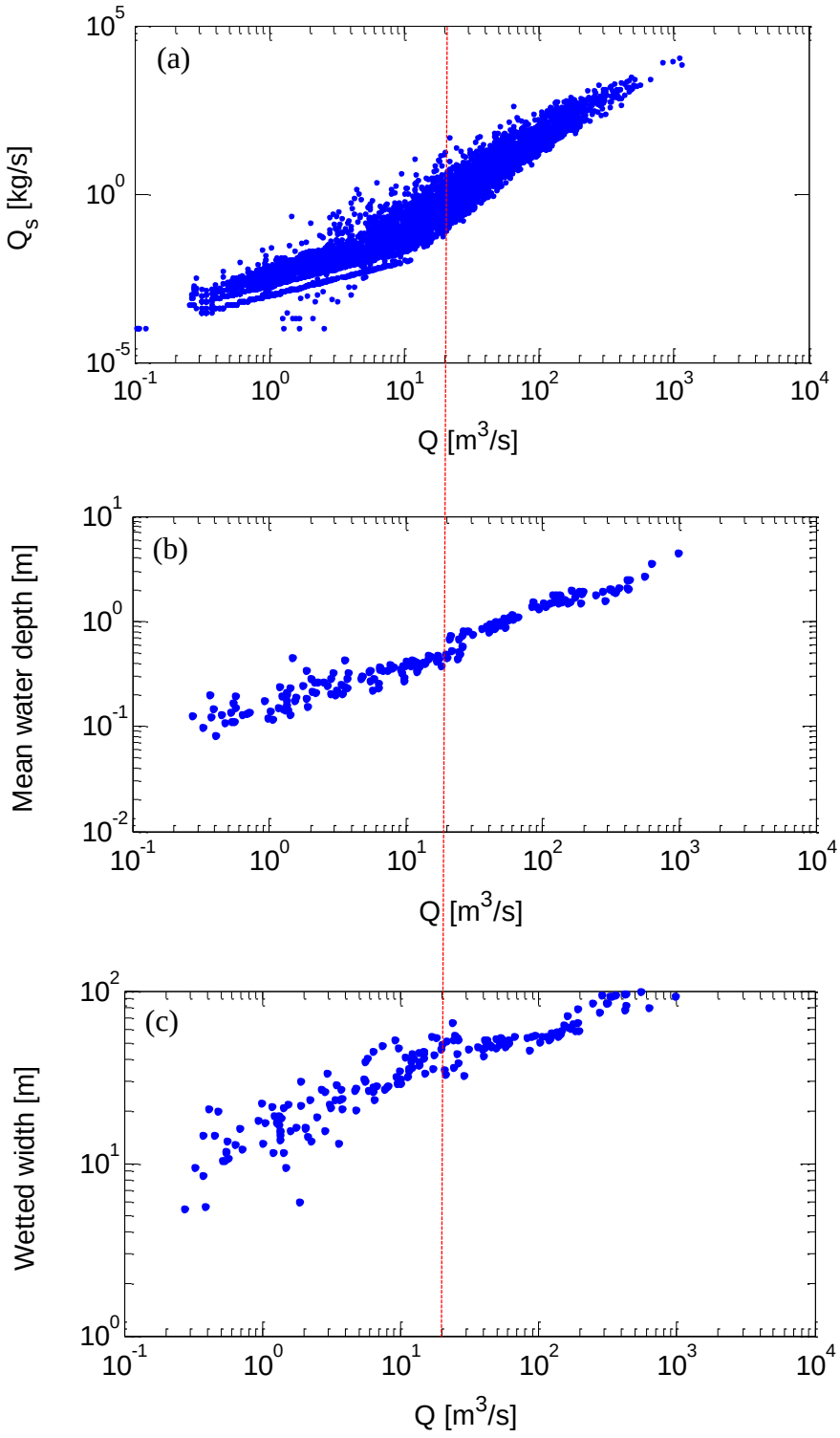

Figure 2.3. Daily suspended load and field measurements reported by USGS in Redwood Creek at Orick between 1970 and 2001. The vertical red line represents a transition at $Q \sim 20$ m^3/s referred to as a slope break.

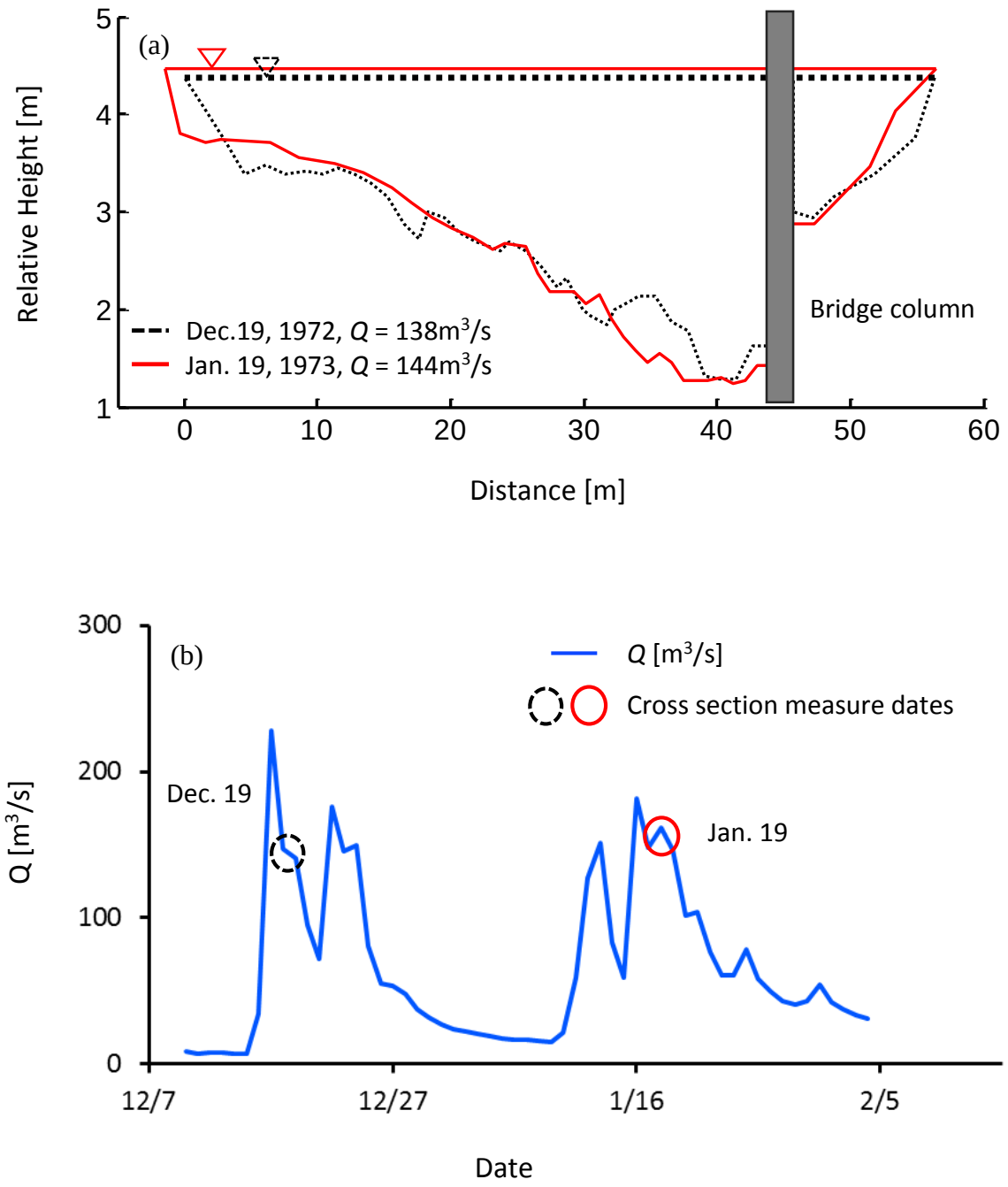

Figure 2.4. USGS channel cross section measurements and hydrograph in Redwood Creek at Orick, (a) Wetted cross section measurements, (b) Hydrograph with dates of cross section measurements indicated.

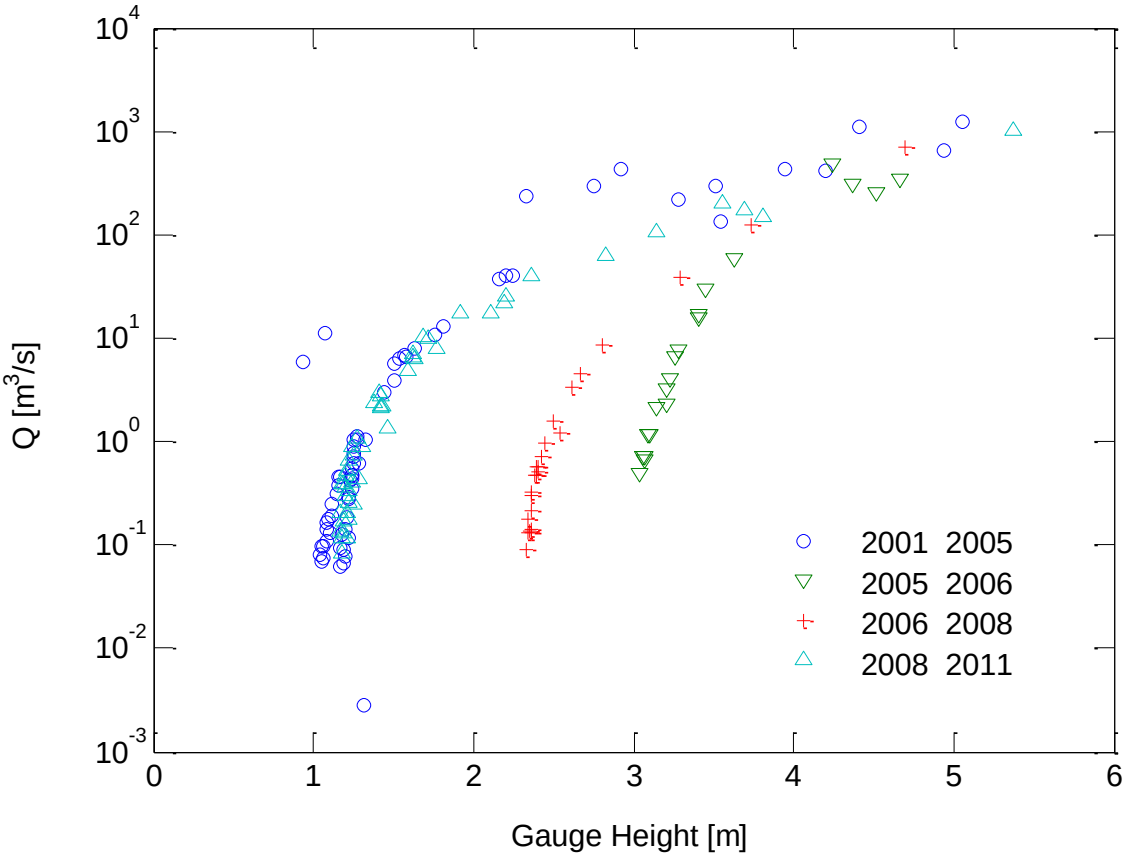

Figure 2.5. Selected stage-discharge relationships from 2001 to 2011 for USGS stream gauge site Sespe Creek near Fillmore, California (USGS site number 11113000).

2.1.3 Sites without a Slope Break

While 30 of the 38 research sites show a clear slope break, the other 8 sites do not. Table 2.3 summarizes the observed characteristics of the bed materials at the sites without a slope break. In general, the stream bed was not dominated by gravel. The photos of channel bed materials taken in these 8 sites during the field investigation are included in Appendix A.

Table 2.3. Classification of sites without a slope break in particle loading dependence on flow rate.

Channel bed material	Site Name (USGS Site No.)
Bed rock and sand/fine gravel	Zayante Creek above Zayante, California (11160300)
	Cull Creek near Castro Valley, California (11180960)
Cobble/boulder and sand/fine gravel	Lopez Creek near Arroyo Grande, California (11141280)
	Santa Rita Creek near Templeton, California (11147070)
	Arroyo Valle below Lang Canyon near Livermore, California (11176400)
	Russian River near Ukiah, California (11461000)
	Grass Valley Creek at Fawn Lodge near Lewiston, California (11525600)
Sand	San Antonio River near Lockwood, California (11149900)

Two sites dominated by bedrock contained sand/fine gravel in the bed. These bedrock sites had stage-discharge relationships that are relatively stable which suggests that there is limited scouring or depositional processes (Figure 2.6 and 2.7).

There are five sites with no slope break where the channel bed is composed of cobbles with sand rather than gravel occupying the space between cobbles. The stage-discharge relationship of these sites is also relatively stable over time except for Lopez Creek near Arroyo Grande California. An example stage-discharge curve at Arroyo Valle below Lang Canyon near Livermore, California (11176400) is shown in Figure 2.8 where the channel bed is stable for 38 years.

Lopez Creek near Arroyo Grande, California presents a difficulty in classification due to characterization data collected over different periods. Over the period between 1967 and 1972, suspended particle concentrations were determined along with sediment bed size distributions. Particle loading as a function of flow rate did not show evidence of a slope break (Appendix A), and the sediment size distributions were becoming finer with time (Figure 2.9). Additionally, the stage – discharge relationship between 1967 and 1984 showed one meter of continuous infilling of the sediment bed (Figure 2.10). When the gauging station was relocated in 1984, bed infilling of another meter occurred through 2009 followed by some erosion (Appendix A). The field observations conducted in 2014 classified the stream bed as cobbles armoring sand, which likely

did not reflect the stream's suspended particle data in the 1967 to 1972 period or the fining of sediment bed materials over the 1969 to 1972 period.

A channel composed of sand was observed in the San Antonio River near Lockwood, California (USGS site number 11149900) (Appendix A). The frequent changes in the stage-discharge relationship suggests that the channel bed at this site is un-stable (Figure 2.11).

In summary, sites without slope breaks have sediment beds composed of bedrock, boulders and cobbles that are infrequently moved, or sandy materials that is usually in motion at the flows encountered in the watershed. At the 25 sites having evidence of a slope break that were visited, none had bed material dominated by bedrock, boulders, cobbles, or sand. It thus appears that gravel-bedded stream beds lead to conditions that alter fine particle capture and release unlike these other bed materials. The next section in this chapter explores conditions for the initiation of sediment motion in gravel-bedded streams.

(a) Zayante Creek above Zayante, California (USGS site number 11160300)

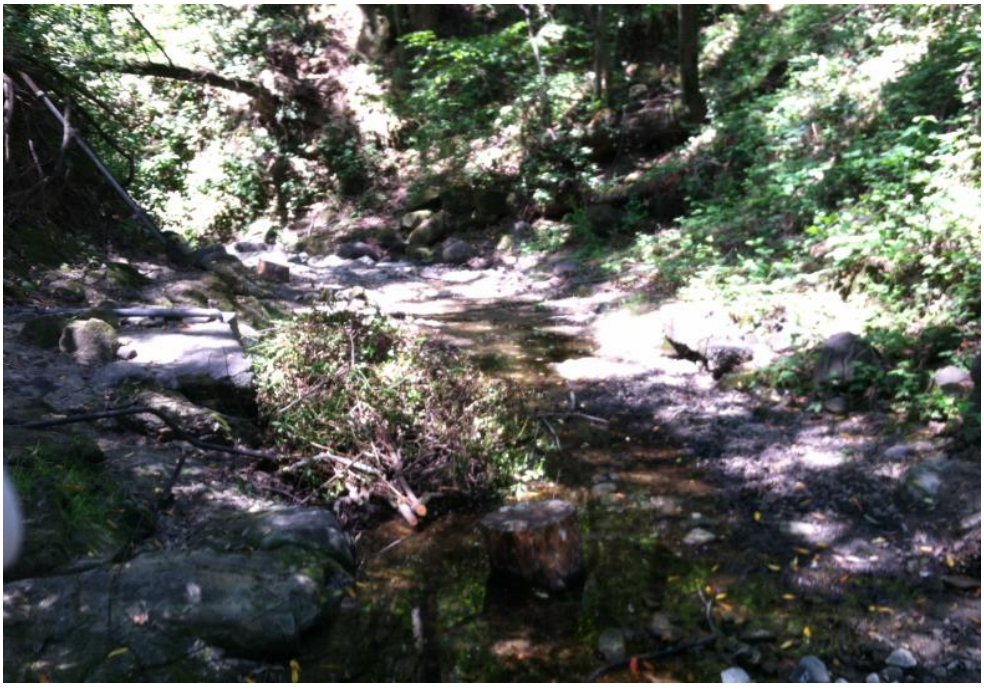

(b) Cull Creek near Castro Valley, California (USGS site number 11180960)

Figure 2.6. Two bedrock sites with sand and fine gravel present in depressions.

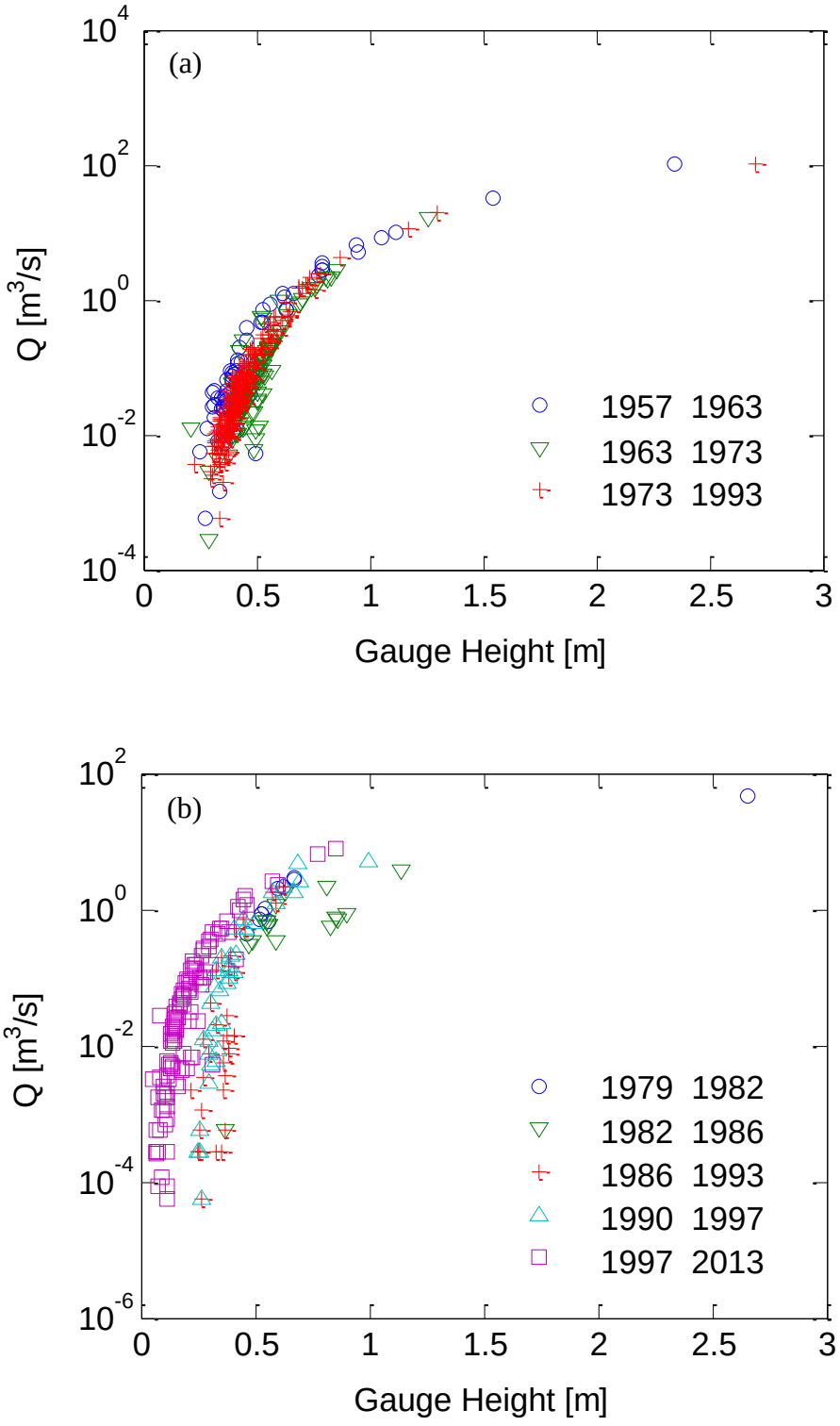

Figure 2.7. Stage-discharge curves in bedrock dominated stream channels reported by USGS at (a) Zayante Creek above Zayante, California (USGS site number 11160300) and (b) Cull Creek near Castro Valley, California (USGS site number 11180960).

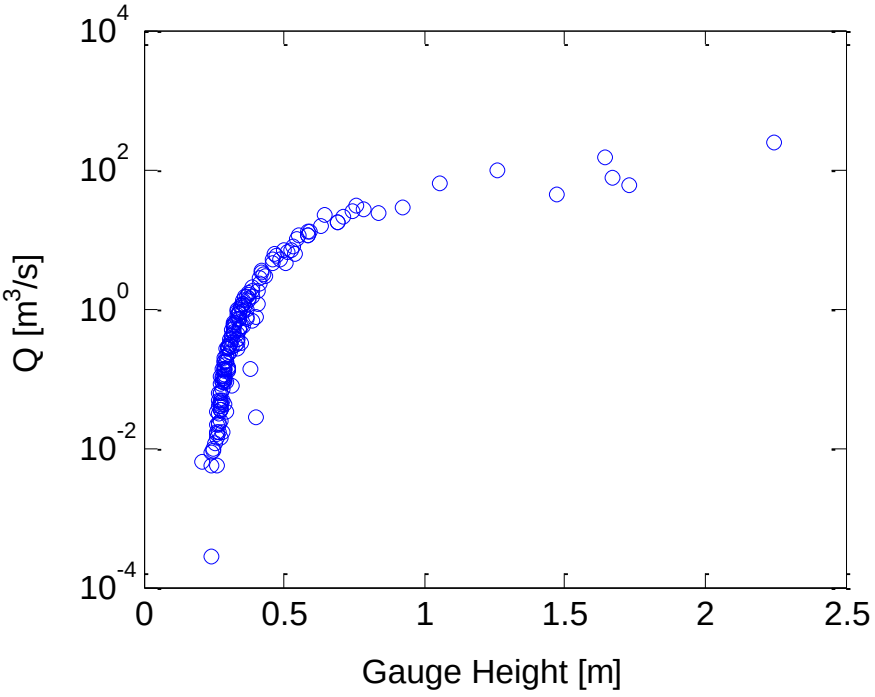

Figure 2.8. Selected stage-discharge measurements at Arroyo Valle below Lang Canyon near Livermore, California (11176400) over the period of 1975 to 2013. The sediment bed surface is dominated by cobbles and boulders with sand and gravel occupying the space between and beneath the cobbles.

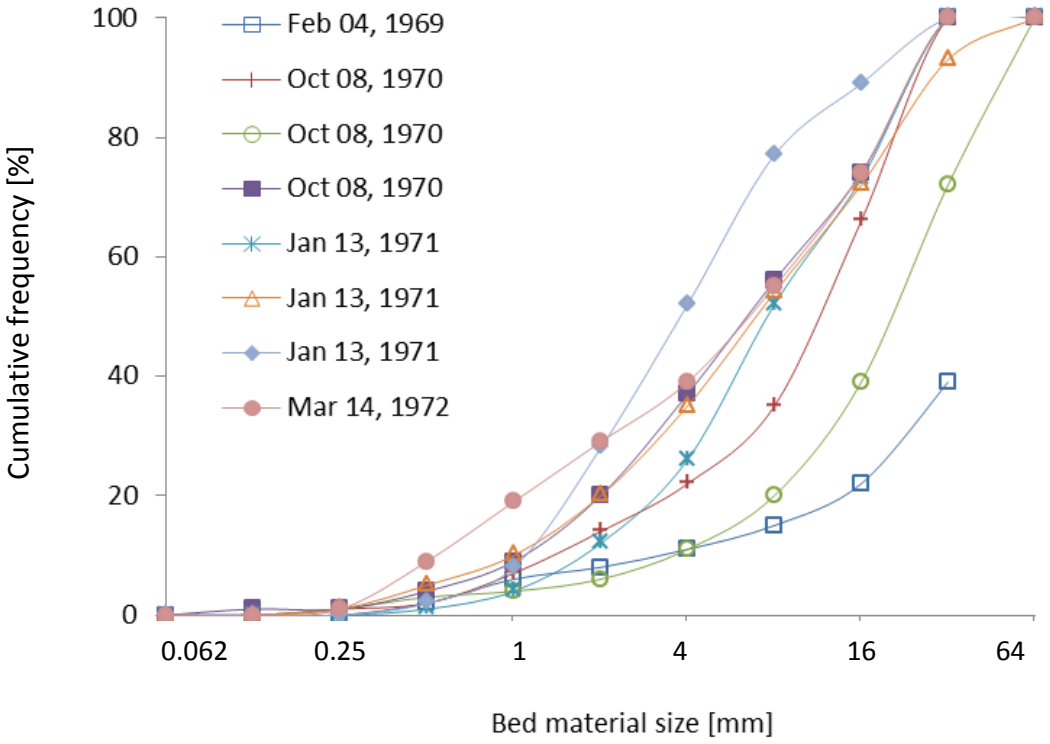

Figure 2.9. Bed material size distribution measurements between 1969 and 1972 at Lopez Creek near Arroyo Grande, California (USGS site number 11141280) reported by USGS.

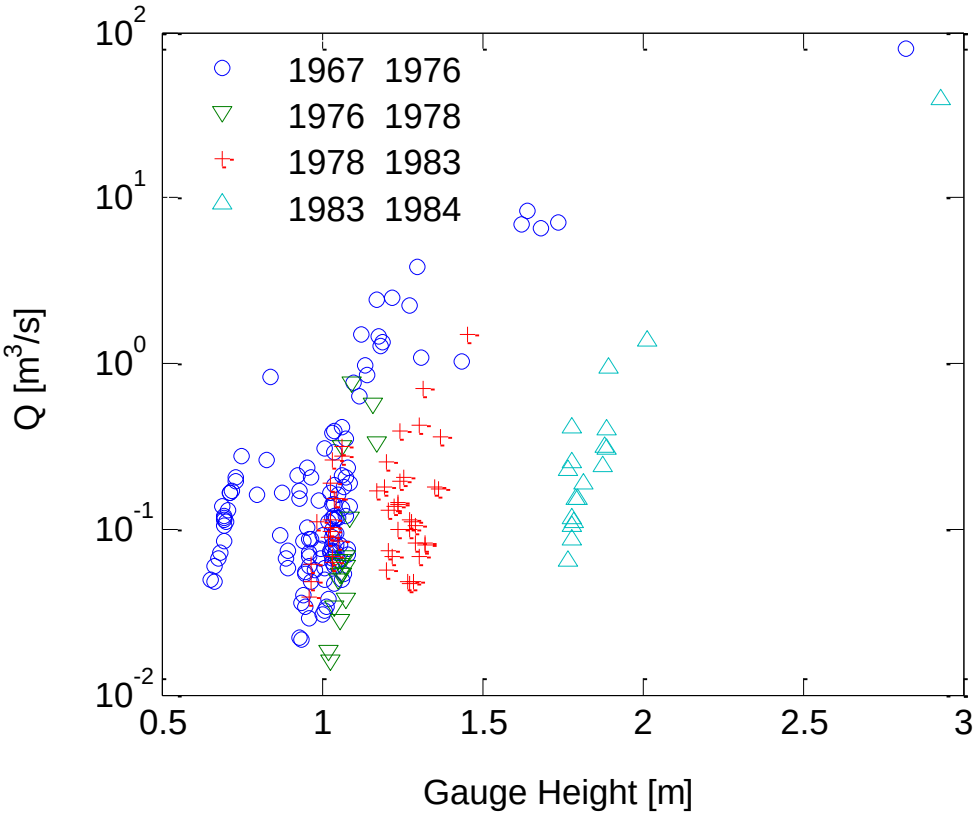

Figure 2.10. Selected stage-discharge curves at Lopez Creek near Arroyo Grande, California (USGS site number 11141280) from 1967 to 1984 reported by USGS.

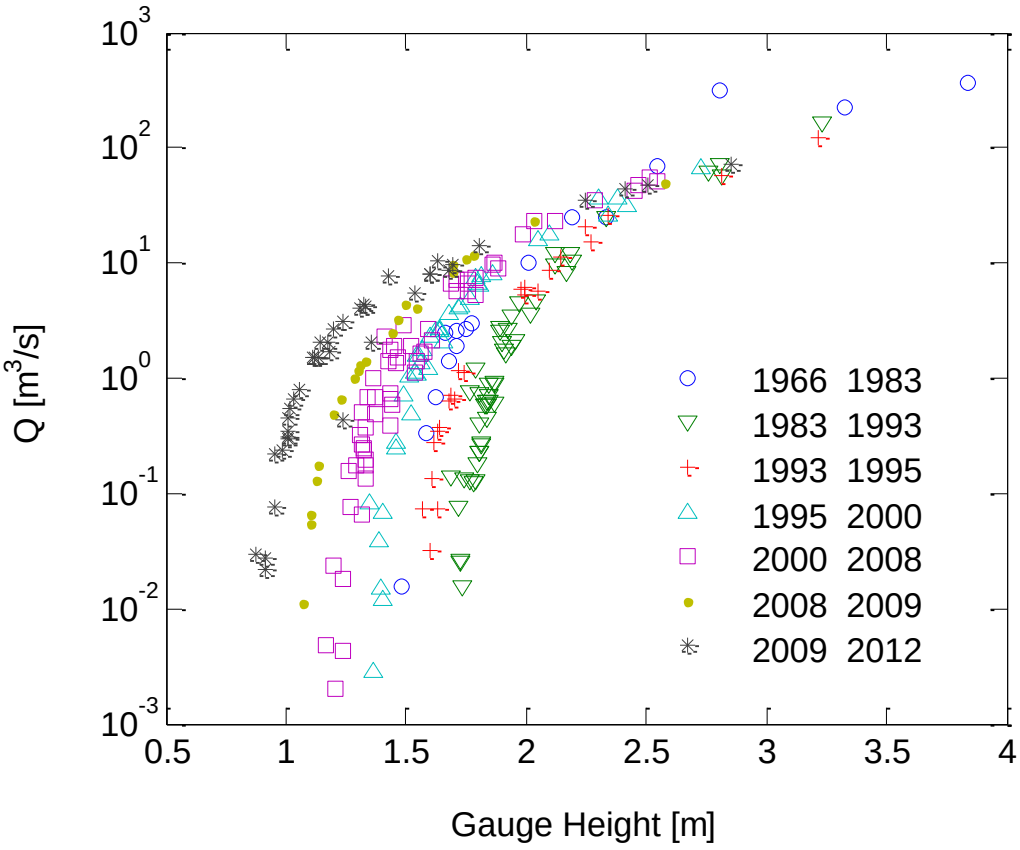

Figure 2.11. Stage-discharge relationship reported by USGS at San Antonio River near Lockwood, California (USGS site number 11149900) showing a progressive erosion of the sediment bed over a 19-year period from 1993 to 2012.

2.1.4 Shear Stress and Bed Mobilization

There has been considerable speculation and data interpretation that high flow events contribute to the fine particle loads in streams [*Collins and Walling*, 2004; *Navratil et al.*, 2010; *Harvey et al.*, 2012]. The slope break observed in particle loading relationships for gravel-bedded streams indicates the increased fine particle loading corresponds to a change in channel hydraulics from relatively shallow to increased water depth at flows above the slope break. This section calculates the shear stresses associated with this change in channel geometry and the data suggest there is a one-to-one correlation with shear stresses required for sediment bed mobilization. While the data have considerable variability, the flow at the slope break imposes a bottom shear stress sufficient to initiate sediment bed motion.

In order to calculate bed shear stresses at slope breaks and the critical shear stresses required for sediment bed mobilization, sediment bed size distributions are needed. Of the 30 minimally developed sites showing evidence of a slope break, only 13 sites have five or more sets of sediment bed material size measurements from which average properties can be estimated. Table 2.1 includes the mean sediment bed sizes (D_{50}) obtained from USGS (http://co.water.usgs.gov/sediment/ancillary.cfm). The watershed areas of these sites ranged from 58 to 8063 km^2 and D_{50} ranged from 1.6 to 18 mm.

The shear stresses at flow rates corresponding to slope breaks were estimated for the 13 sites with sediment bed material size data by

$$\tau = \rho_w g R S_f \tag{2.2}$$

where the frictional slope (S_f) is calculated from Manning's equation:

$$S_f = \frac{V^2 n^2}{R^{4/3}} \tag{2.3}$$

with V representing the mean flow velocity over the channel cross section [m/s], n is Manning's roughness coefficient and is calculated from

$$n = \frac{1}{21.1} D_{50}^{1/6} \tag{2.4}$$

which is suggested by USGS for gravel-bedded rivers (http://il.water.usgs.gov/proj/nvalues/) where D_{50} [m] is mean bed material size, and R is the mean water depth [m] estimated from wetted area divided by channel width. The mean water velocity and the mean water depth were estimated from the field measurement data reported by USGS (http://waterdata.usgs.gov/nwis) for flow rates near the slope break. The range in R and V leads to a range in predicted shear stresses at the slope break.

The critical shear stress (τ_c) to initiate sediment bed movement was calculated for each site using Shields equation [*Shields*, 1936]:

$$\tau_c = \tau_c^* \, g \, (\rho_s - \rho_w) \, D \tag{2.5a}$$

where τ_c^* is a dimensionless critical shear stress, or the Shields parameter, generally assumed as a constant value of 0.03 for a sediment bed Reynolds number, $Re^* = u^*D/v$, greater than 1000 in gravel-bedded streams (Buffington and Montgomery, 1997; Neill, 1968; Parker et al., 2003); ν is the kinematic viscosity [L^2/T], and u^* is the shear velocity defined as

$$u^* = \sqrt{\frac{\tau}{\rho_w}} \qquad (2.5b)$$

The variable D is the bed material size of interest [L] and is generally taken as D_{50}.

Calculated shear stress (τ) at a slope break and critical shear stress for bed mobilization (τ_c) are compared in Figure 2.12 for the 13 gauging station sites having the necessary data on sediment bed material sizes. The field measurement data used for calibration were not measured exactly at the flow rate where the slope break was observed. Even though the channel beds were mobile the relationship between flow rate and mean water depth or channel wetted width show consistency through the entire measurement period with scatter (for example, Figure 2.3). The shear stresses were calculated with all available field measurement data even if the calibration period did not always overlap with the measurement period of the daily suspended particle load. However, when the two periods did overlap with sufficient data for the calculation of shear stress, only the overlap periods were used for the calculation of shear stress. The calculated shear stresses varied even near comparable flow rates for different measurement periods which caused the range of values plotted in Figure 2.12.

The range in estimates of shear stress at slope break and the critical shear stress for bed mobilization are substantial. A range in critical shear stress for bed mobilization arises from the spread in reported D_{50}'s at each site. For the calculated shear stress at the flow rate corresponding to the slope break, the range in values is a consequence of variations in the stage-discharge relationship and geomorphic estimates near that flow rate. In spite of the range of calculated values, the bed shear stress at slope break is comparable to the critical shear stress required to initiate bed movement for these minimally developed sites. This comparison implies that for flow rates greater than the critical flow rate, increased fine particle transport is caused by sediment bed erosion and fluidization. Henceforth, the flow rate corresponding to the flow rate required to initiate bed fluidization and where the slope break occurs will be referred to as the critical flow rate, Q_c.

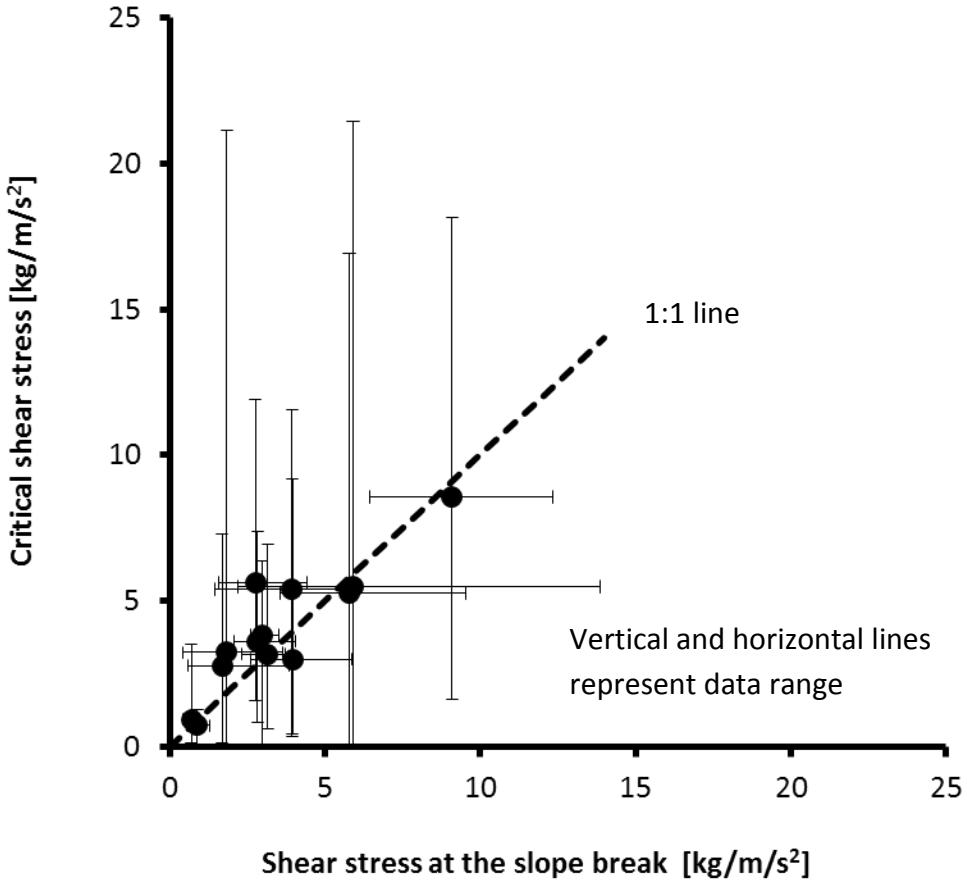

Figure 2.12. The mean and range of calculated bed shear stress ($\boldsymbol{\tau}$) at the observed slope break and critical shear stress ($\boldsymbol{\tau_c}$) for bed mobilization in 13 minimally developed streams.

An analysis of the dynamics for stream beds with boulders and cobbles is challenging because of the irregularity and variation of bed form, form drag, and infrequent cobble mobilization. In this research the dynamics of a channel bed with cobbles/boulders having sand/fine gravel between and beneath cobbles/boulders is explored from the measurements reported by USGS. The observation of stable stage – discharge relationships in five sites with cobbles/boulders and sand/fine gravel between and beneath cobbles/boulders in this research demonstrates that the channel bed is infrequently mobilized at these sites.

The channel bed of Grass Valley Creek at Fawn Lodge near Lewiston, California (USGS site number 11525600) is composed of cobbles/boulders and sand. The mean bed material size of this site is 7.7 mm reported by USGS. The critical shear stress to mobilize this size sediment grain is 3.6 kg/m/s^2 and the corresponding flow rate is about 2 m^3/s which is about 23% of bank-full discharge. However as discussed previously, the stage – discharge relationship and channel bed are relatively stable. The cobbles/boulders were not easily mobilized and secondly, the cobbles and boulders cause form drag reducing the shear stress on any sand or gravel present between and beneath cobbles/boulders [*Andrews*, 2000]. For example, the critical shear stress to mobilize the smallest cobble 65 mm in size is 30 kg/m/s^2. The flow rate corresponding to this shear stress is larger than 20 m^3/s, having a recurrence interval of about 4 years where bank-full discharge is only 8.6 m^3/s. The critical shear stress to mobilize 100 mm sized cobbles is 47 kg/m/s^2 and the corresponding flow rate is larger than 50 m^3/s which was rarely observed at this site. Thus, the cobbles and boulders at this site were rarely mobilized.

Frequent mobilization is observed for sand dominated sediment beds. The San Antonio River near Lockwood, California (USGS site number 11149900) has a sandy channel bed with a mean bed material size of 2 mm reported by USGS. The critical shear stress needed to mobilize this size bed material is 1 kg/m/s^2, and the corresponding flow rate is about 0.6 m^3/s which is only about 2% of bank-full discharge at this site. Under these conditions sand size particles are mobilized by relatively low flow rates and this prevents identification of a slope break in the available data. The frequent mobilization of bed materials is apparent in the stage – discharge relationship.

2.1.5 High Frequency Measurements of Turbidity and Flow Rate for Hysteresis Analysis

The data utilized thus far in the analysis of particle transport in stream channels were based on daily averages of flow and particle concentration provided by the USGS. For watersheds less than about 5000 km^2 there is considerable variability in flow and particle concentration during a 24-hour period. Previous researchers have observed hysteresis loops when particle concentration is plotted as a function of flow rate to qualitatively describe particle transport during flood events and between floods. In the analysis of the 30 sites with evidence of a slope break in the particle loading curve, watershed areas ranged from 20 to 8000 km^2, which led to examination of higher frequency data that would offer insight into particle dynamics.

In a search of available USGS data sets with 15-minute flow and turbidity data, the Russian River gauge near Guerneville was selected because the record spanned multiple years, the individual readings were complete with limited missing or questionable data, and there was an

established calibration between turbidity and fine particle concentration. The stream flow is partially regulated by two reservoirs not on the main stem of the river. Coyote Valley Dam was completed in 1958 and formed Lake Mendocino 123 km upstream, and Warm Springs Dam formed Lake Sonoma in 1983 42 km upstream (USGS Water Data Report). These reservoirs have slightly altered the higher flow records since watershed areas above Coyote Valley Dam and Warm Spring Dam are 7% and 10% of total watershed area, respectively. Releases of water from the flood storage pool in Lake Mendocino can alter the hydrographs at Guerneville [*Leonardson*, 2010].

Table 2.4. Available USGS data in the Russian River at Guerneville

Available data	1930s	1940s	1950s	1960s	1970s	1980s	1990s	2000s	10s
Near-monthly field calibration*									
Daily particle load (Q_s)									
15-min flow rate(Q) & Turibidty									

* Field cross section measurements of channel wetted area and width, and water depth

An example of 15-minute turbidity and flow rate data during four sequential floods was obtained for the Russian River near Guerneville. Data were aggregated to a 2 hour interval for the plotting of Figure 2.13 (a) to reduce visual complexity of the 15-minute interval data and to provide better visual identification. Figure 2.13 (a) shows the flow hydrograph and turbidity during the two-month period with the main flood events sequentially numbered. Floods 1 and 2 happened only a few days apart followed by a gap of about three weeks when floods 3 and 4 occurred. Even though the magnitudes of floods 3 and 4 are greater than floods 1 and 2, the peak turbidities are smaller in floods 3 and 4 than floods 1 and 2. This demonstrates that more fine particles were released from the watershed during first two floods, likely because the next two floods had fewer fine particles available for erosion. In addition, flood 4, while of greater flow rate than flood 3, had a lower peak turbidity. Hysteresis loops are shown for floods 1 and 2 in Figure 2.13 (b) and floods 3 and 4 in Figure 2.13 (c). The rising limb of each flood is distinguished from the falling limb by different symbols, and all four floods demonstrate clockwise hysteresis where turbidity peaks sooner than flow rate and the rising limb turbidity is greater than falling limb turbidity. The dashed black lines in Figures 2.13 (b) and (c) are drawn with the same slope and demonstrate a consistency in the falling limb recession following flood events. These data show that fine particle release from watersheds is operating at short time scales and there is not a one-to-one relationship between fine particle concentration and flow rate.

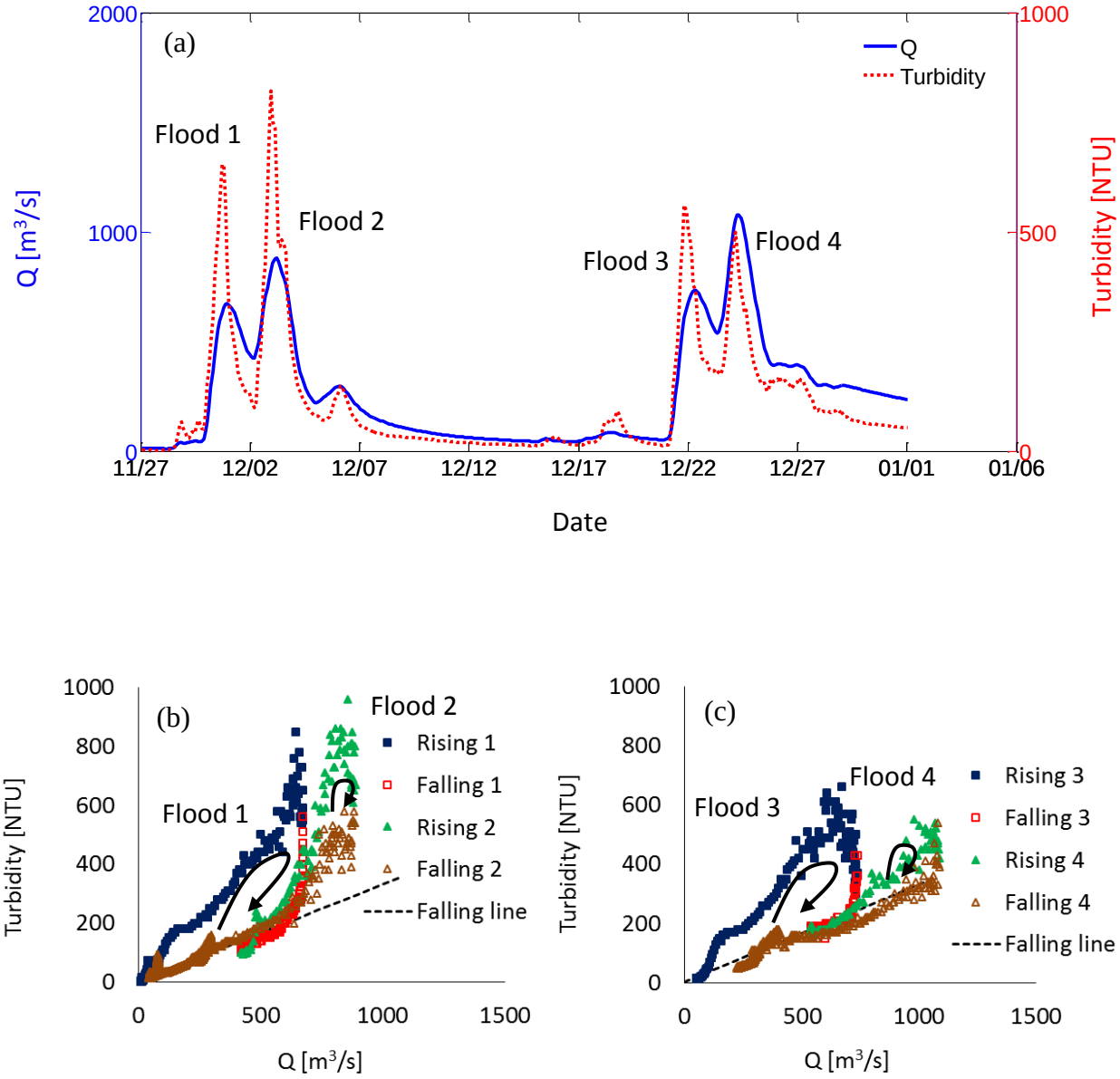

Figure 2.13. Flow rate and turbidity reported by USGS in the Russian River, at Guerneville between November and December in 2012. (a) Hydrograph, (b) and (c) Clockwise hysteresis in the relationship of flow rate to turbidity.

2.2 Conceptual model for the Fine Particle Storage and Release in Gravel-Bedded Streams

The data analysis in the prior section utilized long-term monitoring data available for a range of California watersheds that have been minimally altered by human activities. The initial observation of slope breaks in the particle loading rate dependence on flow rate led to an identification that these sites were associated with gravel-bedded streams rather than sand, cobble, boulder, or bedrock streambeds. Grain size analysis of the sediment bed and frequent measurements of channel geometry during calibration of stage-discharge relationships further showed slope breaks were associated with the initiation of sediment bed erosion. An examination of high frequency flow and turbidity data for a few sequential flooding events on the Russian River demonstrated that particle dynamics are controlled by processes at the sub-daily time scale during high flow events. The observed clockwise hysteresis loops in plots of particle concentration versus flow rate contribute to the observed vertical scatter in the dependence of particle loading on flow rate. These observations and field data analysis lead to the following conceptual model that presents a consistent explanation, guided the organization of the literature review in Chapter 3, which supported quantitative model development and testing in Chapters 4 and 5.

A sequential view of fine particle accumulation and release in minimally developed streams is shown in Figure 2.14 in terms of three separate phases. During Phase 1, the flow rate is below the critical flow rate required for bed fluidization and fine particles suspended in the stream flow accumulate within the gravel sediment bed through hyporheic flow and particle filtration or settling. During Phase 2, the flow rate exceeds the critical flow rate for bed fluidization and particles in storage within the sediment bed that is partially fluidized are eroded into the water column. With increased fluid flow rate, greater depth of fluidization occurs and additional fine particles are eroded. Following the peak flow rate, the sediment bed starts to reform in Phase 3. In this period there are limited opportunities for the release of fine particles since higher flows removed erodible particles. Clockwise hysteresis is represented by particle release during increasing bed fluidization up to the peak flow rate in Phase 2 and background fine particle concentrations during flood flow recession in Phase 3. When the sediment bed is completely reformed into a porous medium, Phase 1 repeats with renewed particle accumulation into the bed with greater pore space for fine particle accumulation. The existence of a common falling limb recession depicted by the dashed lines in Figures 2.13 (b) and (c) suggest there is an additional source of fine particles from the watershed rather than the stream bed.

The conceptual model in Figure 2.14 captures the processes identified from the monitoring data and analysis. The slope break in Q_s vs. Q marks when fine particles are released by bed fluidization showing the coupling of fine and coarse sediment transport. This conceptual model is translated into a quantitative model in Chapter 4.

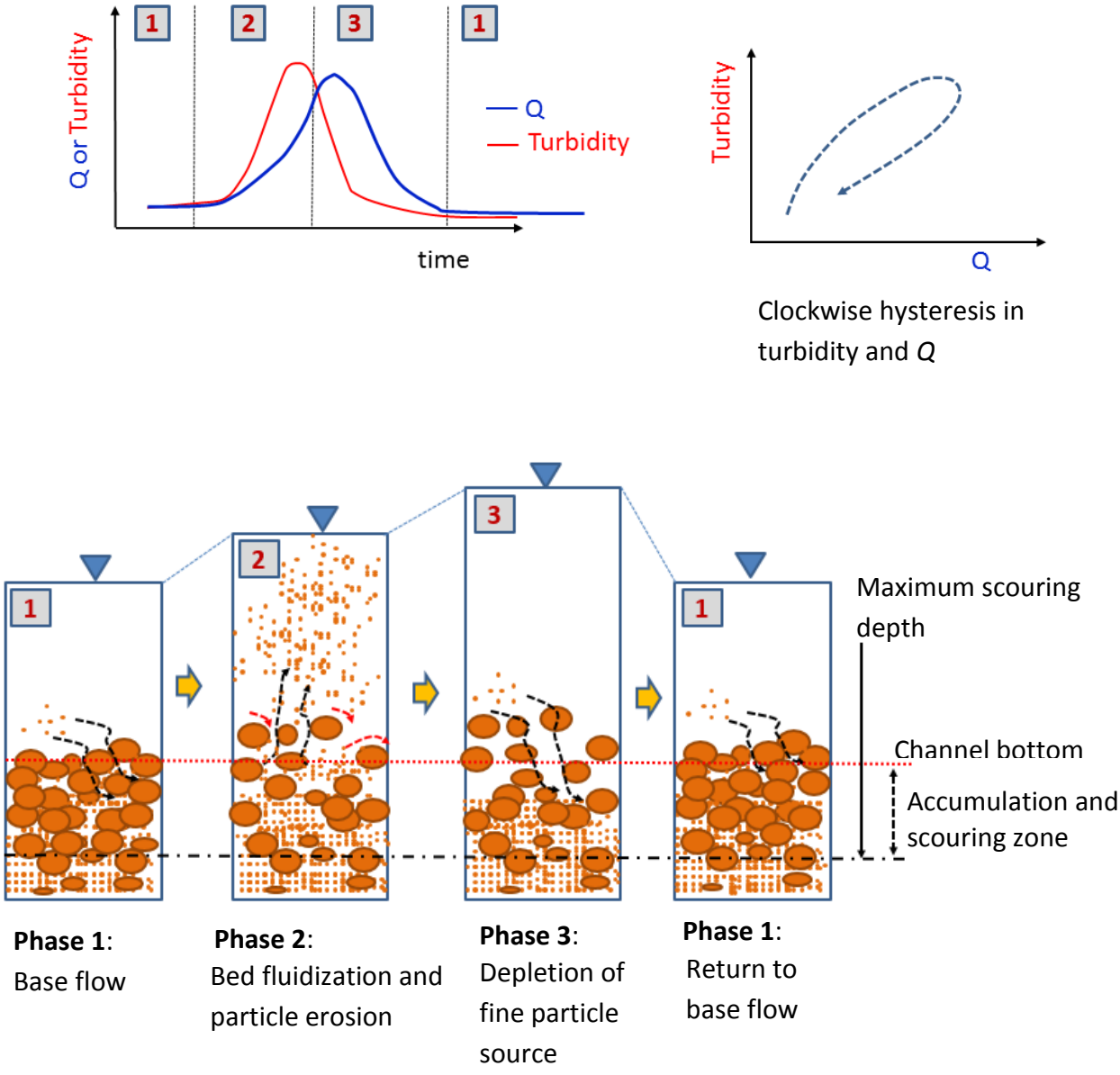

Figure 2.14. Conceptual model of fine particle accumulation and release by a flood.

Chapter 3. Current Understanding

Preliminary analysis in Chapter 2 found that fine particle transport is closely related with incipient motion of stream bed materials. There is a vast literature about fine particle and bed material movement in streams, numerous reasons proposed for variations in the relationship of Q_s to Q, and a range of models for quantifying particle erosion, deposition and release in response to hydrologic variability. This chapter explores the interconnected themes that must be integrated to address fine particle dynamics within streams.

3.1 Historical Perspective

Research and engineering practice related to suspended and bedload sediment transport diverged in their approach about 1950. There were early efforts to unify the two approaches, but with limited success. One example was *Hjulström* [1935] in Sweden who was driven by the opportunity of applying recent advances in turbulence theory to land surface erosion, along with the need to understand watershed responses to the physical and chemical alternation of watersheds brought about by urbanization and intensified agricultural production. In the United States the 1930s' Dust Bowl in the Great Plains led to a rapid expansion of research on soil erosion and fine particle transport in rivers, canals and reservoirs. As a consequence of these circumstances, research on suspended particle transport within watersheds adopted a more empirical approach compared to bedload transport studies.

Some of the early researchers who jointly considered suspended and bedload transport attempted to unify the approach, but there were too many methodological differences. *Einstein et al.* [1940] noted that prior advancements in bedload transport did not have a correspondence in quantifying suspended load transport. In their studies of sediment transport in watersheds during

flooding events, bedload transport was a unique function of discharge given an unlimited supply of material in the sediment bed. In contrast, suspended load was stated as being limited in supply by the watershed without acknowledging fine particle storage in the sediment bed. *Johnson* [1943] made a further distinction by stating that suspended load moves at "a rate that bears no direct relation to discharge". *Johnson* attributed the variability in suspended transport to upstream processes of vegetal cover, soil erosion, and rainfall characteristics. This comment by *Johnson* is in contrast to the thrust of the paper where flow and suspended sediment concentrations are closely aligned during flood events and a procedure is suggested similar to the unit hydrograph in flood flow prediction to estimate suspended particle loading using flow and limited suspended sediment measurements. *Einstein and Chien* [1953] further claimed how suspended load and bedload were different by stating that suspended sediment transport does not depend upon flow rate unlike bedload transport. The data and discussion within the paper emphasized to the contrary that silt-sized particles were exchanging with the sediment bed, were concentrating in the surface layer of the sediment bed, were responding to discharge; but compared to larger particles, the suspendable particles were strongly dependent upon their availability in the flow from upstream sources. It is this supply limitation that has become emphasized in subsequent discussions of the differences between suspended and bedload transport, and the recent compendium [*García*, 2008] continues to reinforce this view. As a consequence, fine particle transport within streams and rivers has been dominated by extensive field-scale monitoring programs of flow and suspended particle concentrations using empirical correlations in a search for generalizations through multiple parameter correlations.

The study of fine particles within watersheds was also driven by unforeseen applied problems and the availability of new measurement techniques. *Wolman* [1977] provides a personal perspective on the emerging needs in quantifying fine particle dynamics within watersheds starting in the 1960s. *Wolman*'s earlier contributions were as a fluvial geomorphologist, but those interests broadened in response to societal questions that required a more integrated view of the natural and altered watershed systems. Of particular relevance to this topic was *Wolman*'s interest in a systems view of sediment sources, their transport, storage, and remobilization over time and space. Additionally, *Wolman* saw an application of erosion and sedimentation to nonpoint source pollution by nutrients, trace metal transport, and the challenges of predicting the transport of particle-associated radionuclides then being introduced into the biosphere. One of the key concepts in these emerging topics was the non-steady dynamics of hydrologic systems when laboratory and field experiments had emphasized steady-state transport.

For many years, fine particles are known to have negative ecological effects and serve as a transport pathway for particle reactive pollutants (see Chapter 1). There remains a continuing need to not only understand fine sediment transport but the residence time of those particles and associated contaminants within watersheds. *Verhoff and Melfi* [1978] recognized that total phosphorus concentrations within rivers were correlated with suspended particle concentration, but more importantly found that a model for total phosphorous in streams required a mass balance modeling approach that included deposition and resuspension processes. Their subsequent work addressed the average travel velocity of total phosphorous within a water course in response to a series of flood events [*Verhoff et al.*, 1979]. Understanding sediment-associated contaminant transport and the efficacy of environmental remediation activities remains a continuing challenge [*Pizzuto*, 2014].

As with much of the hydrologic sciences, the impact of climate variability is placing additional demands on models, measurements, and extrapolation in space and time. Sediment transport models become important is assessing climate change effects with considerable diversity. In the work of *Syvitski et al.* [2003], long-term average sediment loading was determined for 340 watersheds from around the world. The authors' philosophy is that these watersheds provide data on just about all the watershed conditions likely to be encountered in the world and an average sediment loading for each could be correlated with climatic and watershed features such as area, relief, and temperature. The calibrated empirical model could then be utilized to better understand paleo environments where sediment records would be available for model evaluation and forecasting long-term sediment loading under assumed new climatic conditions. In contrast to the long-term average modeling, *Asselman et al.* [2003] explored a highly coupled, spatially resolved sediment transport model to assess climate change in the River Rhine over decadal time scales. The modeling system coupled a land surface hydrology model with sediment models for mobilization into channels, transport within channels, and sedimentation in the floodplain, all resolved to 1 km^2 grids. The authors identified modeling uncertainties that were dominated by the representation of erosion, sediment supply to channels, and sediment delivery downstream. *Forzoni et al.* [2013] provides another example of an integration of models to address long-term sediment contributions to continental shelves for use in paleo environment analysis in support of climate modeling.

There is a continuing need to quantitatively model fine particle dynamics within watersheds. The challenge remains in establishing an appropriate of model resolution that represents the dominant processes controlling fine particle release by hydrologic cycles and is still supported by observational records.

3.2 Fine Particle Dynamics in Streams

The focus of this research is the transport of fine particles in streams and rivers. To address the dominant processes requires some review of the relevant literature on the source of those particles, how particle concentration and fluxes have been quantified in streams during monitoring programs, the processes that determine particle exchange between the sediment bed and the water column, how larger scale watershed processes alter fine particle transport, and additional information that is gained from the analysis of hysteresis loops. While the dominant approach in the literature usually involves representation of fine particle loading rate, Q_s, as a function of flow rate, Q, the resulting particle loading relationships are not unique functions of flow rates and additional variables are added to the correlations. This section identifies those other factors that contribute to observed watershed responses.

3.2.1 Source of Fine Particles

Fine particles are generated within watersheds by erosive processes caused by physical, chemical and biological processes such as tectonic uplift, abrasion, glacial scour and weathering. These particles are mobilized at various spatial scales by raindrop impact, overland flow, hill slope failures, rill formation, gully erosion, stream bank erosion, and sediment bed resuspension. Once

mobilized by any of these processes, the fine particles are re-deposited and their motion restarted after brief or long periods. The fraction of particles generated within a watershed that leave the watershed, sometimes called the delivery ratio, has spatial and temporal scales that are difficult to quantify as initially summarized by *Walling* [1983] and revisited by *de Vente et al.* [2007]. With increasing watershed size, additional particle transport processes arise such as the existence of topographic variability, stream channels, flood plains, and lakes. Calculations of sediment release from watersheds are complicated by the time period adopted for averaging over noting that a year is certainly too short to sample hydrologic variability, but much longer periods challenge data collection efforts unless there are downstream particle traps such as lakes and coastal margins that integrate long periods which usually precludes annual analysis. Finally, assessment of uplift rates have uncertainties such that *de Vente et al.* [2007] place more emphasis on reporting suspended sediment yield [Mg/km^2/a] for watersheds rather than normalizing by an uplift rate.

There are a number of sources proposed for the suspended particles present in surface flows. *Johnson* [1943] attributed fine particles as being directly contributed to stream flow from rainfall impact, land disturbance, gullies, stream bank erosion, and possibly the stream bed. *Walling and Webb* [1982] assumed the fine particles observed at their monitoring location had their origin from hillslopes and undertook separation of streamflow components to correlate suspended particles with surface runoff. Base flow was assumed to dilute suspended particle concentration from surface flows. This approach of attributing fine particles directly to upland sources shifted in later publications with *Collins and Walling* [2007a] measuring fine particles within stream sediment beds and finding that the fine particles in active storage were on the order of the annual fine particle release by the watershed. Additionally, sediment tracers were used to identify sediment sources, and in the case of atmospherically deposited radionuclides, the timing of tracer releases [*Collins and Walling*, 2004]. *Hicks et al.* [2000] suggests that suspended sediment transport in the channel system is dominated by low intensity rainfall with less than 1-year return period floods in stable watersheds. On the contrary, high intensity, low frequency floods are more important in watersheds where suspended sediment supply is dominated by hill slope erosion.

Within semi-arid environments, fine particle transport by infrequent surface runoff events has received considerable attention as an exploitable water resource but with a possible limit to reservoir capacity from sedimentation. The determination of sediment loading rates as a function of flow rate and other environmental variables arrived at empirical correlations with considerable scatter [*Achite and Ouillon*, 2007; *Alexandrov et al.*, 2007; *Gao et al.*, 2013]. In the case of the arid Southwest United States, nested watersheds from 0.01 km^2 to over 100 km^2, both hillslope and sediment bed processes were important in determining suspended sediment release, and they found sediment release was linearly correlated with runoff depth [*Gao et al.*, 2013].

3.2.2 Limitation of Power Law Model

The quantification of suspended particles in flowing water since the 1950s is largely empirical with correlations of suspended particle concentration, C, or particle loading rate, $Q_s = CQ$, with flow rate. One of the most commonly used models for representing these data is a power law of the form $Q_s=aQ^b$ or $C = aQ^{b-1}$ where a and b are empirical coefficients. Power law relationships are typically utilized in hydrologic systems given the orders of magnitude variability in key

hydrologic variables, in this case flow and suspended particle concentrations, each varying by multiple orders of magnitude. Figure 3.1 illustrates typical data encountered within coastal watersheds of California using daily USGS data from the Redwood Creek gage at Blue Lake as an example. The flow rate varies by three orders of magnitude and the particle loading rate by almost seven orders of magnitude. The data ranges require plots of logarithmically transformed data for both variables in order to visualize the data. A power law representation of these data has two problems, first, there is not a single linear regime in the plot, and second, there is orders of magnitude variability in Q_s at a given Q.

While extensively utilized for representing fine particle loading, power law relationships are often criticized. *Walling* [1974] identified the inadequacies of correlating particle concentration only with discharge. He attributed the scatter in his data to numerous causes such as seasonal effects related to more intense summer rainfall patterns compared to the winter and vegetal cover. During flood events the sediment concentration increased at a similar rate as the discharge often peaking prior to the discharge, but the concentration decreased more rapidly than discharge during the falling stage. When concentration is plotted against discharge clockwise hysteresis loops are typically observed. Additionally, in sequential flood events the latter floods had less and less suspended particle mass released and this was attributed to the exhaustion of the source of particles within the watershed.

Multiple linear regression of log transformed data was proposed as a means of representing the suspended particle concentration leaving a watershed. *Walling* [1977] provided a review of the literature from the 1960s and 1970s that developed power law relationships for C or Q_s and noted that such relationships resulted in 30% errors in estimating annual sediment loss from fitted relationships. Greater errors were obtained when monthly loadings were calculated from daily flow data and the fitted power law relationship. The proposed solution was to collect suspended sediment data at hourly or more frequent intervals to improve estimates of seasonal and annual fine particle releases from watersheds rather than refining functional relationships between suspended solids concentrations and watershed discharge and other environmental factors. Continuous recording turbidity monitors were utilized for obtaining high frequency data in conjunction with calibration curves between turbidity and suspended solids concentration.

There are alternatives to the static power law representation of sediment loading relationships. *Hicks et al.* [2000] recognized that log C vs log Q plots were not linear and they used a locally-weighted scatter smoothing curve fitting technique called LOWESS [*Cleveland*, 1979] to represent the data. Watersheds also undergo episodic events that can dramatically alter sediment releases. One of the early examples was the study by *Ritter and Brown III* [1971] who followed increased turbidity for four years within the Russian Rivers following a December 1964 flood event. A broader study by *Warrick et al.* [2013] followed the impact of the 1964 California flood in multiple watersheds and documented decadal long alterations to sediment rating curves. The combination of wildfires followed by flooding before the watersheds become revegetated provided another example where average sediment rating curves were inadequate in representing extreme events [*Warrick et al.*, 2012]. Longer term changes in the relationship of C to Q are attributed to climate change [*Achite and Ouillon*, 2007]. Additionally, log-transformed data consistently underestimate the actual fine particle transport rate [*Ferguson*, 1986]. U.S. Geological survey (USGS) suggests several stochastic techniques to avoid the continuous bias from simple power law model such as MLE(Maximum Likelihood Estimation) [*Runkel et al.*, 2004].

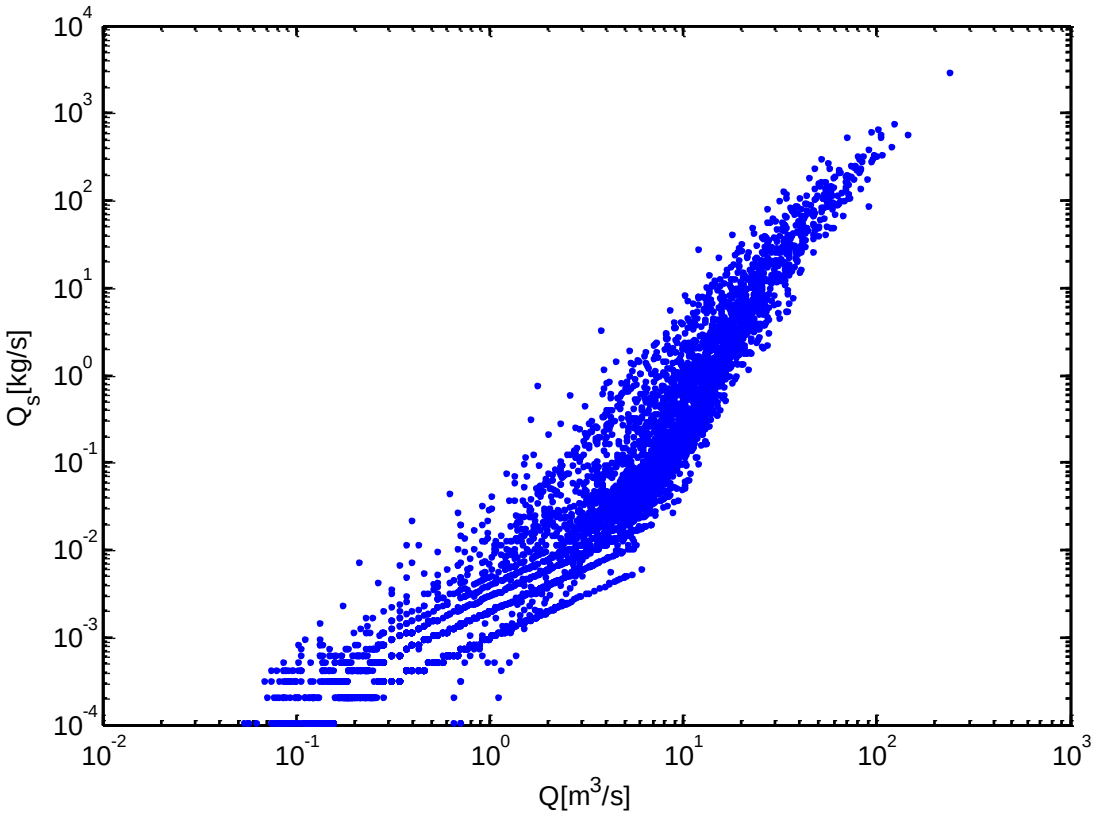

Figure 3.1. Daily values of Q_s and Q reported by USGS for Redwood Creek at Blue Lake (USGS site number 11481500) between 1972 and 2002.

3.2.3 Storage Process of Fine Particle in Channel System

The storage of fine particles in the channel bed is frequently observed in natural streams [*Navratil et al.*, 2010] and in many flume studies [*Einstein*, 1968; *Beschta and Jackson*, 1979; *Diplas and Parker*, 1992; *Packman and MacKay*, 2003]. The fine particle infiltration depths are affected by the ratio of particle size to bed material size [*Leonardson*, 2010]. In *Einstein*'s 1968 flume studies, fine particles filled the pore space from the bottom of the stream bed towards the surface due to the dominance of settling [*Einstein*, 1968]. The bed material was 100 times larger than the fine particles and that minimized particle straining. On the other hand, *Beschta and Jackson* [1979] observed that clogging of a gravel bed near the bed surface inhibits additional intrusion of fine particles into the lower gravels, where bed material was 30 to 70 times larger than the fine particles. *Diplas and Parker* [1992] observed in his flume study that fine particles clogged the bed surface when bed material was 30 times larger than the fine particles and the bed was poorly sorted.

The amount of fine particle storage in the stream bed is variable within watersheds and during measurement periods [*Collins et al.*, 2005; *Collins and Walling*, 2007b]. For example, *Collins and Walling [2007a]* suggest that the amount of fine particle stored in channel bed ranged from 20% to 60% of the mean annual suspended sediment load in their field study at Frome and Piddle watersheds in UK [*Collins and Walling*, 2007b]. They measured the fine particles within the sediment bed by enclosing the upper 5 cm of channel bed and water within a cylinder. The channel bed was manually disturbed with a metal rod, and turbid water in the cylinder was sampled to estimate fine particle storage using a method developed by *Lambert and Walling* [1988]. In another field study, *Collins and Walling* [2007b] also observed that temporary fine particle storage in the channel bed ranged from 7% to 92% of the mean annual suspended sediment load from their field study in the Pang sub-catchment, UK. They also found that about 50% of the fine particles stored in the channel bed are from erosion of soil during the winter period following cultivation during autumn. Radionuclides were useful in fingerprinting bare soil erosion [*Collins and Walling*, 2007a]. More recently, *López-Tarazón et al.* [2009] show the seasonal variation in the amount of fine particle storage in a channel bed subsurface layer in their field study at Isábena River in Southern Pyrenees where the watershed area is about 445 km^2. Though the annual average fine particle storage in the channel bed was about 5% of the total suspended sediment yield, the storage amount increased to 55% of the total suspended sediment yield in a winter season with minimal flooding. In contrast, fine particles in storage decreased to 0.8% in spring flooding season [*Lopez-Tarazon et al.*, 2011].

Einstein [1968] suggests a model for sediment removal by channel bed deposition in his flume study. He observed fine particle removal in the water column by filtration through the channel bed pore space in his flume study under various flow rates. *Einstein* assumed that fine particle deposition rate was proportional to suspended sediment concentration just above channel bed, and that sediment concentration decreases exponentially downstream by infiltration. *Carling* [1984] found that the suspended sediment deposition rate is related to suspended sediment concentration and the exchange velocity just below channel bed surface which he referred as the "zero" velocity plane in his flume study. He also observed an exponential decay of sediment deposition rate with distance from the sediment source.

The penetration depth of fine particles into the stream bed is related to the hyporheic flow depth which is watershed dependent. *Harvey and Wagner* [2000] argue that the hyporheic depth is related to the stream cross section area, and they suggest the ratio of hyporheic flow area to stream cross sectional area is an empirical function of channel friction factor. As fine particles accumulate in the subsurface layer, the permeability of the stream bed is reduced which alters the subsurface flow and decreases filtration opportunities [*Packman and MacKay*, 2003]. This clogging process is commonly observed in natural streams [*Frostick et al.*, 1984; *Lisle*, 1989; *Greig et al.*, 2005; *Zimmermann and Lapointe*, 2005]. It is generally accepted that most fine particles would be stored within 10 cm from channel bed surface [*Collins and Walling*, 2007b].

Elliot and Brooks [1997a, b] presented a bed-form driven hyporheic flow model for non-sorbing solutes in a stream [*Elliott and Brooks*, 1997a; 1997b]. In this model the retention of fine particles in the sediment bed is modeled by hyporheic flow combined with particle settling and filtration. Later, *Packman and MacKay* [2003] modified this model for sediment storage in the subsurface layer [*Packman et al.*, 2000a; 2000b; *Packman and MacKay*, 2003]. In this model, particle settling and filtration are considered as the two main mechanisms for fine particle removal by hyporheic flow. More recently *Drummond et al.* [2014] suggested that fine particles are transported into the channel bed by advection, turbulent diffusion and gravitational settling. They developed a stochastic model for particle deposition by reversible filtration dynamics of fine organic particles during base flow, rather than re-suspension during flood events. However these current models do not consider the dynamic alteration of bed permeability following particle accumulation in the stream bed which is a limitation.

3.2.4 Suspended Load Variation in Watersheds

Suspended sediment yield is affected by various environmental characteristics of a watershed such as climate, watershed area, and land cover characteristics [*Syvitski et al.*, 2000; *Warrick and Mertes*, 2009; *Pelletier*, 2012]. Because of the spatial variability of these environmental characteristics, developing a universally applicable suspended sediment transport model is not easy. Not only the spatial configuration of watersheds but also the size of watersheds causes variations of sediment transport processes. Smaller watersheds tend to have more homogeneous environmental characteristics than larger watersheds. For example, *Gao et al.* [2013] suggest that suspended load is dominated by short time interval processes in smaller watersheds (watershed area less than 0.1 km^2) such as intensity or amount of precipitation and overland flow where large channels are usually absent. However as watershed size increases the homogeneity of watershed environments is reduced, and effects of in-channel processes such as channel bed or bank erosion become greater [*Gao et al.*, 2013].

The functional dependence of fine particle transport on flow rate is also temporally dependent. The relationship between log C vs log Q from daily data often show orders of magnitude scatter [*Warrick et al.*, 2013]. During a flood event there is a different relationship between C and Q for the rising limb of the flood compared to the falling limb leading to hysteresis in the relationship between C and Q [*Carson et al.*, 1973; *Klein*, 1984; *Alexandrov et al.*, 2003; 2007; *Gao et al.*, 2013; *Harrington and Harrington*, 2013; *Warrick et al.*, 2013]. *Carson* [1973] suggested that extra supply of sediment from the channel system is a significant additional source of sediment. *Klein*

[1984] interpreted clockwise hysteresis arising from a sediment source in the channel bed while anticlockwise hysteresis is observed when sediment is supplied from upstream hill slopes. These hysteresis patterns are one of the main reasons why a single power law model is not sufficient to explain the scatter in the relationship between Q_s to Q. More detailed explanations about the relationship between hysteresis and sediment source are included in next section, 3.1.5. Seasonality of precipitation and land cover also causes scatter in C at a given Q [*Negev*, 1969; *Brasington and Richards*, 2000; *Alexandrov et al.*, 2007; *Alexandrov et al.*, 2009]. For example, *Alexandrov et al.* [2007] show that autumn-spring convective storms with higher intensity rainfall often produce higher fine particle transport rates than winter frontal storms with lower intensity from their study in a semi-arid region. *Negev* [1969] suggested that the first flood in given water year could have higher suspended sediment concentration than later floods even though they have similar peak flow rates. *Cantalice et al.* [2013] also observed the highest suspended sediment concentration in the first flood of a given water year in their field study in the Exu River, a sand-bed river in the semi-arid region in Brazil. After that first flood the suspended sediment concentration decreases in later floods. They suggest that the high suspended sediment concentration in the first flood is related to re-suspension of deposited sediment from the previous year. Seasonal variations of flow rate by snowmelt also induce additional sediment supply from the channel bed, and cause variations in the functional relationship of C to Q. *Stubblefield et al.* [2009] observed increased sediment supply from the channel bed when flow rate increased by snowmelt from his field study in Lake Tahoe. Inter-annual variations of loading rate relationships are also caused by various factors such as climate change and related variability of discharge [*Achite and Ouillon*, 2007], or extreme events such as large floods [*Warrick et al.*, 2013]. There are various spatial and temporal scales important in fine sediment transport, and they are conceptually compared in Figure 3.2.

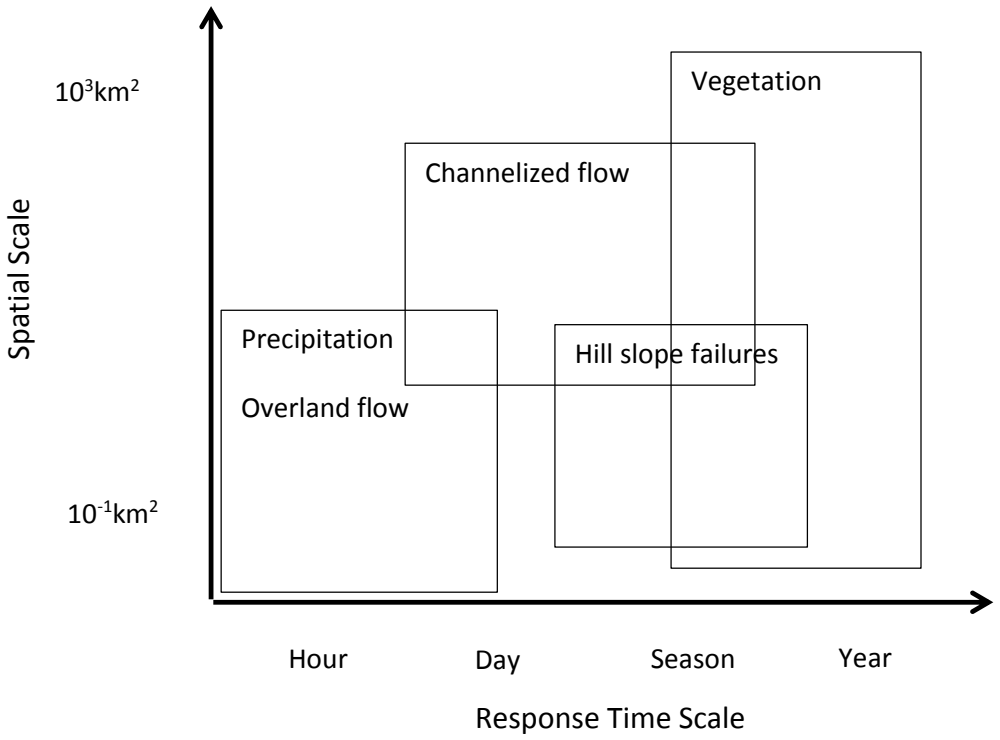

Figure 3.2. Spatial and temporal scales important in fine particle transport.

3.2.5 Hysteresis in the Fine Particle Concentration and Flow Rate Relationship

The relationship between suspended sediment concentration (C) and flow rate (Q) during flood events has been used to identify different sediment sources [*Walling and Webb*, 1982; *Asselman*, 1999; 2000; *Poulenard et al.*, 2012]. By comparing C to Q between rising and falling periods of flood events *Williams* [1989] proposed five classes of hysteresis in the relationship between C and Q (Table 3.1). Clockwise hysteresis is often observed when peak concentration arrived earlier than peak flow rate, and counter clockwise hysteresis is often observed in reverse case as show in Figure 3.3.

Table 3.1. Classes of hysteresis in the relationship between C and Q from *Willimas* [1989]'s Table C1

Class	Relation	C/Q criteria
I	Single-valued line	Slopes of two subsections of the overall relation are equal for straight line. Slopes of two subsections of the overall relation are unequal for curve, slope of which increases or decreases as Q increase
II	Clockwise loop	C/Q in rising limb > C/Q in falling limb
III	Counter clockwise loop	C/Q in rising limb < C/Q in falling limb
IV	Single line plus a loop	C/Q in rising limb ≈ C/Q in falling limb for single line but unequal for loop period
V	"Figure 8"	C/Q in rising limb > C/Q for one range of Q C/Q in rising limb < C/Q for other range of Q

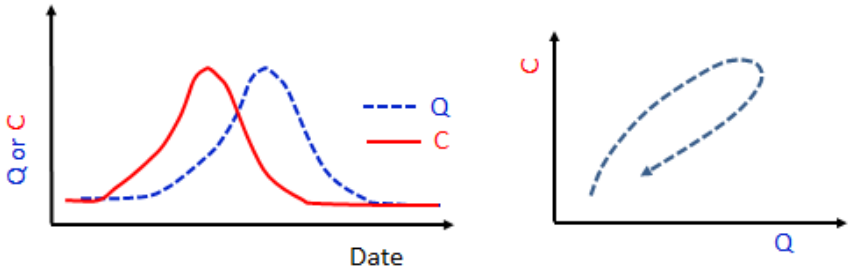

(a) Clockwise hysteresis

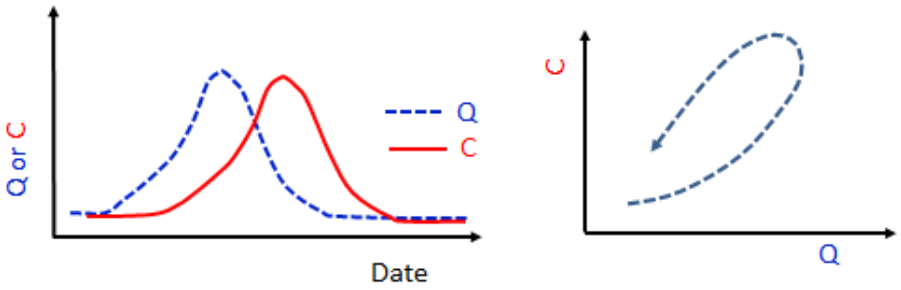

(b) Counter clockwise hysteresis

Figure 3.3. Illustration of clockwise and counter clockwise hysteresis.

Earlier arrival of fine particles than flow rate and clockwise hysteresis are the most commonly observed patterns in natural streams [*Einstein et al.*, 1940; *Johnson*, 1943; *Banasik et al.*, 2005; *Bisantino et al.*, 2011; *Gao et al.*, 2013]. There are numerous qualitative explanations for the observed clockwise hysteresis. Firstly, the earlier depletion of a fine particle source during a flood can cause clockwise hysteresis [*Walling*, 1974; *McCaig*, 1981; *Amos et al.*, 2004; *Megnounif et al.*, 2013]. Secondly, entrainment of stored fine particles during a flood from the channel bottom causes earlier arrival of suspended sediment than flow rate [*Williams*, 1989; *Lenzi and Marchi*, 2000; *Landers and Sturm*, 2013; *Megnounif et al.*, 2013]. Finally, clockwise hysteresis is often observed in streams where diurnal snow melting causes re-suspension of deposited fine particles from stream channels [*Hjulström*, 1935; *Bogen*, 1980].

Counter clockwise hysteresis has been attributed to the delayed transport of fine sediments from distant sources such as hillslopes [*McCaig*, 1981; *Klein*, 1984; *Lenzi and Marchi*, 2000; *Megnounif et al.*, 2013]. Flood peaks tend to travel at the wave velocity, and suspended sediment travels at the water velocity in streams [*Marcus*, 1989; *Williams*, 1989; *Leonardson*, 2010]. The different velocities cause a time lag between peaks of suspended sediment and flow rate when both suspended sediment and water flow are from watershed hillslopes. Thus, earlier arrival of flow peak than suspended sediment peak could cause counter clockwise hysteresis [*Klein*, 1984; *Lenzi and Marchi*, 2000]. *Baca* [2008] observed predominantly counter clockwise hysteresis in the relationship between Q_s and Q in his field study in Rybárik, a small watershed in western Slovakia, and attributed counter clockwise hysteresis to sediment supplied from distant sources such as hillslopes.

Clockwise hysteresis loops are also observed annually in large basins where runoff is slowed by topography or snowmelt. The upper Niger River basin with an area of 250,000 km^2 has annual flood wave that lasts for multiple months as the river flows from the tropical zone to the arid zone in relatively flat topography. *Picouet et al.* [2001] have examined seven annual clockwise hysteresis loops using weekly flow and suspended sediment data that reflected more easily erodible materials at the start of the rainy season. In the Southwestern United States, the Colorado River serves numerous water resource needs through regulation by dams. Prior to the construction of Glen Canyon Dam monitoring data revealed that silts, clays and fine sand displayed multiple-month clockwise hysteresis loops that were attributed to the limited supply of these fine particles within the river system [*Topping et al.*, 2000].

3.3 Bedload

3.3.1 Bedload Transport

There is a threshold for streambed movement that was observed and then modeled by *Shields* [1936] which is utilized in Chapter 2. Steady state bedload transport models are often correlated to boundary shear stress (τ) above a critical shear stress and a non-dimensional version is shown in equation (3.1) [*Meyer-Peter and Müller*, 1948; *Wong and Parker*, 2006]

$$q^* = \alpha(\tau^* - \tau_c^*)^{\beta} \tag{3.1}$$

where:

τ^*: the dimensionless bed shear stress, $\tau^* = \tau / g(\rho_s - \rho_f)D$

$q^* = \frac{q_s}{\sqrt{(\rho_s / \rho - 1)gD^3}}$: non-dimensional bed sediment transport rate with q_s as the volumetric bedload transport rate per unit channel width [$L^3/T/L$], and α and β are empirical coefficients where $\beta \sim 1.5$ is commonly adopted [*García*, 2008]. Measured non-dimensional bedload transport rates at three Redwood Creek sites are compared with the bedload transport model of Wong and Parker [*Wong and Parker*, 2006] in Figure 3.4. The scatter is caused by the variation of environmental characteristics within the nested watershed. While the *Meyer-Peter and Müller* [1948] bedload transport representation does well in comparison to other models for laboratory and controlled field experiments, the model does not demonstrate any predictive capability for bedload transport in Redwood Creek. This is disappointing since Redwood Creek is one of the more well studied watersheds within California in terms of long-term measurements of flow, suspended load and bedload transport. Given the need for a model that can represent sediment bed mobilization of fine particles by bedload transport during flood events, an alternative approach is needed to these steady state bedload transport rates. The next section provides an alternative approach based on net fill and scour during flood events.

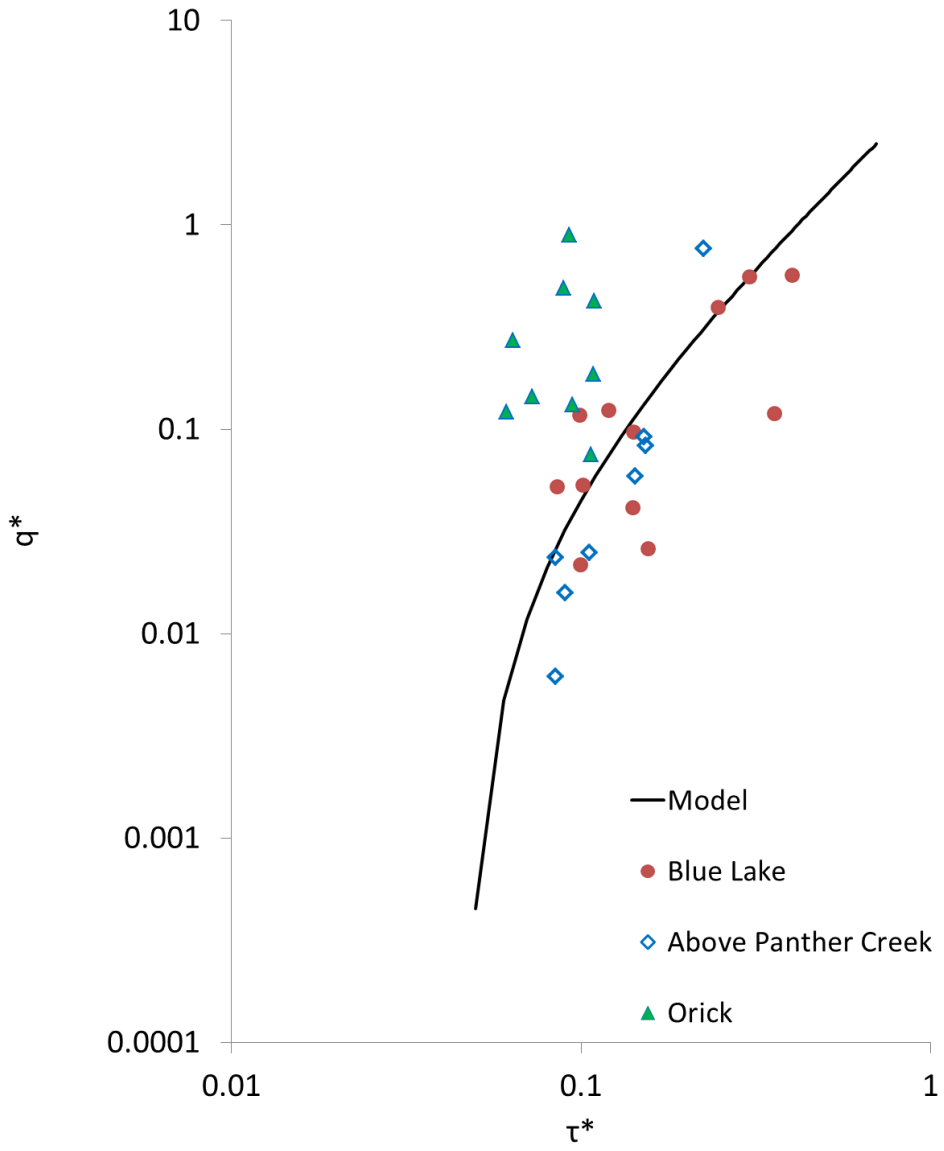

Figure 3.4. Non-dimensional bedload transport rates in three Redwood Creek sites, where the model equation is $q^*=4.93(\tau^*-0.047)^{1.6}$.

3.3.2 Scour, Fill, and Change of Channel Bed Elevation

This study employs channel cross section analysis with data reported by USGS. The USGS regularly (near monthly) measures channel wetted area and width at their gauge sites to calibrate stage - discharge relationships. Sediment transport studies have previously used channel cross section data to quantify channel aggradation or erosion from changes in mean bed elevation [*Madej and Ozaki*, 1996; *Stover and Montgomery*, 2001; *Radoane et al.*, 2010].

Madej and Ozaki [1996] analyzed long-term change of channel bed elevation in Redwood Creek in northern California where the watershed area is 720 km^2. They note that a large flood in December 1964 caused sediment to fill in the channel system of Redwood Creek, and this sediment moved downstream continuously over the next 20 years. Their analysis shows that from 1980 to 1990 about 25% of total suspended sediment load and 95% of bedload in this basin are from the remobilization of this temporarily stored sediment in the channel system.

About a meter of scour and fill depths are observed over time in different watersheds [*Madej*, 1995; *Stover and Montgomery*, 2001; *Radoane et al.*, 2010]. *Madej* [1995] directly measured 0.2 to 1.2 m of scour and fill in the channel bed at Redwood Creek, California by installing scour chains. *Stover and Montgomery* [2001] analyzed historical channel cross section data at Skokomish River in Washington which was monitored by the USGS between 1932 and 1997. They calculated channel elevation change and observed no net changes in channel bed elevations in a year to year period, but channel bed elevations actively oscillated about one meter within each year. *Cohen and Laronne* [2005] observed about 0.5 m scour or fill in Rahaf which is a gravel-bedded ephemeral channel in the arid Southern Judean Desert, Israel where the watershed area is 78 km^2. More recently *Radoane et al.* [2010] also found active changes in channel bed elevation of 0.5 to 1 m each year in his field study in Eastern Carpathians.

The considerable changes of channel bed elevation by scour or fill are also often observed within relatively short time periods such as months [*Hassan*, 1990; *Bourke*, 2002]. *Hassan* [1990] measured the change of channel bed elevation by using tagged particles and scour chains in his field experiments, and reported that the scour and fill depths were about 20 cm during individual floods in his field study at the Negev and Judean Deserts in Israel. He also showed that burial depths of sediment grains was 3 to 30 times the median size of the bed material. In later research he suggested that burial depths of mobile particles are exponentially distributed during single floods, and most sediment grains are buried near the surface of the stream bed [*Hassan and Church*, 1994]. More recently *Bourke* [2002] observed scouring of the channel bed up to 0.5 m in his field study in Todd River, Australia which is an ephemeral sand bed channel between the January 1995 and March/May 1995 floods.

Montgomery et al. [1996] also observed an exponential distribution of scour depth ranging from 0 to 60 cm in their field study at Kennedy Creek, Washington by using scour chains for floods from November 1991 to February 1992. At about 50% of the measured locations, scour was only 10 cm. They also found there was an effect of salmonid spawning on channel scour depth. Fine particles are removed from the channel bed by winnowing during spawning which coarsens bed material sizes. In addition the construction of redds alters the channel bed geomorphology, forming higher bed forms. A coarsened bed with higher bed forms increases the shear stress needed to

mobilized the bed resulting in a decreased depth of scour, and consequently reducing the loss of salmonid eggs during floods [*Montgomery et al.*, 1996].

There have been attempts to relate scour depth of a flood to bedload transport rate, but the two concepts are not compatible. During bedload transport there is an active layer of bed materials in motion, and the depth of this layer is a function of sediment bed size. *DeVries* [2002] observed that the disturbance depth was generally less than a depth of $2D_{90}$ with higher flow rate causing faster movement in this layer, not a greater depth. The application of disturbance depth to bedload transport using a continuity equation from *Einstein* [1950]

$$q_B = d\, U_B \rho_s (1 - \lambda) \tag{3.2}$$

where q_B is the bedload transport rate per unit stream width, d is the disturbance depth assumed equal to the mean active layer thickness, U_B is the transport velocity of the bed layer, ρ_s is the density of the sediment grains, and λ is the bed porosity. *DeVries* [2002] notes that application of this equation to field conditions is difficult and *Carling* [1987] demonstrated that bedload transport was poorly predicted by equation (3.2) under field conditions. The measured scour and fill depths are integrated responses of the sediment bed to a rising and falling flood wave and dependent upon upstream sediment supply.

Haschenburger [1999] used an exponential probability density function to represent scour and fill depths in the field. For two locations on Carnation Creek in British Columbia about 119 scour chains were distributed across 25 cross sections. Each scour chain was excavated after each of the 25 flood events.. The results at these two sites and observations at five other sites were fit to an exponential probability density function given in equation (3.3).

$$f(x) = \theta e^{-\theta x} \tag{3.3}$$

where $f(x)$ is the probability density function for the distribution of scour or fill depth where x is depth and θ is the model parameter such that $1/\theta$ is both the mean and the standard deviation of the probability density function. *Haschenburger* also derived that the model parameter (θ) has an exponential relationship with shear stress at the channel bed (equation 3.4).

$$\theta = 3.33 \exp(-1.52 \frac{\tau^*}{\tau_c^*}) \tag{3.4}$$

where τ^* is the dimensionless bed shear stress defined in equation (3.1) and τ_c^* is the critical nondimensionalized shear stress for bed mobilization.

Haschenburger [1999] reported values of the θ parameter separately for scour and fill depth distributions for a range of floods at three research sites. Figure 3.5 is a plot of the inverse of the θ parameters for observed fill and scour events as a function of peak flow rate (Q_{peak}) for each flood event at two sites in Carnation Creek. In general, average scour depth ($1/\theta$) is close to the average fill depth for each flood at a site, and the average depth of scour and fill increase exponentially with the flood's peak flow rate. The data at another site, Great Eggleshope Beck, also support scour and fill depths being exponentially dependent upon flow rate. These observational data led to the development of an empirical model for sediment bed scour in Chapter 4.

The distribution of measured scour depths at Kennedy Creek from 1991 to 1992 [*Montgomery et al.*, 1996] are also compared with the *Haschenburger* [1999] probability model for various values of the parameter θ in Figure 3.6. *Bigelow* [2005] compared the simulation results with observations at his field study in Freshwater Creek, California and speculated that the differences between model prediction and observation are influenced by various environmental factors such as sediment supply, the particular location within the channel network, the time series of peak flows rather than a single event, and form roughness from boulders and woody debris.

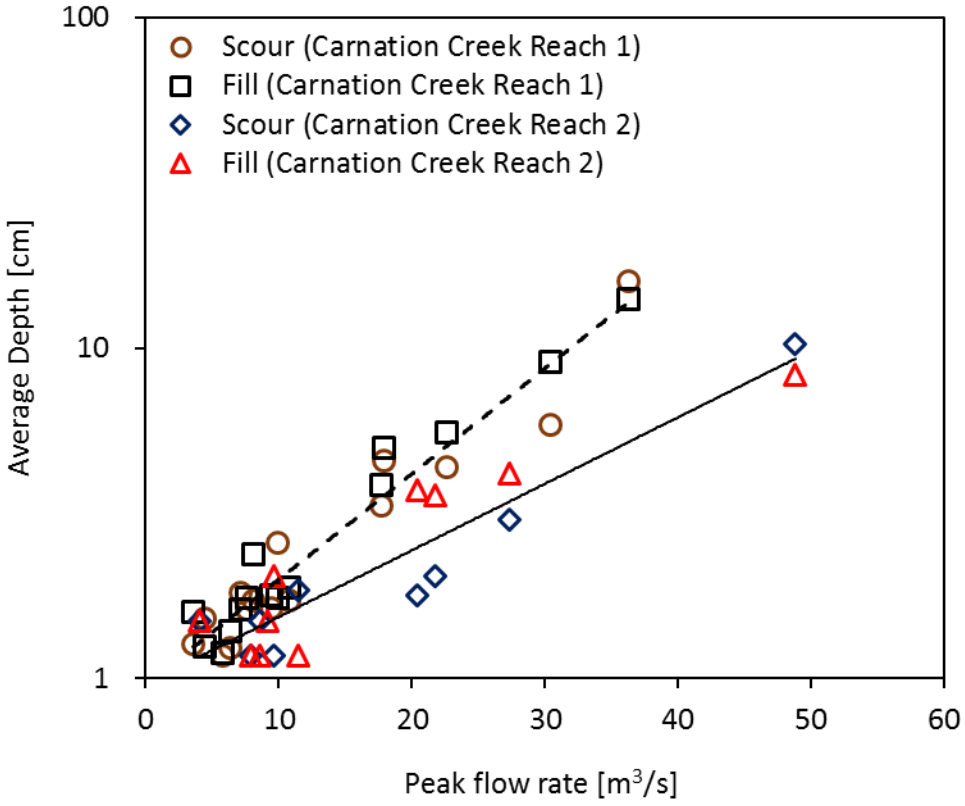

Figure 3.5. Average scour and fill depths as a function of peak flow rates at two research sites reported by *Haschenburger* [1999]. Regression lines of average scour and fill depth as exponential function of flow rates is represented by black dashed line in Reach 1 and black solid line in Reach 2.

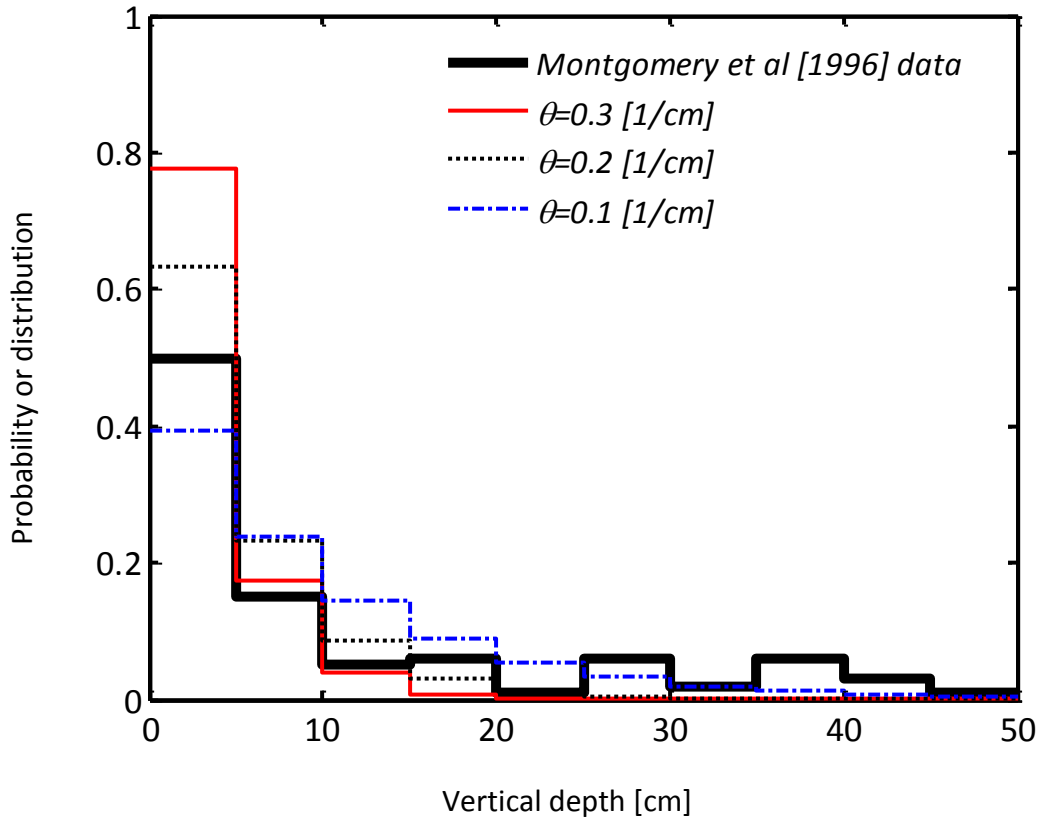

Figure 3.6. Comparison of the scour depth distribution observed by *Montgomery et al.* [1996] with the probability model by *Haschenburger* [1999]. The vertical axis is the probability of disturbance depth within 5 cm intervals for the observations of *Montgomery et al.* [1996] and exponential distribution function of *Haschenburger* [1999] for three possible parameter values.

3.3.3 Channel Geomorphology

The cross section of channels is determined by local characteristics of flows. Bank-full discharge is a parameter which characterizes channel form, although there are various ways to define it [*Wolman*, 1957; *Knighton*, 1998; *García*, 2008]. One usage is that bank-full discharge is the effective discharge which transports the maximum fraction of the annual sediment load [*Wolman and Miller*, 1960; *Andrews*, 1980; *García*, 2008]. This also generally corresponds to the flow at which stream flow reaches a flat flood plain [*Woodyer*, 1968; *Williams*, 1978; *Andrews*, 1980]. The return period of bank-full discharge also varies from 1 to 10 years except the 1.5-year recurrence interval flow rate is commonly adopted [*Wolman*, 1957; *García*, 2008].

Alternatively, *Knighton* [1998] suggests at low flows there is a transition from a rapid increase in wetting channel width with flow rate to a much slower increase in channel width at a critical flow rate, Q_c. This transition, illustrated in Figure 3.7, happens when flows are sufficient to mobilize bed materials. When $Q < Q_c$ there is an inactive phase where the sediment bed is not in motion, the flow is shallow. For flow rates above a critical flow rate, Q_c, bed material is entrained, the flow is constrained between steep banks and the width changes little with substantial increases in flow rate [*Knighton*, 1998].

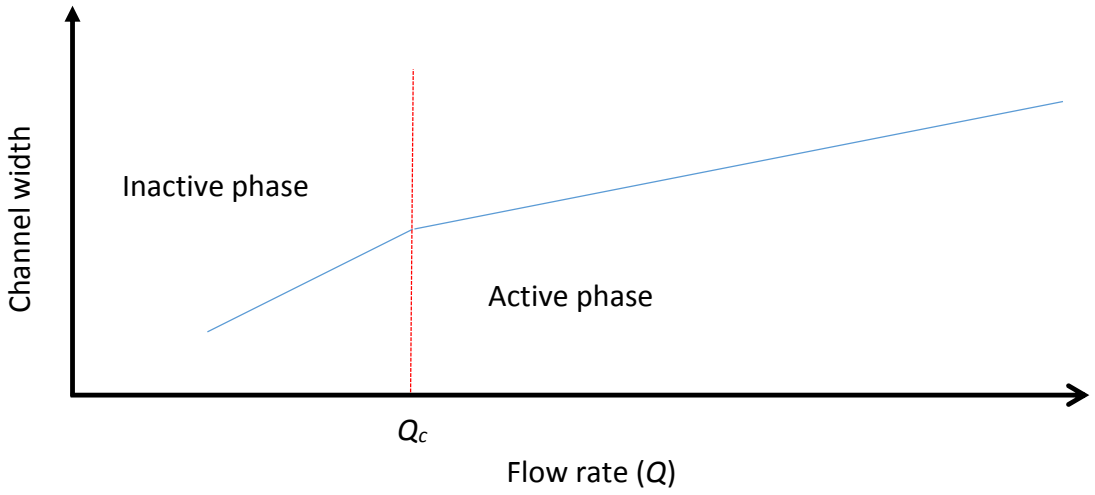

Figure 3.7. Hypothetical relationship between channel width and flow rate where Q_c is the threshold discharge for entrainment. Figure adopted from *Knighton* [1998].

3.4 Interrelationship between Fine Particle Re-suspension and Bedload

Previous studies suggest that fine particles accumulated in the stream bed during the low flow periods become re-suspended as the flow rate increases and bed materials start to move [*Diplas and Parker*, 1992; *Harvey et al.*, 2012]. More recently, *Francalanci et al.* [2013] states that the sediment transport rate in terms of total load which is dominated by the suspended sediment load is coupled with stream bed mobility and bed material mixture conditions. This section reviews observations of fine particle re-suspension when the sediment bed is mobilized.

Frostick et al. [1984] observed increased suspended sediment concentration (*C*) in his field study and attributed the increase to the supply of fine particles by erosion of channel banks, drainage ditches, and the stream bed itself. *Navratil et al.* [2010] measured the mass of fine particles stored in the channel bed and compared this with annual suspended sediment yield. As there was no particular highly erodible zone in the study watershed, they assumed that the channel bed was the major source, and this local source is the reason for clockwise hysteresis during flood events. *Harvey et al.* [2012] also found that fine particles stored in the channel bed are released when the bed form is mobilized by a flood event. They introduced a solute tracer along with a particle tracer during base flow into Clear Run, a shallow, fast flowing sand bedded stream in North Carolina. They observed solute and particle penetration into the mobile bed forms and found that 71% of the introduced particle tracer was retained within the stream bed by hyporheic flow and filtration. A moderately high flow event rapidly eroded 31% of the deposited particle tracer. The remainder of the particle tracers were retained within the stream channel and some were detected below the depth of bed mobilization [*Harvey et al.*, 2012]. These researchers included a modeling component that only addressed the transport processes of conservative solute tracers and particle tracers during the steady, low flow period. The researchers did not address how to represent bed scour and partial bed fluidization as well as the observed instantaneous release of particles when the flow rate was increased.

The above studies lead to the assumption that fine particles accumulated within the channel bed become the source of suspended sediment particles during floods and caused clockwise hysteresis. In addition, the declining erosion of fine particles during closely spaced flood events shows that there is depletion of particles retained in storage. In general the longer the duration between flood events, the greater the mass of fine particles available for release. Many previous studies qualitatively described fine particle accumulation in the sediment bed and subsequent re-suspension by various factors such as peak flow rate, flood duration, intensity of preceding floods, rainfall intensity, and seasonal variation in rainfall [*Negev*, 1972; *McCaig*, 1981; *Frostick et al.*, 1984; *Bourke*, 2002]. However, development and testing of quantitative models that represent these factors on particle accumulation and re-suspension are limited.

A few modeling efforts have appreciated the coupling of fine sediment transport with sediment bed fluidization and transport. *Vansickle and Beschta* [1983] developed a modified power law model by accounting for fine particles stored in the upstream channel. The fine particles were reduced during flood events by an empirical washout function, and fine particles were replenished between flood events through the addition of fine particles into the sediment bed. Specification of the mass of particles placed into the sediment bed prior to each flood allowed the model to agree

with suspended sediment concentrations measured after each flood. *Asselman* [1999] showed the applicability of *VanSickle and Beschta* [1983]'s 'supply base model' for the prediction of fine particle concentration during flood events on the River Rhine. *Asselman* recognized the limitation of the model since it can only be used when the amount of stored fine sediment and the timing of re-supply are known. More recently, *Picouet et al.* [2001] also suggests a conceptual model to predict weekly suspended sediment concentration in the upper Niger River Basin based on the *VanSickle and Beschta* [1983] model. *Picouet et al.* [2001] assumed two different reservoirs of fine particles. The first reservoir represented hillslope erosion with a limited particle supply and depletion during the flood season. The second reservoir accounted for particle supply from bank erosion and re-suspension of deposited particles in the channel network which they assumed had an unlimited source of particles.

Long-term data on flow and suspended solids in the Meuse River formed the basis for model development along similar lines by *Doomen et al.* [2008]. They assumed that suspended particles are stored in the channel bed when the flow rate is lower than the critical flow rate causing bed erosion. The amount of fine particles in storage was decreased by erosion when the flow rate exceeded the critical flow rate. They also suggested a modified power law model for particle loading rate which allowed for sediment storage under low flow conditions and depletion under high flow events. The transition from accumulation to depletion occurred at the critical flow rate of 240 m^3/s corresponding to the flow rate where there is an observed slope break in the particle loading curve. *Baca* [2008] observed the rising limb of the first flood had a much higher fine particle concentration than the rising limb of the second flood event because most of the available particles are eroded during first flood. With sufficient time between floods the particle were accumulated in the bed and clockwise hysteresis returned in the next flood event. In a study of particle-associated phosphorus transport, *Bowes et al.* [2005] observed clockwise hysteresis when total phosphorus was plotted against flow rate for storm events. Additionally, the magnitude of hysteresis loops decreased during a sequence of flood events which caused the depletion of mobile phosphorus-containing particles in the channel system. They assumed that the change in hysteresis can only occur by the additional supply or removal of phosphorus and included an empirical response factor in the model to explain the hysteresis between phosphorus concentration and flow rate.

Within the Colorado River system, silts, clays and fine sand were depleted from the water column and the sediment bed during flood events leading to clockwise hysteresis loops. *Rubin and Topping* [2001; 2008] developed a one-dimensional geomorphic model that represented the particle size distribution within the sediment bed coupled with size-dependent erosion into the water column [*Rubin and Topping*, 2001; 2008]. This model was applied for a distribution of sand-sized particles that composed the mobile sediment bed of the river to model sediment limitations and the evolution of the grain size distribution within the sediment bed [*Wright et al.*, 2010]. While such an approach was necessary for addressing sand transport in the Colorado River, the extension to silts and clays for gravel bedded streams is not straightforward.

3.5 Moving Forward

In Chapter 2 an empirical analysis of fine particle loading rates as a function of stream flows was conducted for 38 watersheds within California. The combined data from these watersheds led to a conceptual model for fine particles within streams that focused on the dynamic coupling of particle transport with bedload transport. This chapter has attempted to selectively summarize the vast literature that is relevant to qualitatively and quantitatively describe the relevant fine particle and bedload transport processes that are compatible with the conceptual model. The desire within the hydrological sciences to emphasize the complexity of watershed processes and to over specialize have hindered an integrated analysis that represents the dominant processes at relevant temporal and spatial scales. An integrated model could address a number of important applied questions related to fine particle accumulation and release within the sediment bed of watersheds.

The coupling of fine particle and sediment bed transport was recognized at least 75 years ago. The divergence of fine particle transport from bedload transport studies arose from initial successes in steady-state bedload transport that could not be replicated for fine particles either in the laboratory or under controlled field conditions. As a consequence, the effort devoted to fine particle transport evolved into watershed monitoring efforts combined with a search for empirical correlations based on flow rate and other environmentally relevant factors. As a consequence, predictability and generalizability were limited. Advancements in measuring and modeling hyporheic flows within sediments beds have helped to better understand fine particle accumulation within sediment beds, but demonstration of predictive models is still a challenge for non-steady conditions as well as instances where particle accumulation reduces sediment bed permeability. Steady-state bedload transport models do not easily couple with episodic fine particle release from sediment beds and the state of the art particle transport models for watersheds depend upon many site specific parameters. The challenge faced in the next chapter is the translation of the conceptual model from Chapter 2 using quantitative process descriptions for the dominant processes covered in this chapter into an integrated model that minimizes site specific parameterization and has some ability to generalize.

Chapter 4. Modeling Fine Particle Accumulation and Release in the Russian River Basin

Previous research and preliminary analysis in Chapter 2 imply that fine particles accumulate in the sediment bed during low flows and re-suspend during higher flows. Suspended fine particles accumulate in the sediment bed by filtration during hyporheic flow through the sediment bed. These fine particles are only released when stream flows exceed a critical level that initiates the mobilization of bed sediments. The analysis in Chapter 2 indicates that the accumulation of fine particles during low flows and their release at higher flows causes a shift in the Q_s versus Q relationship seen as a slope break in the log Q_s vs log Q plots for gravel-bedded streams. An empirical model for deposition and release of fine particles is explored based on the processes identified from data analysis in the Russian River watershed of California. The model is calibrated for two locations within the Russian River, and some data are available for partial verification. In addition, the ability of the model to capture the variability in observed sediment loading curves is explored.

4.1 Model for Fine Particle Storage and Release in the Sediment Bed

Previous research suggested the source of fine particles released during flood events is the sediment bed as summarized in Section 3.4. The accumulated fine particles were deposited into the sediment bed from the overlying water column during base flow. When the flow rate exceeds a critical flow rate, Q_c, required to initiate the mobilization of sediment bed materials, fine particles are released. Analysis of the time series of flow rate and suspended particle concentration also found that particle concentration quickly decreases during the falling limb of high flow events. This leads to the additional assumption that the fine sediments can accumulate within the porous

media portion of the sediment bed during the falling limb of a flood event even though some of the bed is fluidized. The conceptual model of fine particle storage in the sediment bed and re-suspension is illustrated in Figure 4.1 with the identification of three distinct phases:

Phase 1: base flow with $Q \leq Q_c$

In this phase, the sediment bed is not fluidized since the flow rate is less than the critical flow rate for bed fluidization. The fine particles in the water column accumulate in the sediment bed pore space by settling and filtration.

Phase 2: rising flood with $dQ/dt > 0$ and $Q > Q_c$

The sediment bed is partially fluidized for flow rates larger than the critical flow rate during the rising limb of a flood. Fine particles are released from the fluidized portion of the sediment bed into the water column.

Phase 3: flood recession with $dQ/dt < 0$ and $Q > Q_c$

Observations reported in the literature and model iterations led to the inclusion of fine particle removal from the water column while flows partially fluidize bed sediments. Fine particles can be removed by filtration into the remaining sediment bed, but the available capacity is limited by partial fluidization.

The modeling of each of these phases is described separately. The approach in the modeling is to continuously represent particle accumulation in Phases 1 and 3, but particle erosion is modeled discretely on a flood event basis for Phase 2.

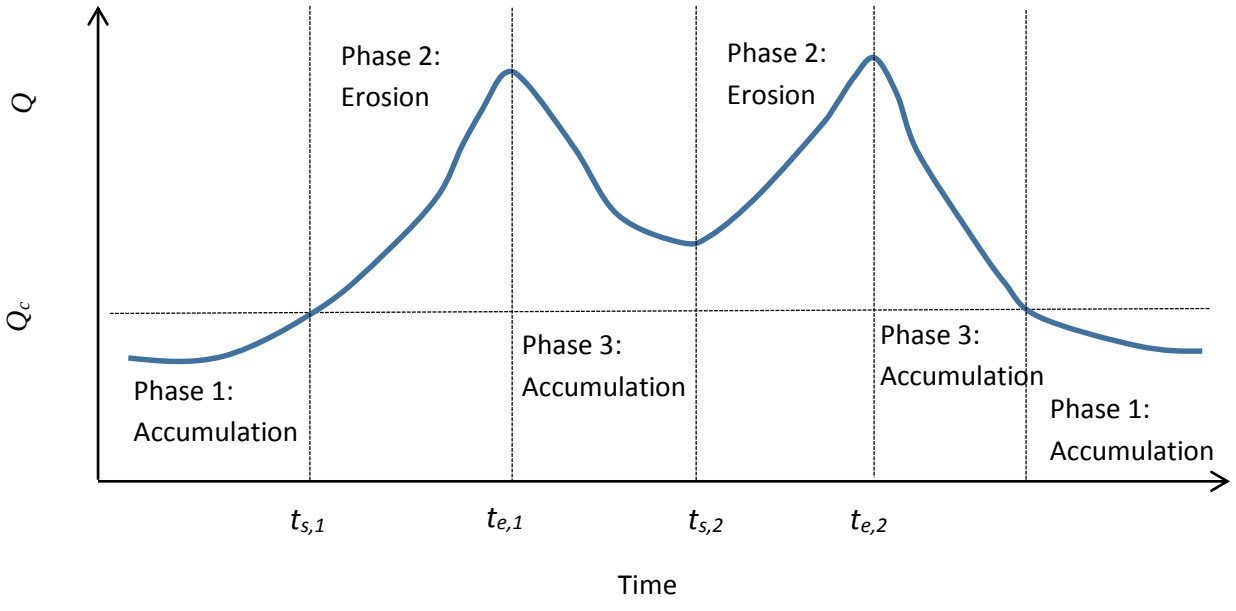

Figure 4.1. The three phases of fine particle exchange between the sediment bed and the overlying water column.

4.1.1 Phase 1: Particle Accumulation

Previous research has extensively documented in laboratory and field studies that fine particles are retained in the sediment bed by hyporheic flow. The adopted modeling for particle accumulation within the pore space of the sediment bed is a simplification of filtration models utilized in the hyporheic flow literature. The model is applicable to the low-flow regime when the flow rate, *Q(t),* is less than the critical flow rate, Q_c, required to fluidize the sediment bed. Particle accumulation in the sediment bed is proportional to the fine particle concentration in the surface water, *C(t),* with a correction for sediment bed clogging. The expression for the change in accumulated fine particle mass during the time period from *t* to *t* + *Δt,* is

$$\Delta M(t) \;=\; \alpha C(t)\left[1-\frac{M(t)}{M_{max}}\right]\Delta t \quad \text{for } Q < Q_c \tag{4.1}$$

where α is a particle removal parameter representing filtration and settling of fine particles within the sediment bed of the watershed. The bracketed term on the right hand side is an approximate expression for the reduction in particle filtration as fine particles accumulate within the sediment bed leading to no filtration when $M(t) = M_{max}$.

4.1.2 Phase 2: Fine Particle Erosion

Fine particles accumulated in sediment bed are re-suspended during flood events when the sediment bed is fluidized as summarized in Chapter 3 [*Navratil et al.*, 2010; *Harvey et al.*, 2012]. Sediment bed scour by individual flood events was measured by *Haschenburger* [1999], and she found that the average depth of scour was an exponential function of bed shear stress. An analysis of her data in Chapter 3 led to:

$$\text{scour depth} \;\propto\; \exp\left(\beta' Q_{peak}\right) \tag{4.2}$$

where β' is a scour parameter and Q_{peak} is the peak flow rate for the flood event. This modeling effort assumes a maximum scour depth occurs at the maximum recorded flow rate (Q_{max}) with:

$$\text{maximum scour depth} \;\propto\; \exp\left(\beta' Q_{max}\right) \tag{4.3}$$

The mass of fine particles released from the sediment bed by a flood with peak flow Q_{peak} is assumed proportional to the scour depth through equation (4.2). Correspondingly, the maximum peak flow rate of all floods, Q_{max}, would potentially release the mass of all fine particles, M_{max}, which is proportional to the maximum scour depth through equation (4.3). The ratio of mass of fine particles released from the sediment bed in the model, $M_{f,m}$, to the maximum possible mass of fine particles in storage is:

$$\frac{M_{f,m}}{M_{max}} = \exp\left[\beta' Q_{peak} - \beta' Q_{max}\right] = \exp\left[-\beta\left(1 - \frac{Q_{peak}}{Q_{max}}\right)\right] \quad (4.4)$$

where β is defined as $\beta' Q_{max}$ and is a dimensionless sediment bed scour parameter.

The functional dependence of equation (4.4) on parameter β is explored in Figure 4.2 which suggests β values should be in the relatively narrow range of $2 < \beta < 20$. When β is 2 or less, even small floods release significant retained mass, something that is not observed. When β approaches 20, only flow events greater than 80% of Q_{max} release any of the retained particles which is again not observed in the watershed data.

The approach suggested by *Haschenburger* [1999] for modeling scour by flood events is based only on the peak flow rate. The application of *Haschenburger*'s results to fine particle release from bed sediments for discrete flood events requires identification of these flood events and accounting for particle mass accumulating in storage, *M(t)*, during Phases 1 and 3. Flood event *i* is assumed to start at time $t_{s,i}$ which is depicted in Figure 4.1 and occurs when either Q first becomes greater than Q_c ($t_{s,1}$ in Figure 4.1) or dQ/dt transitions from negative to positive for $Q > Q_c$ ($t_{s,2}$ in Figure 4.1). The end of flood event *i* is denoted as $t_{e,i}$ and occurs at the time of the peak flow rate for that flood. This representation of fine particle release from bed sediments does not account for the depth distribution of retained particles in the sediment bed before or after partial fluidization. In the notation to follow, the mass of fine particles released by flood event *i* in the model is

$$M_{fi,m} = M_{max} \exp\left[-\beta\left\{1 - \frac{Q(t_{e,i})}{Q_{max}}\right\}\right] \quad (4.5a)$$

The mass of fine particles remaining in the sediment bed after flood event *i* is

$$M(t_{e,i}) = M(t_{s,i}) - M_{max} \exp\left[-\beta\left\{1 - \frac{Q(t_{e,i})}{Q_{max}}\right\}\right] \quad (4.5b)$$

There is the added restriction in the model that $M(t_{e,i})$ is non-negative.

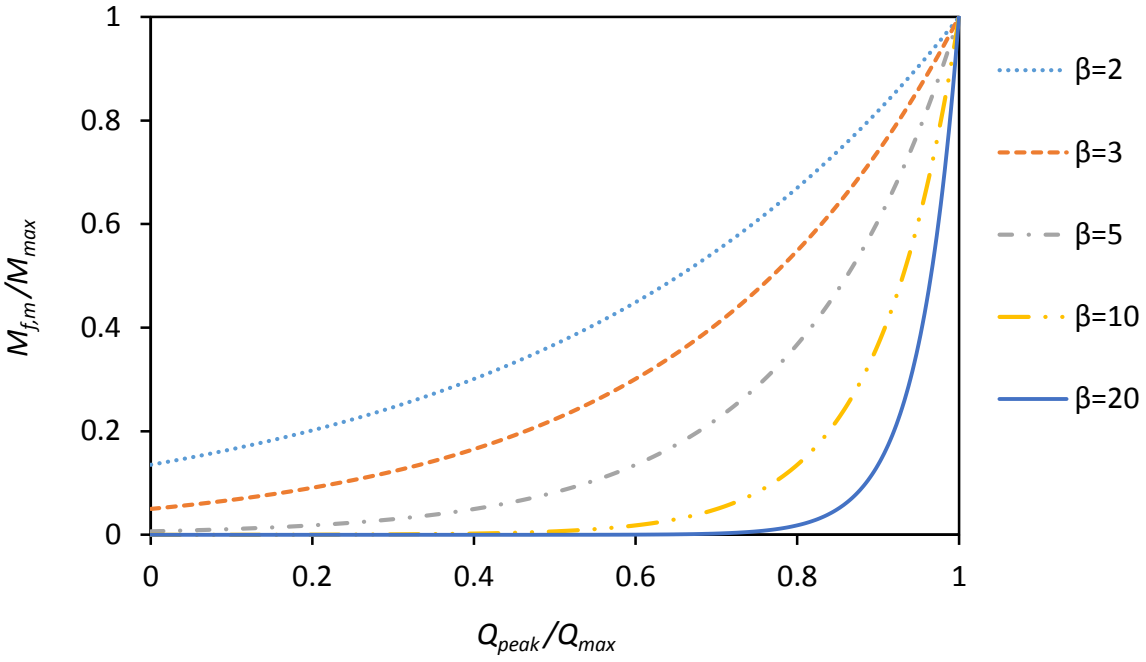

Figure 4.2. Sensitivity of parameter β in the erosion model of equation (4.4).

4.1.3 Phase 3 Fine Particle Accumulation during Flood Recession

This research assumes that the fine particle storage capacity in the sediment bed is finite and that capacity is reduced when the peak flow rate of a flood event is higher than the critical flow rate which fluidizes bed sediments. Partial bed fluidization or scour reduces the volume of porous media available for particle accumulation during flow recession following the peak flow rate. Flowing the representation of scour in Phase 2, the scouring depth is proportional to an exponential function of flow rate and equations (4.2) and (4.3) are modified using the substitution of $\beta = \beta' Q_{max}$ and applying the model to flood flow recession with flow rates of $Q(t)$

$$\text{scour depth at } Q(t) \propto e^{\beta \frac{Q(t)}{Q_{max}}} \tag{4.6}$$

$$\text{maximum scour depth at } Q_{max} \propto e^{\beta} \tag{4.7}$$

The capacity of the sediment bed for accumulating particles during partial fluidization is proportional to sediment bed depth which is not mobilized during the recession period of a flood event. The available capacity normalized by the maximum capacity is estimated by subtracting the scour depth during flow recession at a flow rate $Q(t)$ from the maximum scour depth and normalizing by the maximum scour depth. The available capacity normalized by the maximum capacity is then:

$$\frac{M_{cap}[Q(t)]}{M_{max}} = \frac{e^{\beta} - e^{\beta \frac{Q(t)}{Q_{max}}}}{e^{\beta}} = 1 - \exp\left[-\beta\left(1 - \frac{Q(t)}{Q_{max}}\right)\right] \tag{4.8}$$

Thus, the capacity for fine particle storage in the sediment bed is represented during the flow recession period as:

$$M_{cap}[Q(t)] = M_{max}\left\{1 - exp\left[-\beta\left(1 - \frac{Q(t)}{Q_{max}}\right)\right]\right\} \tag{4.9}$$

During Phase 3 the change in fine particle mass in the sediment bed from t to $t+\Delta t$ is:

$$\Delta M(t) = \alpha C(t)\left\{1 - \frac{M(t)}{M_{cap}[Q(t)]}\right\}\Delta t \quad \text{for } Q > Q_c \text{ and } dQ/dt < 0 \tag{4.10}$$

4.1.4 Model Summary

The model simulation processes are summarized in Figure 4.3. This sketch assumes the sediment bed initially has the particle mass set to M_{max}. During the accumulation period A1, there are no erosion events and the particle mass remains fixed at M_{max}. A flood event with a flow rate exceeding Q_c, erodes mass, $M_{f1,m}$, into the water column during discrete erosion event E1. Following the first erosion event, the flood recession period allows for particle accumulation in period A2. During this period the sediment bed is partially fluidized which reduces the sediment bed capacity, M_{cap}, below M_{max}, suspended particles are captured, and particle mass accumulates in the sediment bed. As the flow rate recedes, the sediment bed is less fluidized and the sediment bed capacity increases. A second flood event (E2) causes additional particle erosion, $M_{f2,m}$, which includes some of the particle mass deposited during the preceding recession period. The final accumulation period (A3) has continuous particle accumulation and increasing bed capacity over time while the sediment bed reforms with reduced flows. When the flow rate is below Q_c, particles can accumulate in the porous sediment bed up to the maximum capacity, M_{max}, with the rate limited by the availability of fine particles in the water column. These cycles are expected to repeat numerous times over a wet season. This model incorporates clockwise hysteresis with fine particles only released from the sediment bed during the rising limb of the flood event and the source of fine particles present during flood recession is assumed to be the background fine particle concentration. The complexity of observed clockwise hysteresis loops is represented by the total mass of fine particles released by individual flood events based only on the peak flow rate.

The model includes a number of watershed-specific parameters that are estimated from observations and others determined through calibration. Section 4.2 describes the model input data, Section 4.3 covers model calibration, Section 4.4 explores the model results at two Russian River gauging stations, and Section 4.5 examines the sensitivity of the model to the calibration parameters. Section 4.6 provides a limited validation of the model and Section 4.7 describes how the model can be extended to other time periods. Finally Section 4.8 provides an overall summary.

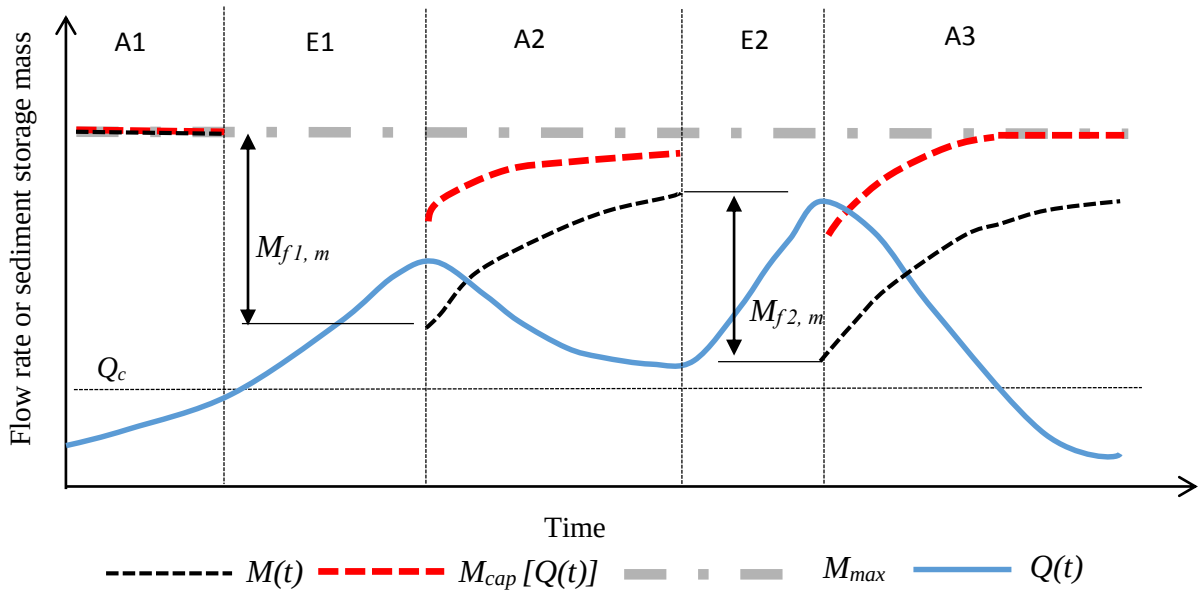

Figure 4.3. Illustration of three phases within the model with E1 and E2 designating periods when fine particles are eroded from the sediment bed; and A1, A2, and A3 indicating periods when fine particle could accumulate in the sediment bed.

4.2 Model Data Sources

The fine particle accumulation and erosion model is evaluated for data available in the Russian River watershed of northern California, a watershed selected for the length and completeness of the data records. Chapter 5 explores model application within other watersheds along with a comparison of model parameters among the watersheds. High frequency 15-minute turbidity and flow rate data between 2003 and 2013 are available for the United States Geological Survey (USGS) stream gauging stations on the Russian River. Calibration data from the USGS were downloaded (http://waterdata.usgs.gov/nwis) in May, 2014 and Table 4.1 summarizes the sub-watershed characteristics of the two gauging stations. The methodology for determining bank-full discharge is covered in Chapter 2, section 2.1.1, and Appendix B contains additional information on channel geomorphology, stage-discharge relationships, and wetted width vs. flow rate observations. Figure 4.4 is a map of the Russian River system and also indicates the locations of two major reservoirs. The water years (October through September) used in model development and calibration were limited to 2011, 2012 and 2013 at Hopland and 2010 and 2013 at Guerneville because of incomplete earlier records and the frequent occurrence of turbidity values that suggested the instrument was reporting the maximum possible reading.

Table 4.1. Characteristics of the two Russian River watersheds.

Site Name	USGS Site No.	Watershed Area [km^2]	Bank-full Discharge [m^3/s]	D_{50} [mm]			
				mean	*min.*	*max.*	Measurement period
Hopland	11462500	938	210	7.9	0.15	22.9	1990-1993
Guerneville	11467000	3465	875	7.1	0.19	26.2	1968-1986

The suspended sediment concentration (C) in the two watersheds is estimated from the turbidity (T) data. *Leonardson* [2010] fitted a relationship between turbidity and suspended sediment concentration at Guerneville from data collected by USGS:

$$C = \begin{cases} 4.35\,T^{0.71} & for\ Q \leq 10\ m^3/s \quad (R^2 = 0.50) \\ 3.0\,T^{0.96} & for\ Q > 10\ m^3/s \quad (R^2 = 0.94) \end{cases} \tag{4.11}$$

where C is in mg/L and T is in Turbidity Units [NTU]. In this dissertation the suspended particle concentrations at Guerneville are estimated from 15−minute turbidity data by equation (4.11). There were insufficient data to develop a relationship between turbidity and suspended particle concentrations at the Hopland site, and equation (4.11) was utilized. Since Hopland is contained within the drainage basin at Guerneville and there are similar hydrological and geological characteristics, this is a reasonable approach. This assumption is supported by *Brown III and Ritter*

[1971]'s observations within the nearby Eel River basin where they found a linear relationship between turbidity and suspended solids concentration that was similar at multiple locations within the basin.

4.3 Model Calibration

The model includes a combination of measured quantities specific to the watersheds as well as empirical parameters lumping the complexities of depositional and erosive processes. Watershed data allow a determination of the critical flow rate required to scour bed sediments, Q_c, maximum capacity of the sediment bed for fine particles, M_{max}, the flow rate that releases those particles, Q_{max}, and the background fine particle concentration dependence on flow rate, $C_b[Q(t)]$, during flood event recession. These quantities were not adjusted during model calibration. The two parameters representing particle filtration (α) and erosion (β) require determination through model calibration. This section describes how these input parameters were determined.

4.3.1 Critical Flow Rate

The analysis in Chapter 2 observed a slope break in the relationship of Q_s to Q that occurs when flow initiates sediment bed mobilization. At Guerneville, a slope break in the relationship of Q_s to Q happens at about 20 m^3/s which also corresponds to a transition of flow from a flat, wide stream to flow constrained by steep banks [Appendix B]. At Hopland, the flow rate at slope break is approximately 10 m^3/s. The available bed sediment size distribution data at both sites permit calculation of the critical shear stress to mobilize bed material. Additionally the shear stress at the flow rate corresponding to the slope break is estimated from USGS site monitoring data. For both Hopland and Guerneville, the critical shear stresses to mobilize bed materials are similar to the shear stresses at the slope break in agreement with the 13 minimally developed sites described in Chapter 2. Figure 4.5 is an expansion of Figure 2.12 which now includes Hopland and Guerneville results in the comparison.

Figure 4.4. The Guerneville and Hopland sub-watersheds of the Russian River, California watershed. The boundary GIS data are from USGS Blue Line Stream.

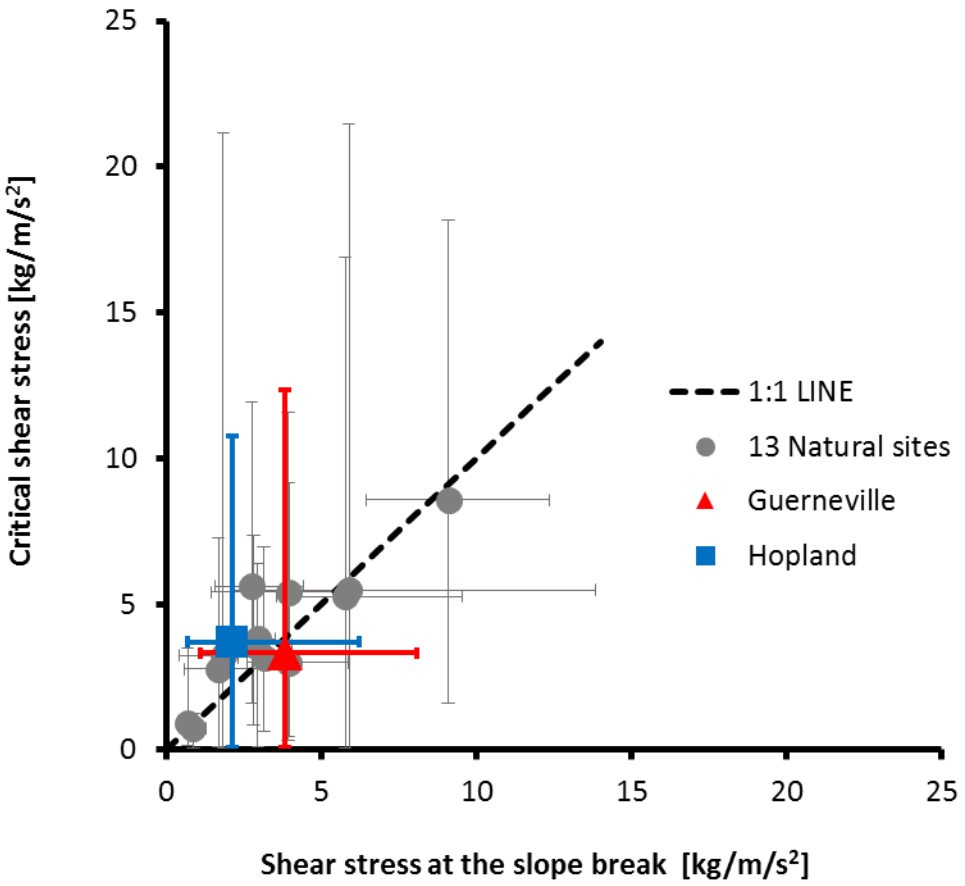

Figure 4.5. Shear stress at the observed slope break and calculated critical shear stress for bed mobilization at Hopland and Guerneville combined with the calculations at the 13 minimally developed sites analyzed in Chapter 2 (Figure 2.12).

4.3.2 Background Suspended Particle Concentration

Stream flow carries suspended particles originating from various sources within watersheds such as hill slopes, channel banks and the channel bed. Analysis in Chapters 2 and a review of the relevant literature in Chapter 3 suggested that during flood events, fine particles accumulated in the sediment bed are released into the flowing water and contribute to suspended particles. A method was needed to quantify the mass of fine particles released from bed sediments during flood events based on the measured particle concentrations. The hysteresis loops for the 2013 floods on the Russian River at Guerneville in Figure 2.13 revealed a consistent linear dependence of particle concentration on flow rate during the falling limb of all four flood events. The resulting conceptual model suggested that particles are only released from the sediment bed during the rising limb of flood events (Phase 2), and the falling limb of flood events asymptotically approaches the background suspended particle concentrations from the watershed (Phase 3). Based on the analysis of those hysteresis loops, the background suspended particle concentration is represented as

$$C_b(t) = \gamma\, Q(t) \tag{4.12}$$

where γ is the slope, and for C_b in [mg/L] and Q in [m^3/s], γ has units of [mg-s/L/m^3].

Data on fine particle concentration as a function of flow rate during flood recessions are available for the Russian River sites at Hopland and Guerneville. Figure 4.6 plots Hopland data in three panels representing the water years: 2011, 2012, and 2013. In each panel, different symbol colors represent unique flood events and show a rapid decline in particle concentration after the peak flow rate with an asymptotic approach to a linear dependence of concentration on flow rate. A single linear representation of these data is shown on these plots as the red line that quantifies the dependence of the fine particle background concentrations on flow rate. Figure 4.7 shows the data and linear fit for the two water years available for the Russian River at Guerneville. These data led to the following estimates for background particle concentrations at these two locations

$$C_b(t) = 2\, Q(t) \qquad \text{(Hopland)} \tag{4.13a}$$

$$C_b(t) = 0.5\, Q(t) \qquad \text{(Guerneville)} \tag{4.13b}$$

The background concentration relationships in equations (4.13a) and (4.13b) give comparable concentrations under similar conditions. There is a factor of 4 increase in watershed area at Guerneville compared to Hopland and flows within a watershed are generally proportional to watershed area. Then at a given time the flow at Guerneville will be four times the flow at Hopland, and the background concentrations would be about the same. Such consistency in these relationships is expected within the relatively homogeneous watershed of the Russian River.

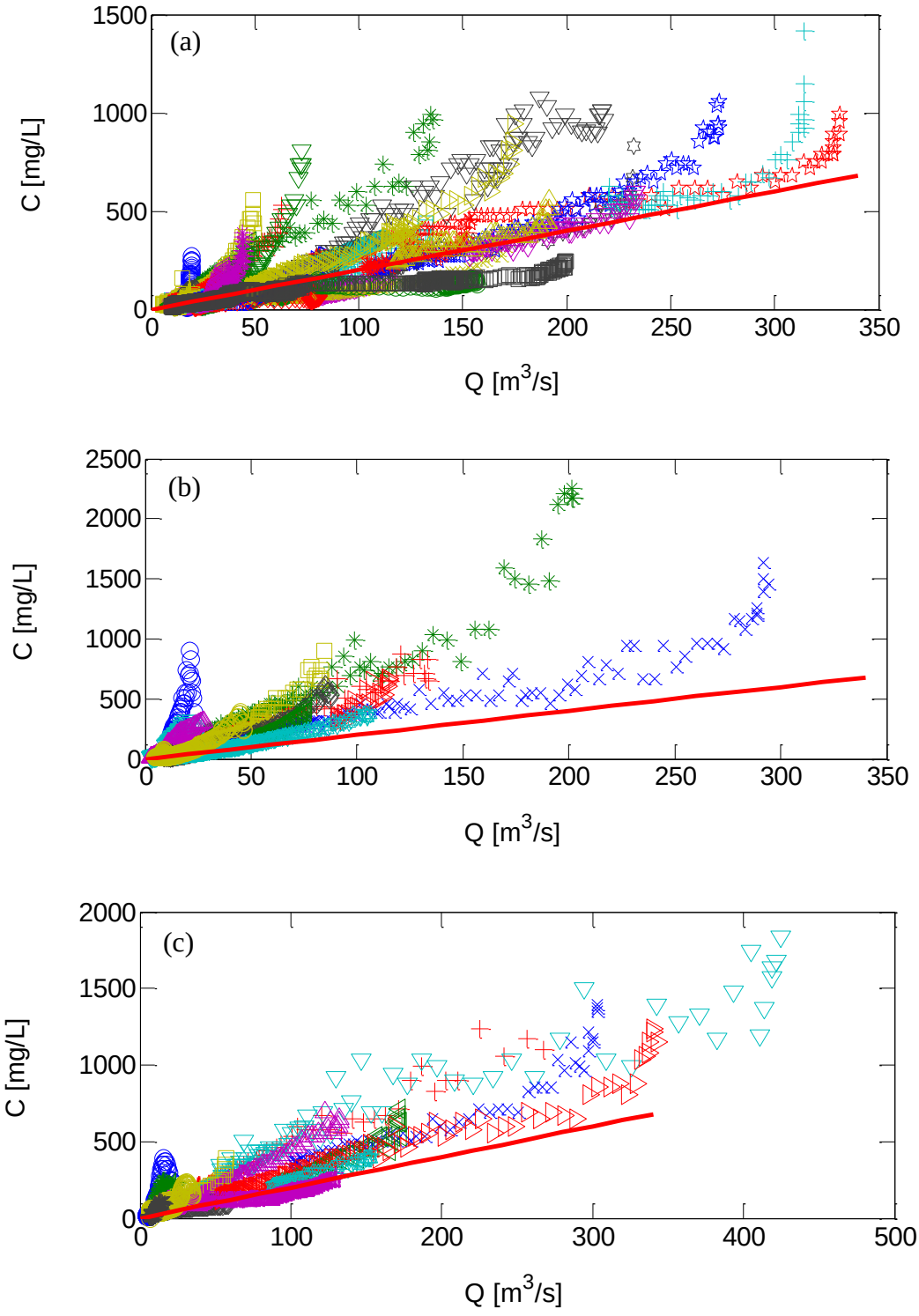

Figure 4.6. Fine particle concentration data during falling limb recession in the Russian River at Hopland for water years (a) 2011, (b) 2012, and (c) 2013. The plotting symbols represent different flood events and the red line is the assumed linear dependence of background suspended particle concentration on flow rate given by equation (4.13a).

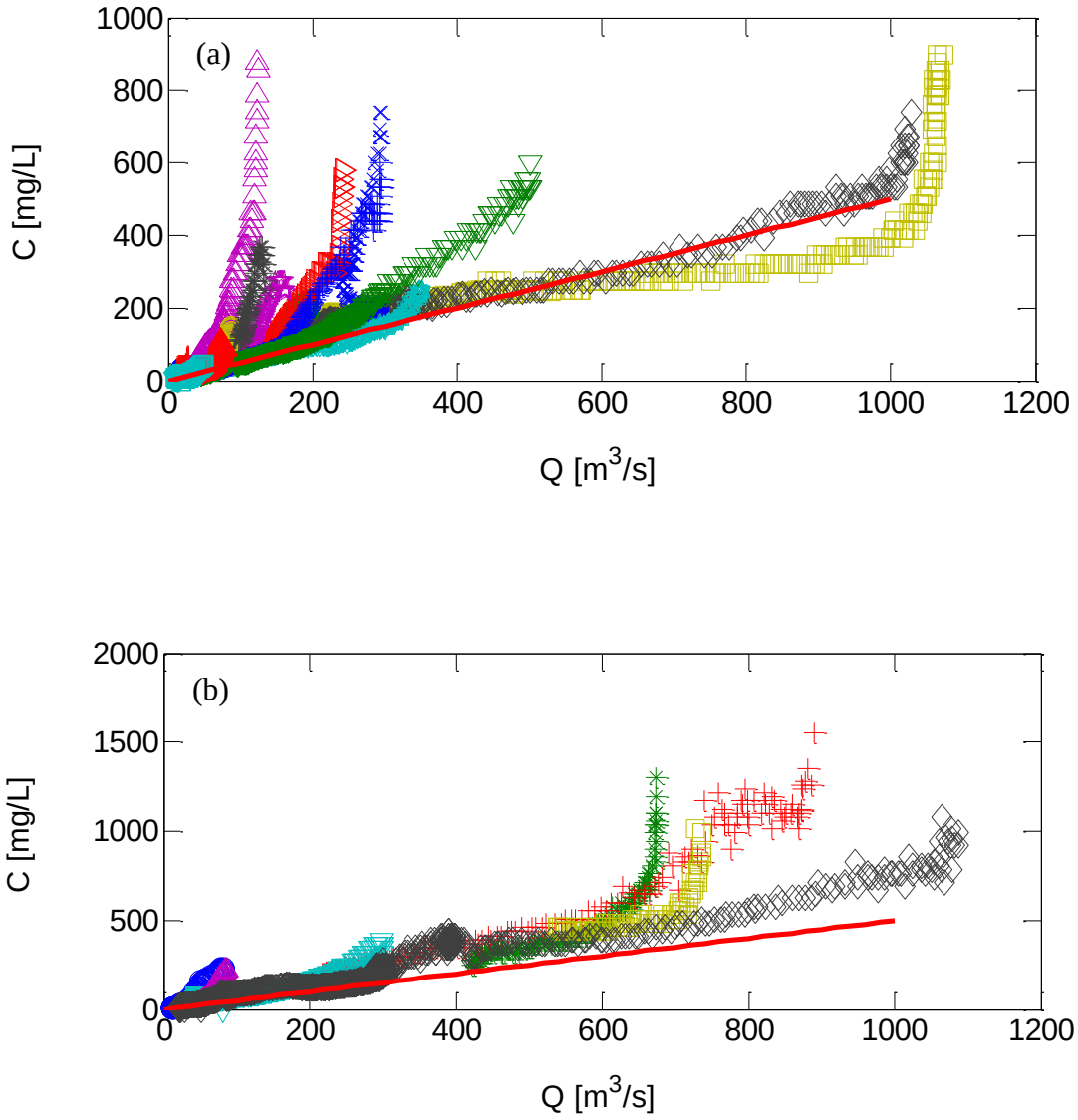

Figure 4.7. Fine particle concentration data during the falling limb recession in the Russian River at Guerneville for water years (a) 2010 and (b) 2013. The plotting symbols represent different flood events and the red line is the assumed linear dependence of background concentration on flow rate given by equation (4.13b).

4.3.3 Particle Mass Release

The model is formulated in terms of fine particle accumulation in the sediment bed, *M(t),* but there are no widely available measurements of this quantity for comparison with the model. Instead, the modeled mass of fine particles released by a flood event is compared to the mass of fine particles eroded from the sediment bed estimated by subtracting the assumed contribution by background particles from the measured mass of fine particles. For flood event *i* the data-determined mass released from the bed is calculated by

$$M_{fi,d} = \int_{t_{s,i}}^{t_{e,i}} Q(t)[C(t) - C_b(t)]\, dt \qquad (4.14a)$$

The lower limit of integration, $t_{s,i,}$ is the start of the flood event *i*, which is either the first occurrence when $Q(t_s) > Q_c$ or when d$Q(t)$/dt transitions from negative to positive while $Q > Q_c$ during multiple high flow events. The upper limit of integration, $t_{e,i}$, represents the end of the erosive component of the flood which is the time of peak flow. The reported concentration data are *C(t)* and the background suspended particle concentrations are approximated with a linear dependence on flow rate

$$C_b(t) = \gamma Q(t) \qquad (4.14b)$$

where γ is the site-specific slope as discussed in Section (4.3.2). While $M_{fi,d}$ is referred to as the data-determined mass of fine particle release from the sediment bed, the calculation does require this assumed background concentration relationship. Sensitivity of the model to this assumption is addressed in Section 4.7.

The total particle mass released from the channel bed is the cumulative sum of $M_{fi,d}$ for the measurement period, and the total fine particle mass passing the gauging station is the total suspended load and calculated by integrating over the period of measurement:

$$\text{Total suspended load} = \int Q(t)C(t)\, dt \qquad (4.15)$$

Table 4.2 provides a comparison of the total suspended load to the mass released from the sediment bed by flood events. The mass released from the sediment bed is at most 35% of the total suspended load and this is typical of what is encountered when fine particle sources are estimated from upland and local sources as covered in section 3.2.3 of the literature review.

Table 4.2. Summary of the total fine particle mass passing the two gauging stations on the Russian River by water year along with estimated fine particle mass released from the sediment bed

Watershed	Water Year	Total Particle Mass [Mg]	Particle Mass Released from Sediment Bed [Mg]	Fine Particles Released from Sediment Bed as percent of Total
Hopland	2011	153,000	26,000	17%
	2012	53,000	14,000	26%
	2013	124,000	44,000	35%
Guerneville	2010	441,000	120,000	27%
	2013	467,000	144,000	31%

The model-derived mass of fine particles released by flood event i, $M_{fi,m}$, is determined from equation (4.5) as

$$M_{fi,m} = M(t_{s,i}) - M(t_{e,i}) = M_{max} \exp\left[-\beta\left(1 - \frac{Q_{fi}}{Q_{max}}\right)\right]$$

The comparison of model and data is through an examination of the mass released from the sediment bed by individual floods as well as the cumulative mass of fine particles released up to and including flood i

$$A_{i,d} = \sum_{j=1}^{i} M_{fj,d} \qquad (4.16a)$$

$$A_{i,m} = \sum_{j=1}^{i} M_{fj,m} \qquad (4.16b)$$

where $A_{i,d}$ and $A_{i,m}$ represent the cumulative mass of fine particles released in the first i flood events of the season based on data and the model, respectively. The data-determined and the model-determined cumulative mass released during the first i floods are useful in both comparing model performance for individual flood events, but also for visualizing the model's ability to reproduce the dynamics of particle capture and erosion compared to the data available over a wet season. One final measure of the model fit is the ratio of the modeled particle mass released to the data-determined particle mass released, which can be represented as

$$R = \frac{\sum_{j=1}^{n} M_{fj,m}}{\sum_{j=1}^{n} M_{fj,d}} \qquad (4.16c)$$

where n is the number of flood events in the total simulation period.

4.3.4 Peak Flow Rate and Maximum Storage Capacity

The maximum fine particle storage capacity (M_{max}) in the sediment bed is estimated as the maximum mass released from the sediment bed by a flood event during the calibration period. The peak flow rate of this flood event is taken as Q_{max}. Table 4.3 summarizes the model parameters determined for the two locations. The peak flood event for Hopland in Dec 2, 2012 had a constant turbidity reading of 1000 NTU during a 4-hour period suggesting the turbidity sensor reached its maximum value. The turbidity signal during this peak period was estimated by smoothly connecting the hysteresis loop of turbidity versus flow rate from which M_{max} was obtained. The details of this correction are included in Appendix B.

Table 4.3. Model parameters for Hopland and Guerneville sub-watersheds identified from the analysis of data

Site Name	Q_{max} [m^3/s]	M_{max} [Mg]	Date
Hopland	425	20,800	Dec 2, 2012
Guerneville	1070	66,500	Jan 21, 2010

4.3.5 Parameter Optimization

The modeling effort minimized the number of calibration parameters in order to determine what were the dominant processes and the coupling between bed erosion and particle accumulation. The only parameters that were utilized for calibration where the empirical parameters representing particle accumulation (α) and bed scour (β). With only two parameters, visual techniques of parameter fitting were possible and quantification of goodness of fit was evaluated initially by three different statistical methods commonly used in hydrology [*Moriasi et al.*, 2007]. These possible measures of model performance are summarized and then their applicability to the model evaluation within the Russian River locations demonstrates only a single goodness-of-fit statistic is needed.

1. Percent bias (PBIAS) provides information on systematic deviation of the model away from observations through

$$PBIAS = \frac{\frac{1}{n}\sum_{i=1}^{n}(M_{fi,d} - M_{fi,m}) \times 100}{\overline{M_{f,d}}} \tag{4.17}$$

where n is the number of flood events and the mean data-determined mass released for all flood events is

$$\overline{M_{f,d}} = \frac{1}{n}\sum_{i=1}^{n} M_{fi,d} \tag{4.18}$$

Values of PBIAS can range from 0, which is optimal, to very large positive or negative values.

2. Root Mean Square Error − Observation Standard Deviation Ratio is represented by the acronym RSR (**R**oot mean square error to data **S**tandard deviation **R**atio) and is calculated by

$$\text{RSR} = \frac{\sqrt{\sum_{i=1}^{n}\left(M_{fi,d} - M_{fi,m} \right)^2}}{\sqrt{\sum_{i=1}^{n}\left(M_{fi,d} - \overline{M_{f,d}} \right)^2}} \tag{4.19}$$

Values of RSR range from 0 when the model and data are equal to very large positive values when the model is a poor fit to the data.

3. The Nash-Sutcliffe Efficiency (NSE) is commonly utilized in the evaluation of hydrologic time series models and is calculated by

$$NSE = 1 - \frac{\sum_{i=1}^{n}(M_{fi,d} - M_{fi,m})^2}{\sum_{i=1}^{n}(M_{fi,d} - \overline{M_{f,d}})^2} = 1 - (RSR)^2 \tag{4.20}$$

Values of NSE range from -∞ to 1, with NSE = 1 corresponding to a model identical with the observations.

These three statistical measures of the goodness of fit are compared for the Guerneville 2010 water year in Figure 4.8. The contour plots were generated by running the simulation model for a fine grid of α and β pairs. The range of α values was determined through model exploration of reasonable values and the range of β values was constrained by the scour model performance illustrated in Figure 4.2. The optimal parameter values are not uniquely determined by the PBIAS statistic. NSE and RSR show similar patterns of parameter dependency as expected from their interdependence. The RSR statistic is easier to identify the optimal range of model parameters than NSE, and was used to determine the optimal parameter pairs in this analysis.

Model refinement was also suggested by inspection of the time sequences of particle mass in storage, $M(t)$, bed capacity, $M_{cap}(t)$, and cumulative mass released according to the data, $A_{i,d}$, and the model, $A_{i,m}$. For example, fine particle filtration was included within Phase 3 (flow recession) in order to achieve particle accumulation within the sediment bed during a series of flood events where all flows were greater than Q_c. Without the model modification there was continual depletion of fine particles predicted in the sediment bed even though the data suggested continuing particle deposition and release. This required inclusion of particle accumulation during flood recession when the sediment bed was partially fluidized. This model modification is also in agreement with observations reported in the literature that stream turbidity rapidly cleared during flood recessions.

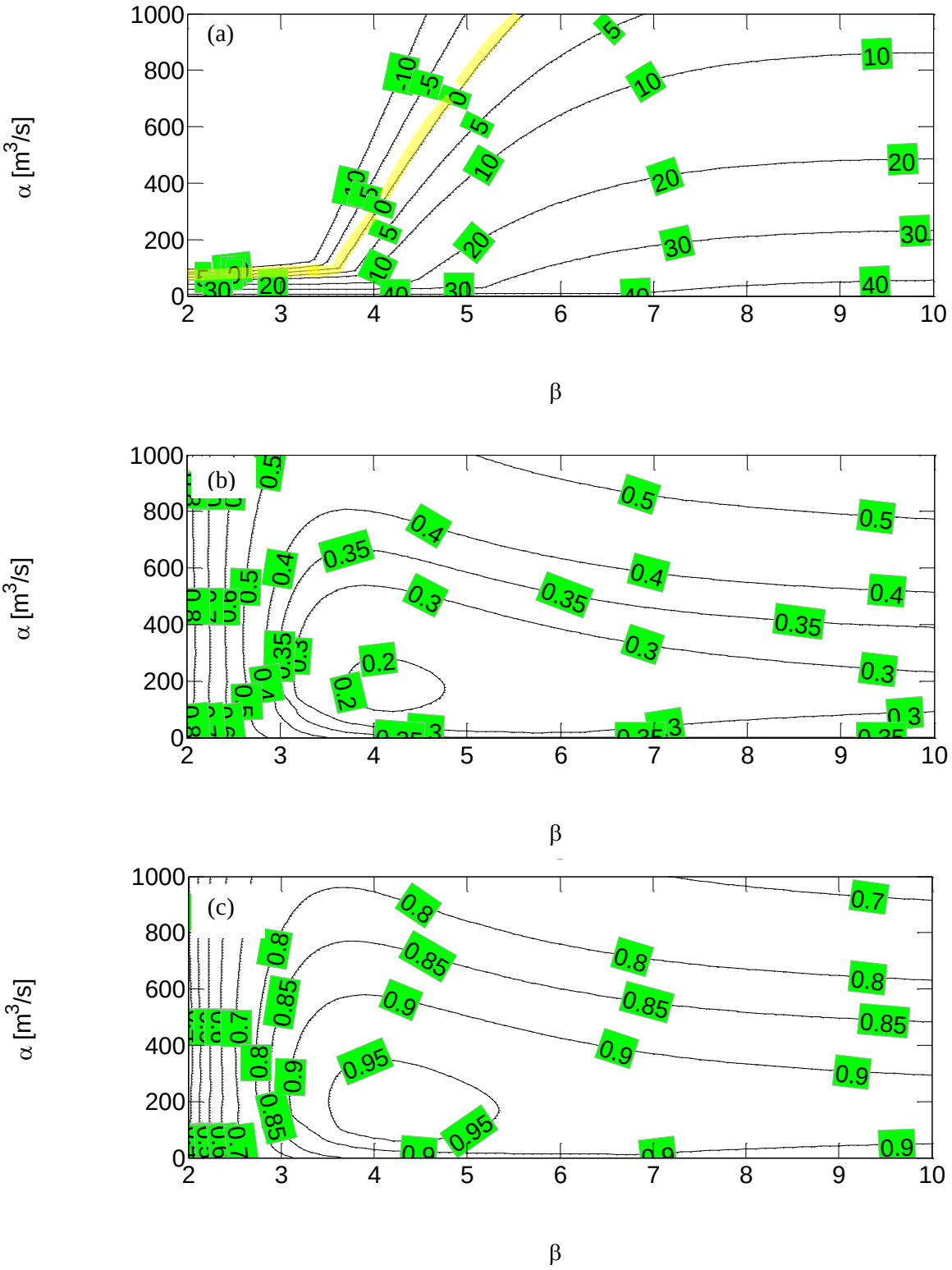

Figure 4.8. Comparison of three statistical measures applied to water year 2010 Guerneville station on Russian River (a) PBIAS, (b) RSR, and (c) NSE. The PIBAS statistic does not identify a unique set of optimal parameters as indicated by the highlighted PBIAS = 0 line.

4.4 Model Results

This section illustrates the ability of the model to represent fine particle dynamics within the two gauged locations in the Russian River watershed. The search process for the optimal values of the filtration and scour parameters permitted an assessment of the sensitivity of the model to these two parameters.

The contour plots of RSR for the three continuous water years at Hopland and the two-year record at Guerneville are shown in Figure 4.9. The goodness of fit statistic, RSR, is evaluated for all flood events in each record to determine the multi-year optimum parameter values. For Hopland the model results are relatively insensitive to the filtration parameter, α, when it is larger than about 200 m^3/s and the scour parameter, β, is constrained within the interval of 4.5 to 5.5. At Guerneville, the particle filtration parameter is within the interval of 200 to 600 m^3/s while the scour parameter has a relatively narrow range between 3 and 4. Table 4.4 summarizes the multi-year optimal parameter values at these two watersheds as well as the individual year values of RSR and *R*. There is some variability year to year and this is better described in an analysis of the yearly series of flood events comparing data with modeling results.

Table 4.4. Optimal parameters and goodness of fit for the Hopland and Guerneville gauging sites on the Russian River

Watershed	Optimal Parameters		Multi-year		Water year	RSR	*R*
	α [m^3/s] (range)	β (range)	RSR	*R*			
Hopland	300 (>200)	5 (4.5 - 5.5)	0.25	1.04	2011	0.48	1.45
					2012	0.48	0.72
					2013	0.16	0.90
Guerneville	340 (200 - 600)	3.4 (3 - 4)	0.32	0.97	2010	0.26	1.19
					2013	0.45	0.79

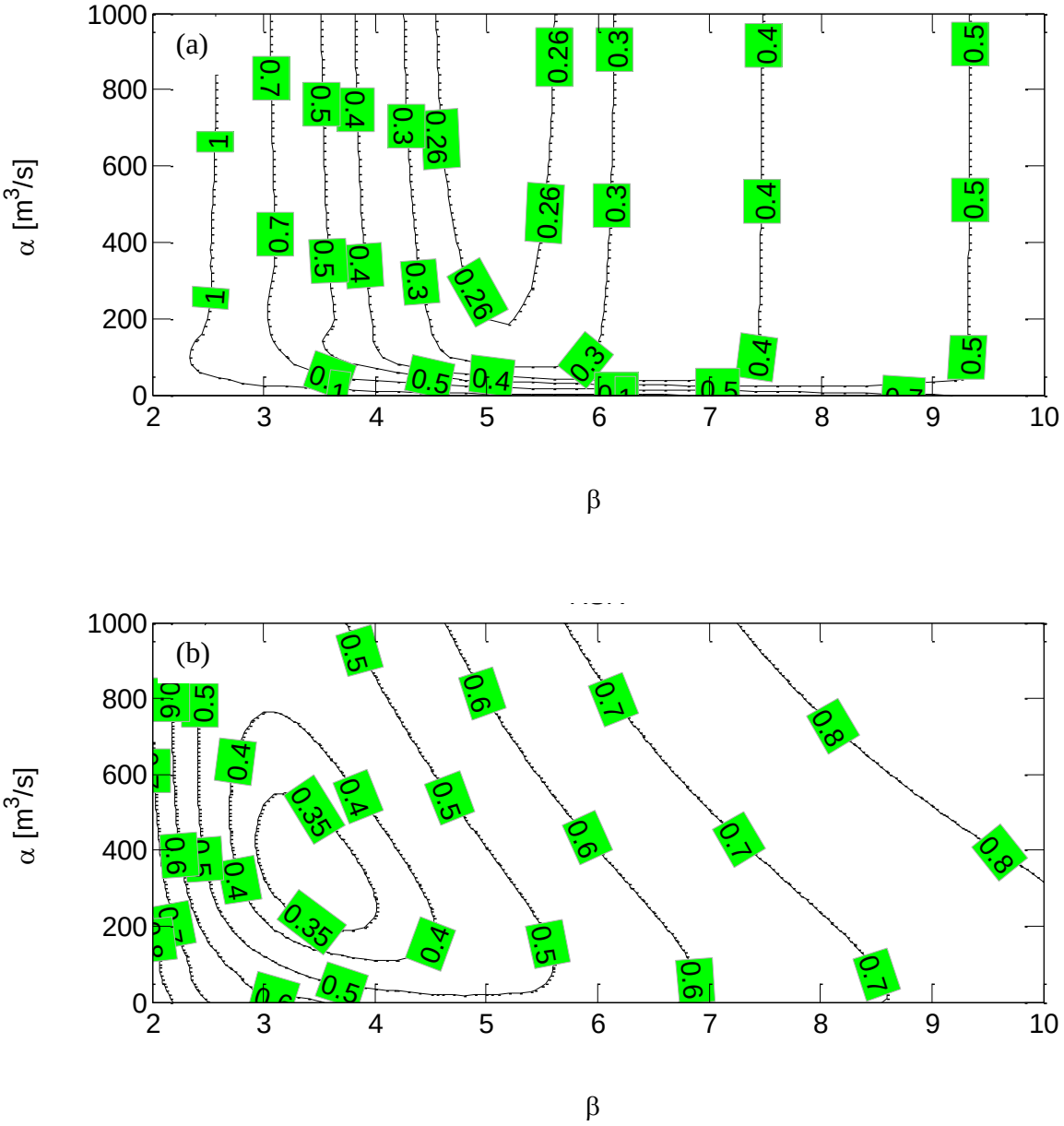

Figure 4.9. Sensitivity of RSR for model simulation with model parameters α and β (a) Hopland, combining measurements of 2011, 2012 and 2013 water years, and (b) Guerneville, for 2010 and 2013 water years.

Figures 4.10 and 4.11 illustrate the model output for the continuous simulation over the water years 2011 to 2013 at Hopland, and for water years of 2010 and 2013 at Guerneville. The vertical axis on the left is fine particle mass, and the vertical axis on the right side is flow rate, plotted as a blue line. Multiple lines represent fine particle mass where the dashed magenta line is the capacity of the sediment bed for fine particles, $M_{cap}\ [Q(t)]$, and the dotted black line is the mass of fine particles in the sediment bed, $M(t)$. The cumulative mass of fine particles released from the bed by the first i flood events based on data, $A_{i,d}$, is plotted as a black line with a triangle symbol for each flood event. The model-generated cumulative mass of particles released for the first i flood events, $A_{i,m}$, is plotted as a red line with a circle for each flood event.

The Hopland data set was continuous for three hydrologically different years. This permitted having only one initial condition for the complete period with the sediment bed at the maximum mass of fine particles, M_{max}. In Figure 4.10 (a) the comparison of the data with the model for the three water years illustrates the coupling of fine particles with sediment bed fluidization where the overall value of R for three years is 1.04. The model output also demonstrates that the mass of fine particles in the sediment bed returns each fall to near M_{max}. The model output by year is included in Figure 4.10 (b), (c), and (d) for easier visual identification of model functioning.

During the first few months in 2011 water year, there were a number of small flood events that caused a limited depletion in particles from the sediment bed as shown in Figure 4.10 (b). The first big flood event in early January eroded about half of the particles from the bed with an initial rapid recovery in stored mass (Phase 3) followed by slow accumulation (Phase 1). In late March two closely spaced flood events caused additional removal of particles from the sediment bed followed by a slow accumulation during the remainder of the water year. The modeled particle release is greater than the observational data with the ratio R =1.45 for that year.

The 2012 water year in the Russian River watershed had few flood events as depicted in Figure 4.10 (c). Only two flood events had significant particle release and the model under-estimated the mass eroded with R = 0.72. The particle mass stored in the bed was only partially depleted by the flood events and accumulation was slow during the summer months because the mass in storage was close to M_{max}.

Water year 2013 was a drought year in northern California and there were only four significant flood events as shown in Figure 4.10 (d). One of these floods was at Q_{max} and that flood event eroded all particles from storage. The model represented the accumulation of the fine particles during December prior to the second major flow event of the year and then for the remainder of the water year as fine particles accumulated in the sediment bed and approached the maximum capacity. The modeled mass of particles released from the sediment bed over the water year was 90% of the measured mass. These Hopland results illustrate the need for multiple years of data to provide hydrologic variability needed in testing model assumptions of erosion, accumulation and bed capacity reduction during partial fluidization.

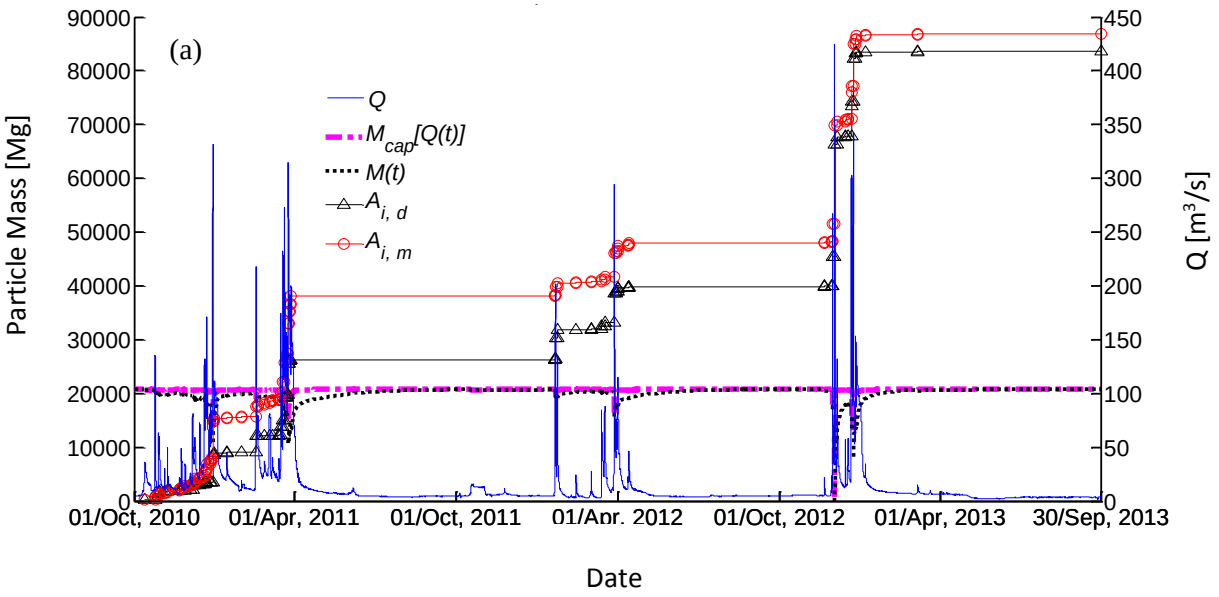
(a)
Q
$M_{cap}[Q(t)]$
M(t)
$A_{i,d}$
$A_{i,m}$
Particle Mass [Mg]
Q [m³/s]
90000
80000
70000
60000
50000
40000
30000
20000
10000
0
450
400
350
300
250
200
150
100
50
0
01/Oct, 2010
01/Apr, 2011
01/Oct, 2011
01/Apr, 2012
01/Oct, 2012
01/Apr, 2013
30/Sep, 2013
Date

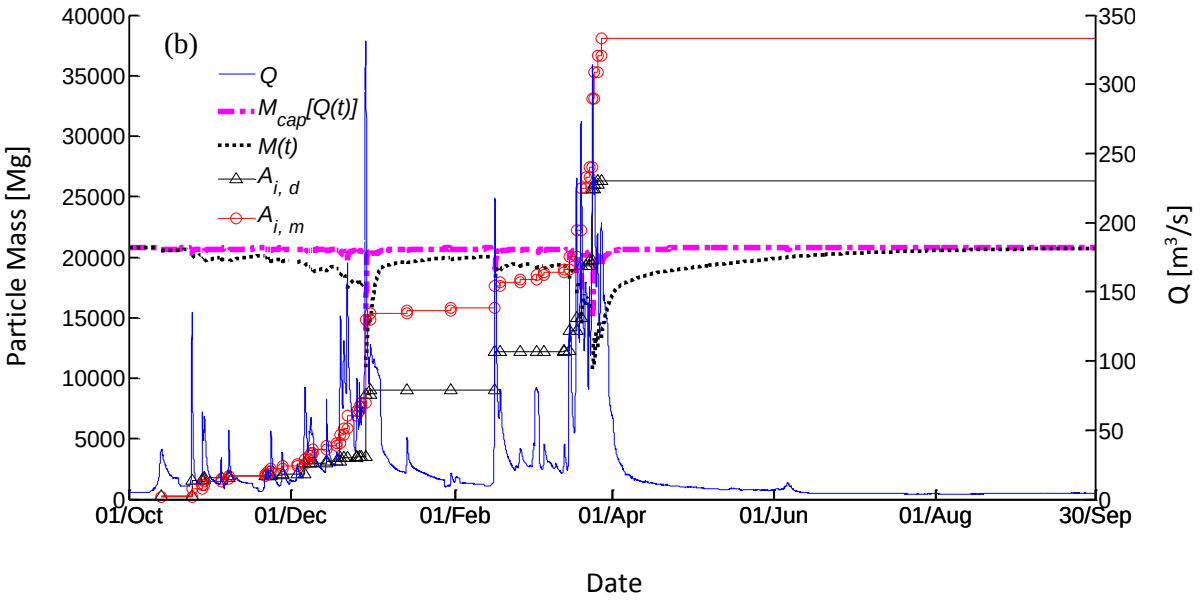
(b)
Q
$M_{cap}[Q(t)]$
M(t)
$A_{i,d}$
$A_{i,m}$
Particle Mass [Mg]
Q [m³/s]
40000
35000
30000
25000
20000
15000
10000
5000
0
350
300
250
200
150
100
50
0
01/Oct
01/Dec
01/Feb
01/Apr
01/Jun
01/Aug
30/Sep
Date

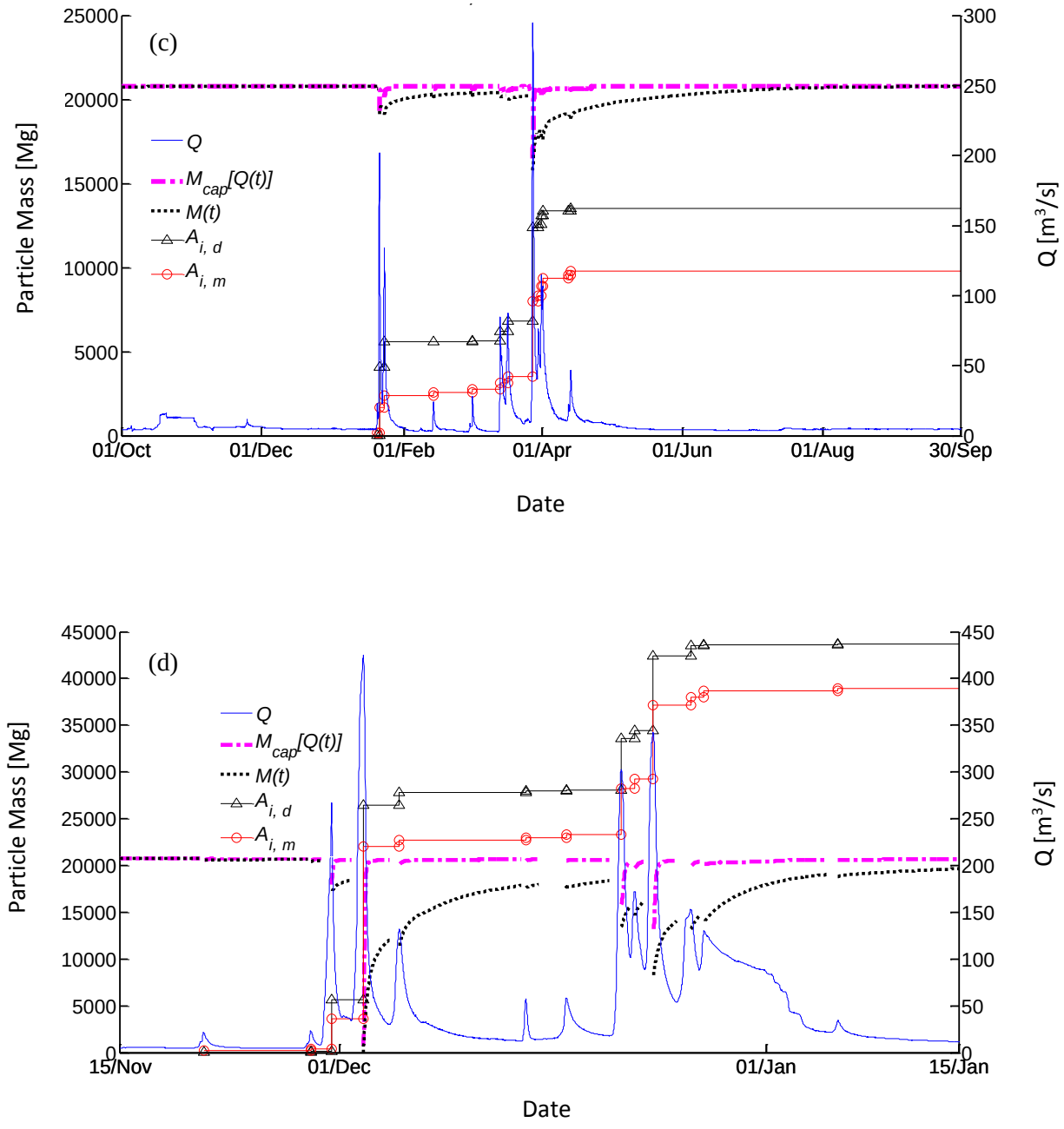

Figure 4.10. Russian River at Hopland model comparison with data for water years (a) from 2011 to 2013 (b) 2011, (c) 2012, and (d) 2013 only for the flooding period between November 15, 2012 and January 15, 2013. The blue line represents flow rate, the dashed magenta line is the capacity of the sediment bed for fine particles, M_{cap} *[Q(t)]*, and the dotted black line is the mass of fine particles in the sediment bed, *M(t)*. $A_{i,d}$, is plotted as a black line with a triangle symbol for each flood event and $A_{i,m}$, is plotted as a red line with a circle for each flood event.

The model performed reasonably well for the two separate water years of data available at Guerneville. The fine particle storage mass was assumed to be at capacity at the beginning of both the 2010 and 2013 water years at Guerneville based on the Hopland modeling results where the low-flow summer period could refill the sediment bed to near M_{max}. These two water years were hydrologically different with 2010 having 18 flood events while 2013 had only 7 (Figure 4.11 (a), (b)). In January of 2010 the first of two flood events had a flow rate of Q_{max} resulting in the complete erosion of fine particles from the sediment bed. At the time of the second flood there was limited particle accumulation and all particle mass was removed by that second flood. The model successfully represented this sequence of events with far greater particle mass removed during the first flood compared to the second. During the rest of the 2010 water year the model tracked the observed release of fine particles and the overall ratio of modeled mass released to measured mass released (R) was 1.19. For 2013 the relatively small number of flood events observed at Guerneville was similar to Hopland, and the model was able to reproduce the dynamics of fine particle release from the bed sediments. The overall ratio of modeled mass released to the measured mass released was 0.79 for 2013. Given the differences in hydrology in the 2010 and 2013 water years, the optimum values of the filtration and scour parameters resulted from a compromise resulting in model over prediction in 2010 and under prediction in 2013.

The modeled and measured mass of fine particles released from sediment bed in 69 flood events at Hopland between 2011 and 2013 water years and 25 flood events at Guerneville in 2010 and 2013 water years are compared in Figure 4.12. The model shows a good fit with released mass of fine particles for larger flood events. The model estimates released mass of fine particles from sediment bed within about 1 to 40% bias for the 8 largest flood events which represent 73% of total released mass at Hopland between 2011 and 2013 water years and within about 13 to 60% bias for the 7 largest flood events which represent 90% of total released mass of fine particles at Guerneville in the 2010 and 2013 water years. The bias of the model for smaller flood events is a consequence of minimizing RSR which weighs more heavily absolute deviation of modeled mass from observed mass.

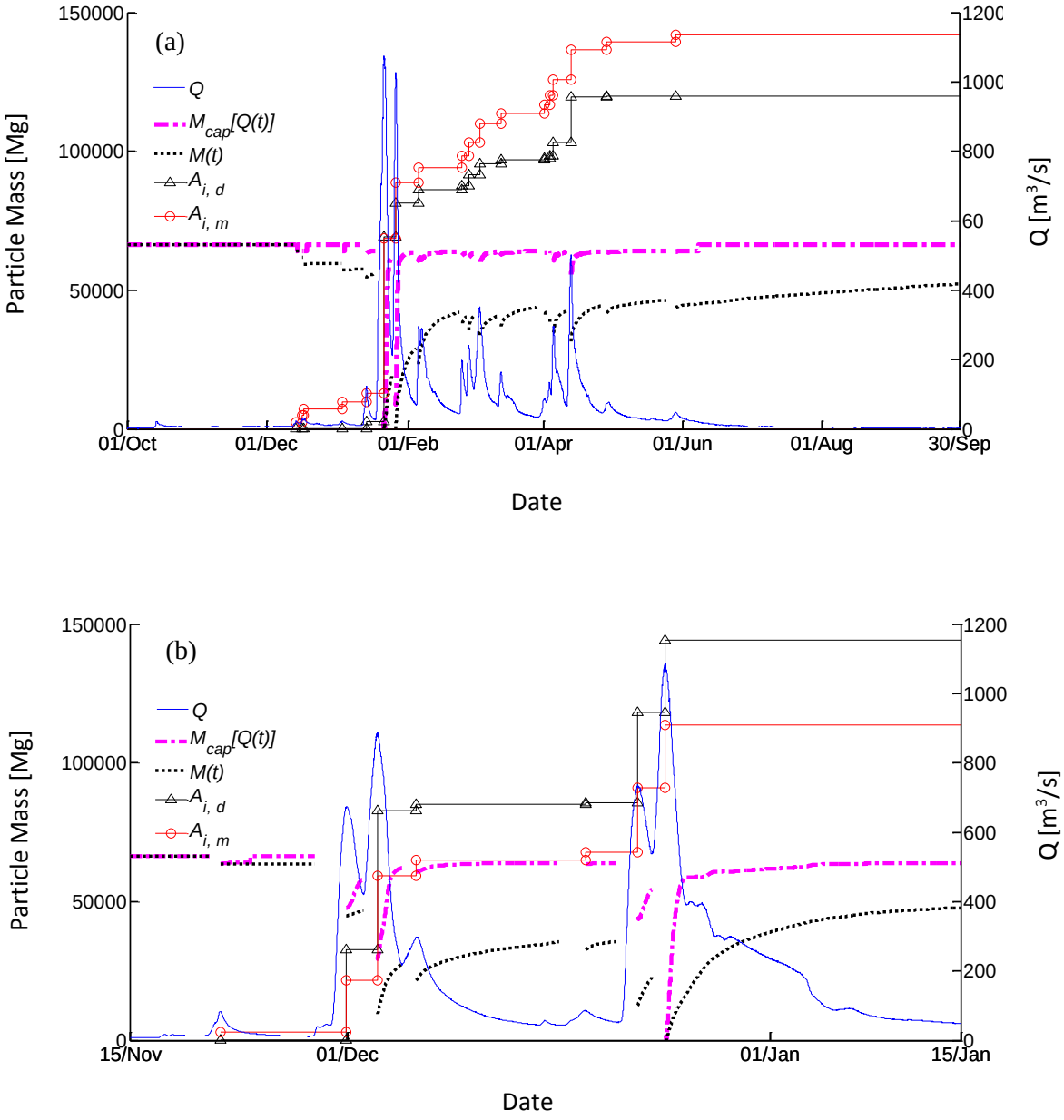

Figure 4.11. Russian River at Guerneville model comparison with data for (a) 2010 and (b) 2013 only for flooding periods between November 15, 2012 and January 15, 2013. The blue line represents flow rate, the dashed magenta line is the capacity of the sediment bed for fine particles, $M_{cap}\,[Q(t)]$, and the dotted black line is the mass of fine particles in the sediment bed, $M(t)$. $A_{i,d}$, is plotted as a black line with a triangle symbol for each flood event and $A_{i,m}$, is plotted as a red line with a circle for each flood event.

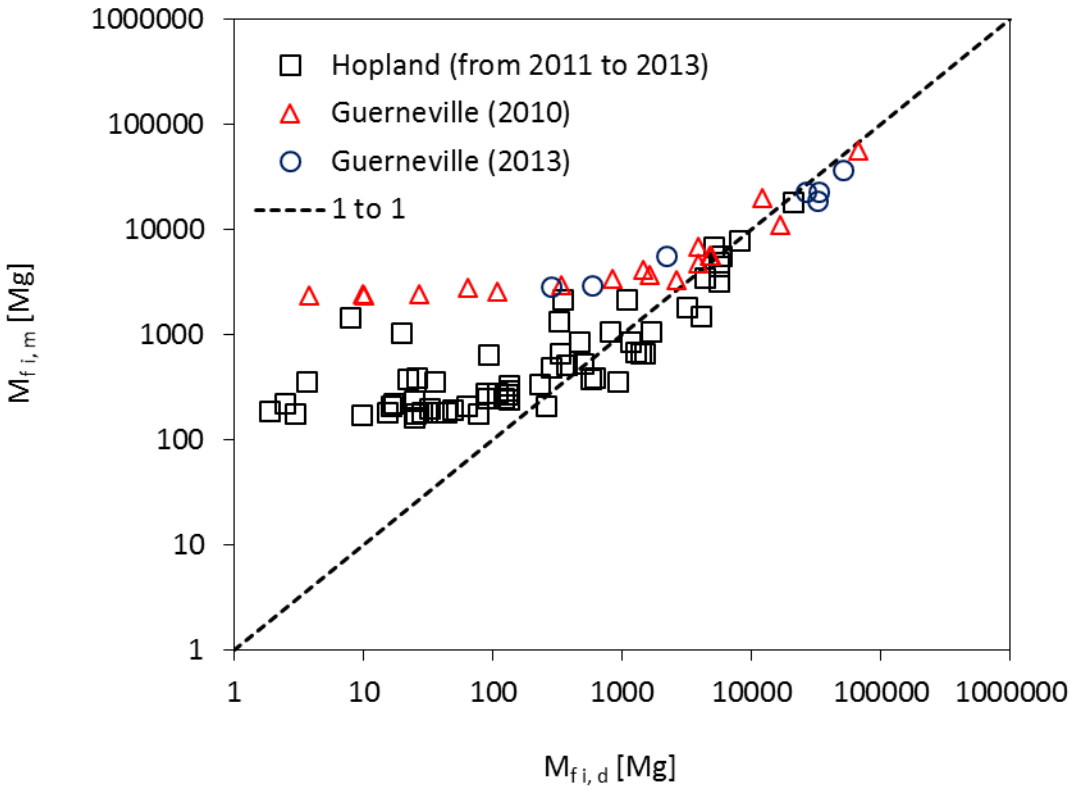

Figure 4.12. Comparison of modeled and measured mass released from individual floods for Hopland between 2011 and 2013 water years and Guerneville in 2010 and 2013 water years.

4.5 Model Sensitivity to Background Suspended Particle Concentration

The model has numerous parameters, but only the filtration and scour parameters were determined by optimization through inspection of the contour plots of RSR values. Another model parameter, γ, appears in the linear dependence of background suspended particle concentration on flow rate. In this section, model sensitivity to the γ parameter is explored, which is potentially important given the need to distinguish fine particle releases between watershed and sediment bed contributions.

The sensitivity of the model to the γ parameter is given in Table 4.5 at Guerneville by exploring values of γ above and below the fitted value of 0.5. When γ is altered, the model requires recalibration of the other parameters because a change in background concentration alters the mass released from the sediment bed by flood events and this leads to changes in M_{max} and new optimal values for α and β as shown in the table. The model performance as evaluated by RSR is better for smaller values of γ. It is possible this goodness of fit statistic with smaller γ values reflects more mass being released from the sediment bed and this increases the standard deviation of the measured mass released as appears in the denominator of the RSR expression in equation 4.19 leading to a reduction in RSR. The ratio of total modeled mass released to measured mass released (R) also improves with decreasing γ. It is clear from the plot of fine particle concentration versus flow rate during falling limb recession (Figure 4.7) that $\gamma = 0.5$ is a good fit to the asymptotic relationship between concentration and flow rate rather than slightly larger or smaller values. This sensitivity analysis led to the parameter γ obtained from actual observations rather than an automated optimization scheme.

Table 4.5. Model sensitivity for the slope (γ) of background suspended particle concentration applied to the Russian River at Guerneville

Slope (γ)	M_{max} [Mg]	Q_{max} [m^3/s]	Optimal parameters (combining measurements of 2010 and 2013 water years)			Yearly Results			
						RSR		R	
			α	β	RSR	2010	2013	2010	2013
0.3	88,200	1070	480	3.6	0.24	0.19	0.35	1.12	0.85
0.5	66,500	1070	340	3.4	0.32	0.26	0.45	1.19	0.79
0.7	44,900	1070	210	3.1	0.45	0.39	0.59	1.31	0.69

4.6 Model Validation

Hydrologic modeling is usually conducted with long-term datasets with some period used in calibration and another period used for validation. The availability of long-term, continuous 15-minute data on flow rate and turbidity calibrated to fine particle concentration limited the analysis to the Russian River system. Three years of continuous data from Hopland and two discontinuous years at Guerneville were used in model calibration in order to sample some of the natural hydrologic variability. During the period of model development and calibration, additional data became available for the period Oct 1, 2013 through Dec 31, 2014 that are used for partial model validation. The approach does not follow the recommended usage of word "validation" promoted by *Beven and Young* [2013] since the validation period is limited and there is no attempt to predict flow rate using a continuous watershed simulation model. Measured flow rates continue to be utilized in this modeling effort.

For validation testing of the model, the model input is limited to model parameters and measured flow rates over the period of validation. The model parameters determined during data analysis and the calibration process over the 2010 to 2013 water years were the slope of the line representing the relationship between background suspended particle concentration (γ) and flow rate; the flow rate required to initiate sediment bed movement, Q_c; the maximum flow rate, Q_{max}; the maximum mass of fine particles within the sediment bed, M_{max}; the filtration parameter (α); and the scour parameter (β). The initial mass of fine particles within the sediment bed at the start of the validation period is taken as the mass at the end of the calibration period, Sept 30, 2013.

The extension of the model for use in the validation period requires modification during the three phases of the hydrologic cycle described in Section 4.1.

Phase 1: During base flow, $Q < Q_c$, the suspended particle concentration is given by the background particle concentration determined from the linear relationship between concentration and flow rate during falling flood recession as shown in Section 4.3.2

$$C(t) = C_b(t) = \gamma Q(t) \quad \text{for} \quad Q(t) < Q_c \tag{4.21}$$

The mass of fine particles added to the sediment bed during this phase through filtration and settling is a modification of equation (4.1)

$$\Delta M(t) = \alpha\, \gamma\, Q(t) \left(1 - \frac{M(t)}{M_{max}}\right) \Delta t \quad \text{for} \quad Q(t) < Q_c \tag{4.22}$$

Phase 2: During the rising period of a flood where $Q > Q_c$ and $dQ/dt > 0$, particle erosion predicted for the flood event, does not change from equation (4.5a)

$$M_{fi,m} = M_{max} \exp\left[-\beta \left\{1 - \frac{Q(t_{e,i})}{Q_{max}}\right\}\right] \tag{4.5a}$$

Phase 3: The extended particle filtration model during flow recession requires modification of equation (4.10) by substituting in the background suspended particle concentration's dependence on flow rate for *C(t)* as was done in Phase 1 of validation

$$\Delta M(t) = \alpha\, \gamma\, Q(t) \left[1 - \frac{M(t)}{M_{cap}[Q(t)]}\right] \Delta t \qquad \text{for } Q > Q_c \text{ and } dQ/dt < 0 \qquad (4.23)$$

Model comparison to observations was undertaken two different ways because of constraints imposed by what validation data were available. For the Hopland site the turbidity record was not continuous in the 2014 water year with only three floods in March having continuous turbidity records for the determination of flood event releases. The first three-month period of the 2015 water year (October 1, 2014 to December 31, 2014) had continuous flow and turbidity data available for the seven flood events. Thus for Hopland the modeled mass released for each individual flood event is compared with observed mass released by that flood when available. The Guerneville site has continuous flow and turbidity data allowing for a comparison of individual flood event mass released from the sediment bed as well as the cumulated release over the entire validation period.

The overall comparison for all flood events in the validation period is given in Figure 4.13 which combines results from both the Hopland (10 flood events) and Guerneville (14 flood events) sites. In general, the Hopland flood events show less than a factor of 2 difference between the measured and modeled mass release except for the 4 smallest flood events where the modeled mass releases are considerably greater than the measurements. At Guerneville the largest flood in the validation period had a flow rate greater than Q_{max} and the estimated mass released by that flood from the bed sediments was almost twice M_{max}. The calibrated model prediction for this flood was unable to match this release. This demonstrates the importance of having a sufficiently long calibration period that includes high flow events with high particle mass releases to achieve the best estimates of M_{max} and Q_{max}. Additionally at Guerneville, the smaller floods had much greater predicted mass released than observed. As explained in previous section 4.4, this model bias in small flood events is a consequence of minimizing RSR.

Comparison of the continuous model simulation and data at Guerneville are shown in Figure 4.14 over the validation period of October 2013 to December 2014. The initial mass of fine particles in the sediment bed, *M(t)*, in October 1, 2013 is the value of *M(t)* at the end of 2013 water year. The model over predicts particle mass released from the bed sediments in the 2014 water year, but under predicts particle mass release in December 2014 due to the large flood event with peak flow rate higher than calibration parameter Q_{max} and with more mass released than M_{max}. Overall, the ratio of total modeled mass released to total observed mass release, *R*, is 0.65 and RSR is 0.72 at Guerneville while *R* is 1.11 and RSR is 0.18 for the 10 flood events at Hopland.

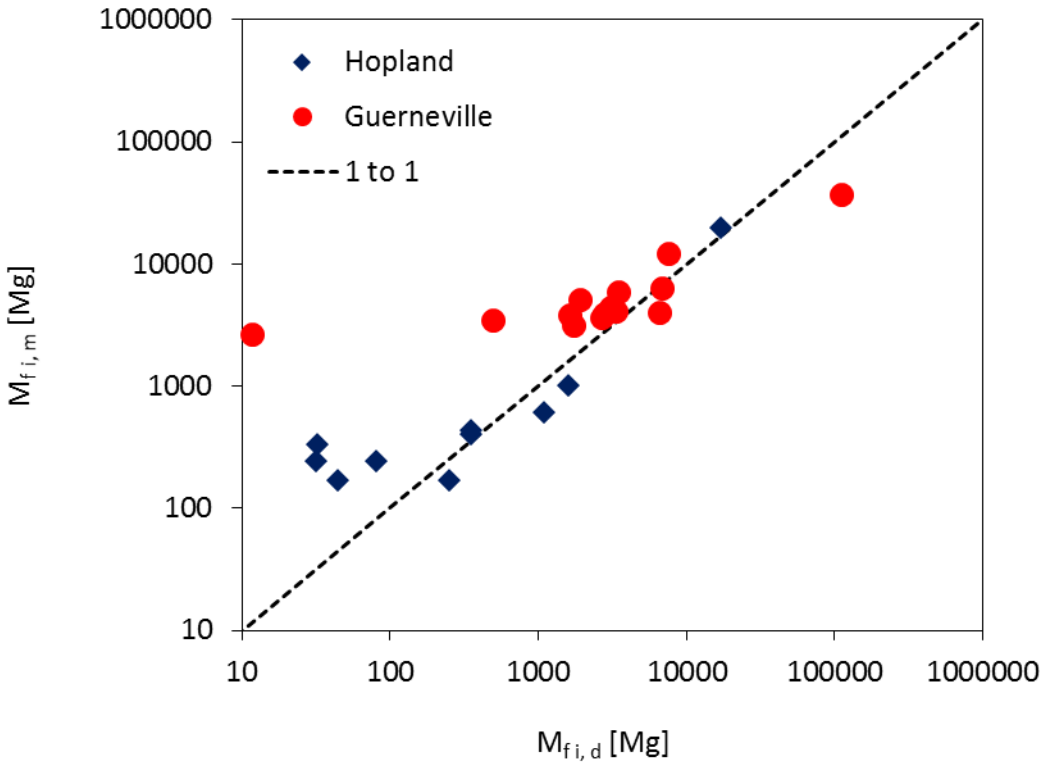

Figure 4.13. Comparison of modeled and measured mass released from individual floods in the validation period of Oct 1, 2013 to Dec 31, 2014 for Hopland and Guerneville sites on the Russian River.

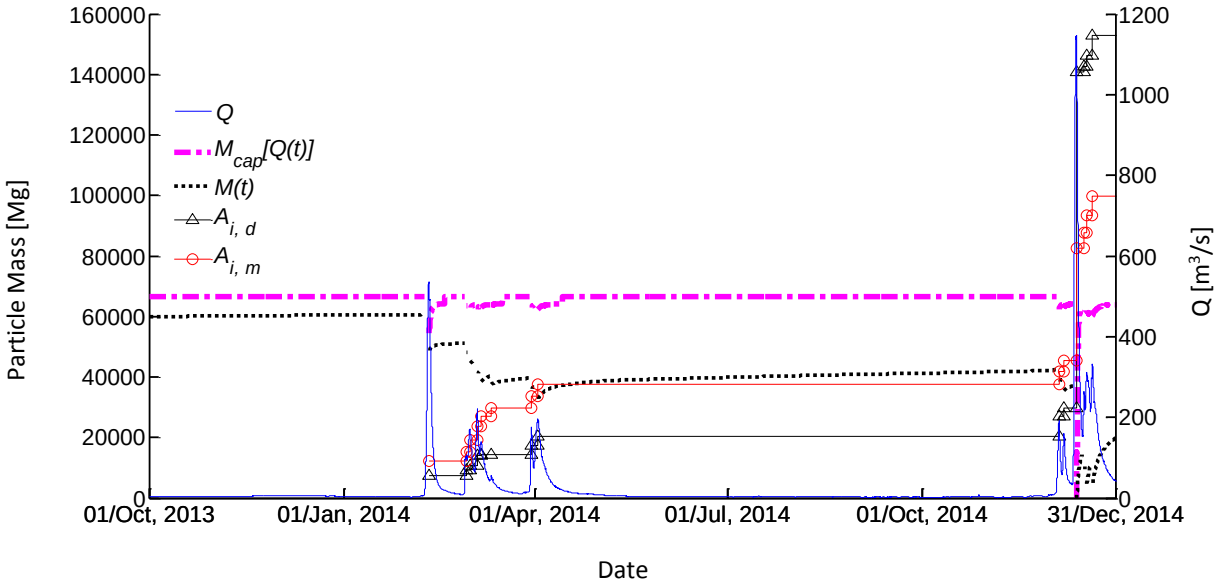

Figure 4.14. Validation test of the model with data from the Guerneville gauge on the Russian River over the period October 1, 2013 to December 31, 2014.

4.7 Model Extension

The prior section on model validation was constrained by the lack of hydrologic data fulfilling the requirements for long, continuous records of flow and turbidity at 15-minute intervals. This section provides an additional approach in model evaluation by using observed flow rates as input to the calibrated model to generate particle loading rates and examine how these generated rates compare with observations. There are two parts to this analysis. The first effort generates particle loading rates from the model and compares those predicted particle loading rates with observed loading rates when data are available. The second part is to compare the model-generated loading rates with historically observed loading rates prior to 2010 which is only available at Guerneville. As discussed in Chapter 2, there are extensive daily records of particle loading and flow rate that have considerable scatter in log Q_s vs log Q plots at Guerneville between 1967 and 1986. This analysis provides an additional examination of the stability over time of fine particle dynamics within coastal California watersheds because model calibration was done on data from 2010 to 2013 and the model results are compared with loading rates from an earlier period.

The model is as described in the prior section on model validation where only continuous flow rate and model calibration parameters are used as input. The transformation of model output into loading rate requires some clarification. During Phases 1 and 3, the loading rate is quantified as the background concentration multiplied by the flow rate. With the linear dependence of background concentration on flow rate, the particle loading rate is given by

$$Q_s(t) = C_b(t)\,Q(t) = \gamma\,Q(t)^2 \qquad \text{for Phases 1 and 3} \tag{4.24}$$

This assumes that for flow rates less than Q_c, the linear relationship is maintained between background particle concentration dependence on flow rate even though the data used in setting this relationship was for flows substantially greater than Q_c as indicated in Figures 4.6 and 4.7.

During Phase 2 with a rising flow rate of a flood event, particle mass erosion is predicted for the flood event, not continuously during the flood. As a consequence, the model will generate only one value of particle loading rate for that flood, and that loading rate is associated with the average flow rate during the rising limb of flood. The average flow rate for flood *i* is

$$\overline{Q_i} = \frac{1}{t_{e,i} - t_{s,i}} \int_{t_{s,i}}^{t_{e,i}} Q(t)dt \tag{4.25}$$

The average particle concentration during the rising limb of flood *i* is the mass released from the sediment bed, $M_{f\,i,m}$, divided by the volume of the flood event combined with the background particle concentration

$$\overline{C_i} = \frac{M_{fi,m}}{\overline{Q_i}\,[\,t_{e,i} - t_{s,i}]} + C_b(\,\overline{Q_i}\,) = \frac{M_{fi,m}}{\overline{Q_i}\,[t_{e,i} - t_{s,i}]} + \gamma\,\overline{Q_i} \tag{4.26}$$

During Phase 2 the average loading rate for flood *i* is then given by

$$\overline{Q_{s,i}} = \overline{C_i}\ \overline{Q_i} = \frac{M_{fi,m}}{t_{e,i} - t_{s,i}} + \gamma \bar{Q}_i^{\,2} \tag{4.27}$$

The model uses as input the observed flow rate, *Q(t)*, and model calibration parameters to generate $\overline{Q_i}$ and $\overline{Q_{s,i}}$ during the rising limb of flood events and $C_b(t) = \gamma\, Q(t)$ during all other times. There are missing flow rate observations for the 2014 water year at Hopland. Thus, model generated particle loading rates are only for the water years 2011 to 2013 and these are compared with available observations at Hopland for the same period in Figure 4.15. The small blue dots represent every particle loading rate calculated from the 15-minute data. The red line is the particle loading rate during Phase 1 (accumulation) and Phase 3 (accumulation while partially fluidized). Particle loading rate for the rising limb of each flood event is plotted as a single red circle. The background loading rate (red line) provides an approximate lower bound of the observations and the simulated flood events have a variability similar to the observations. Predicted particle loading rates for smaller flood events are slightly biased larger than observed. It is important to note that the flood event simulations represent average loading and average flow rates during each flood event while the blue dots are plotting continuous 15-minute data.

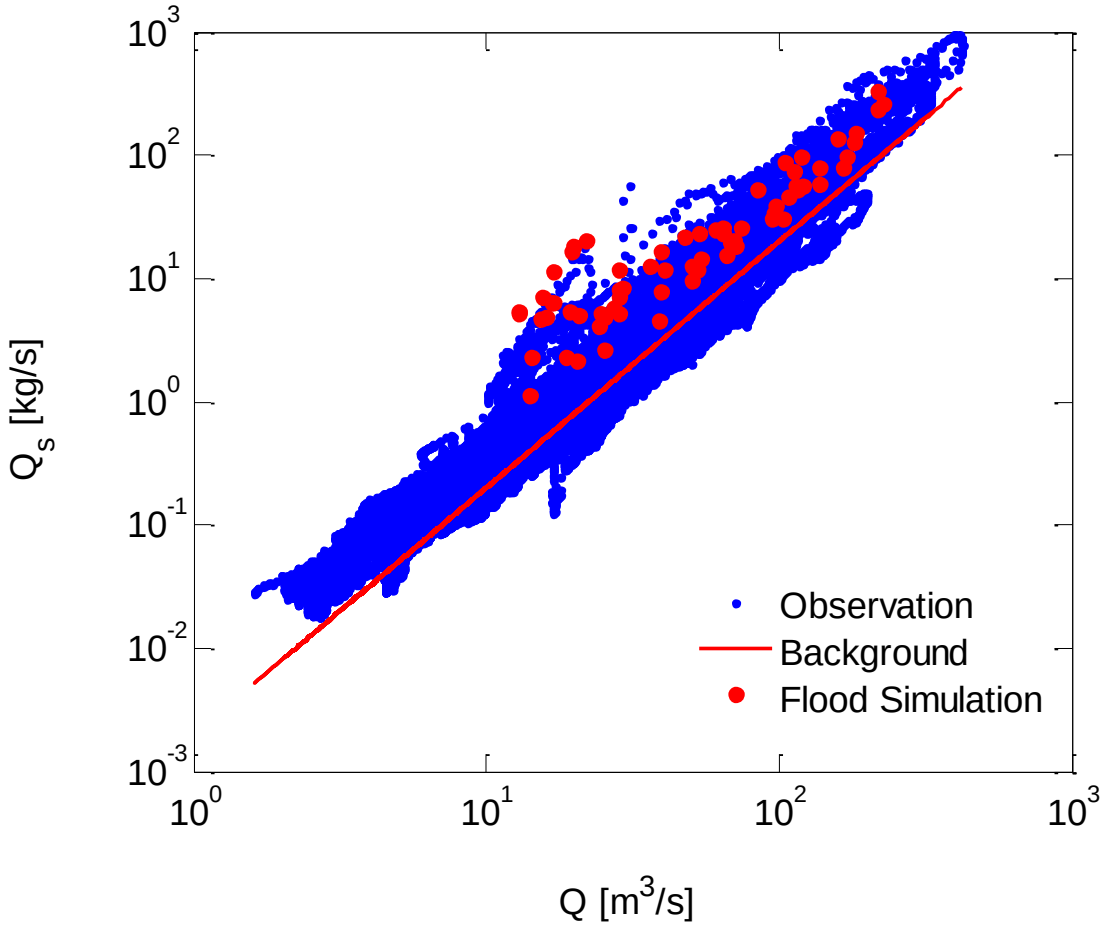

Figure 4.15. Comparison of particle loading rates determined from 15-minute observations at Hopland with the assumed background loading rate (red line) and model generated discrete flood event loading (red dots) for the water years 2011 to 2013.

For Guerneville, observed particle loading rates are compared with the model generated background and flood events in Figure 4.16. The simulation period is from Oct 1, 2009 to Dec 31, 2014. The observations, represented as blue dots, for the water years of 2010, 2013 and 2014, and from Oct 1, 2014 to Dec 31, 2014 are compared with model simulation. The fitted background particle concentration sets a lower bound on the loading rate with the red line and the modeled discrete flood events plotted as red circles generally sample the observed variability in loading rates for flood events above 100 m^3/s. For average flow rates of flood events less than 100 m^3/s, the model bias over predicts mass releases as discussed previously. In spite of this small flood event bias, the model representation of flood events and background particle concentration is able to capture the general shape of the mass loading relationship during this recent period.

Besides the comparison of model generated loading rates loading rates determined with 15-minute data, it is possible to check if loading rates generated by the model are similar to loading rates determined from daily data from an earlier period. Figure 4.17 includes the same model simulation of loading rates for floods and the background period that appeared in Figure 4.16, however the observed data were collected during the period of 1967 to 1986 on a daily basis. The daily particle loading rate data are similar to the more recently determined values from high frequency data. The result of this comparison suggests that the extended model has captured the processes that determine fine particle loading as a function of flow rate, and a continuous simulation of particle dynamics is feasible from flow rate data once calibration parameters are determined.

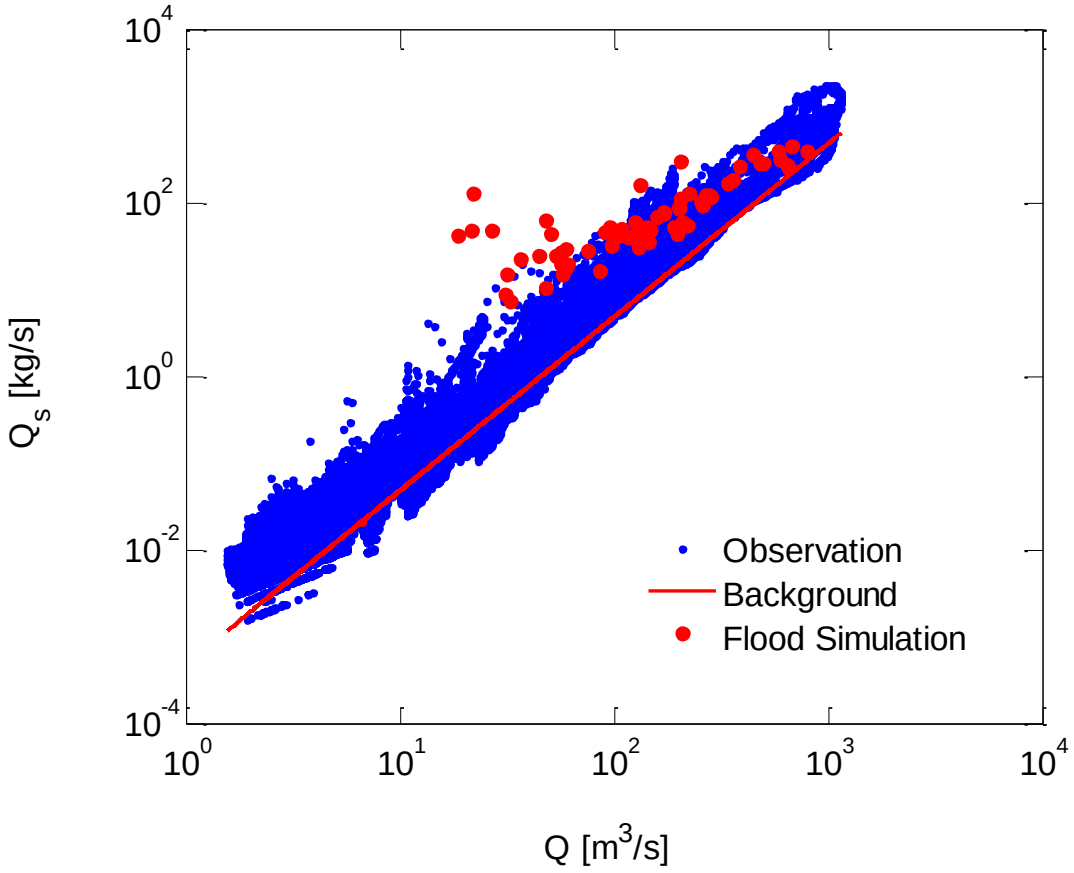

Figure 4.16. Comparison of particle loading rates determined from 15-minute observations at Guerneville for the water years of 2010, 2013 and 2014, and from Oct 1, 2014 to Dec 31, 2014 with the assumed background loading rate (red line) and model generated discrete flood event loading (red dots) from Oct 1, 2009 to Dec 31, 2014.

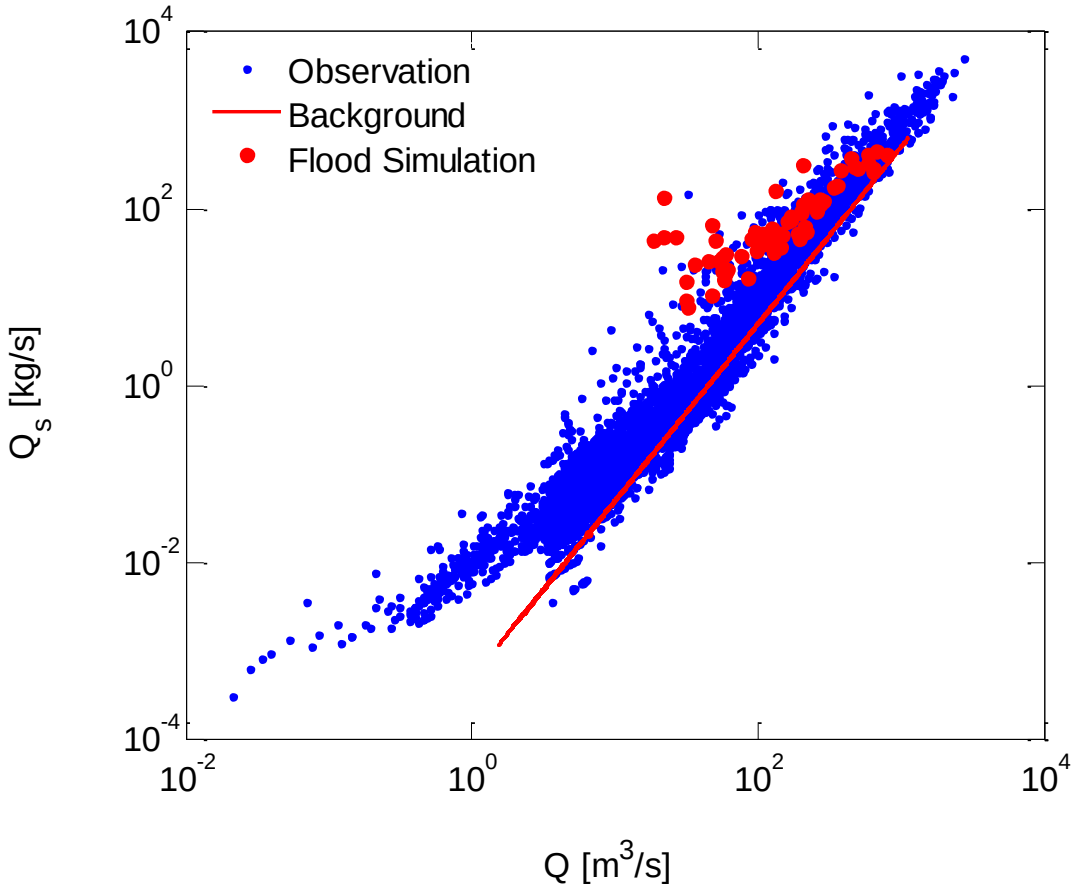

Figure 4.17. Comparison of measured particle loading rates determined from daily suspended sediment data between 1967 and 1986 with the assumed background loading rate (red line) and the model generated discrete flood event loading (red dots) at Guerneville from Oct 1, 2009 to Dec 31, 2014.

4.8 Summary

Empirical observations of fine particle transport over multiple years in California watersheds led to a model that coupled flow, particle filtration, and particle erosion by sediment bed scour. The model was limited in its parameterization and was successfully calibrated using multiple years of data at two gauging stations along the Russian River. The limited duration of the continuous data records constrained testing the model on data not used in model calibration. The model was tested in its ability to generate particle loading rates for comparison with observations during the calibration period and for historical data. The model was able to predict particle loading rates from instantaneous flow rates and calibration parameters that were similar to the observations during the calibration period. Historical daily data on particle loading rates were also replicated at higher flow rates. The prediction captured the observed fine particle loading relationship, including scatter, which has been a source of considerable interest to researchers for many years. This suggests that the pattern observed in the loading curves is a direct consequence of the coupling of fine particle transport with sediment bed erosion in dynamic processes of fine particle filtration and erosion. Chapter 5 explores model applicability to other watersheds and possible generalization of model parameters.

Chapter 5. Model Application to Other Watersheds

Chapter 4 described the development and testing of the coupled filtration and erosion model for fine particles in surface waters. This chapter provides an application of that modeling approach to other watersheds where calibration data are available. With multiple watersheds it is possible to provide a preliminary exploration of parameter dependence on watershed characteristics.

5.1 Owenabue and Bandon Watersheds in Ireland

5.1.1 Data Sources

Two watersheds in southern Ireland were the subject of fine particle transport studies described by *Harrington and Harrington* [2013]. A map of these watersheds is in Figure 5.1, and 90% of the land use in both watersheds is pasture and tillage. Flow and turbidity were measured every 15 minutes and the authors developed correlations between turbidity and suspended particle concentration. The smaller Owenabue watershed (103 km^2) has data available for September 15, 2009 to September 15, 2010 and during this period the rainfall was 97% of the mean. Bandon is the other watershed with an area of 424 km^2 and data are available for a partially overlapping period February 10, 2010 to February 9, 2011, and this period had only 72% of the mean rainfall.

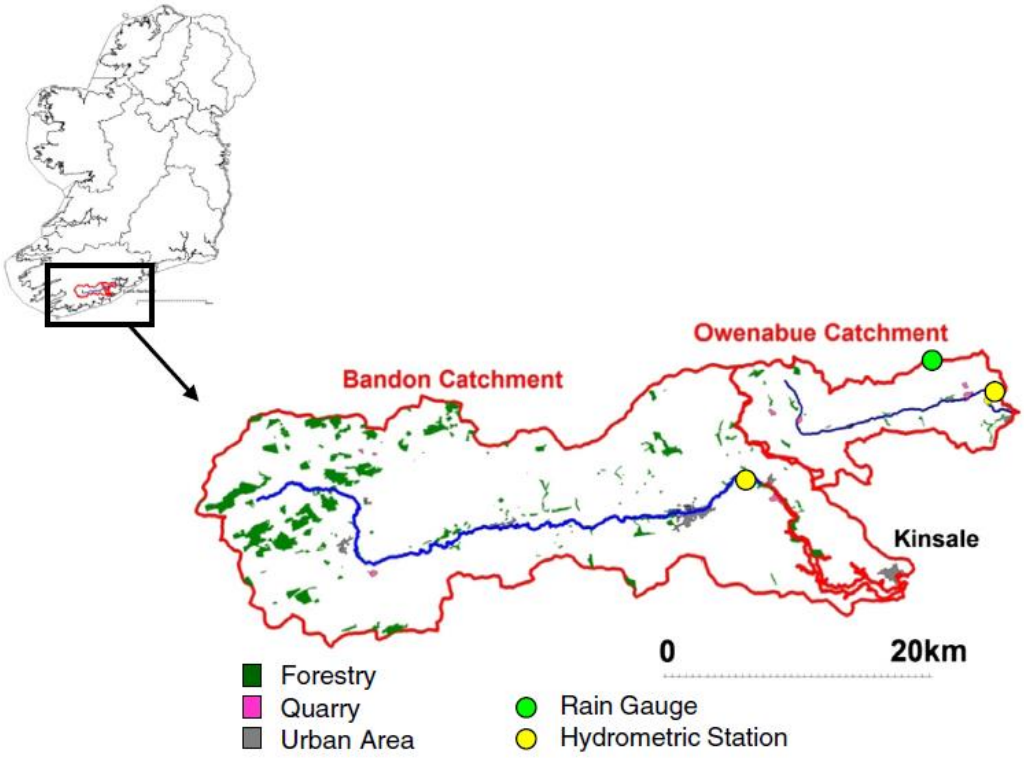

Figure 5.1. Location of Owenabue and Bandon watershed with the figure from *Harrington and Harrington* [2013].

5.1.2 Model Calibration and Sensitivity Analysis

The critical flow rates which initiate the mobilization of sediment bed material at these sites were determined from plots of particle loading rate, Q_s, as a function of flow rate, Q [Appendix C]. Though the data show considerable scatter, mild slope breaks were observed for Owenabue when Q is about 5 m^3/s and 10 m^3/s at Bandon.

Both watersheds usually had clockwise hysteresis loops when particle concentrations were plotted against flow rates for larger flood events. Non-clockwise hysteresis loops were observed under conditions where a second flow event followed only a few days after a comparable or larger flood event which depleted the fine particles accumulated in the sediment bed. The falling limb flow recessions asymptotically approached a linear relationship between suspended particle concentration and flow rate which defined the assumed background suspended particle concentration dependence on flow rate. Figure 5.2 plots the falling limb data and red lines represent the background suspended particle concentration relationships given by

$$C_b = 1.5\,Q \quad \text{(Owenabue)} \tag{5.1}$$

$$C_b = 0.1\,Q \quad \text{(Bandon)} \tag{5.2}$$

The total mass of fine particles released by each watershed was obtained by integrating the particle mass loading rate, Q_s, over the measurement period. The particle mass released from the sediment bed was estimated from the total mass released from the watershed during the rising limb of flood events minus the mass associated with the background concentration as described in section 4.3.3. The results of these calculations are in Table 5.1 with particle mass released from the sediment bed at 24 to 49% of the total suspended particle load for Owenabue and Bandon, respectively.

Table 5.1. Summary of total fine particle mass at the two watersheds in Ireland along with estimated fine particle mass released from sediment bed.

Watershed	Measurement Period	Total Particle Mass [Mg]	Particle Mass Released from Sediment Bed [Mg]	Fine Particles Released from Sediment Bed as percent of Total
Owenabue	Sept 15, 2009 - Sept 15 2010	2500	610	24%
Bandon	Feb 10 2010 - Feb 9 2011	3990	1990	49%

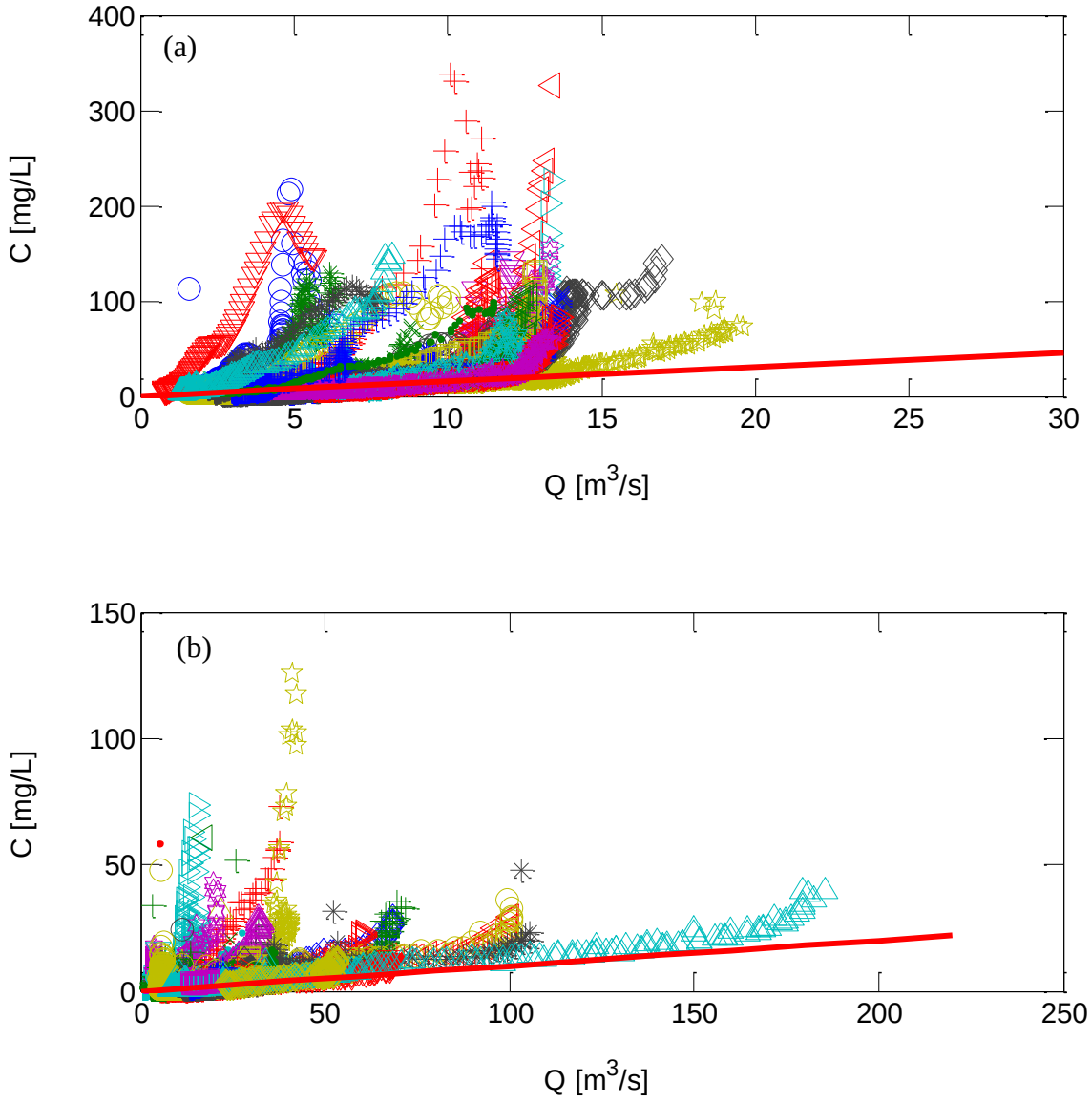

Figure 5.2. Fine particle concentrations data during falling limb recession for watersheds in Ireland (a) Owenabue and (b) Bandon. The plotting symbols represent different flood events. The red lines are the assumed linear dependence of background suspended particle concentration on flow rate given by equations (5.1) and (5.2).

The maximum fine particle storage capacities (M_{max}) in the sediment bed were also determined by the same method used for the sites in the Russian River watershed as in section 4.3.3 and 4.3.4. Table 5.2 includes the values of M_{max} estimated from the maximum fine particle mass released from sediment beds where the peak flow rates are Q_{max}.

Table 5.2. Model parameters for the watersheds in Ireland determined from watershed data

Watershed	Q_{max} [m^3/s]	M_{max} [Mg]	Date
Owenabue	20	100	Nov 20, 2009
Bandon	110	430	Dec 28, 2010

Optimal values of the filtration and scour parameters for the Owenabue and Bandon watershed were determined through a gridded search minimizing RSR similar to the approach adopted for the Russian River watersheds. Figure 5.3 demonstrates that the model is relatively insensitive to the filtration parameter for both watersheds as long as the filtration parameter was greater than 50 m^3/s at Owenabue and greater than 400 m^3/s at Bandon. Optimal parameter values are listed in Table 5.3 along with goodness of fit RSR statistics. There are very close agreements between the modeled total fine particle masses released by the sediment beds and the observed masses released.

Table 5.3. Optimization of the model for the two watersheds in Ireland

Watershed	Area [km^2]	Optimal Parameters		Measurement Period	RSR	R
		α [m^3/s] (lower bound)	β (range)			
Owenabue	103	200 (>50)	4.2 (4 - 4.5)	Sept 15, 2009 - Sept 15 2010	0.47	0.99
Bandon	424	600 (>400)	4.5 (4 - 5)	Feb 10 2010 - Feb 9 2011	0.33	1.00

The comparison of accumulated mass released from the sediment bed obtained from measurements and the model over the yearlong simulations are included in Figure 5.4. There were 32 flood events at Owenabue and 34 flood events at Bandon with the modeled mass released being very close to the measured mass released for each flood event in each watershed.

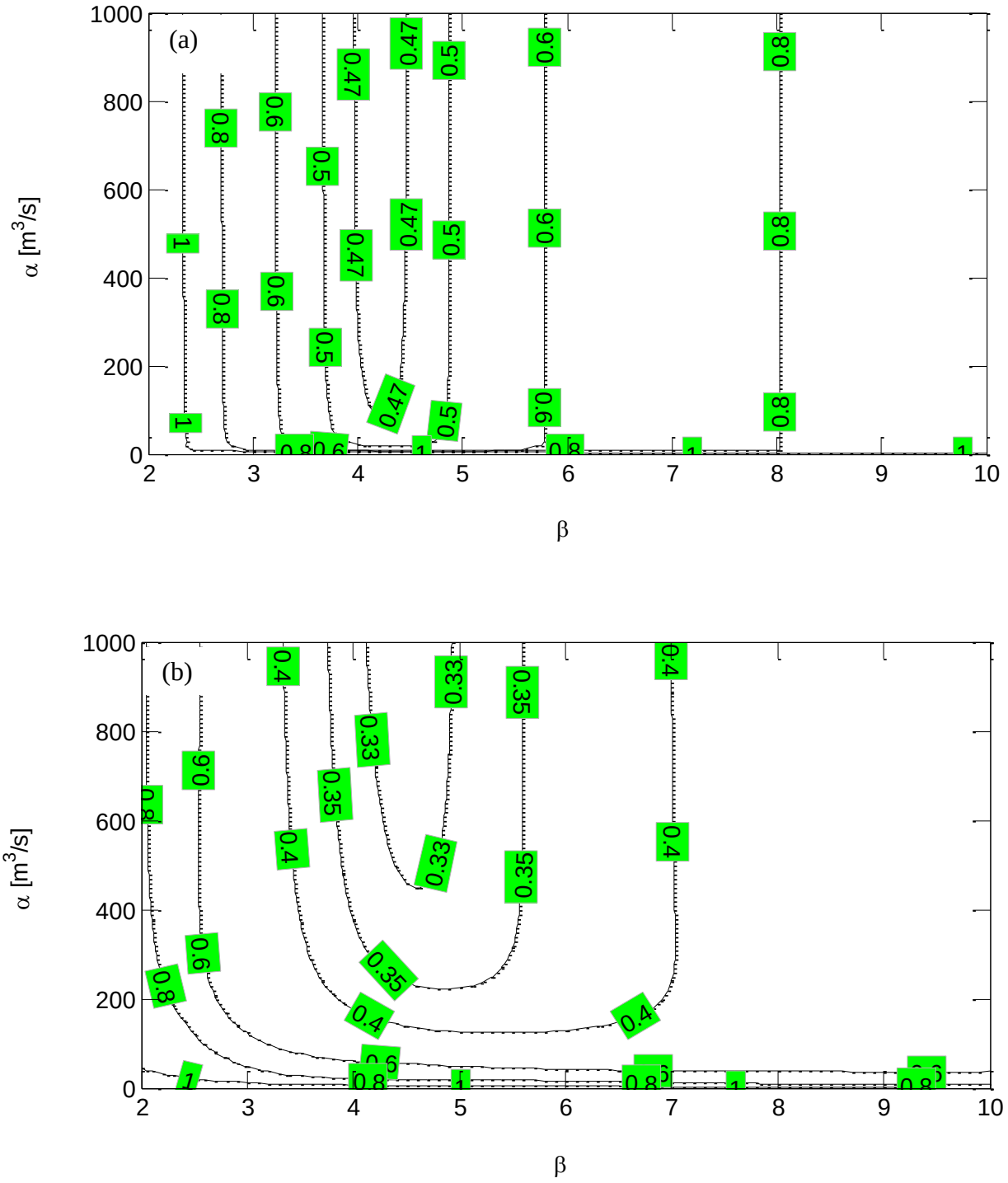

Figure 5.3. Model sensitivity to filtration (α) and scour (β) parameters using contours of RSR for the two watersheds in Ireland (a) Owenabue and (b) Bandon.

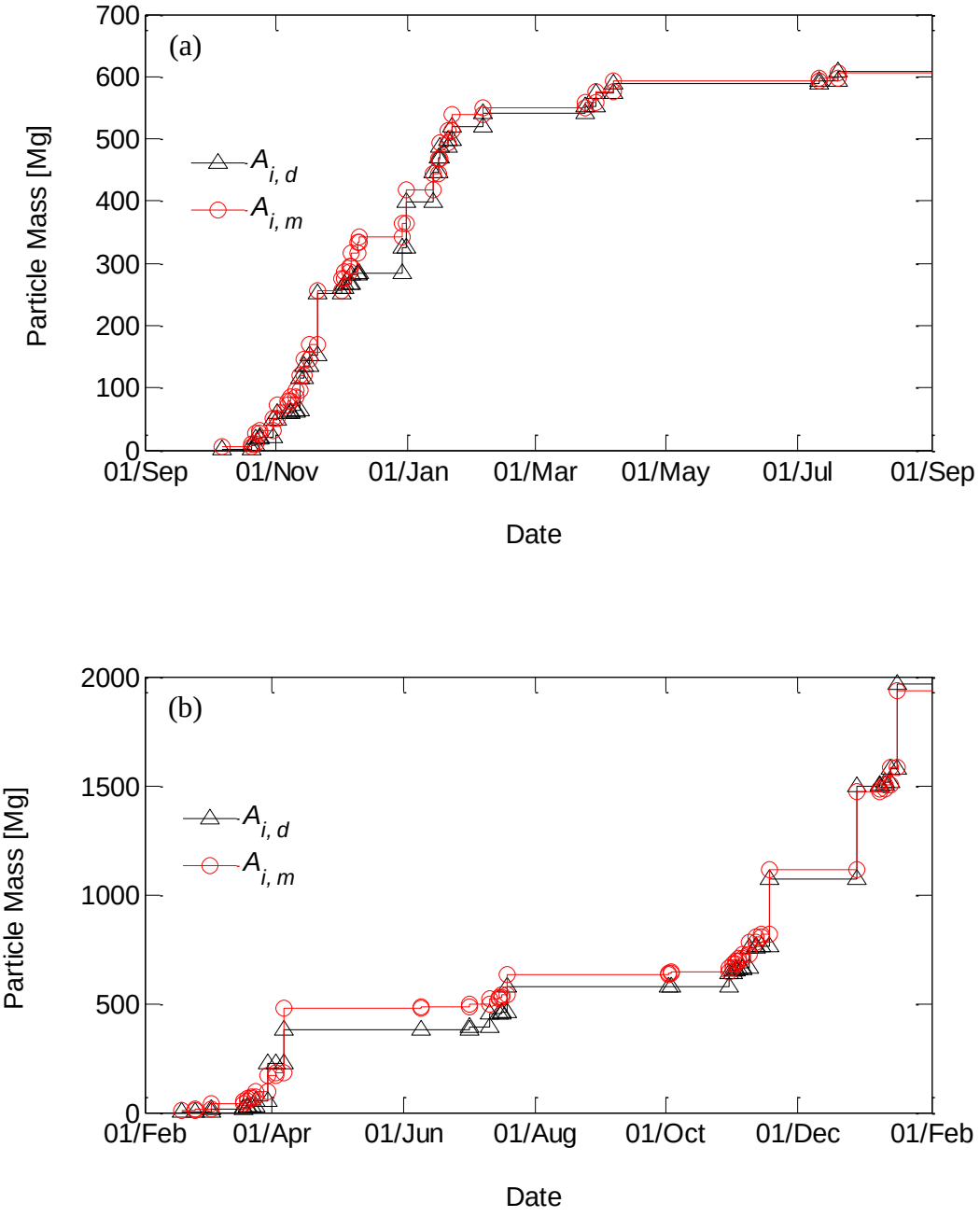

Figure 5.4. Cumulative mass of fine particles released from the sediment bed based on data ($A_{i,d}$) and the model ($A_{i,m}$) for the watersheds in Ireland (a) Owenabue and (b) Bandon.

5.2 Moulinet and Violettes Watersheds in France

Two small watersheds in northwestern France were extensively instrumented to quantify flow and fine particle release for over a year at each location. The Moulinet watershed has an area of 4.5 km^2 and Violette has an area of 2.2 km^2 with the climate characterized as temperate (Figure 5.5). The land is used extensively for dairy cattle farming including pastures, and cattle disturbance has been associated with bank erosion and increased suspended sediments in the stream waters. *Birgand et al.* [2004] describe the instrumentation installed within the watersheds and *Lefrancois et al.* [2007] present the results of their data analysis.

5.2.1 Data Source

Turbidity sensors were installed at the outlet of each watershed, and suspended particle concentration were estimated from the correlation between turbidity and suspended particle concentration. The flow rate was determined from the flow velocity measured by the Doppler Effect multiplied by the wetted cross section of the flume. The flow rate and suspended sediment concentration were measured every 30 seconds, and 10-minute average values were reported. Dr. Francois Birgand (North Carolina State University) and Dr. C. Grimaldi (INRA, UMR Sol-Agronomie-Spatialisation, Rennes cedex, France) provided the data. Continuous data are available for the Moulinet watershed from July 1, 2002 through June 30, 2003 and from October 1 through December 10 in 2007. Other data within 2008 were excluded because the record was not continuous. The Violettes data are continuous from June 1, 2002 through May 31, 2003.

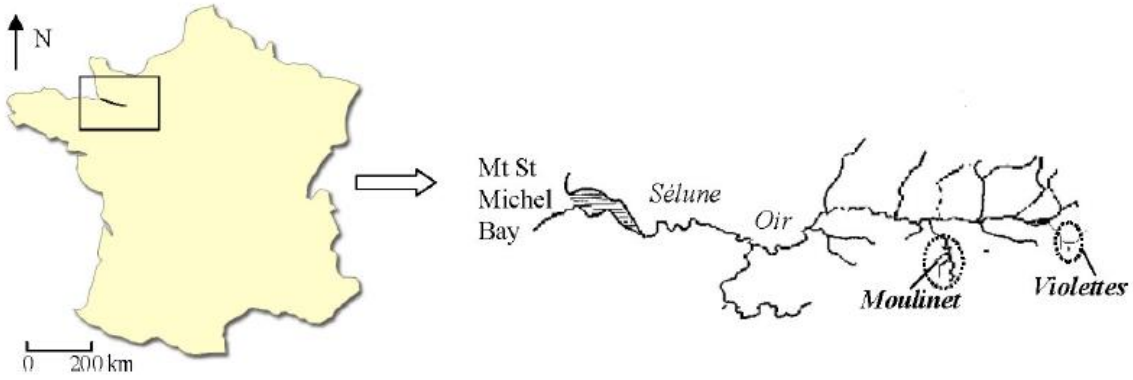

Figure 5.5. Location of Moulinet and Violettes. Figure from *Lefrancois et al.* [2007].

5.2.2 Model Calibration and Sensitivity Analysis

The critical flow rates which initiate the mobilization of channel bed material at both sites were determined from plots of particle loading rate as a function of flow rate [Appendix D]. Though the data show considerable scatter, mild slope breaks were observed at flow rates of 0.1 m^3/s at Moulinet and 0.05 m^3/s at Violettes. There were no reported data on sediment bed size distributions or channel cross sectional information to provide an independent assessment of the critical flow rates for initiation of sediment bed motion.

The background suspended particle concentration relationships are also estimated by the analysis of hysteresis data. Clockwise hysteresis loops were generally observed in larger flood events when the peak flow rates were above 0.2 m^3/s at Moulinet, and above 0.1 m^3/s at Violettes. Similar to other watersheds in the Russian River and the two sites in Ireland, no clockwise loops were observed in floods immediately following large floods which suggests the depletion of accumulated fine particles in the sediment bed. Falling limb flow recessions also had evidence of an asymptotic background suspended solids concentration linearly dependent upon flow rate as

$$C_b = 300\ Q \quad \text{(Moulinet)} \tag{5.3}$$

$$C_b = 4000\ Q \quad \text{(Violettes)} \tag{5.4}$$

with these relationships plotted as the red lines in Figure 5.6. There is considerable variability in the background relationship within each watershed and between watersheds. Unlike the two nested watersheds within the Russian River where comparable runoff conditions had similar background suspended particle concentrations, the estimated background suspended solids concentrations at Violettes would be six times that of Moulinet at comparable runoff rates. Appendix D contains more detailed plots for the falling limb recession data over the particle concentration range of 0 to 2000 mg/L and shows reduced background concentrations in the winter for the Violettes watershed.

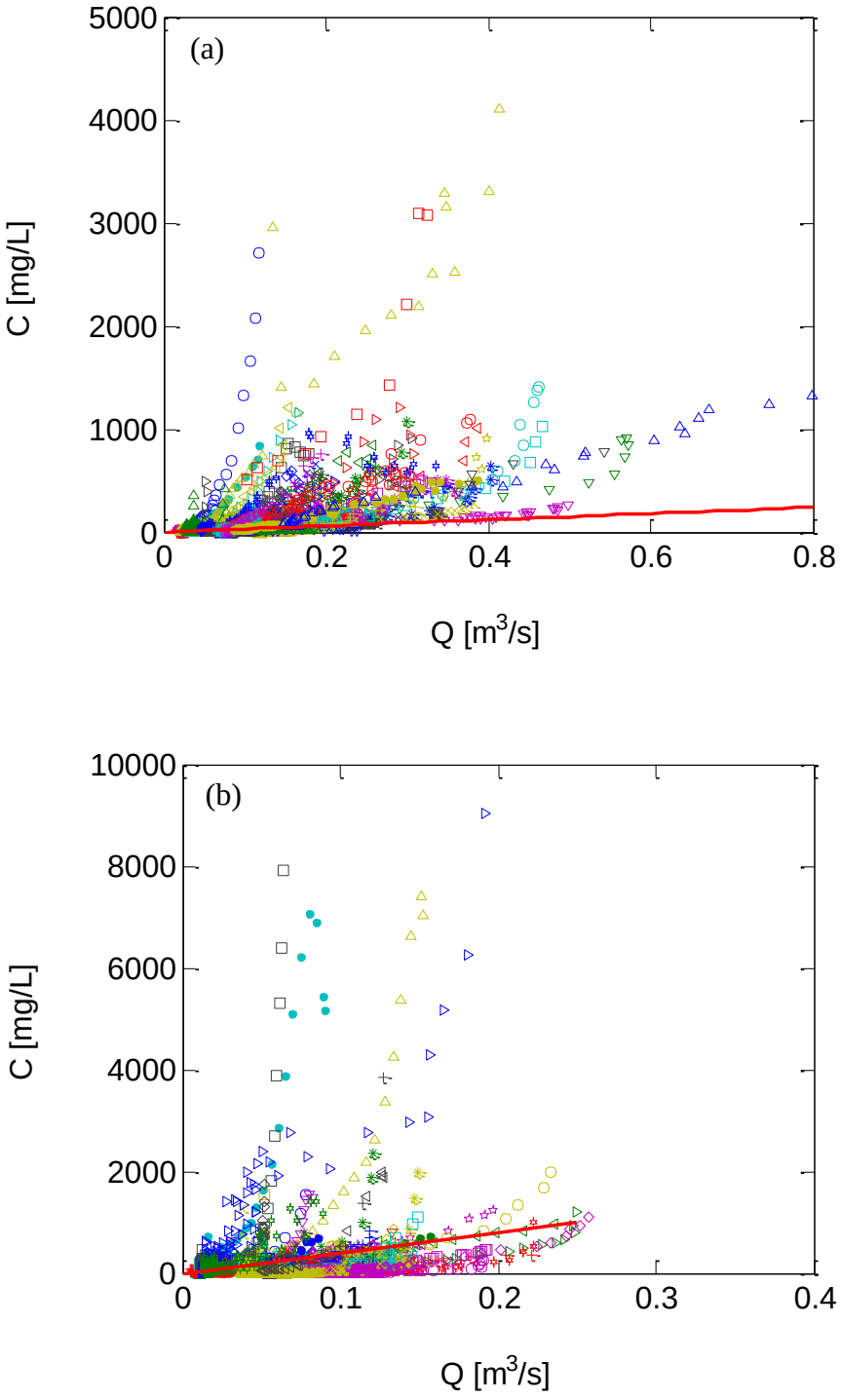

Figure 5.6. Fine particle concentration data during falling limb recession in the French watersheds (a) Moulinet and (b) Violettes. The plotting symbols represent different flood events. The red lines are the assumed linear dependence of background suspended particle concentration on flow rate given by equations (5.3) and (5.4).

The total masses of fine particles released from the two French watersheds were calculated by integrating the measured particle loading rates over the measurement periods. These masses were compared with the estimated masses of fine particles released from the sediment beds during flood events that utilized equation 4.14a. The results appear in Table 5.4 and indicate, as expected, that Violettes had much greater watershed contribution to fine particle release than what was released from the bed sediments. The fine particle mass released from the Moulinet sediment bed in 2003 is approximately twice the mass released by Violettes for the same period. This is reassuring given the watershed area for Moulinet is twice that of Violettes.

Table 5.4. Summary of total fine particle mass at the two watersheds in France along with estimated fine particle mass released from sediment bed

Watershed	Measurement Period	Total Particle Mass [Mg]	Particle Mass Released from Sediment Bed [Mg]	Fine Particles Released from Sediment Bed as Percent of Total
Moulinet	July 1, 2002 - June 30, 2003	116	39	33%
	Oct 1, 2007 - Dec 10, 2007	35	15	44%
Violettes	June 1, 2002 - May 31, 2003	144	23	16%

The maximum fine particle storage capacity (M_{max}) is also determined by the same method used for the sites in Russian River watershed. The values of M_{max} are estimated from the maximum fine particle masses released from sediment bed during the period of record. The peak flow rate at this flood event is taken as Q_{max}. These model input parameters are summarized in Table 5.5.

Table 5.5. Model parameters for the watersheds in France determined from watershed data

Watershed	Q_{max} [m^3/s]	M_{max} [Mg]	Date
Moulinet	0.32	4.9	May 17, 2003
Violettes	0.23	5.0	Nov 23, 2002

The calibrated model can be fit to the observations in these two watersheds with model sensitivity to the filtration and scour parameters shown in Figure 5.7 as contour plots of RSR. Compared to other watersheds, the model calibrations are more sensitive to the filtration parameter than the scour parameter as summarized in Table 5.6. Additionally, the scour parameter for

Moulinet is far larger than for Violettes, something not expected based on the results for the Russian River and Ireland watersheds. Figure 5.8 plots the cumulative fine particle mass released from the sediment bed based on observational data and the optimal model. In general the model tracks the observed release of fine particles from the sediment bed, although for Violettes in September and October there are two observed particle release events that do not have any significant modeled release. This underestimation of model performance may be related to the additional supply of sediment by episodic events such as bank erosion related to cattle trampling in riparian pastures generally from March to October [*Lefrancois et al.*, 2007]. Though the model tends to underestimate the observations for Moulinet in 2008, the period of observation was only two months. The combined 14 month period for Moulinet had an overall RSR = 0.69.

Table 5.6. Optimized model for the two watersheds in France

Watershed		Optimal Parameters (Multi-year)			Measurement Period	RSR	*R*
Site name	Area [m^3/s]	α [m^3/s] (range)	β (range)	RSR			
Moulinet	4.5	0.085 (0.07 - 0.10)	15.8 (12 - 18)	0.69	July 1, 2002-June 30, 2003	0.43	0.83
					Oct 1, 2007-Dec 10, 2007	1.33	0.68
Violettes	2.2	0.013 (0.01 - 0.02)	5.7 (5 - 7)	0.73	June 1, 2002-May31, 2003	0.73	0.90

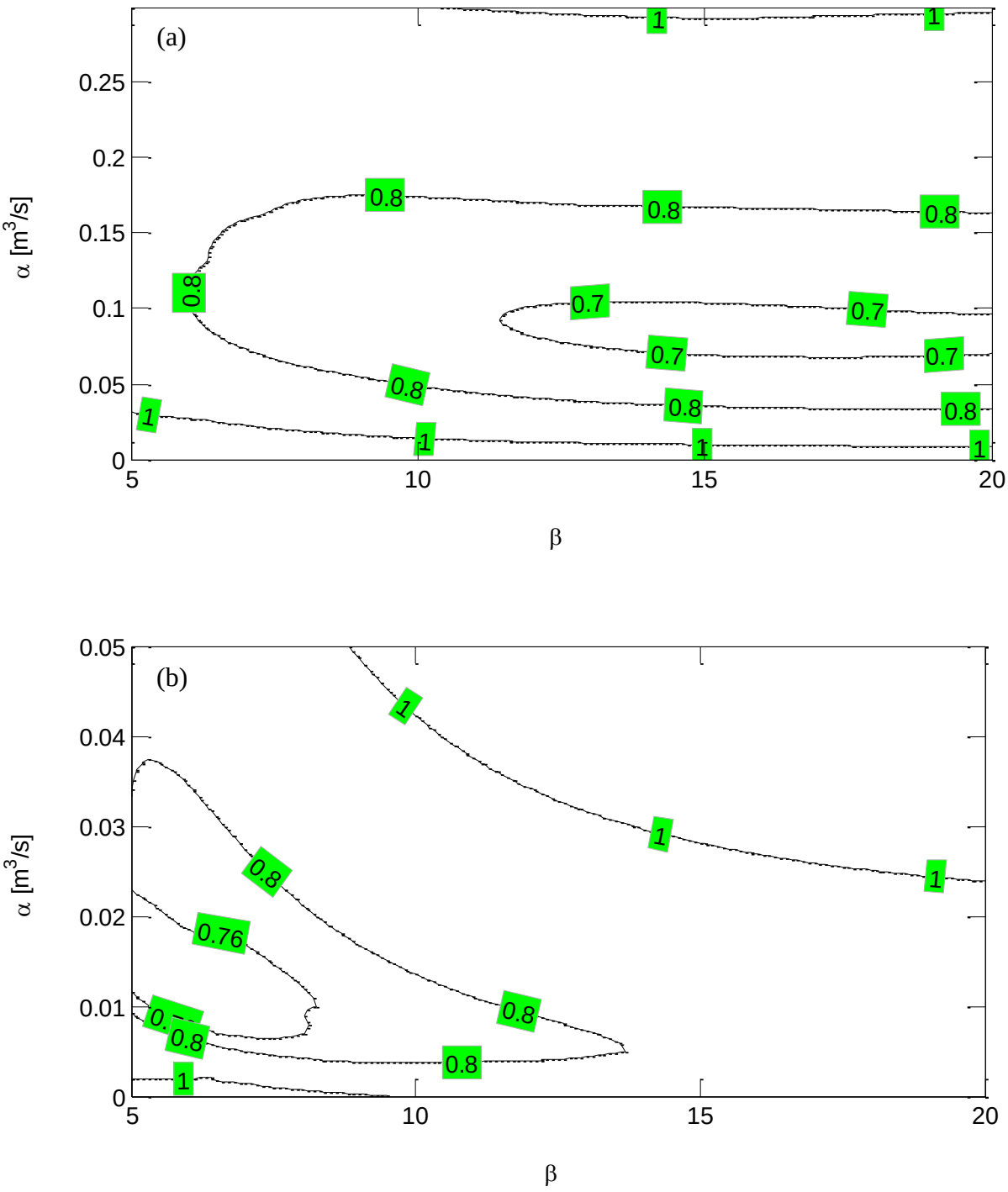

Figure 5.7. Model sensitivity to filtration (α) and scour (β) parameters using contours of RSR for the two watersheds in France (a) Moulinet combining measurements in 2003 and 2008 and (b) Violettes in 2003.

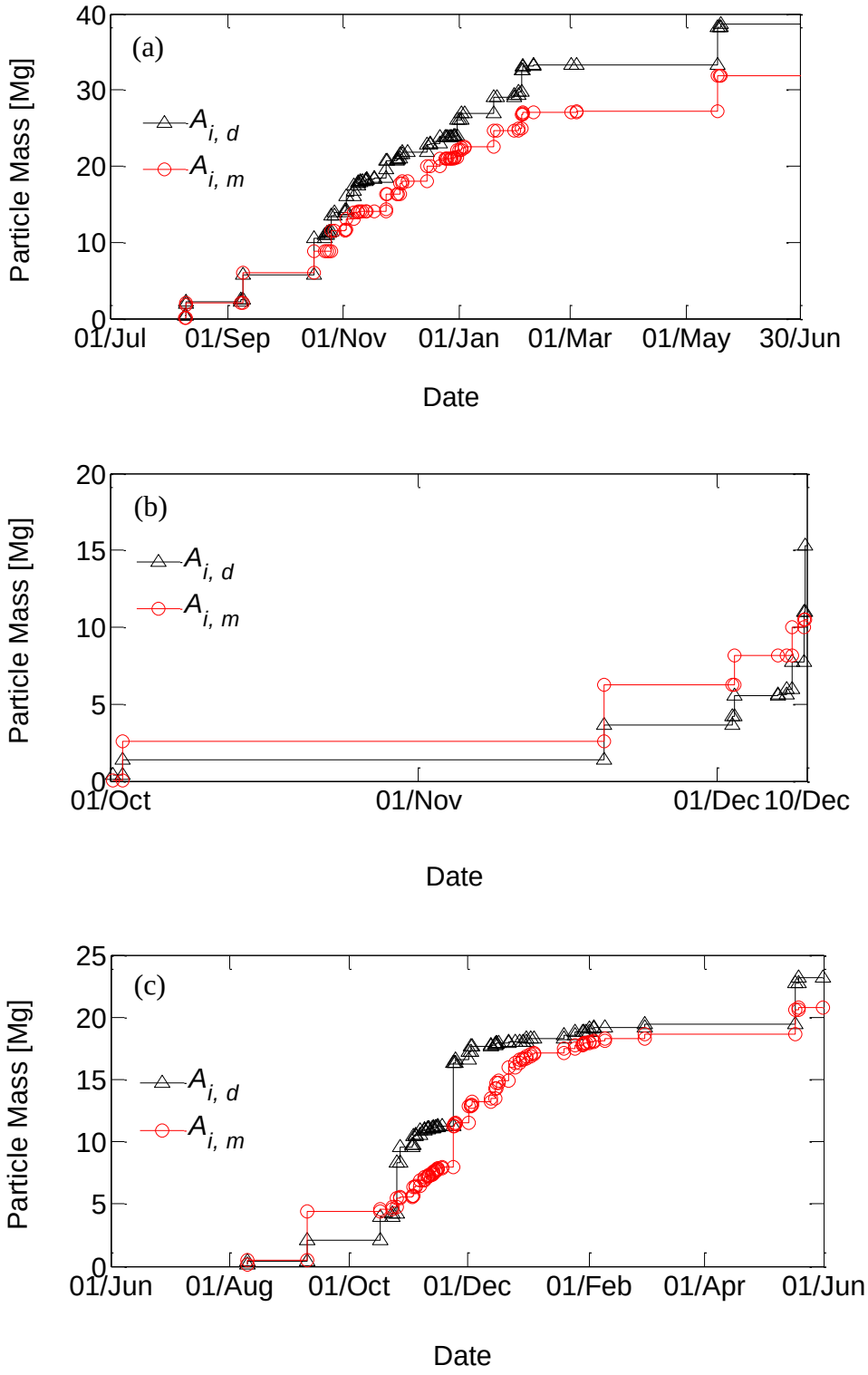

Figure 5.8. Cumulative mass of fine particles released from sediment bed based on data ($A_{i,d}$) and the model ($A_{i,m}$) for watersheds in France (a) Moulinet from July 2002 through June 2003, (b) Moulinet from October 2007 through December 2007, and (c) Violettes from June 2002 through May 2003.

5.3 Incline Creek in Lake Tahoe Basin

As reviewed in Chapter 3 snowmelt and glacial melt dominated streams have periodic flow rates and corresponding fine particle concentration fluctuations. These conditions provided an extreme test of the model given there are only 24 hours between flood events and higher elevation watersheds are unlikely to have soils and gravel bedded streams as encountered in the other watersheds.

5.3.1 Data Sources

The model for fine particle storage and release from the sediment bed was applied to Incline Creek watershed which drains into the Lake Tahoe basin in Nevada (Figure 5.9). The watershed area is 7.4 km^2 and the gauge elevation is 2100 m suggesting winter precipitation was present as snow. *Langlois et al.* [2005] analyzed 15-minute flow rate and suspended particle concentration data at this watershed over a 54-day interval in April and May in 2000, and kindly provided the data for model comparison. The flow rate was measured by USGS (site number: 103366993) and continuous suspended particle concentrations were estimated from continuous turbidity data. The turbidity readings were converted to suspended particle concentrations using a site-specific calibration curve. The flow rate during this period had daily cycles reflecting snowmelt conditions and other periods where cold waves reduced daily periodicity (Figure 5.10). The earlier arrival of suspended sediment peaks compared to peak flow rate gave clockwise hysteresis loops in almost all flood events.

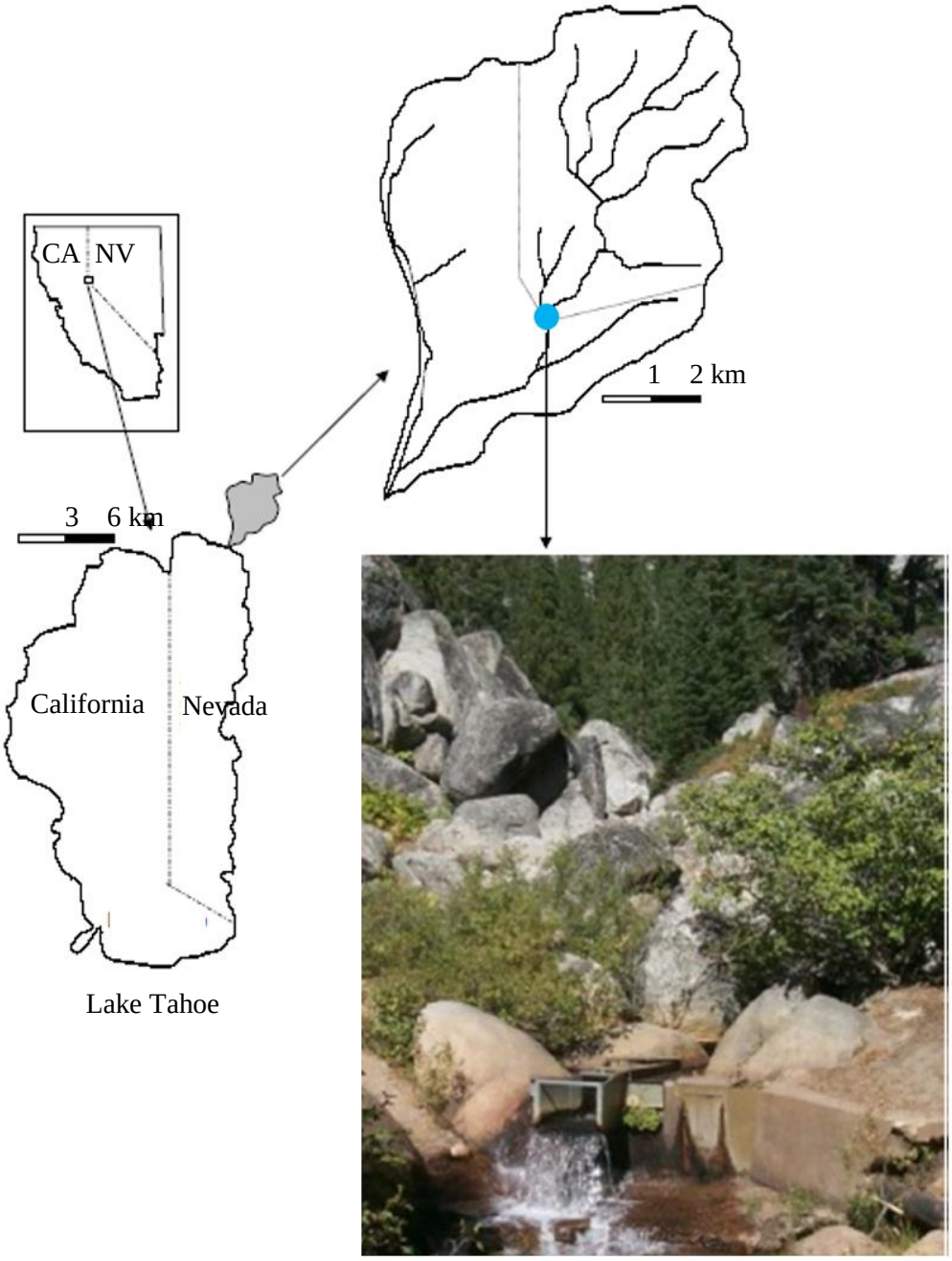

Figure 5.9. Location of Incline Creek. Original figure from *Langlois et al.* [2005]. The broken line represents the limit of the sub-watershed and the blue dot (●) represents the location of measurements.

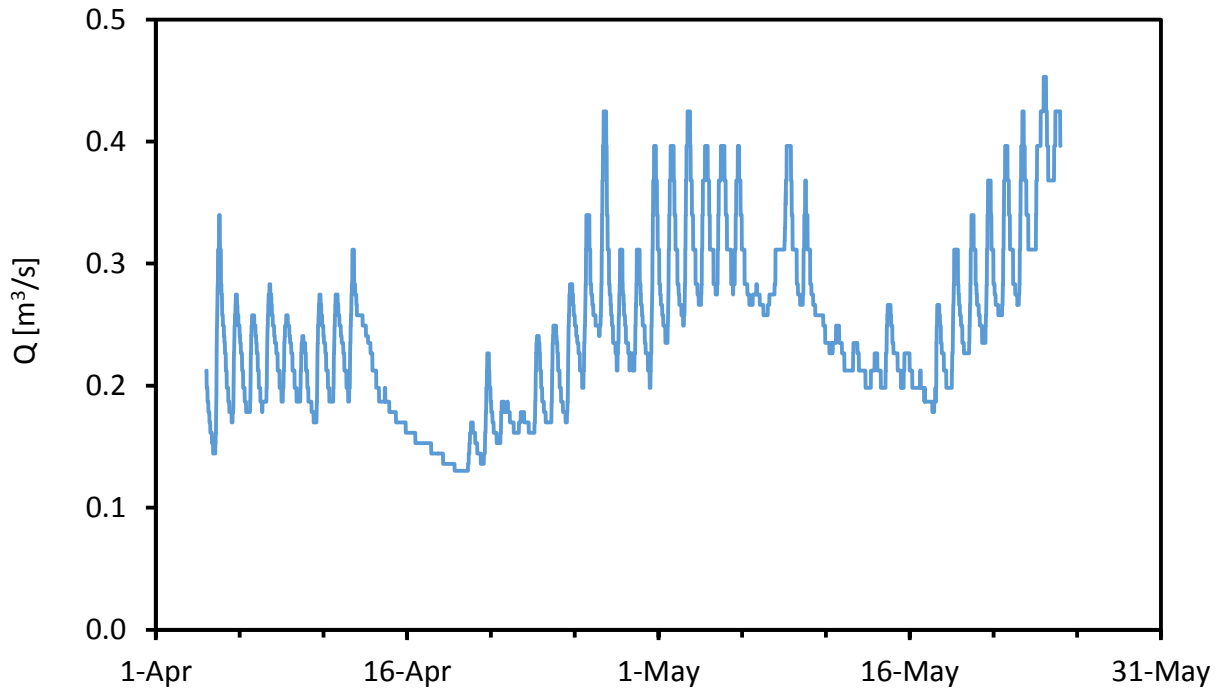

Figure 5.10. Flow rate in Incline Creek, Nevada during sampling period in year 2000.

5.3.2 Model Calibration and Sensitivity Analysis

Although the particle loading versus flow rate plot has considerable scatter, there is a mild slope break when the flow rate is around 0.2 m^3/s which is taken as the critical flow rate, Q_c [Appendix E]. The falling limb recession flow rates during the sampling period are plotted in Figure 5.11, and unlike other watershed data, the range in flow rates is rather small from 0.15 to 0.45 m^3/s. Additionally for this USGS gauging site, flow rates above 10 cfs (0.28 m^3/s) are reported only to within 1 cfs (0.028 m^3/s) leading to limited resolution of the recession curve and the appearance of data aligned vertically beyond flow rates of 0.28 m^3/s in Figure 5.11. An estimate of the background suspended particle concentration is represented by the red line in Figure 5.11 which is

$$C_b = \ 100\ (\ Q - 0.20) \qquad \text{(Incline Creek)} \tag{5.5}$$

The total mass of fine particles released by Incline Creek was obtained by integrating the particle loading rate over the sampling interval. The estimated contribution from the sediment bed is obtained by integrating the particle loading rate in excess of the background loading rate over the rising limb of all flood events. The particle mass released from the sediment bed by all snowmelt floods is 2.1 Mg, which is 18% of total particle mass transported during measurement period, 11.9 Mg.

Following procedures adopted in the other watersheds, the model parameters were determined by inspection of the data to determine M_{max} and Q_{max}, assuming an initial fine particle mass of M_{max} at the start of the sampling period, and α and β parameter optimization by minimizing RSR. Table 5.7 summarizes the model parameters and statistical evaluation of the optimal fit along with the ratio of total modeled mass release to observed mass release (R). The contours of RSR for various filtration and scour parameter values are in Figure 5.12 and show the model is sensitive to both of these parameters. The cumulative fine particle mass lost from the sediment bed according to the observational data and the model are plotted in Figure 5.13 with a good overall agreement, but there is one instance where modeled particle loss precedes by one day the observed particle loss in late April, and another case in late May where the model shows a gradual rise in cumulative mass loss while the observational data suggest a release over only a single day.

Table 5.7. Optimization of the model for the Incline Creek watershed

Observed Model parameters		Optimal Parameters		Measurement Period	RSR	R
M_{max} [Mg]	Q_{max} [m^3/s]	α [m^3/s] (range)	β (range)			
0.3	0.34	0.14 (0.1 - 0.17)	6.3 (6 - 7)	April 4-May 24, 2000	0.86	0.96

Model results are sensitive to the assumption that initial mass of fine particles in the sediment bed is M_{max}. For the other watersheds, the start of simulation was usually following a relatively dry

season with the expectation that the sediment bed would have had time to accumulate the maximum mass of fine particles. For Incline Creek, snowmelt started about March 15, 2000 while the turbidity data became available 20 days later on April 4, 2000. Thus, there was about 3 weeks of active snow melting before the turbidity measurement started. This suggests that fine particle mass stored in the sediment bed could be smaller than M_{max}. However, manipulation of the initial condition opened up considerable difficulties in evaluation and justification.

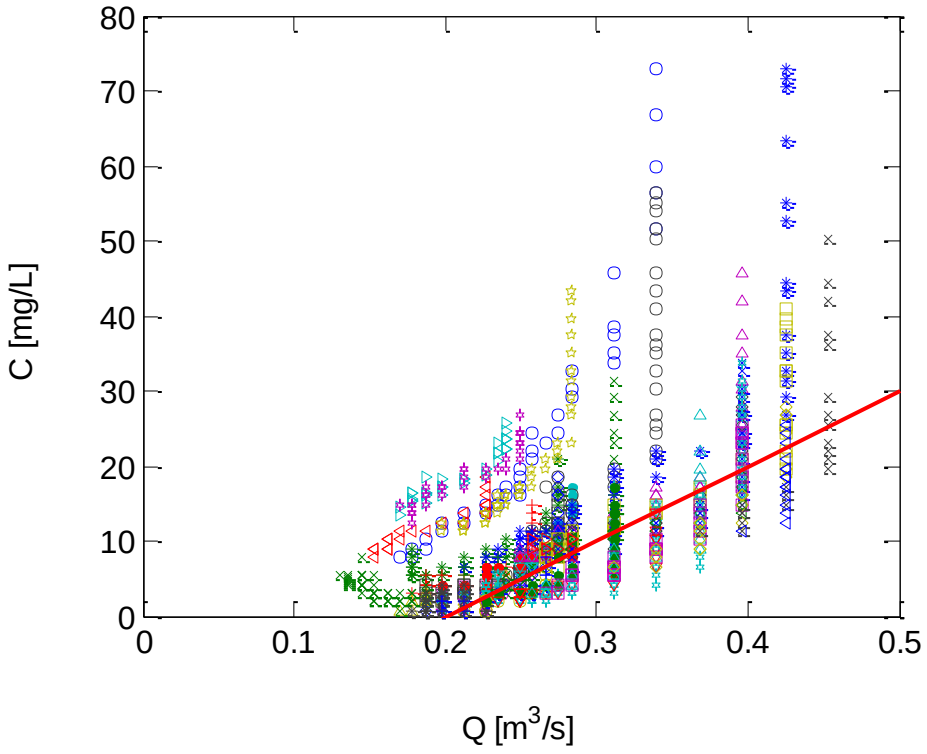

Figure 5.11. Fine particle concentration data during falling limb recessions in Incline Creek, Nevada. Different colored symbols represent different snowmelt events. The red line is the assumed linear dependence of back suspended particle concentration on flow rate given by equation 5.5.

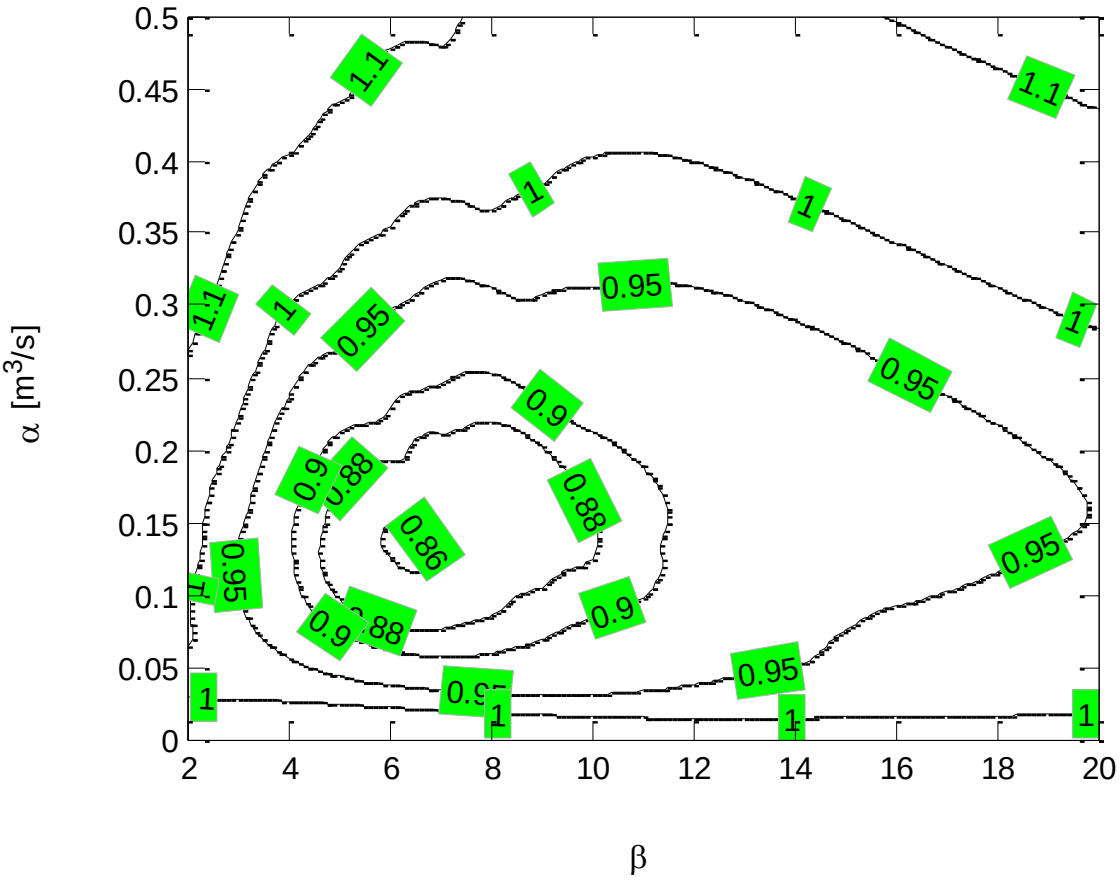

Figure 5.12. Model sensitivity to filtration (α) and scour (β) parameters using contours of RSR at the Incline Creek, Nevada.

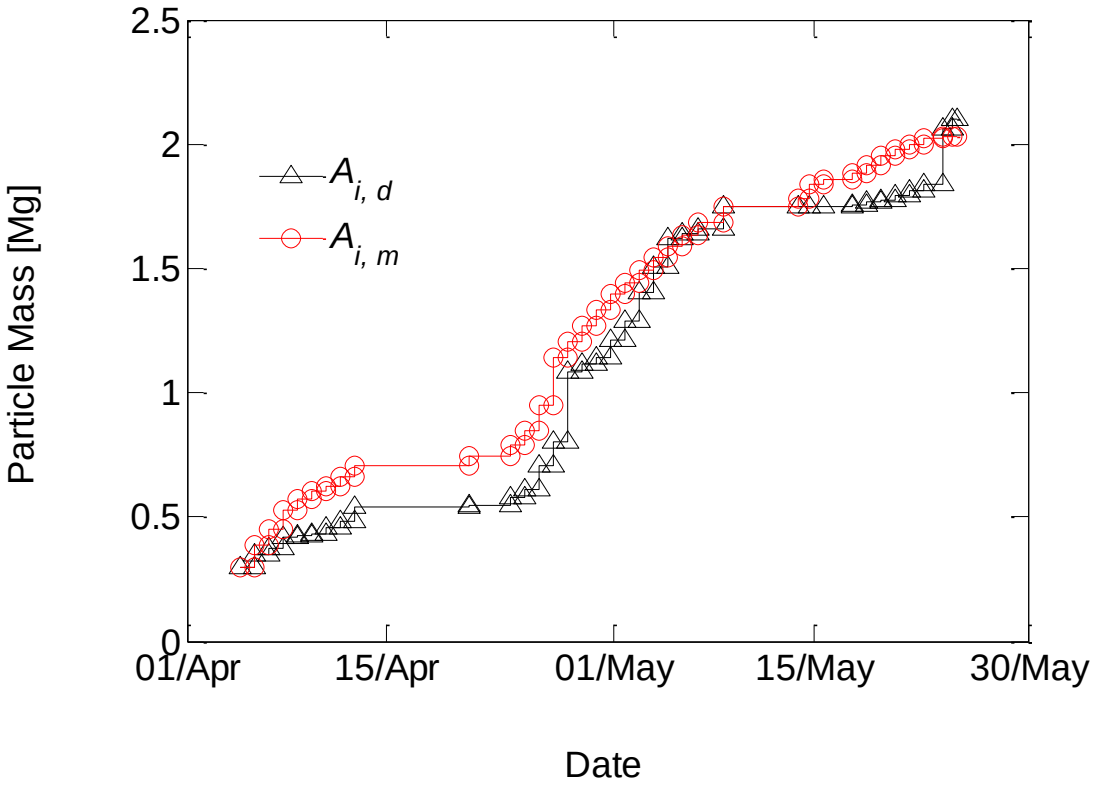

Figure 5.13. Cumulative mass of fine particles released from sediment bed based on data ($A_{i,\,d}$) and the model ($A_{i,\,m}$) for Incline Creek, Nevada from April 4 to May 25, 2000.

5.4 Meuse River at the Belgian-Dutch Border

The Meuse River basin in Europe provides an opportunity to test the applicability of the model for a larger watershed where only daily data are available. Since model parameter identification requires resolution of rising and fall limbs of individual flood events, daily data are only appropriate for watersheds that respond slowly. The daily observations in the Meuse watershed with an area of about 21,000 km^2 were successfully utilized for model calibration and validation.

5.4.1 Data Sources

Fifteen years of daily observations of flow rate and suspended sediment concentration were downloaded for the period of 1995 to 2010. The data were collected at the Eijsden gauging station which is located at the at the Belgian-Dutch border. The Dutch Institute for Inland Water Management and Waste Water Treatment (RIZA) provide electronic access to the data at [http://live.waterbase.nl]. Weekly data are available prior to 1995, and higher frequency flow data are available after 2010. Professor Hans Middelkoop at Utrecht University, the Netherlands, kindly provided the link to the flow and suspended particle data. *Doomen et al.* [2008] described the length of Meuse River at about 935 km with a watershed area of about 36,000 km^2. Upstream of the Eijsden gaging station the river length is approximately 700 km and the watershed area is about 21,000 km^2 according to a contact at the RIZA website (http://www.rijkswaterstaat.nl/).

5.4.2 Model Calibration and Sensitivity Analysis

The data collected between October 1, 1995 and September 30, 2000 were used for the model calibration. The particle loading dependence on flow rate (Q_s vs. Q, plotted in Appendix F) shows a break in slope at about 280 m^3/s, in agreement with the flow rate identified by *Doomen et al.* [2008] as the critical flow rate that initiates channel bed erosion. The relationship of Q to C also show a slope break at this discharge [Appendix F]. The particle concentrations measured during the falling limb of flood events asymptotically approaches a linear dependence on flow rate allowing for the identification of a background suspended particle concentration represented by the red line in Figure 5.14 as

$$C_b = 0.03\,Q \qquad \text{(Meuse River)} \tag{5.6}$$

The mass of fine particles released from channel bed during the calibration period at Eijsden was calculated as 713,000 Mg by integrating the particle loading rate in excess of the background loading rate over the rising limb of all flood events. The release from the sediment bed is about 43% of total particle mass transported during this period, 1,670,000 Mg.

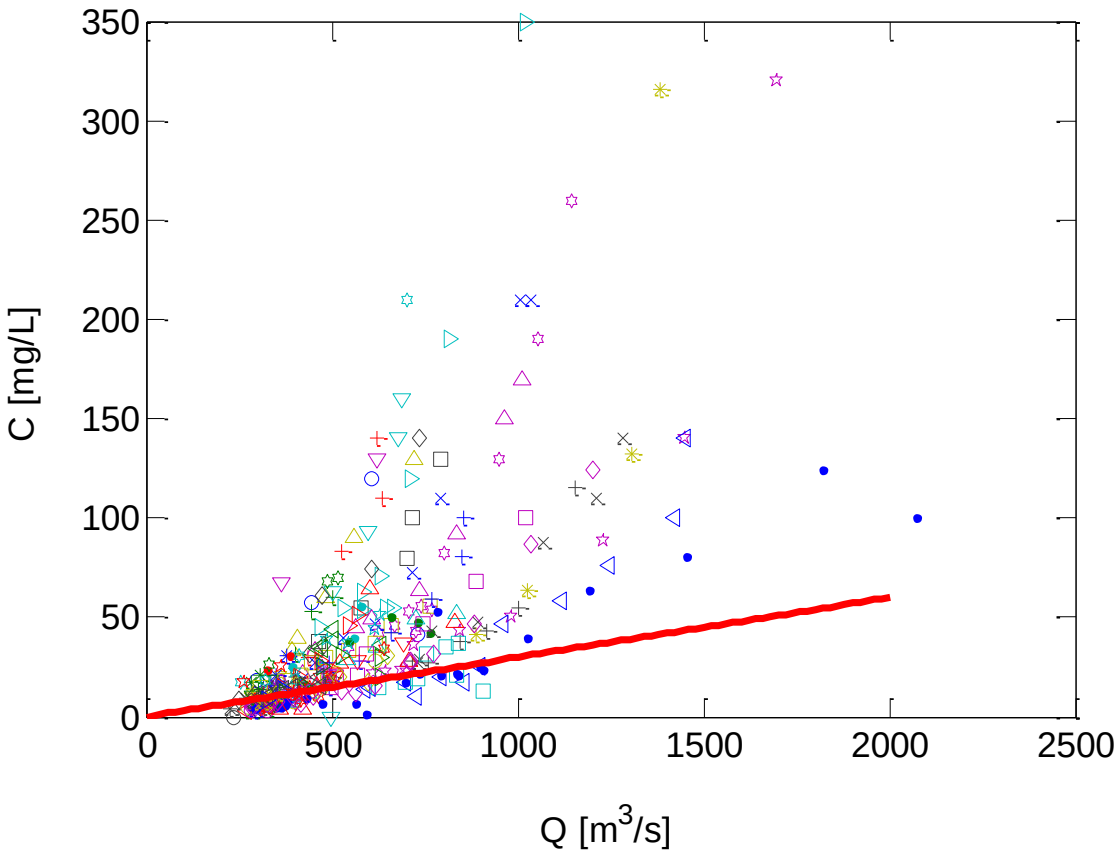

Figure 5.14. Fine particle concentration data during falling limb recessions at Eijsden gaging station in Meuse River between October 1, 1995 and September 30, 2000. The plotting symbols represent different flood events. The red line is the assumed linear dependence of background suspended particle concentration on flow rate given by equation 5.6.

The model parameters were determined following the same procedures used in the other watersheds and the results are summarized in Table 5.8. M_{max} and Q_{max} were determined by inspection of the data while the initial fine particle mass stored at the channel bed at the start of the model calibration period was assumed as M_{max}. Optimal values of α and β were determined by minimizing RSR.

Table 5.8. Optimization of the model for the Meuse River watershed

Observed Model Parameters		Optimal Parameters		Calibration Period	RSR	R
M_{max} [Mg]	Q_{max} [m^3/s]	α [m^3/s] (range)	β (range)			
165,000	1700	950 (900 - 1000)	5.0 (4.5 - 5.5)	Oct. 1, 1995 - Sept. 30, 2000	0.46	1.03

The contours of RSR for a range of filtration and scour parameter values are plotted in Figure 5.15 and show that the model's application to the Meuse River is more sensitive to the scour parameter than the filtration parameter. Figure 5.16 compares the measured and modeled cumulative fine particle release from the sediment bed over the five-year calibration period. Overall there is good agreement between modeled mass released and the measured release with R=1.03.

5.4.3 Model Validation and Extension

The Meuse measurements from October 1, 2000 to November 30, 2010 which were not utilized for model calibration were used for model validation. The same parameters in Table 5.8 were used in the model validation and the initial fine particle mass stored in the sediment bed at the start of model prediction, October 1, 2000 was taken as the value of fine particle mass stored in the sediment bed at the end of the calibration period (108,000 Mg). The model output shows good overall agreement with observations with RSR=0.64 and R=1.12 as shown in Figure 5.17. While RSR is a larger during the verification period and while there is an overall model bias to greater mass released, the agreement is reasonable.

Finally the applicability of the model to generate fine particle loading rates as described in section 4.7 was evaluated using the daily measurements during the calibration period (Figure 5.18). The observations, represented as blue dots, are compared with model generated fine particle loading rates during flood events, represented as red dots, for flow rates greater than the critical flow rate, 280 m^3/s. The model generated suspended loads show good agreement with observations which support the results of section 4.7.

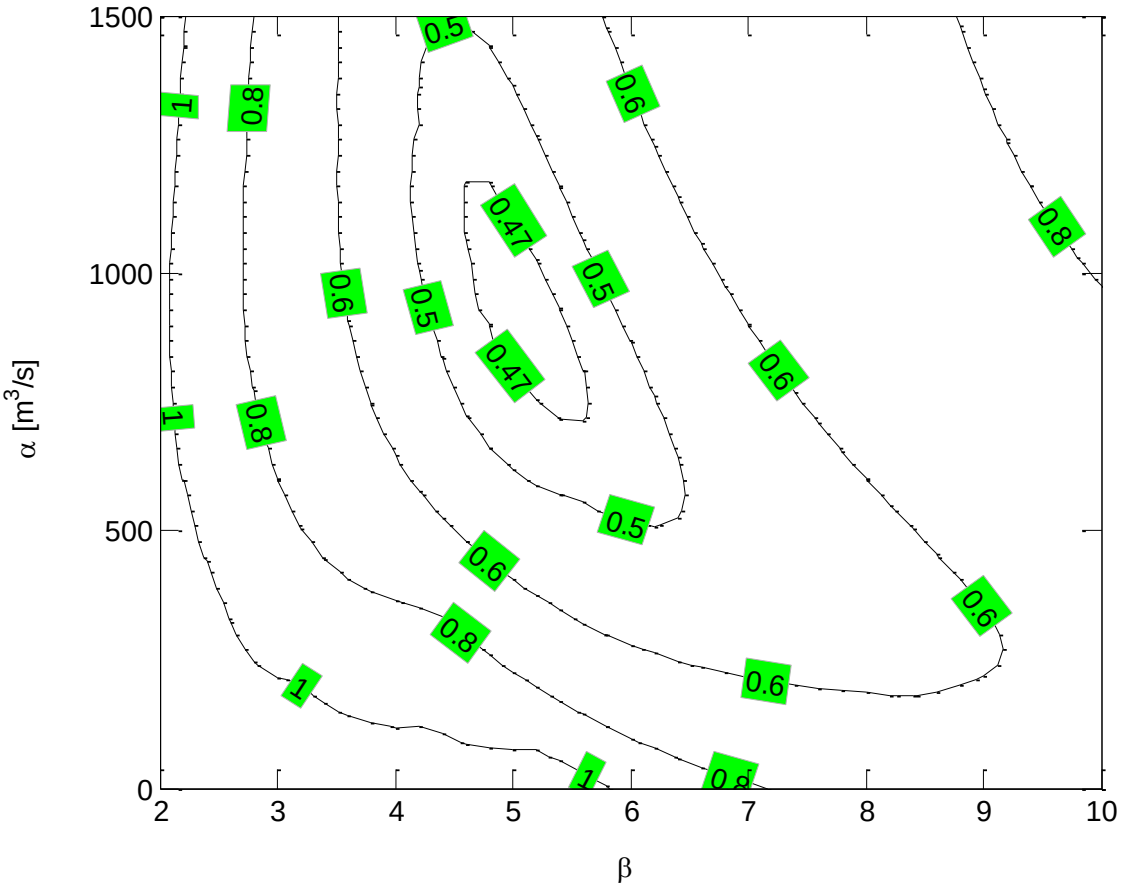

Figure 5.15. Model sensitivity to filtration (α) and scour (β) parameters using contours of RSR for the Eijsden gauging station on the Meuse River from October 1, 1995 to September 30, 2000.

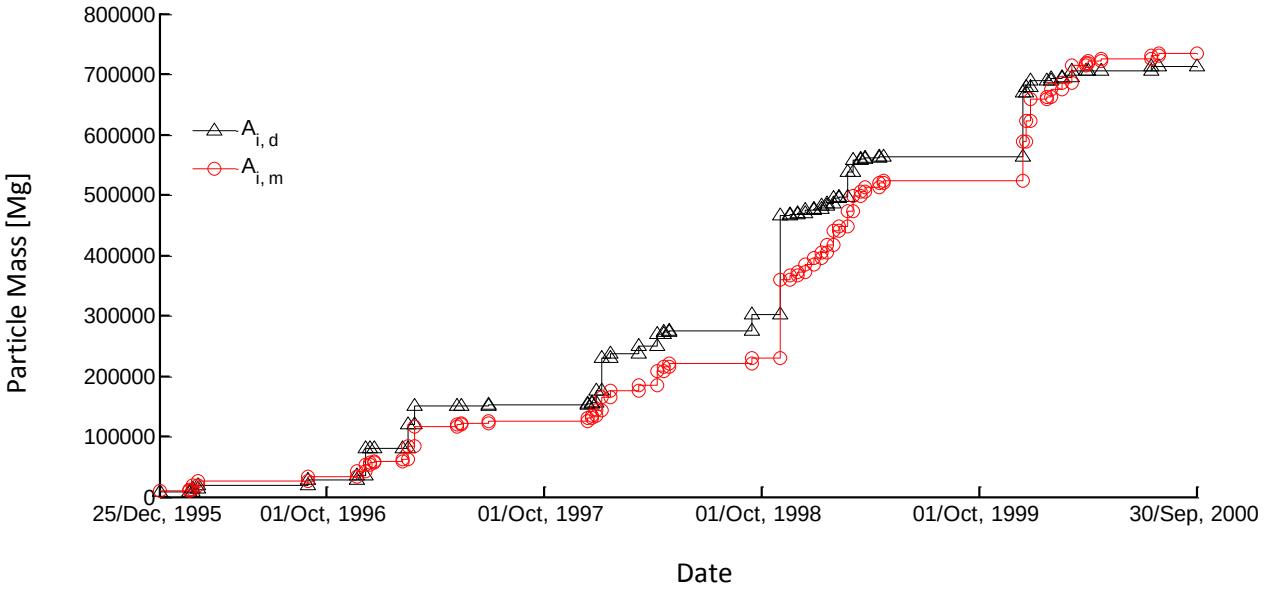

Figure 5.16. Cumulative mass of fine particles released from sediment bed based on data ($A_{i,\,d}$) and the model ($A_{i,\,m}$) for the Eijsden gauging station on the Meuse River, from October 1, 1995 to September 30, 2000.

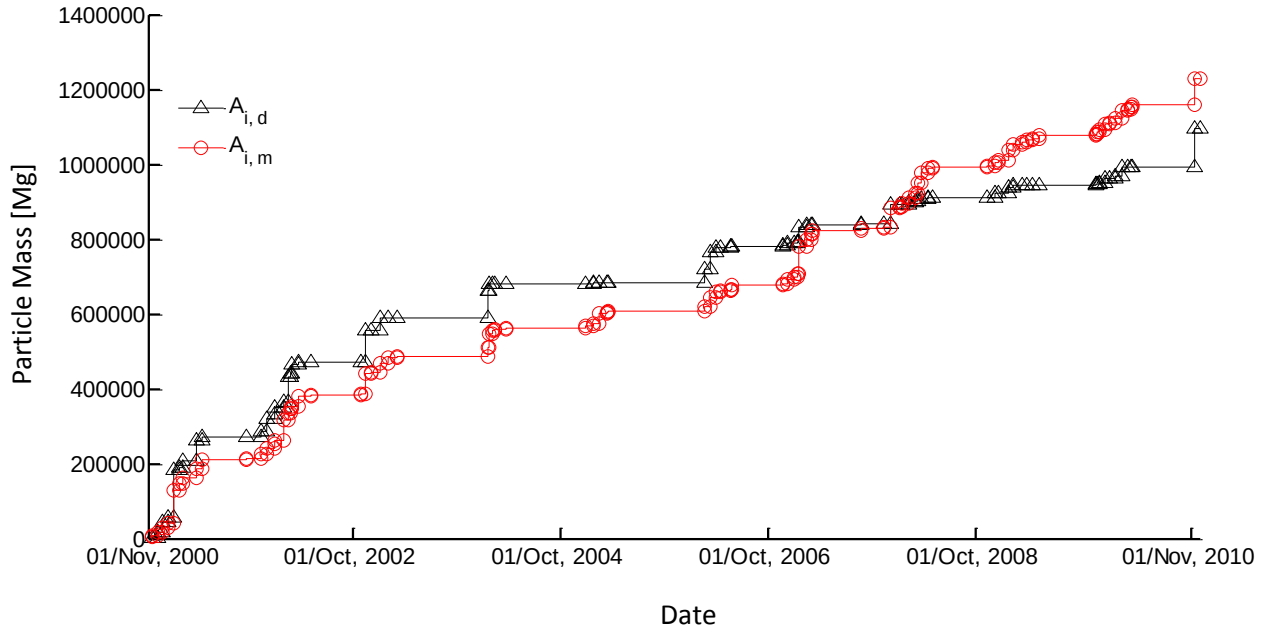

Figure 5.17. Validation test of the model with data from the Eijsden gauging station on the Meuse River over the period October 1, 2000 to November 30, 2010.

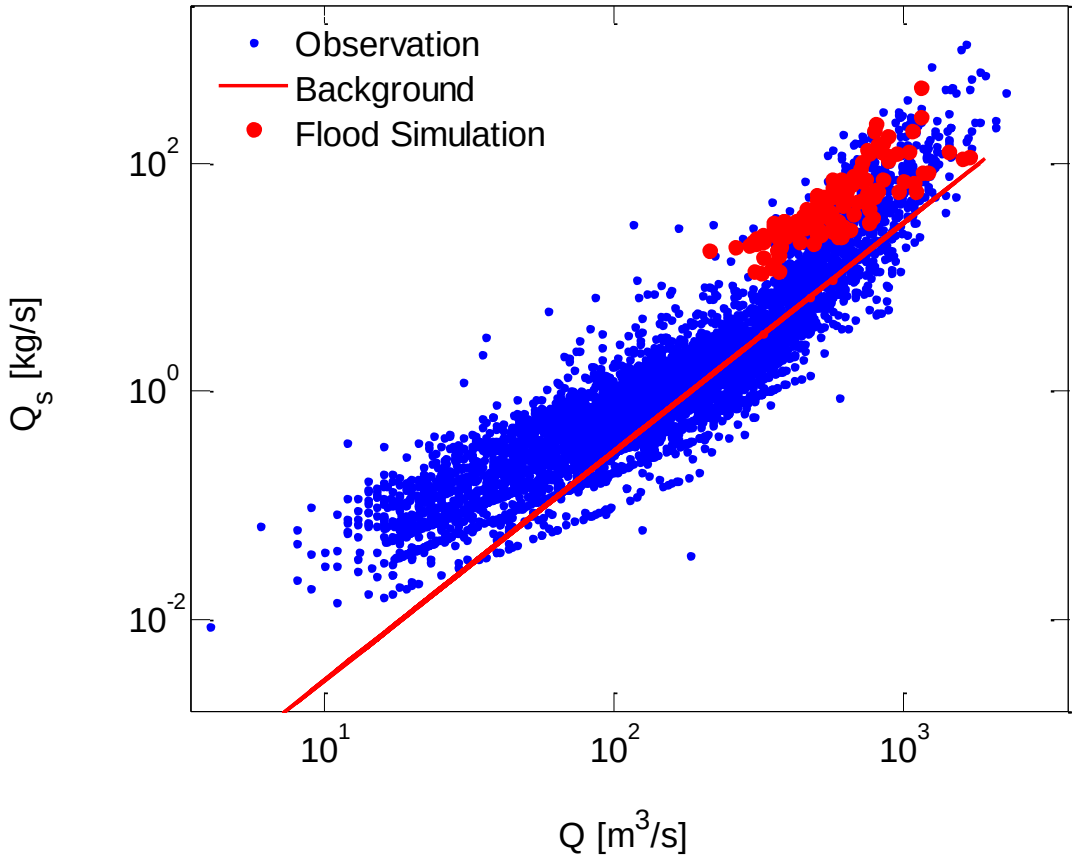

Figure 5.18. Comparison of measured particle loading rates (blue dots) at Eijsden gauging station in the Meuse River with the assumed background loading rate (red line) and the model generated discrete flood event loading (red dots) for the calibration period.

5.5 Model Summary

This chapter applied the model developed in Chapter 4 for two Russian River watersheds to various watersheds with different hydrological characteristics. The selection of these additional watersheds was based on the availability of continuous, high frequency flow and suspended particle concentration data for at least a runoff season. Table 5.9 summarizes the characteristics of all eight watersheds. The model parameters Q_{max} and M_{max} were evaluated directly from the observed data, although the calculation of M_{max} required the subtraction of the fitted background suspended particle concentration from the observed suspended particle concentrations. Forcing a linear correlation during the falling limb recession was an estimate of the background watershed contribution. The mass of fine particles released from channel beds ranged from 16 to 49% of total loads, a result noted by others.

The filtration parameter, α, represents particle accumulation throughout the stream bed within a watershed and thus ought to depend upon watershed area. Figure 5.19 (a) is a plot of log α against log of watershed area showing there is a hint that there is an increase in α with area for the smaller watersheds. For the watersheds with areas of 100 km^2 and larger, limited dependence on area is observed. The watershed data that could be analyzed thus far is limited, but is encouraging that the filtration parameter is reasonably consistent among a wide range of watersheds.

Unlike the filtration parameter the values of the scour parameter varied within only narrow range between about 4 and 6 except for Moulinet (Figure 5.19 (b)). The scour model based on *Haschenburger* [1999]'s data for a single watershed and normalization by Q_{max} appears to have adequately represented the complexity of scour and fill during bedload transport as far as fine particle release is concerned.

Table 5.9. The summary of model parameters

Watershed		Watershed Area [km^2]	Q_{max} [m^3/s]	M_{max} [Mg]	Optimal parameter	
					α [m^3/s] (range)	β (range)
Russian River	Hopland	938	425	20,800	300 (>200)	5 (4.5 - 5.5)
	Guerneville	3465	1070	66,500	340 (200 - 600)	3.4 (3 - 4)
Ireland	Owenabue	103	20	100	200 (>50)	4.2 (4 - 4.5)
	Bandon	424	110	430	600 (>400)	4.5 (4 - 5)
France	Moulinet	4.5	0.32	4.9	0.085 (0.07 - 0.10)	15.8 (12 - 18)
	Violettes	2.2	0.23	5.0	0.013 (0.01 - 0.02)	5.7 (5 - 7)
Lake Tahoe	Incline Creek	7.4	0.34	0.3	0.14 (0.1 - 0.17)	6.3 (6 - 7)
Meuse River	Eijsden gauge	Approximately 21,000	1700	165,000	950 (900 - 1000)	5.0 (4.5 - 5.5)

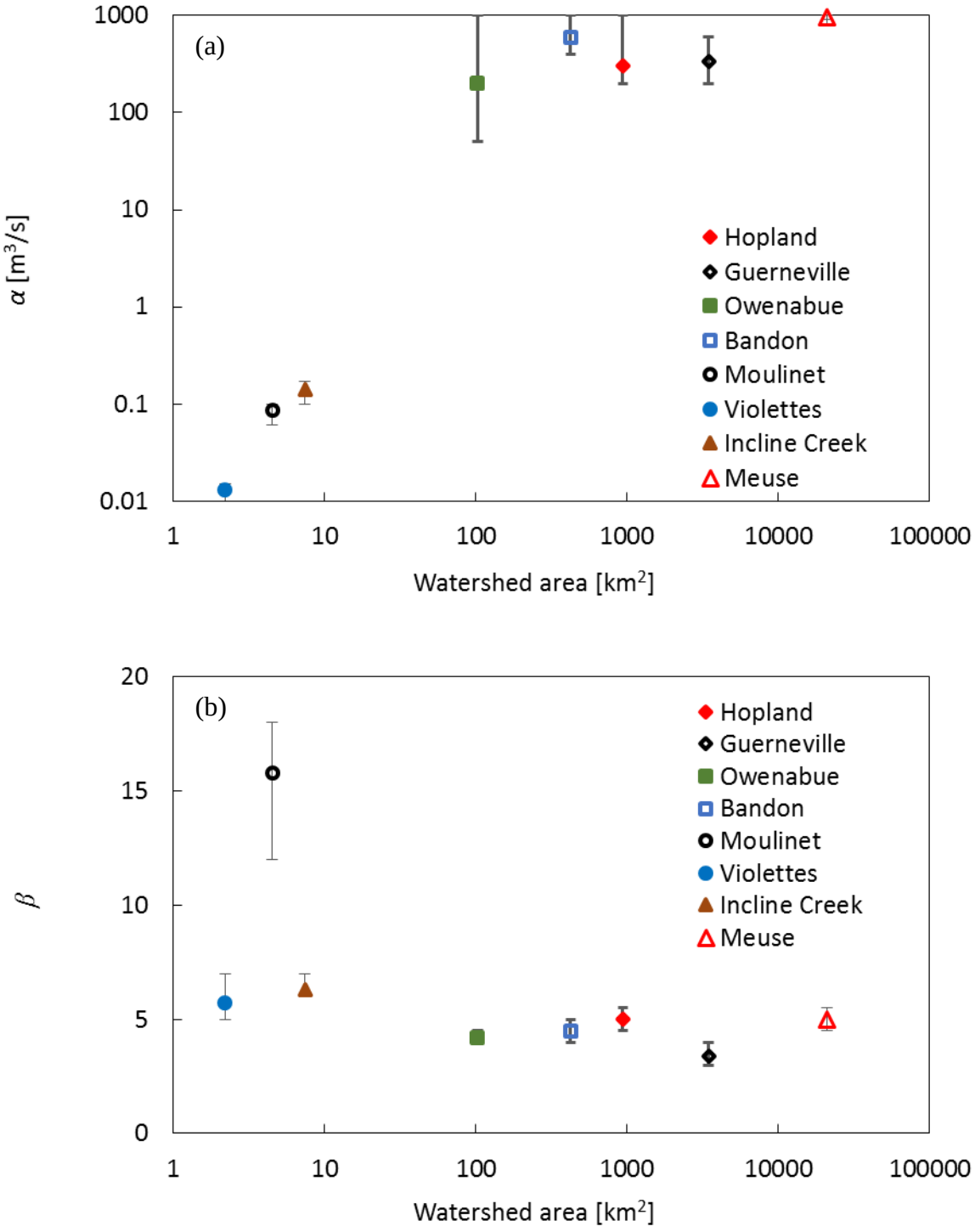

Figure 5.19. Model parameters dependence on watershed area (a) α, filtration parameter and (b) β, scour parameter. The possible range of the parameter for each watershed is indicated by vertical bars.

Chapter 6. Summary and Conclusion

This dissertation analyzed the dynamics of fine particle transport and deposition in streams. The fine particle loading rate is often represented as a function of flow rate with considerable scatter. Besides this scatter, there is a different functional relationship between flow rate and suspended load under high and low flow regimes observed in multiple watersheds in California. While power law models are commonly used for representing the relationship between fine particle loading and flow rate, such an approach has not explained the scatter or the differences between high and low flow regimes. The overall research question is why does the particle loading rate take on the form that it does in multiple watersheds? The high frequency turbidity and flow rate data at Guerneville on the Russian River in California during four sequential flood events suggested the increased suspended load during higher flows is caused by the re-suspension of fine particles from the sediment bed. The particles were previously deposited during lower flow periods by hyporheic flow. The scatter in the particle loading relationship arises from the depletion of fine particles within the sediment bed during sequential higher flow events. From this conceptual model an empirical model is developed to estimate the accumulation and re-suspension of fine sediment from the channel bed. The model is applied to multiple watersheds with different areas and environmental conditions. There are three main contributions 1) explaining observed patterns in environmental data, 2) developing and calibrating a process model, and 3) generalizing model results to multiple watersheds.

The initial contribution is the analysis of the low and high flow regimes in the dependence of particle loading rates on flow rate observed in multiple watersheds in California. The slope break in the dependence of Q_s on Q is observed in 30 minimally developed streams in California out of the 38 sites investigated. The additional analysis of channel cross sectional data and bed material size distribution implies the slope break corresponds to the change in flow from a flat wide stream to a deeper stream constrained by steep banks of the channel. The flow rate at the slope break also corresponds to conditions which initiate the mobilization of the sediment bed. Further analysis

with four sequential flood events with continuous flow rate and turbidity data leads to the conceptual model that the increased suspended load in minimally developed streams during the high flow regime is caused by the re-suspension of fine particles accumulated in the channel bed during base and flood recession flow. Field investigations correlated the existence of a slope break with gravel-dominated sediments where the accumulation and re-suspension processes are possible. For those sites without a slope break, the sediment bed was composed of either bedrock, boulders, cobbles or sand. In bedrock, boulder and cobble dominated streams there is limited storage space for fine particles and infrequent re-suspension opportunities. For sandy sediment beds, the sediment bed is always in motion even under low flow regimes. These observations lead to the development of an empirical model for fine sediment dynamics between the sediment bed and the water column above the bed.

The second contribution is the development of an empirical model to predict fine particle accumulation in the sediment bed and release from the sediment bed by higher flows. This model simplified the complex physicochemical processes into only two parameters, α, the filtration parameter, and β, the scour parameter. The model is calibrated over two discontinuous years of data collected from the Russian River at Guerneville and arrived at estimates of the mass of fine sediment released from the channel bed that had a 20% bias each year. The model overestimates by 19% the observed particle release in the 2010 water year, and underestimates by 21% of the observed values in the 2013 water year when using the same values of α and β. The model was also applied for three continuous water years at Hopland between 2011 and 2013 with an overall bias of 4%. Though this model only requires the fitting of two parameters, the simulation results of this model show good agreement with observed values with minor bias considering the scale of other uncertainties such as variations of fine sediment measurements. This simplicity is another advantage of this model for practical applicability.

The empirical model was partially validated using observational data not included during calibration. The results suggest the model is applicable for estimating fine particle release during flood events based only on flow rate data once the model parameters are determined. When the model uses only flow rate data there is a reasonably good fit with about 35% underestimation at Guerneville and 11% overestimation at Hopland for the released mass of fine particles from the sediment bed during the validation period from October 2013 to December 2014.

In an additional application of the calibrated model, fine particle loading rates were generated at Hopland between 2011 and 2013 water years and at Guerneville from October 2009 to December 2014 both using only measured flow rates. The model generated particle loading rates compared well with observations during the calibration and verification periods. In addition, the generated particle loading rates compared well with the historical daily observations between 1967 and 1986. This demonstrated that the model can estimate fine particle loading rates with the inherent scatter present in the observations based only on observed flow rates once proper model parameters are determined during calibration.

The third contribution was the application of the empirical model to multiple watersheds with different areas and environmental conditions to test its broader applicability. Watersheds were selected that had complete, high frequency data over reasonable periods. Model inputs included M_{max}, the maximum fine sediment storage capacity, Q_{max}, the peak flow rate when the sediment bed released the maximum mass of fine sediment, and a functional dependence of background

suspended particle concentration on flow rate. Filtration and scour parameters were determined to minimize overall error resulting in model estimates of released mass with an acceptable bias from 0 to 31% in the watersheds. The Meuse River was included within these data sets because of its prior use by *Doomen et al.* [2008] in modeling fine particle dynamics and to demonstrate that daily data on a larger watershed provides sufficient resolution of flood events to calibrate and partially validate the model.

A model can estimate measured values more precisely with more parameters. However using multiple parameters makes it more difficult to apply the model in practice. The model developed in this dissertation uses only two adjustable parameters, α and β, which lump together numerous physical, chemical, and biological processes into empirical coefficients. This minimalist approach to modeling fine particle deposition and release from channel beds with an acceptable bias is an obvious advantage in environmental modeling.

Model development required a number of assumptions on filtration and fluidization to represent the dynamics of fine particles in gravel-bedded streams. Improvements in these process sub-models would lessen the empirical nature of the model and assist in greater generalization. There are a couple obvious areas where improvements are needed.

Firstly, the model is developed from the assumption that accumulation rates of fine particles are proportional to the suspended sediment concentration in the water column above the sediment bed. Fine particles entering the pore space of the sediment bed accumulate within the sediment bed by filtration and settling [*Packman and MacKay*, 2003]. The filtration of fine particles within the sediment bed pore space was represented by a single filtration parameter, α. Moreover, as fine sediments are stored in the sediment bed the available pore spaces are continuously reduced [*Packman and MacKay*, 2003]. This clogging effect will reduce the filtration rate of fine particles in the sediment bed, but no models are available for the non-steady, heterogeneous porous media conditions encountered within the sediment bed. Thus, there is a need to better understand and model the details of fine particle accumulation as it occurs within sediment beds.

The second area for improvement is the assumption that the mass of fine particles released from the sediment bed by a flood event is an exponential function of the flood's peak flow rate. Researchers have addressed bedload sediment dynamics through a number of different approaches. Steady-state bedload transport functions do not have direct application to the dynamics encountered within a flood event where scouring and filling can lead to no net change in the sediment bed elevation. The field data collected by *Haschenburger* [1999] demonstrated that the average scouring depth of the sediment bed during a flood event is an exponential function of peak flow rate of the flood event. On the other hand, *Doomen et al.* [2008] made a shear stress argument that fine particle release from the channel bed is proportional to the square of the flow rate. In addition, the model does not attempt to represent the depth distribution of fine particle accumulation or erosion in the sediment bed and this is an obvious oversimplification. A greater understanding of fine particle release during sediment bed scouring during a flood event will improve the model simulation and lessen dependency on completely empirical representations.

Finally the lack of direct measurements of fine particle mass released from the sediment bed requires an approximation for background particle release from the watershed. High frequency flow rate and fine particle concentration data for multiple flooding events had falling limb hysteresis loops that asymptotically approached a linear relationship between particle

concentration and flow rate. This asymptotic relationship was attributed to fine particle contributed by the watershed compared to the sediment bed. Then, indirectly, the mass of fine particles released from the sediment bed was estimated by subtracting the background suspended particle concentration from the observed concentration during the rising limb of flood events. The alternative would be direct measurements of fine particle mass in the sediment bed, but measurements are difficult, highly variable at a site, and rare. *Lambert and Walling* [1988] developed a method to measure the fine particle mass stored within the sediment bed by sampling the sediment bed by inserting a cylinder and manually resuspending fine particles. Several researchers have used this method and reported channel bed fine particles in storage. *Navratil et al.* [2010] applied this method and found that the mass of accumulated fine particles in the sediment bed is approximately 80% of mean annual fine particle yield. These data would need to be collected between flood events, although there is considerable local spatially variability and sampling between floods can be dangerous under wet season flow conditions. This limitation on the availability of field measurements led to the approximate method of estimating fine particle mass in storage by a mass balance calculation based on an assumed background contribution from the watershed.

The filtration and scour model was applied in multiple watersheds with different watershed areas and environmental characteristics such as precipitation and soils. The value of the filtration parameters suggests an increase with area until watersheds had areas above 100 km^2. The reason of this possible area dependence was not explored in this dissertation given the limited number of watersheds. Since the filtration parameter applies to the whole watershed, an area dependency is expected, and any lack of dependency at a larger scale might reflect watersheds of sufficient size that no longer have gravel-bedded sediments throughout the stream channel system. In the case of the scour parameter, the values were within the narrow range of 4 to 6 with no obvious dependence on watershed scale. It is still clear that α and β are affected by the various environmental characteristics in each watershed, but the number of watersheds investigated precludes generalization at this time.

This research provided an empirical model for fine particles which can be applied to the management of the water quality and the improvement of aquatic ecosystems. The filtration and scour model represents the exchange of fine particles between the water column and the stream bed and can provide useful information for planning and managing fresh water environments. Further efforts are needed in improving the theoretical basis of the model and demonstrating its applicability for the assessment and improvement of aquatic environments.

Bibliography

Achite, M., and S. Ouillon (2007), Suspended sediment transport in a semiarid watershed, Wadi Abd, Algeria (1973-1995), *J. Hydrol.*, *343*(3), 187-202.

Alexandrov, Y., J. B. Laronne, and I. Reid (2003), Suspended sediment concentration and its variation with water discharge in a dryland ephemeral channel, northern Negev, Israel, *J Arid Environ*, *53*(1), 73-84.

Alexandrov, Y., J. B. Laronne, and I. Reid (2007), Intra-event and inter-seasonal behaviour of suspended sediment in flash floods of the semi-arid northern Negev, Israel, *Geomorphology*, *85*(1), 85-97.

Alexandrov, Y., H. Cohen, J. B. Laronne, and I. Reid (2009), Suspended sediment load, bedload, and dissolved load yields from a semiarid drainage basin: A 15-year study, *Water Resour. Res.*, *45*, W08408, doi:08410.01029/02008WR007314.

Amos, K. J., J. Alexander, A. Horn, G. D. Pocock, and C. R. Fielding (2004), Supply limited sediment transport in a high-discharge event of the tropical Burdekin River, North Queensland, Australia, *Sedimentology*, *51*(1), 145-162.

Andrews, E. D. (1980), Effective and bankfull discharges of streams in the Yampa river basin, Colorado and Wyoming, *J. Hydrol.*, *46*(3-4), 311-330.

Asselman, N. E. M. (1999), Suspended sediment dynamics in a large drainage basin: the River Rhine, *Hydrol. Process.*, *13*(10), 1437-1450.

Asselman, N. E. M. (2000), Fitting and interpretation of sediment rating curves, *J. Hydrol.*, *234*(3-4), 228-248.

Asselman, N. E. M., H. Middelkoop, and P. M. Van Dijk (2003), The impact of changes in climate and land use on soil erosion, transport and deposition of suspended sediment in the River Rhine, *Hydrol. Process.*, *17*(16), 3225-3244.

Baca, P. (2008), Hysteresis effect in suspended sediment concentration in the Rybarik basin, Slovakia, *Hydrolog Sci J*, *53*(1), 224-235.

Banasik, K., M. Madeyski, J. K. Mitchell, and K. Mori (2005), An investigation of lag times for rainfall-runoff-sediment yield events in small river basins, *Hydrolog Sci J*, *50*(5), 857-866.

Berry, W., N. Rubinstein, B. Melzian, and B. Hill (2003), The biological effects of suspended and bedded sediment (SABS) in aquatic systems: a review. USEPA, Washington DC, 58.

Beschta, R. L., and W. L. Jackson (1979), The intrusion of fine sediments into a stable gravel bed, *J. Fish. Res. Board Can.*, *36*(2), 204-210.

Bigelow, P. E. (2005), Testing and improving predictions of scour and fill depths in a northern California coastal stream, *River Res Appl*, *21*(8), 909-923

Birgand, F., J. Lefrancois, C. Grimaldi, E. Novince, N. Gilliet, and C. Gascuel-Odoux (2004), Mesure des flux et échantillonnage des matières en suspension sur de petits cours d'eau, *Ingénieries-EAT*, *40*, 21-35.

Bisantino, T., F. Gentile, and G. T. Liuzzi (2011), Continuous monitoring of suspended sediment load in semi-arid environments, in Sediment Transport, chap. 15, 296-312, edited by S. S. Ginsberg, doi:10.5772/15373.

Bogen, J. (1980), The hysteresis effect of sediment transport systems, *Norwegian Journal of Geography*, *34*(1), 45-54.

Bourke, M. C. (2002), Suspended sediment concentrations and the geomorphic effect of sub-bankfull flow in a central Australian stream, *Structure, Function and Management Implications of Fluvial Sedimentary Systems, IAHS Publication, No. 276*, , 315-324.

Bowes, M. J., W. A. House, R. A. Hodgkinson, and D. V. Leach (2005), Phosphorus–discharge hysteresis during storm events along a river catchment: the River Swale, UK., *Water Res*, *39*(5), 751-762.

Brasington, J., and K. Richards (2000), Turbidity and suspended sediment dynamics in small catchments in the Nepal Middle Hills, *Hydrol. Process.*, *14*(14), 2559-2574.

Brown III, W. M., and J. R. Ritter (1971), *Sediment transport and turbidity in the Eel River basin, California, Geological Survey water-supply paper 1986*, vi, 67 p. pp., U.S. Govt. Print. Off., Washington,.

Bruton, M. N. (1985), The effects of suspensoids on fish, *Hydrobiologia*, *125*(Jun), 221-241.

Cantalice, J. R. B., M. Cunha, B. D. Stosic, V. C. Piscoya, S. M. S. Guerra, and V. P. Singh (2013), Relationship between bedload and suspended sediment in the sand-bed Exu River, in the semi-arid region of Brazil, *Hydrolog Sci J*, *58*(8), 1789-1802.

Carling, P. A. (1984), Deposition of fine and coarse sand in an open-work gravel bed, *Can J Fish Aquat Sci*, *41*(2), 263-280.

Carling, P. A. (1987), Bed stability in gravel streams, with reference to stream regulation and ecology, in River Channels: Environment and Process, *Spec. Publ. 17, edited by K. Richards, Institute of British Geographers, London*, 321-347.

Carson, M. A., C. H. Taylor, and B. J. Grey (1973), Sediment production in a small Appalachian watershed during spring runoff: the Eaton Basin, 1970-1972, *Can J Earth Sci*, *10*(12), 1707-1734.

Chapman, D. W. (1988), Critical review of variables used to define effects of fines in redds of large salmonids, *T Am Fish Soc*, *117*(1), 1-21.

Cleveland, W. S. (1979), Robust locally weighted regression and smoothing scatterplots, *J Am Stat Assoc*, *74*(368), 829-836.

Cohen, H., and J. B. Laronne (2005), High rates of sediment transport by flashfloods in the Southern Judean Desert, Israel, *Hydrol. Process.*, *19*(8), 1687-1702.

Collins, A. L., and D. E. Walling (2004), Documenting catchment suspended sediment sources: problems, approaches and prospects, *Prog. Phys. Geog.*, *28*(2), 159-196.

Collins, A. L., D. E. Walling, and G. J. L. Leeksz (2005), Storage of fine-grained sediment and associated contaminants within the channels of lowland permeable catchments in the UK, *Sediment Budgets 1*, *291*, 259-268.

Collins, A. L., and D. E. Walling (2007a), The storage and provenance of fine sediment on the channel bed of two contrasting lowland permeable catchments, UK, *River Res Appl*, *23*(4), 429-450.

Collins, A. L., and D. E. Walling (2007b), Fine-grained bed sediment storage within the main channel systems of the Frome and Piddle catchments, Dorset, UK, *Hydrol. Process.*, *21*(11), 1448-1459.

Crowder, B. M. (1987), Economic costs of reservoir sedimentation: a regional approach to estimating cropland erosion damages, *J. Soil Water Conserv.*, *42*(3), 194-197.

de Vente, J., J. Poesen, M. Arabkhedri, and G. Verstraeten (2007), The sediment delivery problem revisited, *Prog. Phys. Geog.*, *31*(2), 155-178.

DeVries, P. (2002), Bedload layer thickness and disturbance depth in gravel bed streams, *J. Hydraul. Eng.*, *128*(11), 983-991.

Diplas, P., and G. Parker (1992), Deposition and removal of fines in gravel-bed streams. In Dynamics of Gravel-Bed Rivers, Chpt 15, *Billi P, Hey RD, Thorne CR, Tacconi P (eds). Wiley: Chichester, UK*, 313–329.

Doomen, A. M. C., E. Wijma, J. J. G. Zwolsman, and H. Middelkoop (2008), Predicting suspended sediment concentrations in the Meuse River using a supply-based rating curve, *Hydrol. Process.*, *22*(12), 1846-1856.

Droppo, I. G., S. N. Liss, D. Williams, T. Nelson, C. Jaskot, and B. Trapp (2009), Dynamic existence of waterborne pathogens within river sediment compartments. Implications for water quality regulatory affairs, *Environ Sci Technol*, *43*(6), 1737-1743.

Drummond, J. D., A. F. Aubeneau, and A. I. Packman (2014), Stochastic modeling of fine particulate organic carbon dynamics in rivers, *Water Resour. Res., 50, 4341–4356, doi:10.1002/2013WR014665.*

Einstein, H. A., A. G. Anderson, and J. W. Johnson (1940), A distinction between bed-load and suspended load in natural streams, *Transactions, American Geophysical Union*, *21*(2), 628-633.

Einstein, H. A. (1950), *The bed-load function for sediment transportation in open channel flows*, USDA Soil Cons. Serv. Tech. Bull., 1026, Washington, D.C.

Einstein, H. A., and N. Chien (1953), Can the rate of wash load be predicted from the bedload function?, *Transactions, American Geophysical Union*, *34*(6), 876-882.

Einstein, H. A. (1968), Deposition of suspended particles in a gravel bed, *J. Hydraul. Eng.*, *94*(5), 1197-1205.

Elliott, A. H., and N. H. Brooks (1997a), Transfer of nonsorbing solutes to a streambed with bed forms: Theory, *Water Resour. Res.*, *33*(1), 123-136.

Elliott, A. H., and N. H. Brooks (1997b), Transfer of nonsorbing solutes to a streambed with bed forms: Laboratory experiments, *Water Resour. Res.*, *33*(1), 137-151.

Farnsworth, K. L., and J. A. Warrick (2007), Sources, dispersal, and fate of fine sediment supplied to coastal California, *U.S. Geological Survey Scientific Investigations Report, 2007–5254, Washington, D.C (77 pp.)*.

Ferguson, R. I. (1986), River loads underestimated by rating curves, *Water Resour. Res.*, *22*(1), 74-76.

Forzoni, A., G. de Jager, and J. E. Storms (2013), A spatially lumped model to investigate downstream sediment flux propagation within a fluvial catchment, *Geomorphology*, *193*, 65-80.

Francalanci, S., E. Paris, and L. Solari (2013), A combined field sampling-modeling approach for computing sediment transport during flash floods in a gravel-bed stream, *Water Resour. Res.*, *49*(10), 6642-6655.

Frostick, L. E., P. M. Lucas, and I. Reid (1984), The Infiltration of fine matrices into coarse-grained alluvial sediments and its Implications for stratigraphical interpretation, *J Geol Soc London*, *141*(Nov), 955-965.

Gao, P., M. A. Nearing, and M. Commons (2013), Suspended sediment transport at the instantaneous and event time scales in semiarid watersheds of southeastern Arizona, USA, *Water Resour. Res.*, *49*(10), 6857-6870.

García, M. H., Editor (2008), *Sedimentation engineering : processes, measurements, modeling, and practice, ASCE Manuals Rep. Eng. Practice, vol. 110*, 1132 pp., Am. Soc. of Civ. Eng., Reston, Va.

Greig, S. M., D. A. Sear, and P. A. Carling (2005), The impact of fine sediment accumulation on the survival of incubating salmon progreny: Implications for sediment management, *Sci. Total Environ.*, *344*(1-3), 241-258.

Harrington, S. T., and J. R. Harrington (2013), An assessment of the suspended sediment rating curve approach for load estimation on the Rivers Bandon and Owenabue, Ireland, *Geomorphology*, *185*, 27-38.

Harvey, J. W., and B. J. Wagner (2000), Quantifying hydrologic interactions between streams and their subsurface hyporheic zones, in Streams and Ground Waters, edited by J. B. Jones and P. J. Mulholland, pp. 3 – 44, Academic, San Diego Calif.

Harvey, J. W., et al. (2012), Hydrogeomorphology of the hyporheic zone: Stream solute and fine particle interactions with a dynamic streambed, *J. Geophys. Res.*, 117, G100N111, doi:110.1029/2012JG002043.

Haschenburger, J. K. (1999), A probability model of scour and fill depths in gravel-bed channels, *Water Resour. Res.*, *35*(9), 2857-2869.

Hassan, M. A. (1990), Scour, fill, and burial depth of coarse material in gravel bed streams, *Earth Surf. Proc. Land.*, *15*(4), 341-356.

Hassan, M. A., and M. Church (1994), Vertical mixing of coarse particles in gravel-bed rivers - a kinematic model, *Water Resour. Res.*, *30*(4), 1173-1185.

Hicks, D. M., B. Gomez, and N. A. Trustrum (2000), Erosion thresholds and suspended sediment yields, Waipaoa River Basin, New Zealand, *Water Resour. Res.*, *36*(4), 1129-1142.

Hjulström, F. (1935), Studies of the morphological activity of rivers as illustrated by the river Fryis, *Bull. Geol. Inst. Upsula*, *25*, 221-527.

Jaramillo, M. (2012), Riverbank filtration: an efficient and economical drinking-water treatment technology, *Dyna*, *171*(148-157).

Jensen, D. W., E. A. Steel, A. H. Fullerton, and G. R. Pess (2009), Impact of fine sediment on egg-to-fry survival of Pacific salmon: a meta-analysis of published studies, *Rev. Fish. Sci.*, *17*(3), 348-359.

Johnson, J. W. (1943), Distribution graphs of suspended-matter concentration, *Trans. Am. Soc. Civ. Eng.* , *108*, 941–956.

Kemp, P., D. Sear, A. Collins, P. Naden, and I. Jones (2011), The impacts of fine sediment on riverine fish, *Hydrol. Process.*, *25*(11), 1800-1821.

Klein, M. (1984), Anti clockwise hysteresis in suspended sediment concentration during individual storms: Holbeck catchment, Yorkshire England, *Catena*, *11*(1), 251–257.

Knighton, D. (1998), *Fluvial forms and processes: a new perspective*, 180-183 pp., Arnold, Hodder Headline, PLC.

Koltun, G. F., M. Eberle, J. R. Gray, and G. D. Glysson (2006), User's manual for the graphical constituent loading analysis system(GCLAS), in techniques and methods, *Book 4, chap. C1, 50 pp., U.S.Geol. Surv., Reston, Va. (Available at http://pubs.er.usgs.gov/usgspubs/tm/tm4C1).*

Kondolf, G. M. (1997), Hungry water: Effects of dams and gravel mining on river channels, *Environ Manage*, *21*(4), 533-551.

López-Tarazón, J. A., R. J. Batalla, D. Vericat, and T. Francke (2009), Suspended sediment transport in a highly erodible catchment: the River Isábena (Southern Pyrenees), *Geomorphology*, *190*(3), 210-221.

Lambert, C. P., and D. E. Walling (1988), Measurement of channel storage of suspended sediment in a gravel-bed river, *Catena*, *15*(1), 65-80, doi:10.1016/0341-8162(1088)90017-90013.

Landers, M. N., and T. W. Sturm (2013), Hysteresis in suspended sediment to turbidity relations due to changing particle size distributions, *Water Resour. Res.*, *49*(9), 5487-5500.

Langlois, J. L., D. W. Johnson, and G. R. Mehuys (2005), Suspended sediment dynamics associated with snowmelt runoff in a small mountain stream of Lake Tahoe (Nevada), *Hydrol. Process.*, *19*(18), 3569-3580.

Lefrancois, J., C. Grimaldi, C. Gascuel-Odoux, and N. Gilliet (2007), Suspended sediment and discharge relationships to identify bank degradation as a main sediment source on small agricultural catchments, *Hydrol. Process.*, *21*(21), 2923-2933.

Lenzi, M. A., and L. Marchi (2000), Suspended sediment load during floods in a small stream of the Dolomites (northeastern Italy), *Catena*, *39*, 267 – 282.

Leonard, R. L., L. A. Kaplan, J. F. Elder, R. N. Coats, and C. R. Goldman (1979), Nutrient transport in surface runoff from a subalpine watershed, Lake Tahoe Basin, California, *Ecol Monogr*, *49*(3), 281-310.

Leonardson, R. (2010), Exchange of fine sediments with gravel riverbeds, PhD thesis, University of California, Berkeley.

Lewis, K. (1973), The effect of suspended coal particles on the life forms of the aquatic moss Eurhynchium riparioides (Hedw.), *Freshwater biol.*, *3*(3), 251-257.

Lisle, T. E. (1989), Sediment transport and resulting deposition in spawning gravels, North Coastal California, *Water Resour. Res.*, *25*(6), 1303-1319.

Lopez-Tarazon, J. A., R. J. Batalla, and D. Vericat (2011), In-channel sediment storage in a highly erodible catchment: the River Isabena (Ebro Basin, Southern Pyrenees), *Z Geomorphol*, *55*(3), 365-382.

Madej, M. A. (1995), Changes in channel-stored sediment, Redwood Creek, northwestern California, Chapter O, *Geomorphic Processes and Aquatic Habitat in the Redwood Creek Basin, Northwestern California. US Geological Survey Professional Paper*, *1454*.

Madej, M. A., and V. Ozaki (1996), Channel response to sediment wave propagation and movement, Redwood Creek, California, USA, *Earth Surf. Proc. Land.*, *21*(10), 911-927.

Marcus, W. A. (1989), Lag-time routing of suspended sediment concentrations during unsteady-flow, *Geol Soc Am Bull*, *101*(5), 644-651.

McCaig, M. (1981), Modelling storm period fluctuations in suspended sediment- an appraisal. Working Paper 311, School of Geography, Univ. of Leeds. .

Megnounif, A., A. Terfous, and S. Ouillon (2013), A graphical method to study suspended sediment dynamics during flood events in the Wadi Sebdou, NW Algeria (1973-2004), *J. Hydrol.*, *497*, 24-36.

Meyer-Peter, E., and R. Müller (1948), Formulas for bed-load transport, Report on 2nd Meeting of International Association for Hydraulic Research, *Rep.*, pp 39–64, Int. Assoc. for Hydraulic Struct. Res., Stockholm, Sweden..

Montgomery, D. R., J. M. Buffington, N. P. Peterson, D. SchuettHames, and T. P. Quinn (1996), Stream-bed scour, egg burial depths, and the influence of salmonid spawning on bed surface mobility and embryo survival, *Can J Fish Aquat Sci*, *53*(5), 1061-1070.

Moriasi, D. N., J. G. Arnold, M. W. Van Liew, R. L. Bingner, R. D. Harmel, and T. L. Veith (2007), Model evaluation guidelines for systematic quantification of accuracy in watershed simulations, *T Asabe*, *50*(3), 885-900.

Navratil, O., C. Legout, D. Gateuille, M. Esteves, and F. Liebault (2010), Assessment of intermediate fine sediment storage in a braided river reach (southern French Prealps), *Hydrol. Process.*, *24*(10), 1318-1332.

Negev, M. (1969), Analysis of data on suspended sediment discharge in several streams in Israel, Israel Hydrological Service, Hydrological Paper No. 12.

Negev, M. (1972), Suspended sediment discharge in western watersheds of Israel, Israel Hydrological Service, Hydrological Paper No. 14.

Packman, A. I., N. H. Brooks, and J. J. Morgan (2000a), A physicochemical model for colloid exchange between a stream and a sand streambed with bed forms, *Water Resour. Res.*, *36*(8), 2351-2361.

Packman, A. I., N. H. Brooks, and J. J. Morgan (2000b), Kaolinite exchange between a stream and streambed: Laboratory experiments and validation of a colloid transport model, *Water Resour. Res.*, *36*(8), 2363-2372.

Packman, A. I., and J. S. MacKay (2003), Interplay of stream-subsurface exchange, clay particle deposition, and streambed evolution, *Water Resour. Res.*, *39*(4).

Palmieri, A., F. Shah, and A. Dinar (2001), Economics of reservoir sedimentation and sustainable management of dams, *J Environ Manage*, *61*(2), 149-163.

Pelletier, J. D. (2012), A spatially distributed model for the long-term suspended sediment discharge and delivery ratio of drainage basins, *J. Geophys. Res.*, *117*(F02028, doi:10.1029/2011JF002129).

Picouet, C., B. Hingray, and J. C. Olivry (2001), Empirical and conceptual modelling of the suspended sediment dynamics in a large tropical African river: the Upper Niger river basin, *J. Hydrol.*, *250*(1), 19-39.

Pizzuto, J. E. (2014), Long-term storage and transport length scale of fine sediment: Analysis of a mercury release into a river. , *Geophys Res Lett*, *41*(16), 5875-5882.

Poulenard, J., C. Legout, J. Nemery, J. Bramorski, O. Navratil, A. Douchin, B. Fanget, Y. Perrette, O. Evrard, and M. Esteves (2012), Tracing sediment sources during floods using Diffuse Reflectance Infrared Fourier Transform Spectrometry (DRIFTS): A case study in a highly erosive mountainous catchment (Southern French Alps), *J. Hydrol.*, *414*, 452-462.

Radoane, M., G. Pandi, and N. Radoane (2010), Contemporary bed elevation changes from the Eastern Carpathians, *Carpath. J. Earth. Env.*, *5*(2), 49-60.

Renard, K. G., G. R. Foster, G. A. Weesies, and D. C. Yoder (1997), *Predicting soil erosion by water: a guide to conservation planning with the revised universal soil loss equation (RUSLE), Agriculture Handbook, No. 703 (Washington).*

Ritter, J. R., and W. M. Brown III (1971), *Turbidity and suspended-sediment transport in the Russian River basin, California, U.S. Geological Survey, Open-file Report 72-316, Menlo Park, California*.

Rowe, M., Essig, D., and Jessup, B. (2003), Guide to selection of sediment targets for use in Idaho TMDLs. Idaho Department of Environmental Quality, Boise.

Rubin, D. M., and D. J. Topping (2001), Quantifying the relative importance of flow regulation and grain size regulation of suspended sediment transport α and tracking changes in grain size of bed sediment β, *Water Resour. Res.*, *37*(1), 133-146.

Rubin, D. M., and D. J. Topping (2008), Correction to "Quantifying the relative importance of flow regulation and grain size regulation of suspended sediment transport α and tracking changes in grain size of bed sediment β", *Water Resour. Res.*, *44*(9), W09701, doi:09710.01029/02008WR006819.

Runkel, R. L., C. G. Crawford, and T. A. Cohn (2004), Load Estimator(LOADEST): A FORTRAN program for estimating constituent loads in streams and rivers, *U.S. Geol. Surv. Techniques Methods, Book 4, Chap. A5, 69 pp.*

Schubert, J. (2006), Significance of hydrologic aspects on RBF performance - Everything is linked to everything else, *Riverbank Filtration Hydrology*, *60*, 1-20.

Shields, A. (1936), Application of similarity principles and turbulence research to bed-load movement (in German), *Mitt. Preuss. Vers. Wasserbau. Schiffbau.*, *26*, 5-24.
Singer, M. B., R. Aalto, L. A. James, N. E. Kilham, J. L. Higson, and S. Ghoshal (2013), Enduring legacy of a toxic fan via episodic redistribution of California gold mining debris, *P. Natl. Acad. Sci. USA*, *110*(46), 18436-18441.
Stevens, L. E., K. A. Buck, B. T. Brown, and N. C. Kline (1997), Dam and geomorphological influences on Colorado River waterbird distribution, Grand Canyon, Arizona, USA, *Regul River*, *13*(2), 151-169.
Stover, S. C., and D. R. Montgomery (2001), Channel change and flooding, Skokomish River, Washington, *J. Hydrol.*, *243*(3-4), 272-286.
Stubblefield, A. P., J. E. Reuter, and C. R. Goldman (2009), Sediment budget for subalpine watersheds, Lake Tahoe, California, USA, *Catena*, *76*(3), 163-172.
Suttle, K. B., M. E. Power, J. M. Levine, and C. McNeely (2004), How fine sediment in riverbeds impairs growth and survival of juvenile salmonids, *Ecol. Appl.*, *14*(4), 969-974.
Syvitski, J. P., M. D. Morehead, D. B. Bahr, and T. Mulder (2000), Estimating fluvial sediment transport: The rating parameters, *Water Resour. Res.*, *36*(9), 2747-2760.
Syvitski, J. P., S. D. Peckham, R. Hilberman, and T. Mulder (2003), Predicting the terrestrial flux of sediment to the global ocean: a planetary perspective, *Sediment Geol*, *162*(1), 5-24.
Syvitski, J. P., C. J. Vörösmarty, A. J. Kettner, and P. Green (2005), Impact of humans on the flux of terrestrial sediment to the global coastal ocean, *Science*, *308*(5720), 376-380.
Tappel, P. D., Bjornn, T. C. (1983), A new method of relating size of spawning gravel to salmonid embryo survival. , *N Am J Fish Manage*, *3*(2), 123-135.
Topping, D. J., D. M. Rubin, and L. E. Vierra Jr. (2000), Colorado River sediment transport, 1. Natural sediment supply limitation and the influence of the Glen Canyon Dam, *Water Resour. Res.*, *36*(2), 515-542.
Tufenkji, N., J. N. Ryan, and M. Elimelech (2002), The promise of bank filtration, *Environ Sci Technol*, *36*(21), 422a-428a.
USEPA (2000), *The quality of our nations waters. A summary of the national water quality inventory: 1998 report to congress. Office of Water, Washington DC. 841-S-00-001*.
USEPA (2009), National water quality inventory: Report to congress, *http://water.epa.gov/lawsregs/guidance/cwa/305b/upload/2009_01_22_305b_2004report_2004_305Breport.pdf*.
Vansickle, J., and R. L. Beschta (1983), Supply-based models of suspended sediment transport in streams, *Water Resour. Res.*, *19*(3), 768-778.
Verhoff, F. H., and D. A. Melfi (1978), Total phosphorus transport during storm events, *J. Environ. Eng. Div.*, *104*(5), 1021-1026.
Verhoff, F. H., D. A. Melfi, and S. M. Yaksich (1979), Storm travel distance calculations for total phosphorus and suspended materials in rivers, *Water Resour. Res.*, *15*(6), 1354-1360.
Walling, D. E. (1974), Suspended sediment and solute yields from a small catchment prior to urbanization, Fluvial Processes in Instrumented Watersheds, Inst. Brit. Geogr. Spec. Publ., 6, 169-192.
Walling, D. E. (1977), Limitations of the rating curve technique for estimating suspended sediment loads, with particular reference to British rivers, *IAHS Publ.*, *122*, 34-48.
Walling, D. E., and B. W. Webb (1982), Sediment availability and the prediction of storm-period sediment yields, *Hydrolog Sci J*, *27*(2), 246-246.
Walling, D. E. (1983), The sediment delivery problem, *J. Hydrol.*, *65*(209-237).

Warrick, J. A., and L. A. K. Mertes (2009), Sediment yield from the tectonically active semiarid Western Transverse Ranges of California, *Geol Soc Am Bull*, *121*(7-8), 1054-1070.
Warrick, J. A., J. A. Hatten, G. B. Pasternack, A. B. Gray, M. A. Goni, and R. A. Wheatcroft (2012), The effects of wildfire on the sediment yield of a coastal California watershed, *Geol Soc Am Bull*, *124* (7/8), 1130-1146.
Warrick, J. A., M. A. Madej, M. A. Goni, and R. A. Wheatcroft (2013), Trends in the suspended-sediment yields of coastal rivers of northern California, 1955-2010, *J. Hydrol.*, *489*, 108-123.
Welsh, B. L. (1980), Comparative nutrient dynamics of a marsh-mudflat ecosystem, *Estuar. Coast. Marine S.*, *10*(2), 143-164.
White, W. R. (2001), Evacuation of Sediment From Reservoirs, Thomas Telford, London.
Williams, G. P. (1978), Bank-full discharge of rivers, *Water Resour. Res.*, *14*(6), 1141-1154.
Williams, G. P. (1989), Sediment concentration versus water discharge during single hydrologic events in rivers, *J. Hydrol.*, *111*(1-4), 89-106.
Wolman, M. G., and J. P. Miller (1960), Magnitude and frequency of forces in geomorphic processes, *J Geol*, *68*(1), 54-74.
Wolman, M. G. (1977), Changing needs and opportunities in the sediment field, *Water Resour. Res.*, *13*(1), 50-54.
Wolman, M. G., and L. B. Leopold (1957), River flood plains: Some observations on their formation, *U.S. Geol. Surv. Prof. Pap. 262-C, pp. 85–107, U.S. Gov. Print. Off., Washington, D. C.*
Wong, M. G., and G. Parker (2006), Reanalysis and correction of bed-load relation of Meyer-Peter and Muller using their own database, *J. Hydraul. Eng.*, *132*(11), 1159-1168.
Wood, P. J., and P. D. Armitage (1997), Biological effects of fine sediment in the lotic environment, *Environ Manage*, *21*(2), 203-217.
Woodyer, K. D. (1968), Bankfull frequency in rivers, *J. Hydrol.*, *6*(2), 114-142.
Wright, S. A., D. J. Topping, D. M. Rubin, and T. S. Melis (2010), An approach for modeling sediment budgets in supply-limited rivers, *Water Resour. Res.*, *46*(10), W10538, doi:10510.11029/12009WR008600.
Zhang, Y. Q., S. Hubbard, and S. Finsterle (2011), Factors governing sustainable groundwater pumping near a river, *Ground Water*, *49*(3), 432-444.
Zimmermann, A. E., and M. Lapointe (2005), Intergranular flow velocity through salmonid redds: Sensitivity to fines infiltration from low intensity sediment transport events, *River Res Appl*, *21*(8), 865-881.

Appendix A. Thirty eight minimally developed sites in California

1. Upper Truckee River at South Lake Tahoe, CA. (USGS site number 10336610)

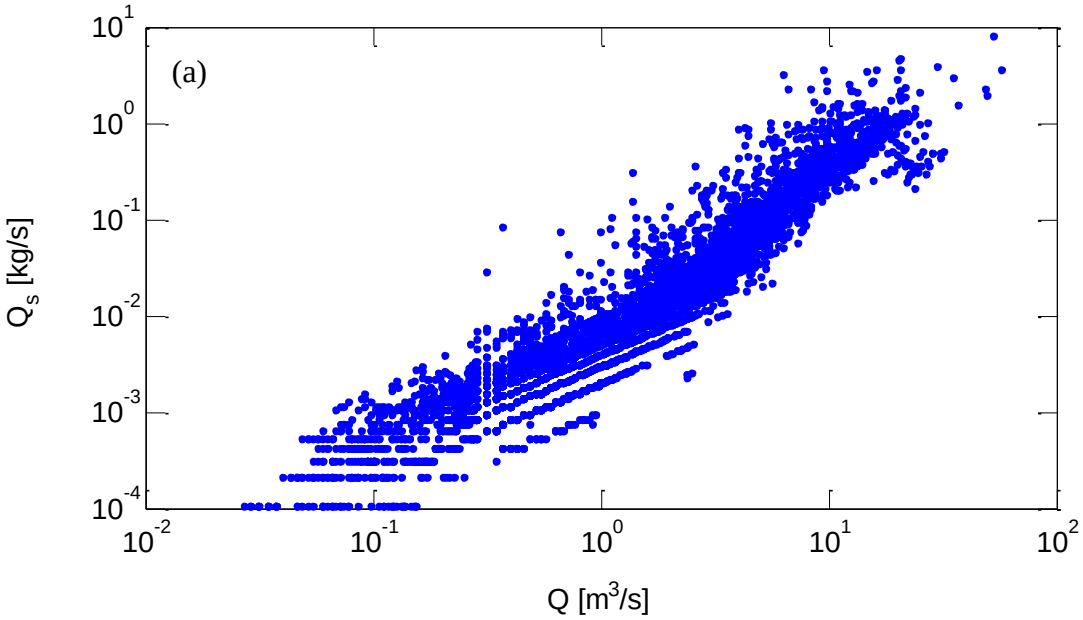

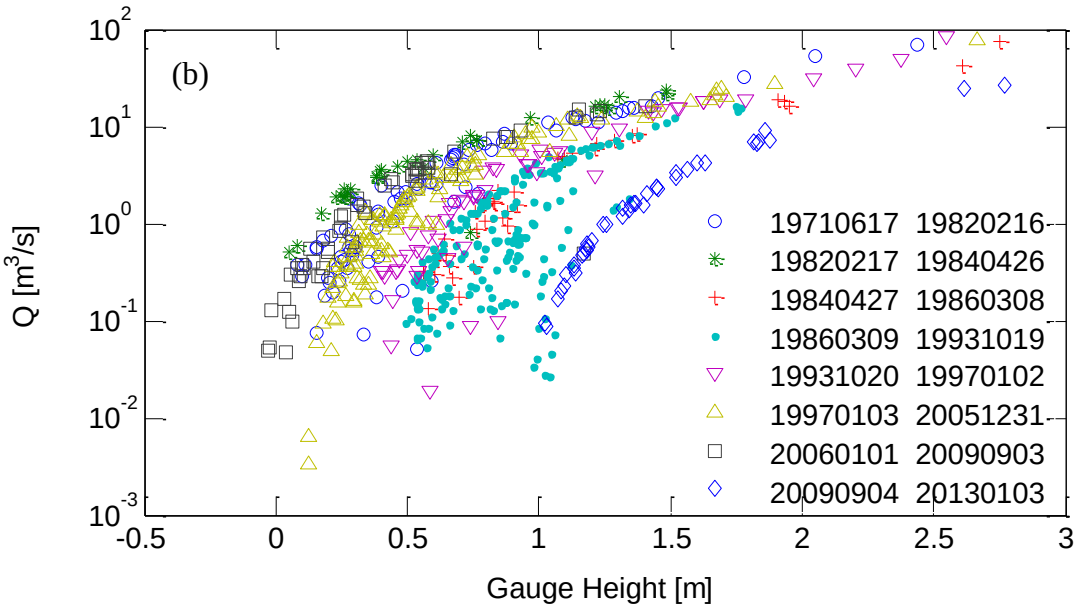

Figure A.1. (a) Q_s vs Q relationship from 1971 to 1992, (b) Q vs Gauge Height, and (c) photo image of site location from Google Earth at Upper Truckee River at South Lake Tahoe, CA.

2. General Creek near Meeks Bay,CA. (USGS site number 10336645)

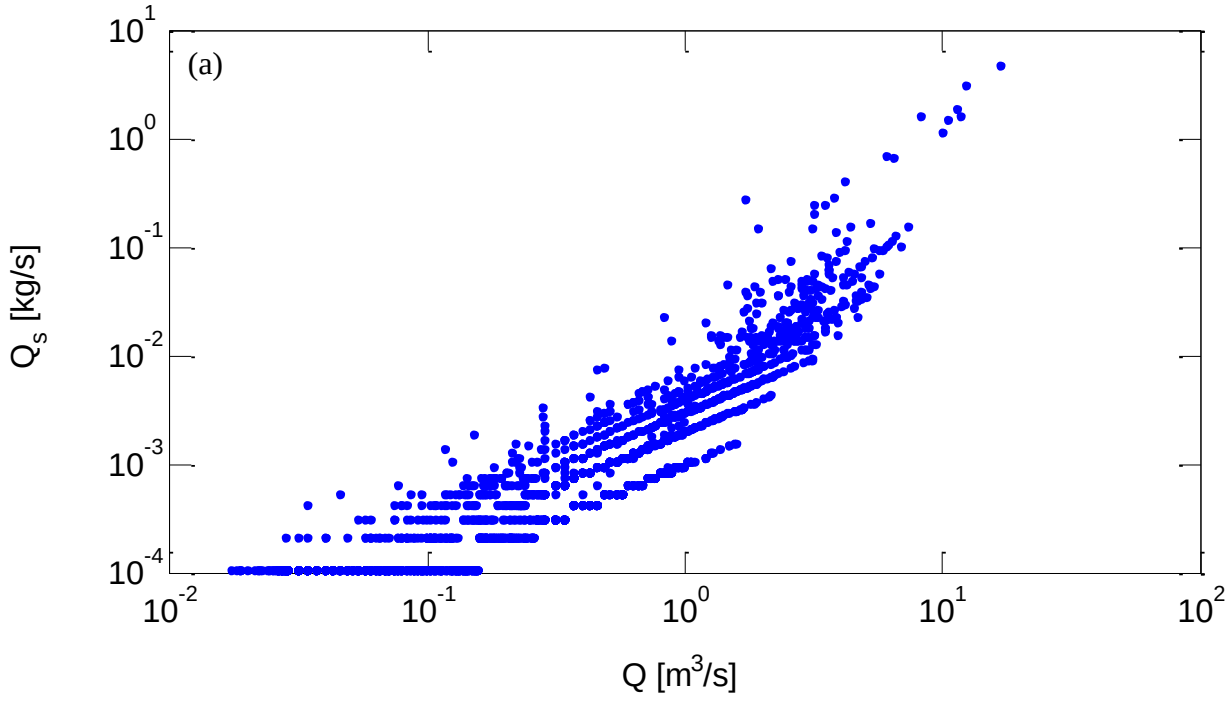

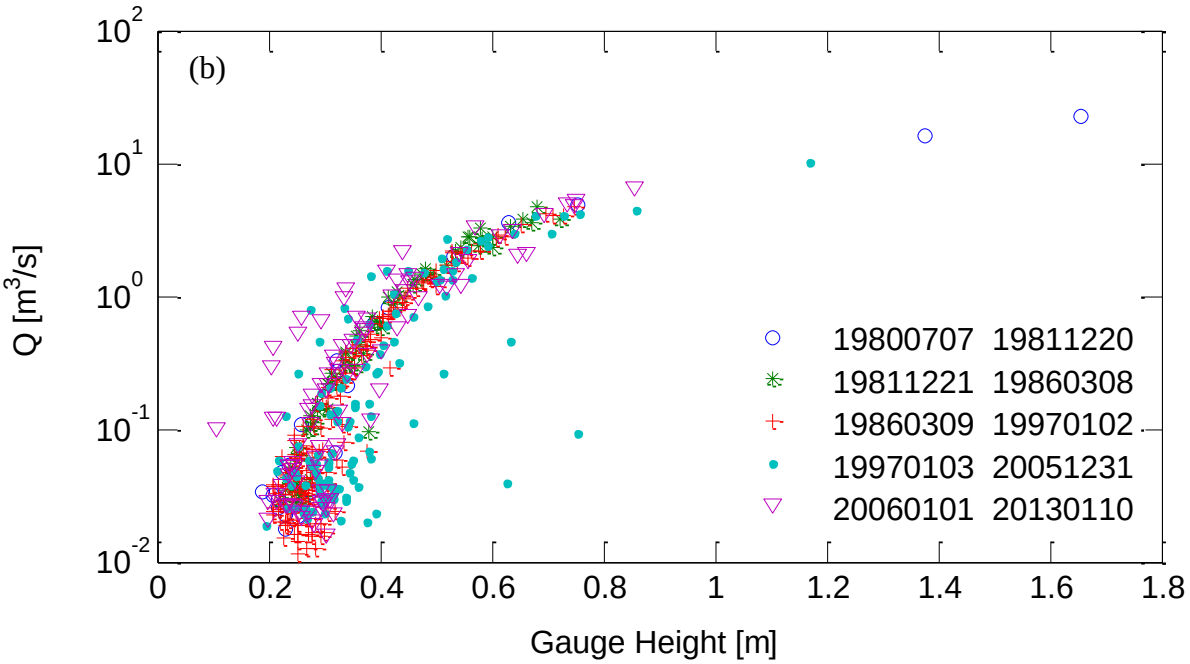

Figure A.2. (a) Q_s vs Q relationship from 1980 to 1992, (b) Q vs Gauge Height, and (c) photo image of site location from Google Earth at General Creek near Meeks Bay, CA.

3. Blackwood Creek near Tahoe City, CA. (USGS site number 10336660)

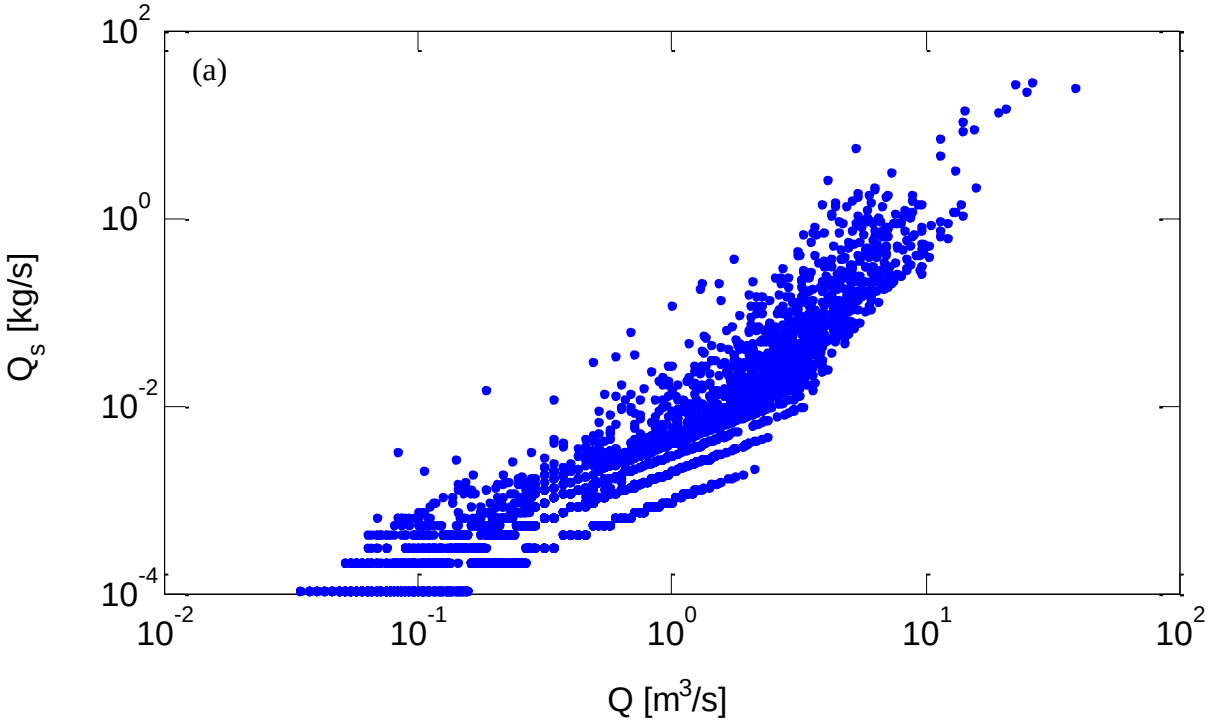

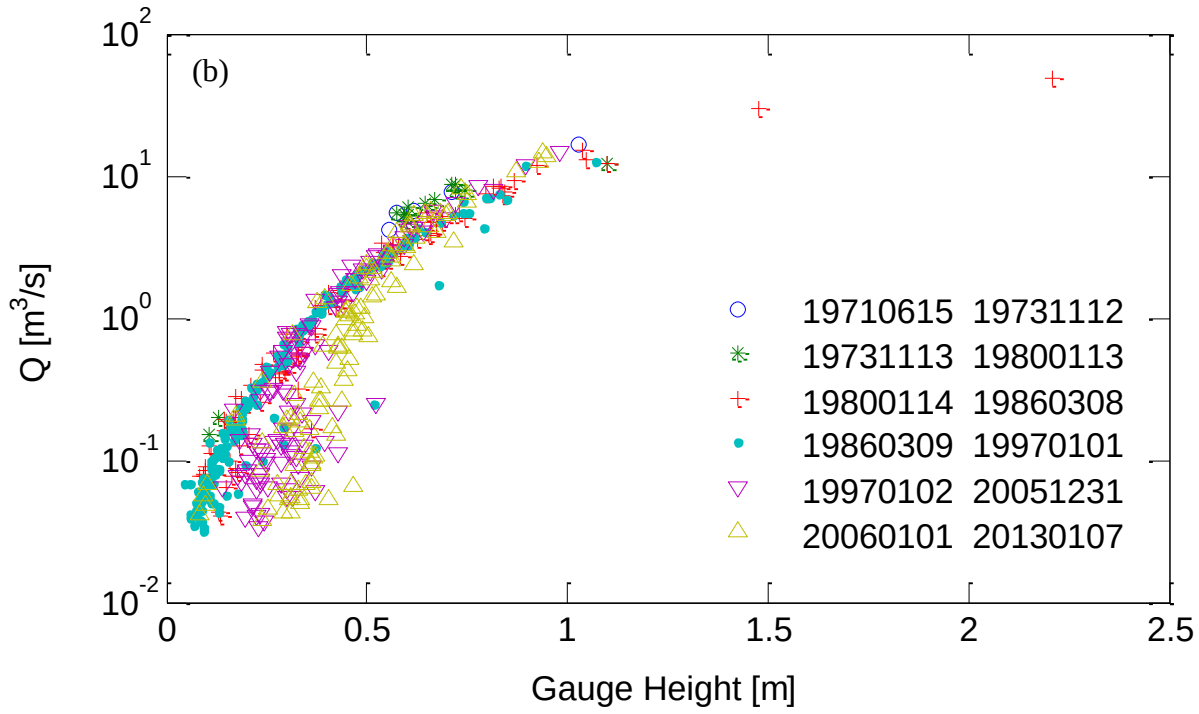

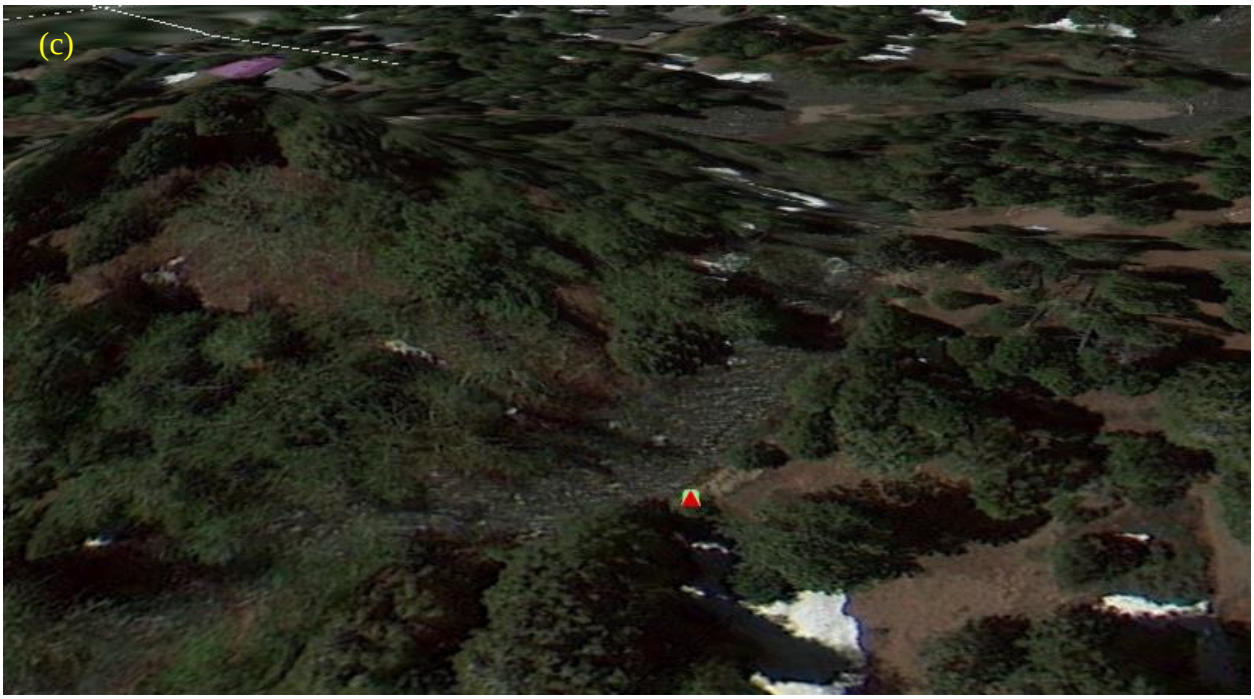

Figure A.3. (a) Q_s vs Q relationship from 1974 to 1992, (b) Q vs Gauge Height, and (c) photo image of site location from Google Earth at Blackwood Creek near Tahoe City, CA.

4. Ward Creek at HWY 89 near Tahoe Pines, CA. (USGS site number 10336676)

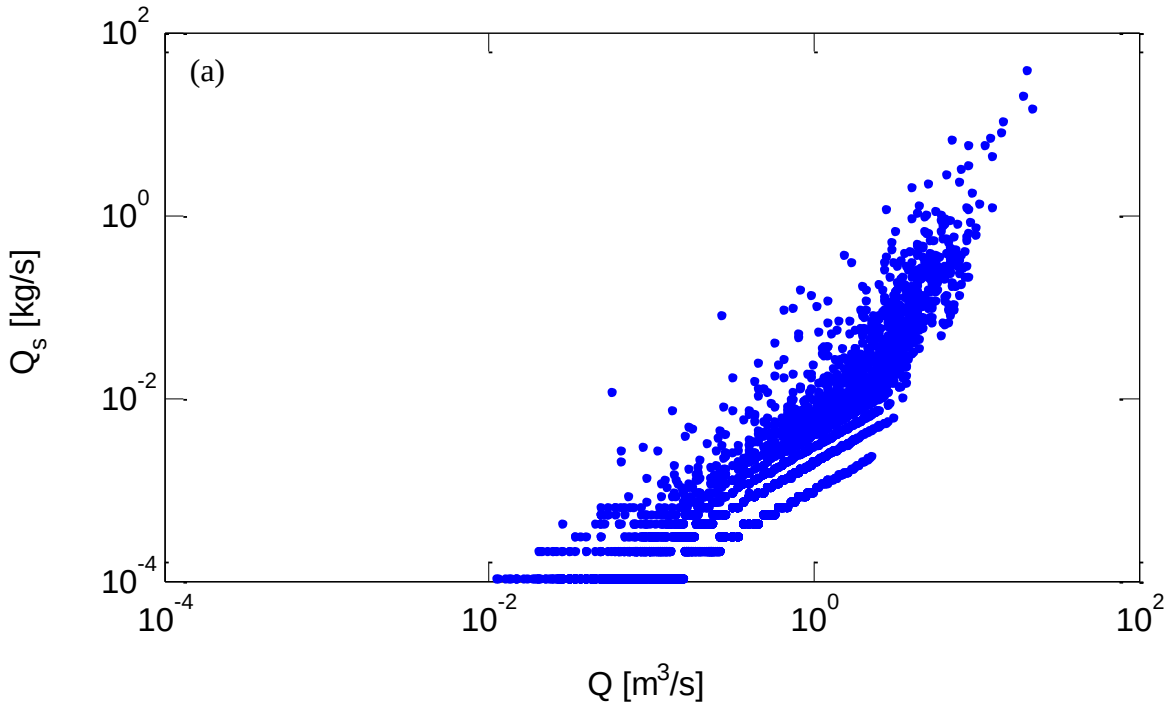

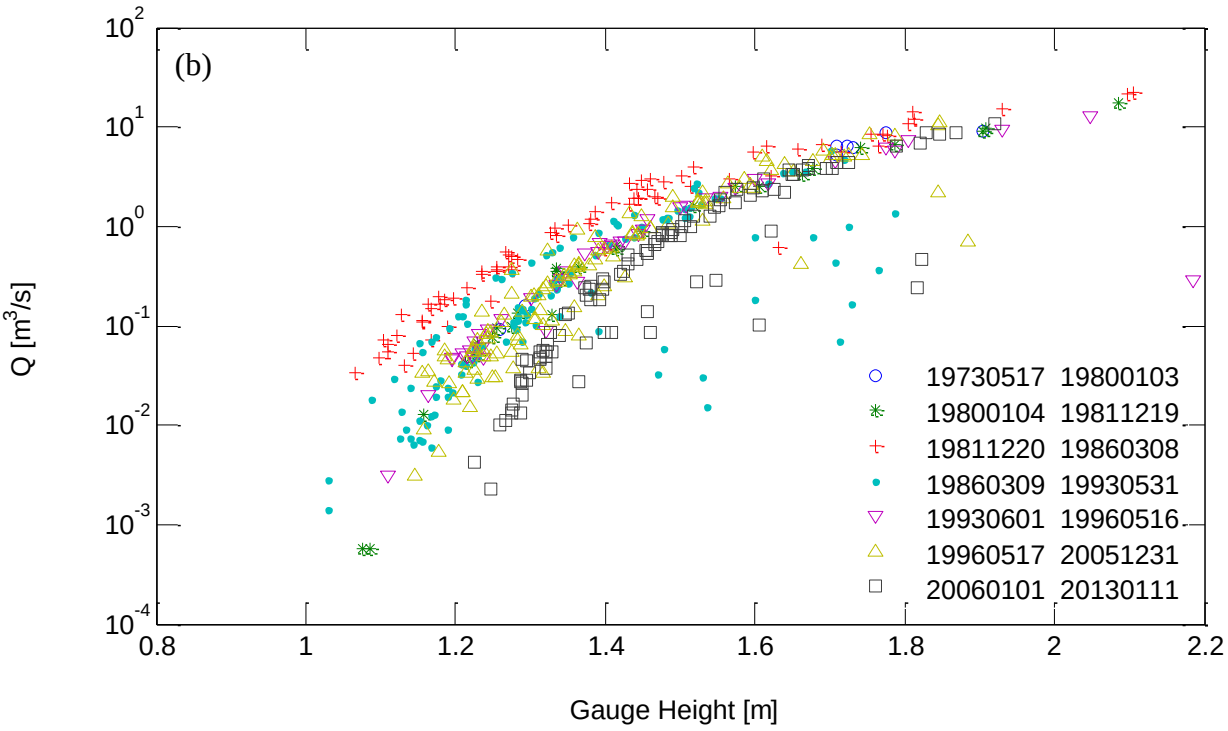

Figure A.4. (a) Q_s vs Q relationship from 1972 to 1992, (b) Q vs Gauge Height, and (c) photo image of site location from Google Earth at Ward Creek at HWY 89 nr Tahoe Pines, CA.

5. Trout Creek near Tahoe Valley, CA. (USGS site number 10336780)

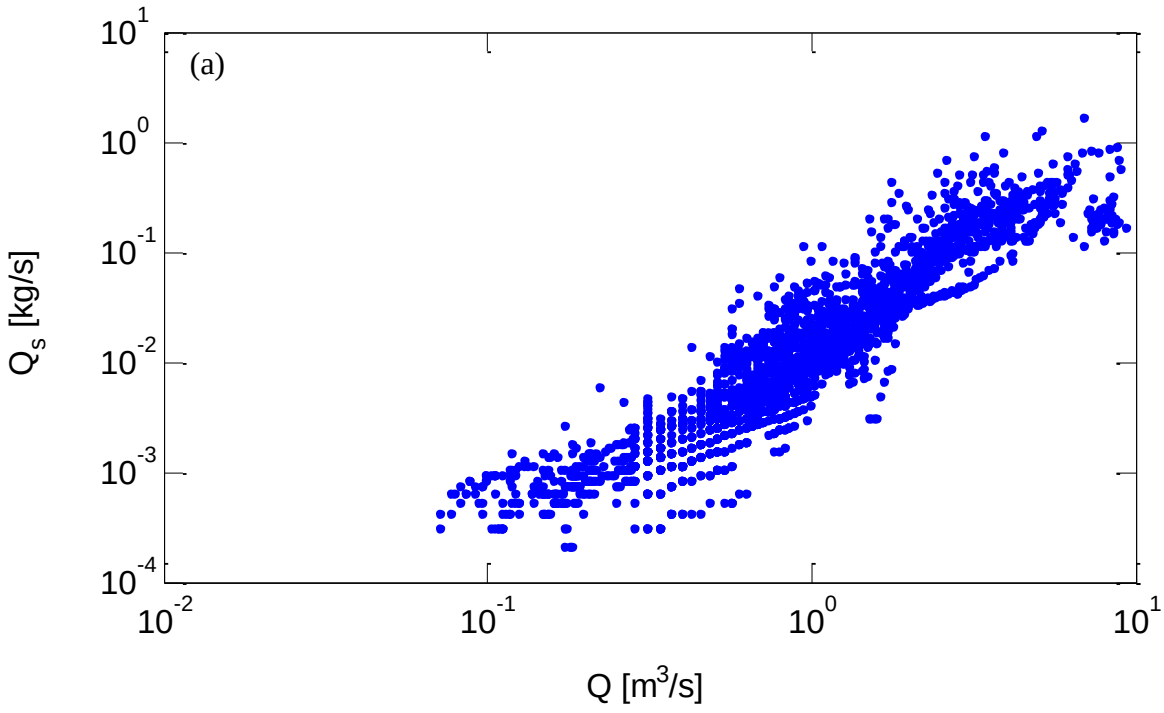

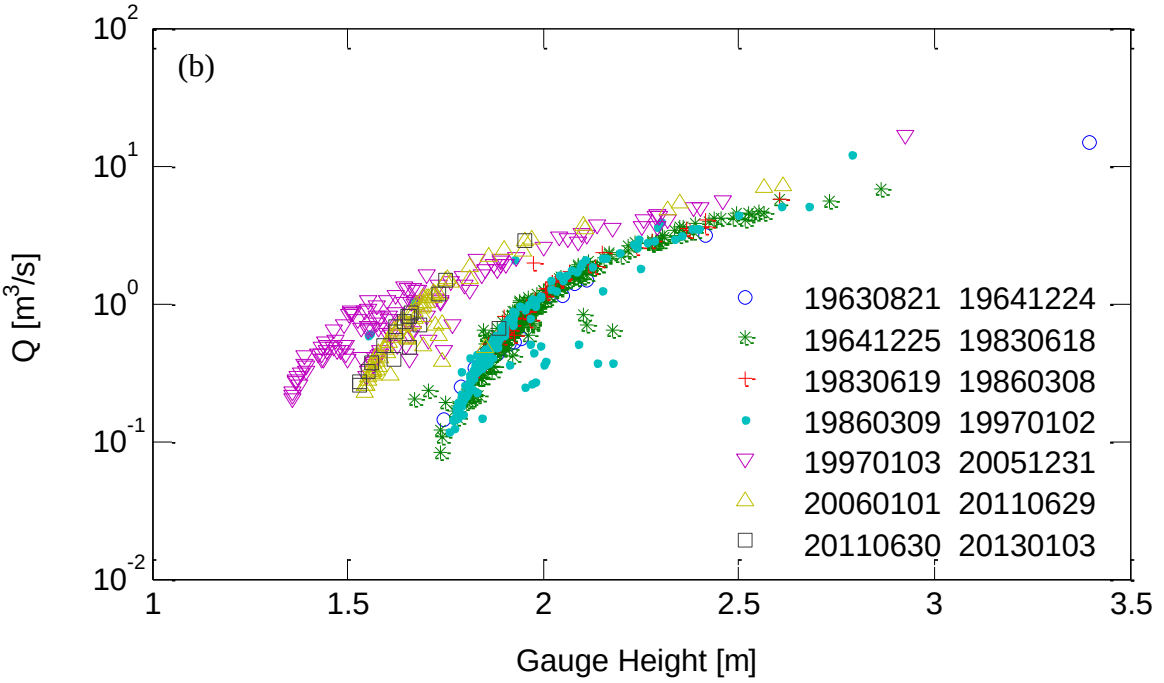

Figure A.5. (a) Q_s vs Q relationship from 1973 to 1988, (b) Q vs Gauge Height, and (c) photo image of site location from Google Earth at Trout Creek near Tahoe Valley, CA.

6. Sespe Creek near Fillmore, CA. (USGS site number 11113000)

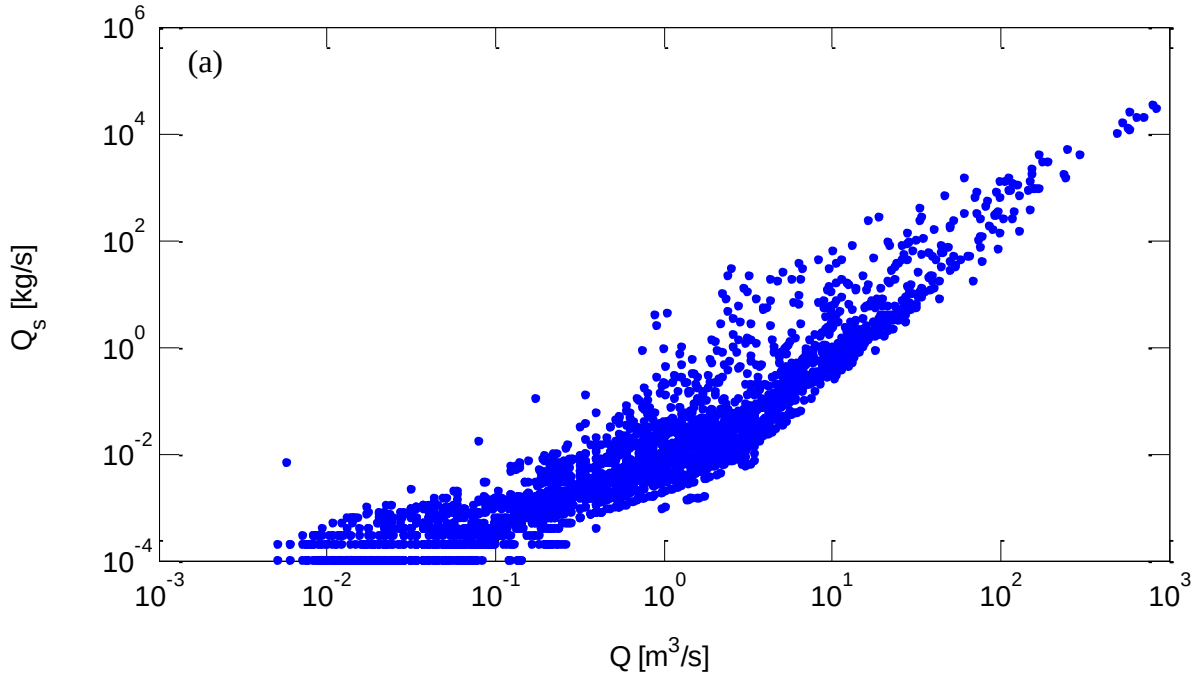

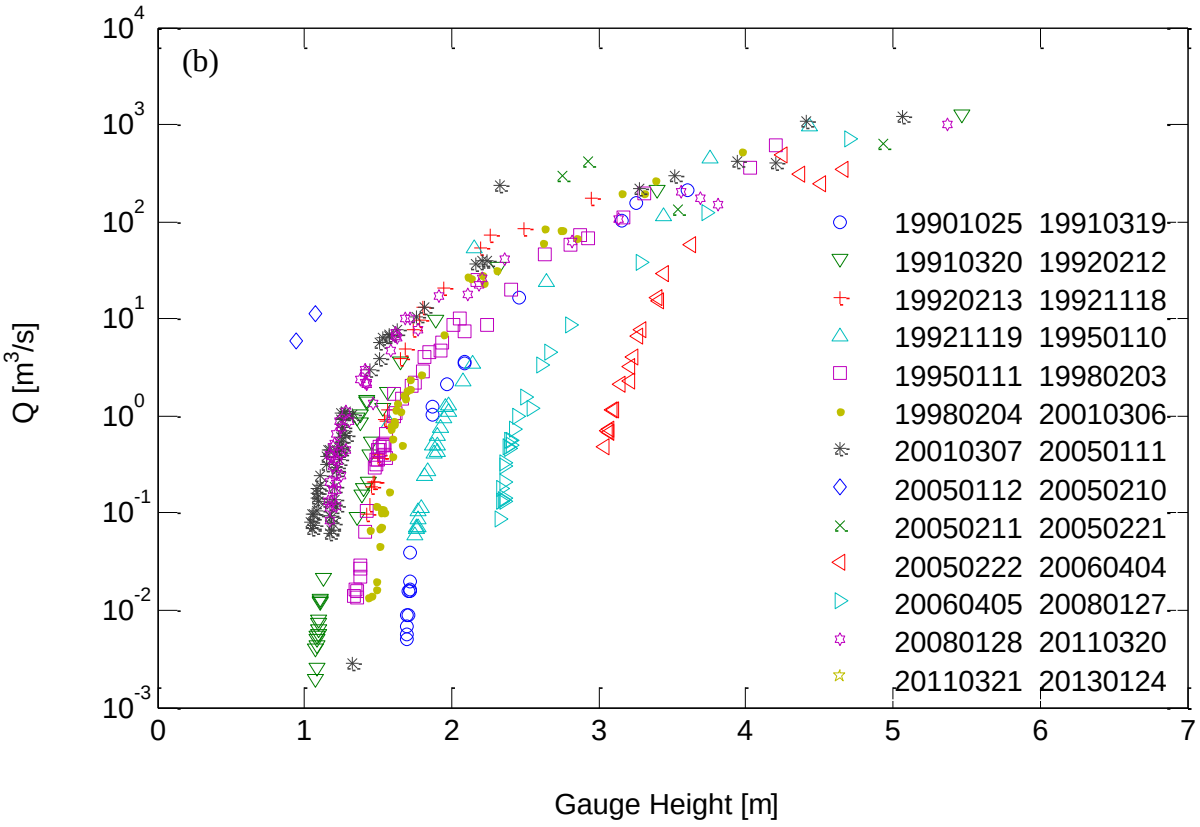
(b)
Q [m3/s]
Gauge Height [m]
19901025 19910319
19910320 19920212
19920213 19921118
19921119 19950110
19950111 19980203
19980204 20010306
20010307 20050111
20050112 20050210
20050211 20050221
20050222 20060404
20060405 20080127
20080128 20110320
20110321 20130124


(c)

Figure A.6. (a) Q_s vs Q from 1966 to 1978, (b) Q vs Gauge Height, (c) stream flow, and (d) channel bed. Photos were taken from field investigation at Sespe Creek near Fillmore, CA.

7. Nacimiento River below Sapaque Creek, near Bryson CA. (USGS site number 11148900)

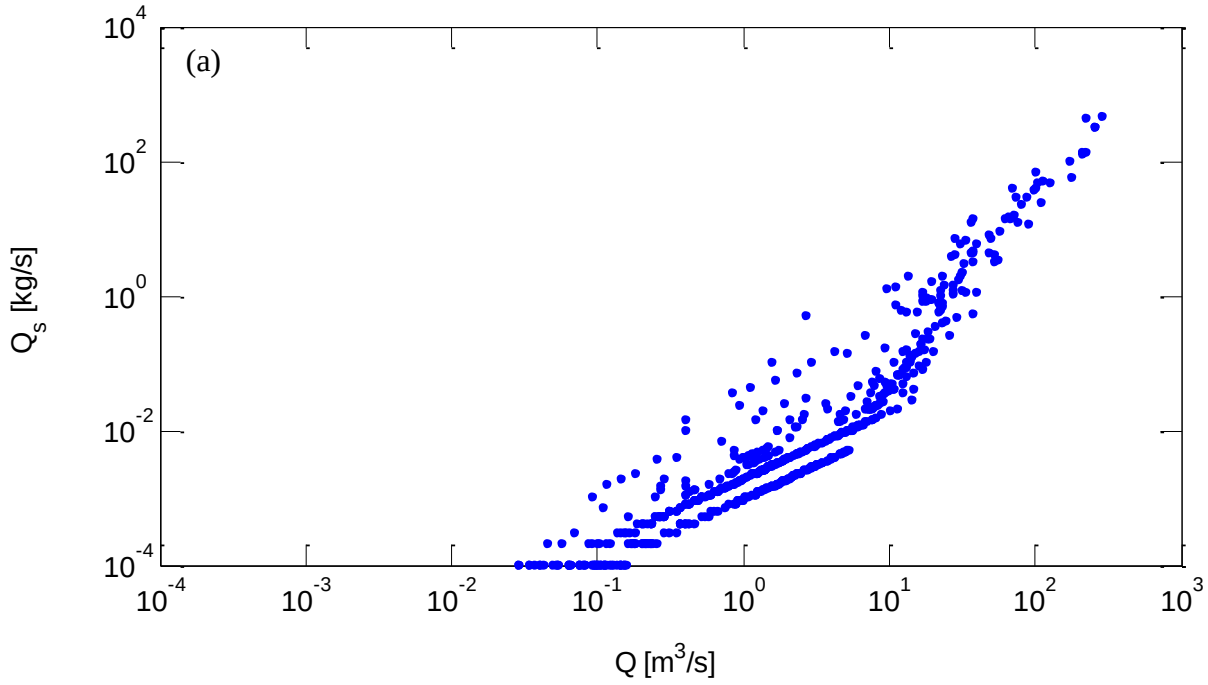

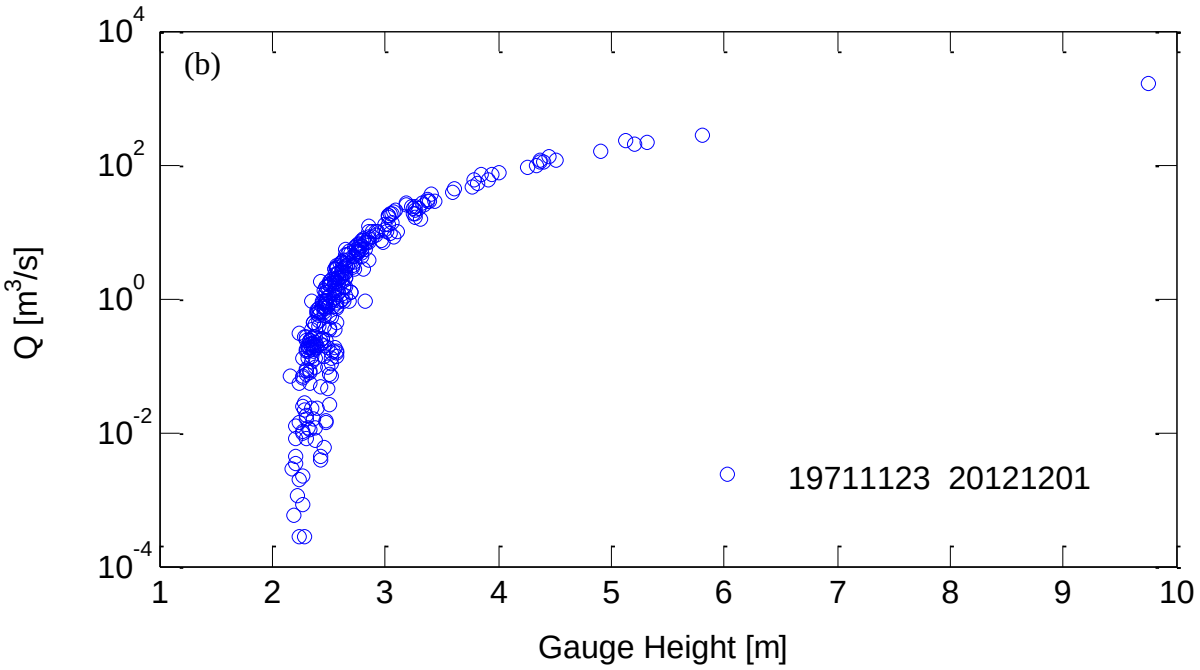

Figure A.7. (a) Q_s vs Q relationship from 1971 to 1974, (b) Q vs Gauge Height, and (c) photo provided by USGS Santa Cruz field office at Nacimiento River below Sapaque Creek, near Bryson CA.

8. Arroyo Seco near Greenfield, CA. (USGS site number 11151870)

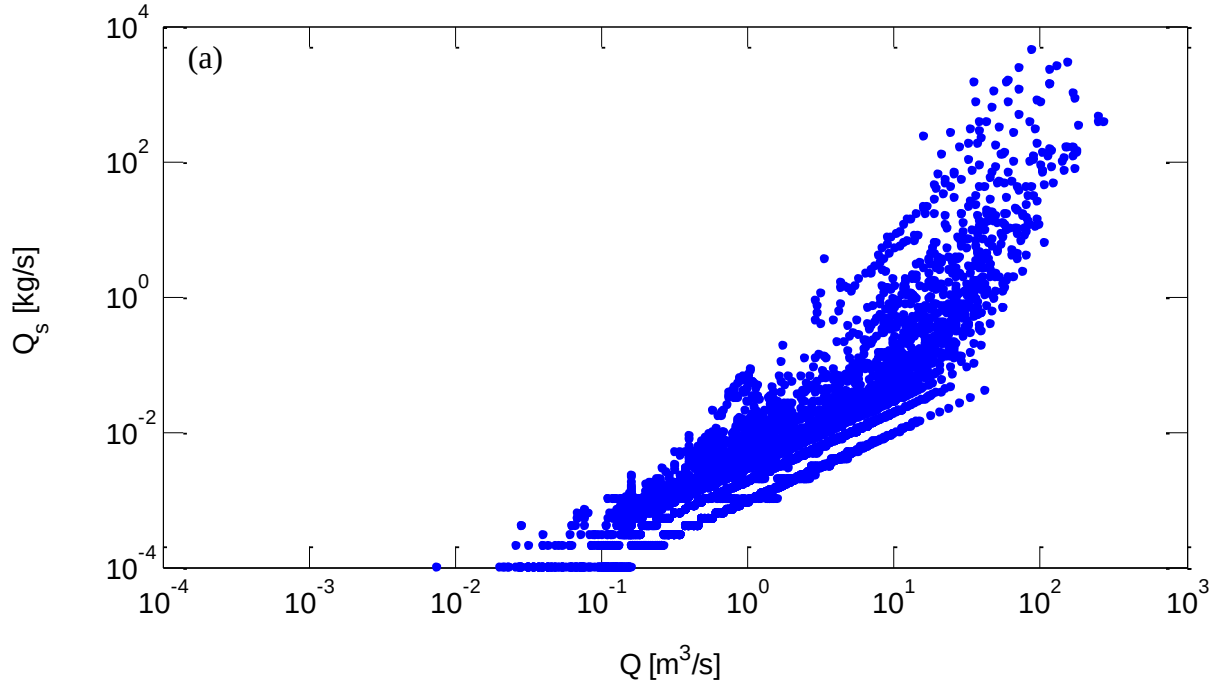

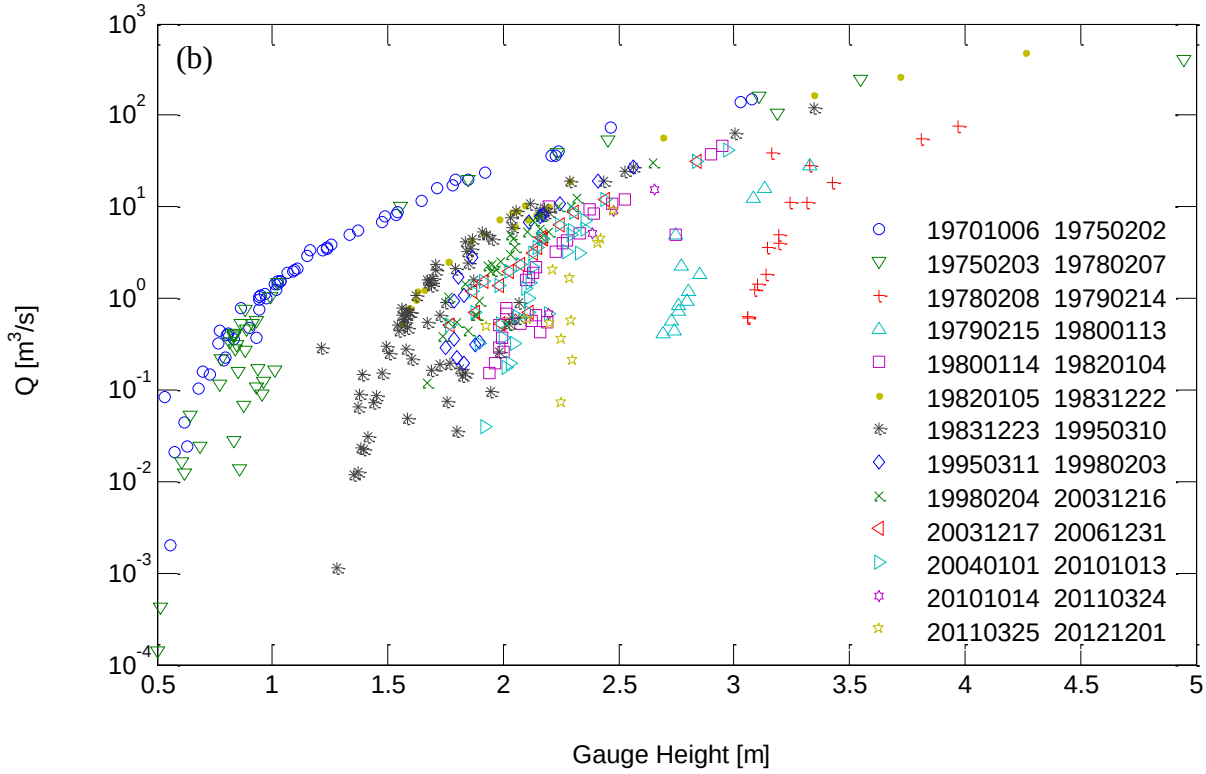

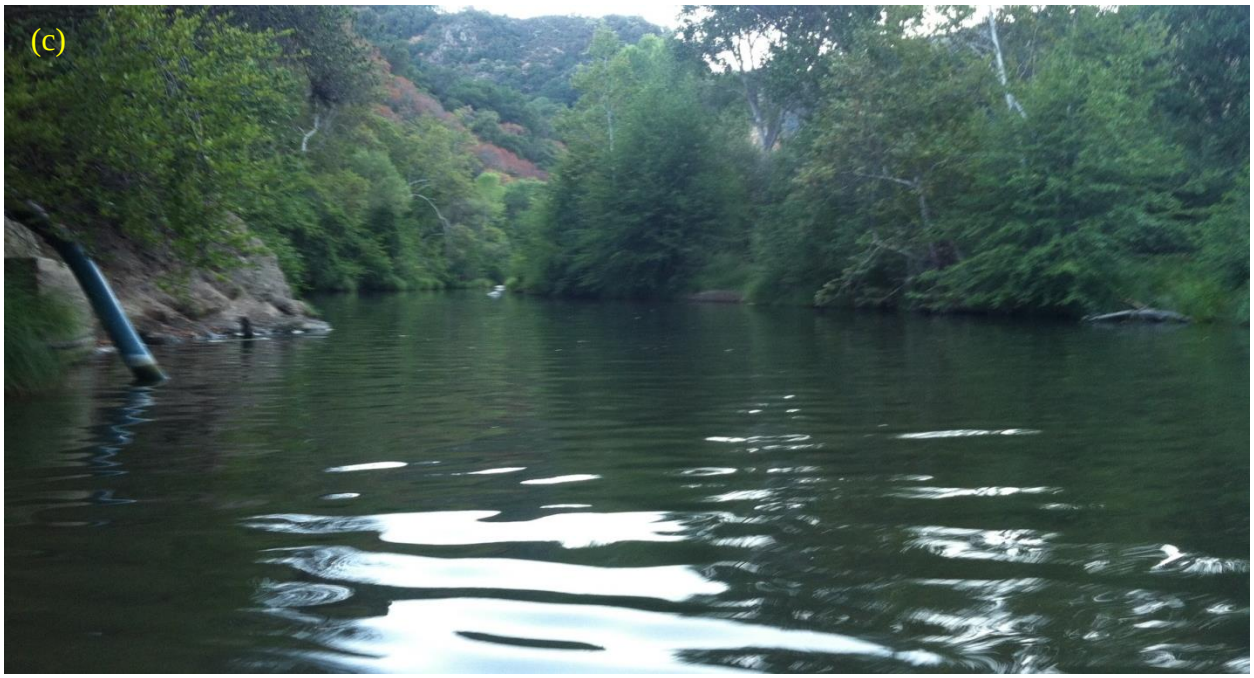

Figure A.8. (a) Q_s vs Q relationship from 1964 to 1984, (b) Q vs Gauge Height, (c) stream flow, and (d) gravel dredged from channel bottom. Photos were taken from field investigation at Arroyo Seco near Greenfield, CA.

9. Coyote Creek near Gilroy, CA. (USGS site number 11169800)

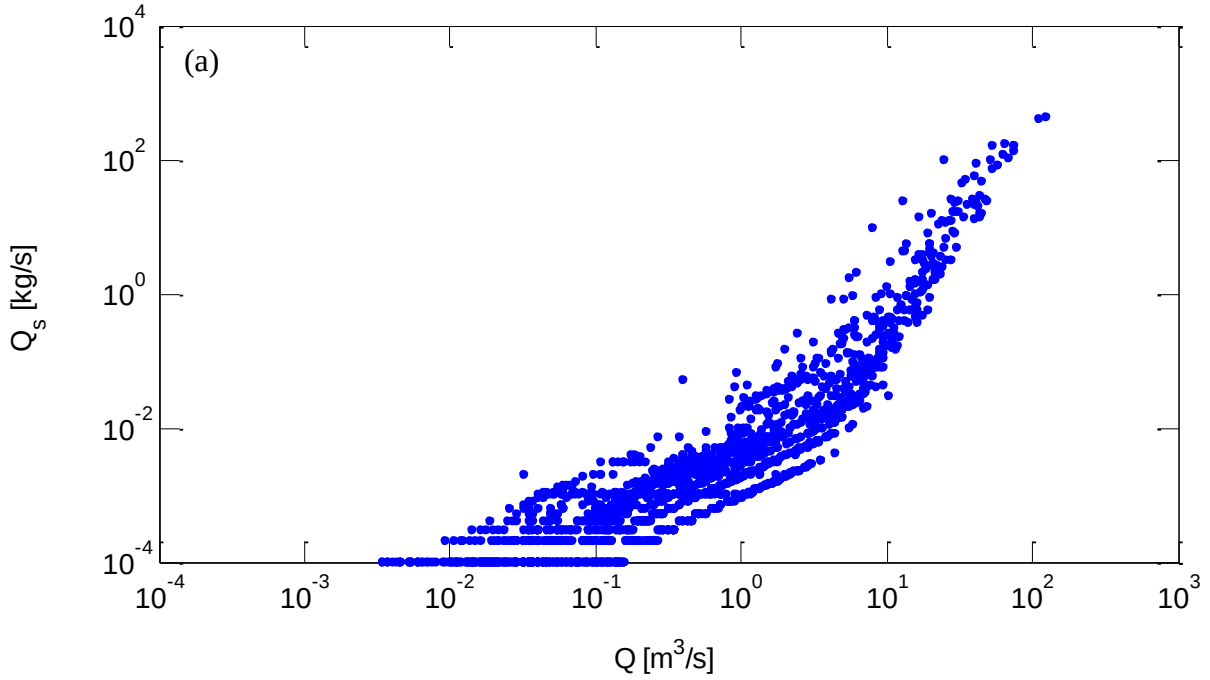

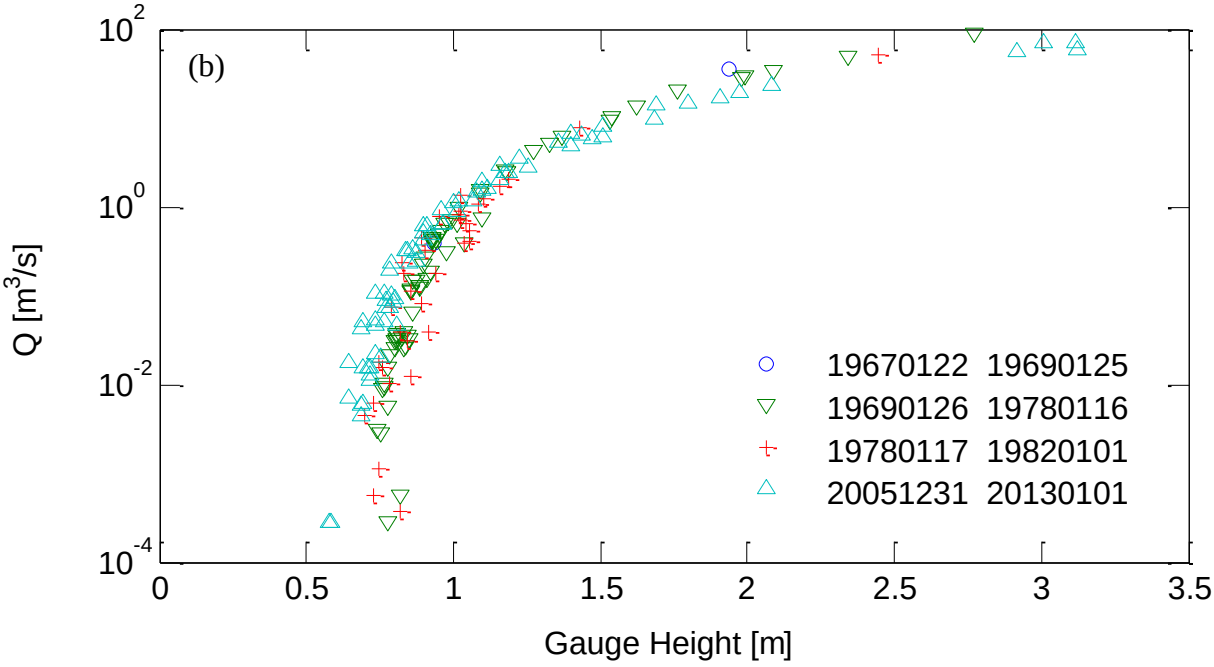

Figure A.9. (a) Q_s vs Q relationship from 1965 to 1976, (b) Q vs Gauge Height, (c) stream flow, and (d) channel bed. Photos were taken from field investigation at Coyote Creek near Gilory, CA.

10. Cosumnes River at Michigan Bar, CA. (USGS site number 11335000)

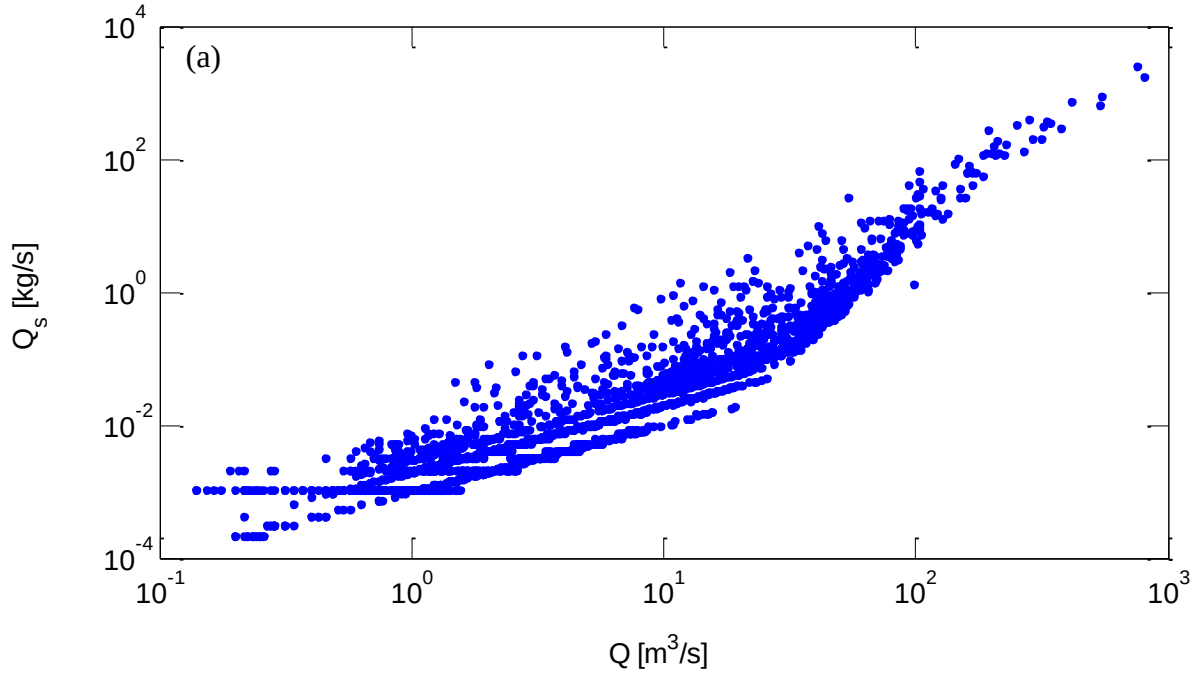

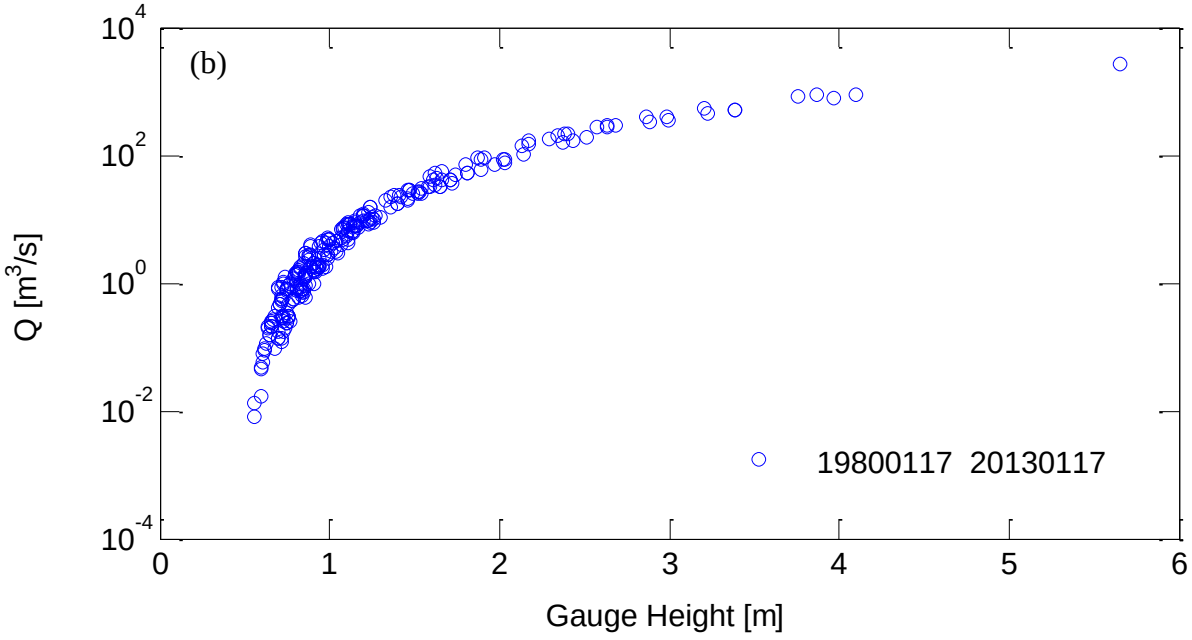

Figure A.10. (a) Q_s vs Q relationship from 1962 to 1970, (b) Q vs Gauge Height, (c) channel with gravels and cobbles. Photo was taken from field investigation at Cosumnes River at Michigan Bar, CA.

11. Thomes Creek at Paskenta, CA. (USGS site number 11382000)

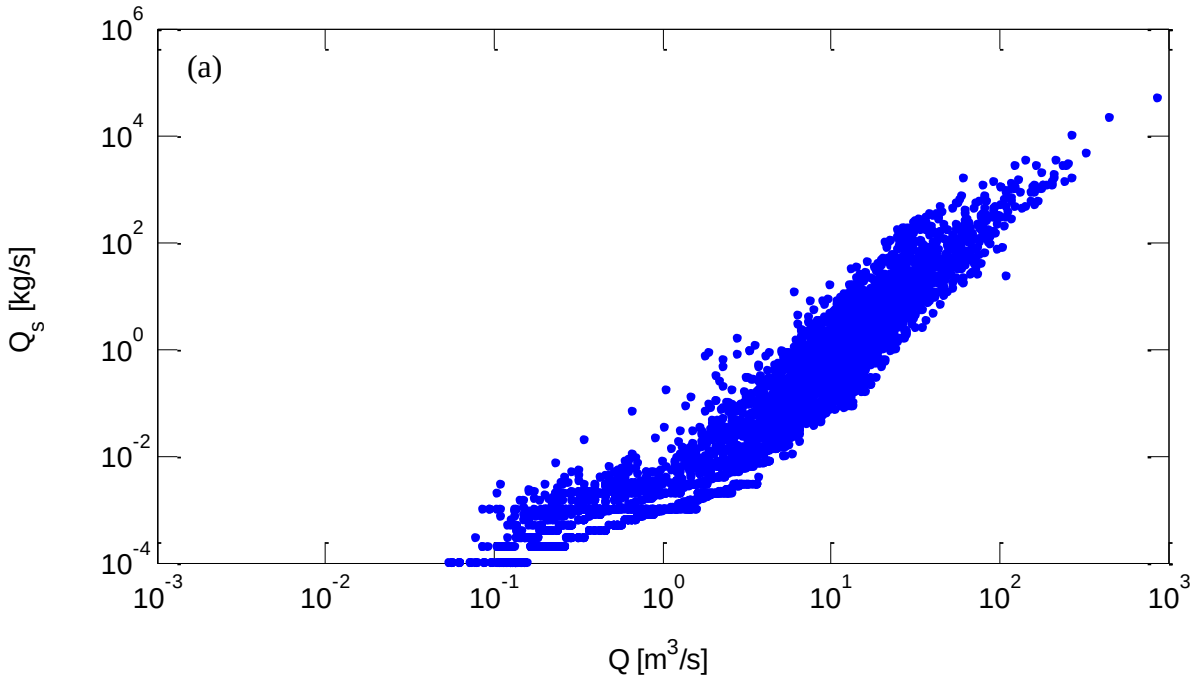

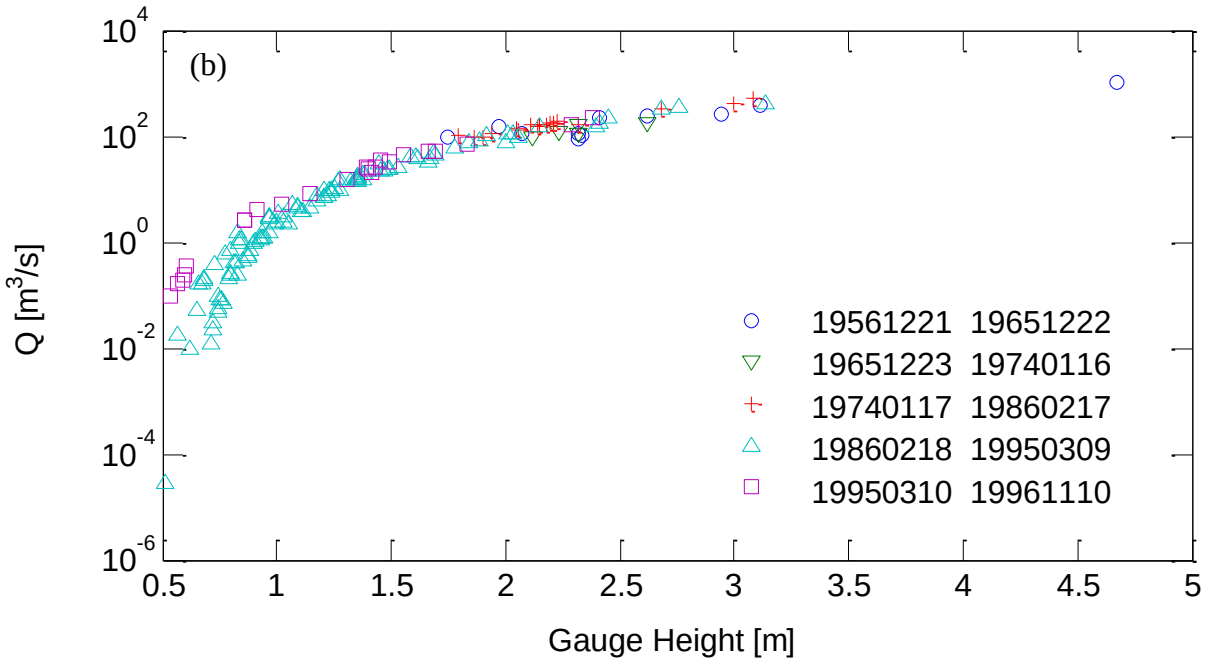
(b)
Q [m3/s]
Gauge Height [m]
19561221 19651222
19651223 19740116
19740117 19860217
19860218 19950309
19950310 19961110


(c)

Figure A.11. (a) Q_s vs Q relationship from 1962 to 1983, (b) Q vs Gauge Height, (c) and (d) photos taken from field investigation at Thomes Creek at Paskenta, CA.

12. Pena Creek near Geyserville, CA. (USGS site number 11465150)

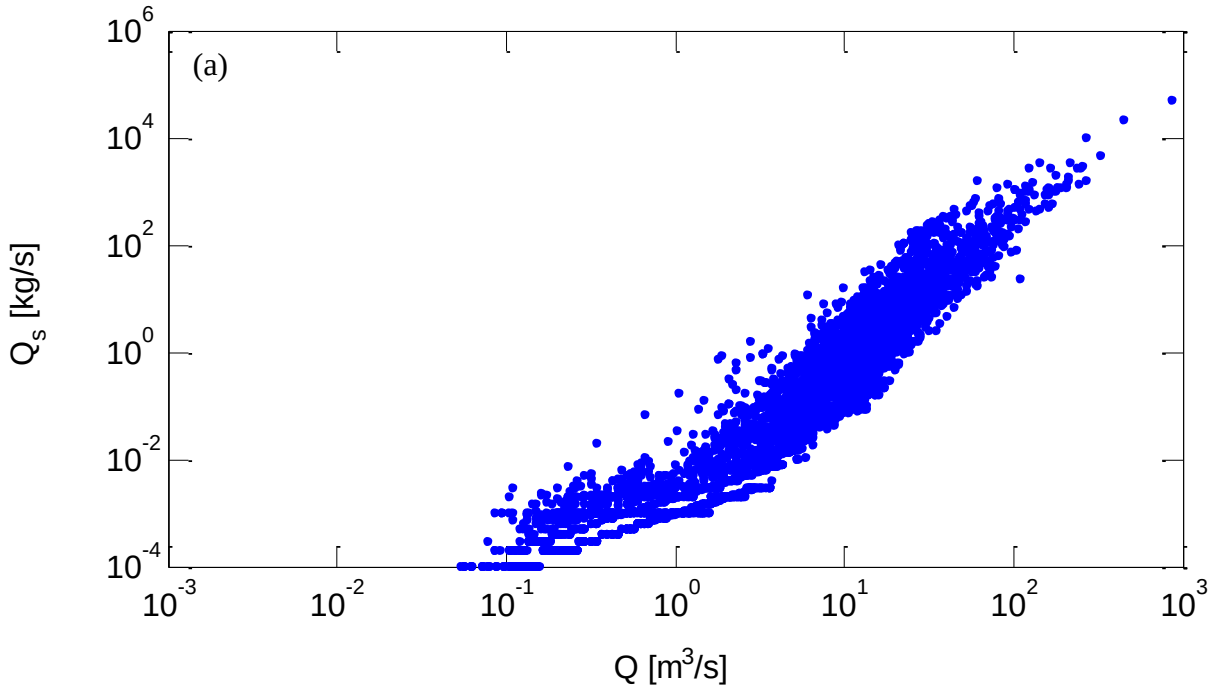

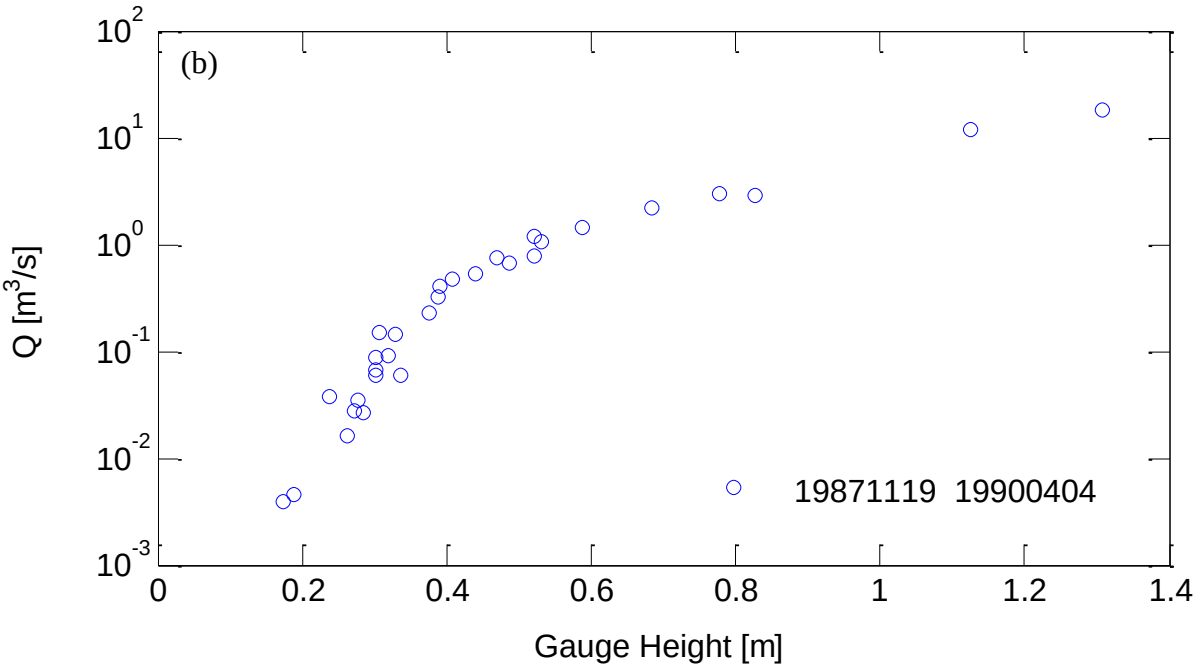

Figure A.12. (a) Q_s vs Q relationship from 1978 to 1986, (b) Q vs Gauge Height, (c) and (d) photos taken from field investigation at Pena Creek near Geyserville, CA.

13. Dry Creek near Geyserville, CA. (USGS site number 11465200)

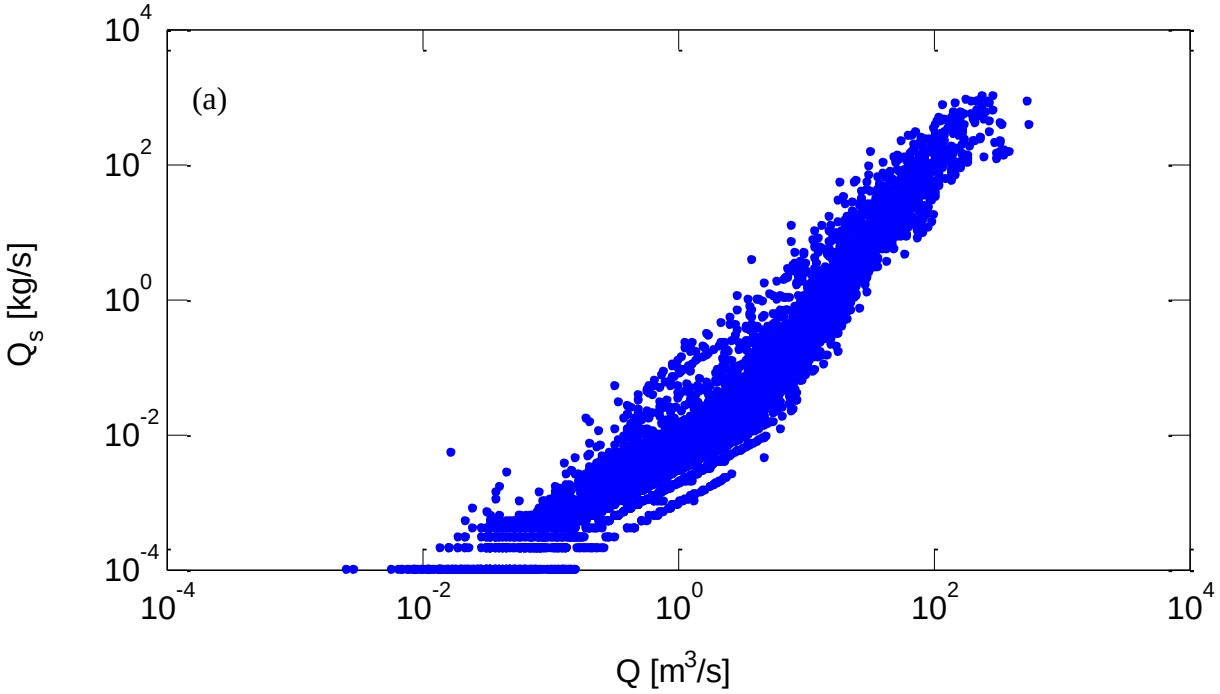

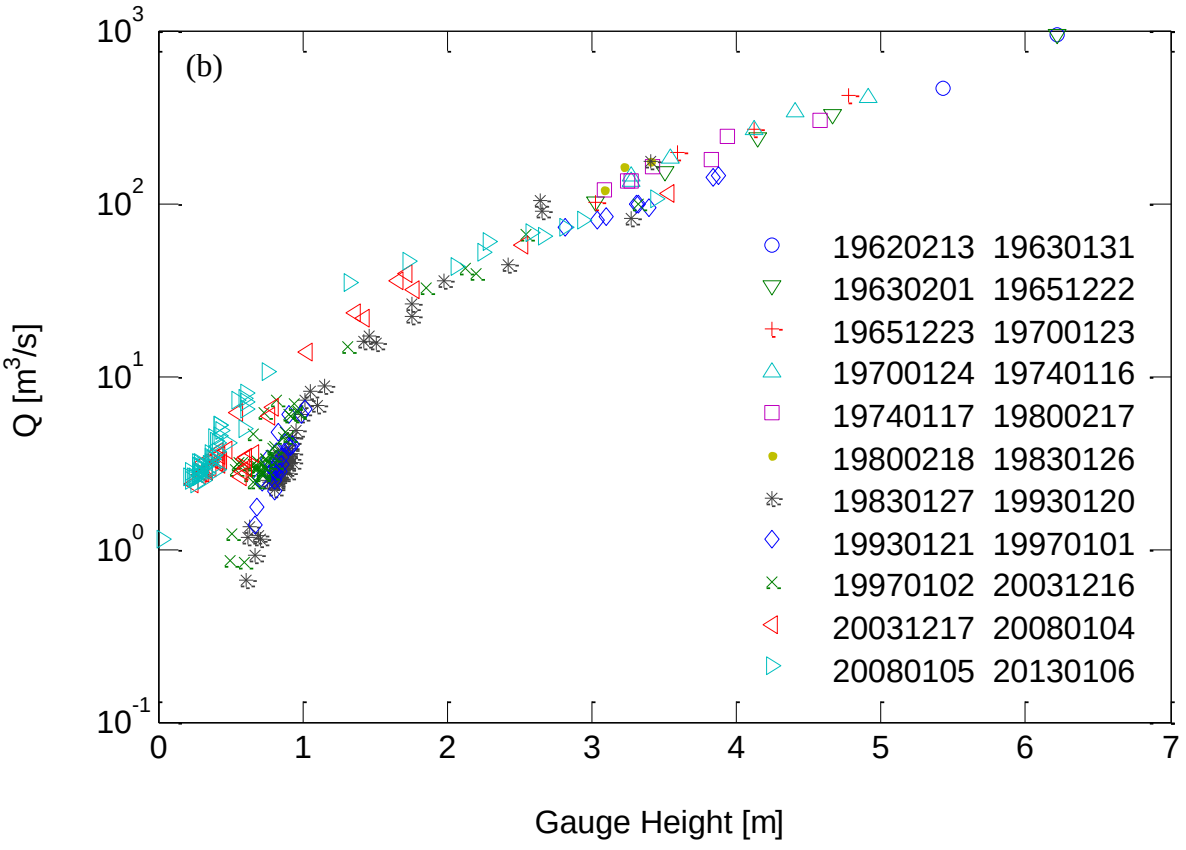

Figure A.13. (a) Q_s vs Q relationship from 1964 to 1986, (b) Q vs Gauge Height, (c) stream flow and (d) gravel channel bed. Photos were taken from field investigation at Dry Creek near Geyserville, CA.

14. Navarro River near Navarro, CA. (USGS site number 11468000)

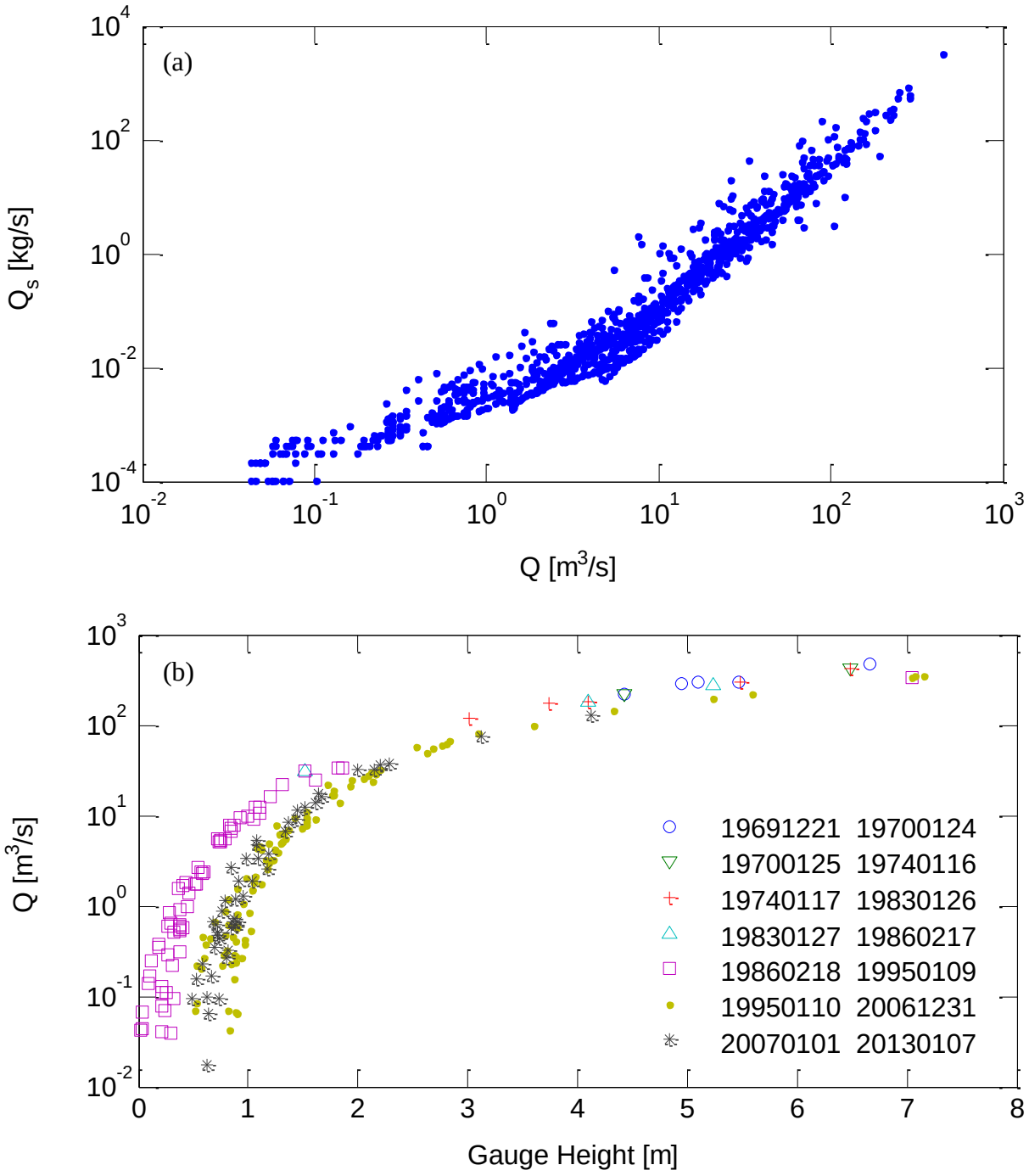

Figure A.14. (a) Q_s vs Q relationship from 1998 to 2003, (b) Q vs Gauge Height, (c) gravelly channel bed. Photo was taken from field investigation at Navarro River near Navarro, CA.

15. Eel River near Dos Rios, CA. (USGS site number 11472150)

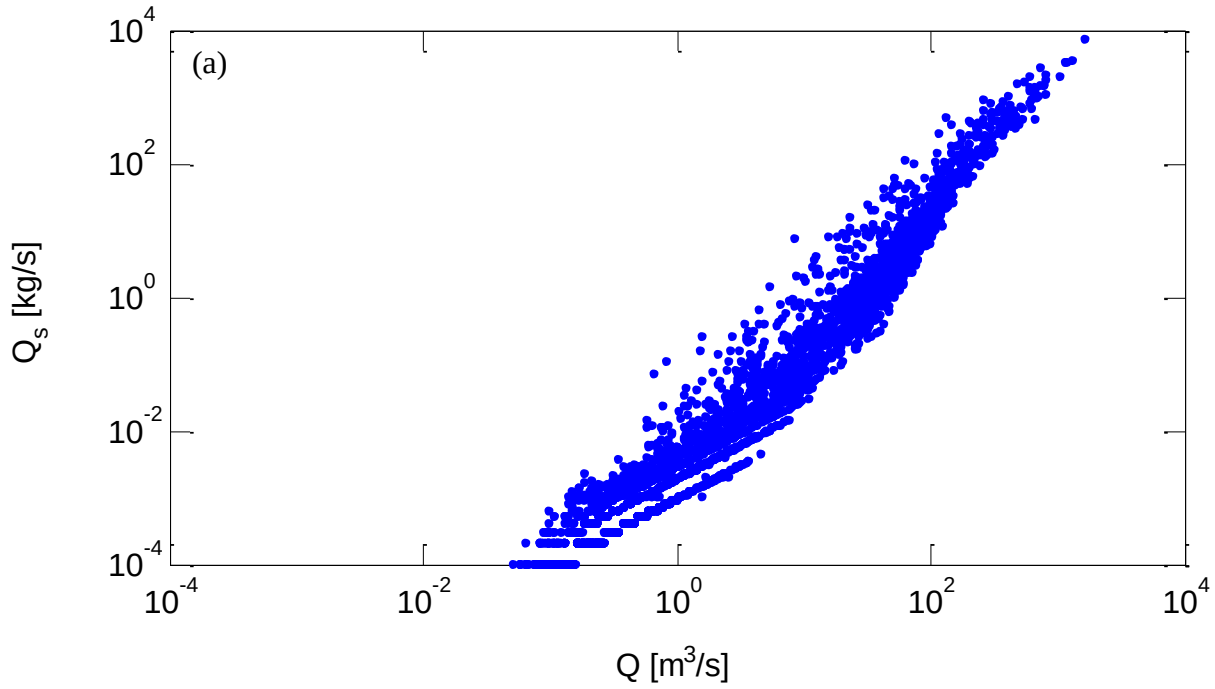

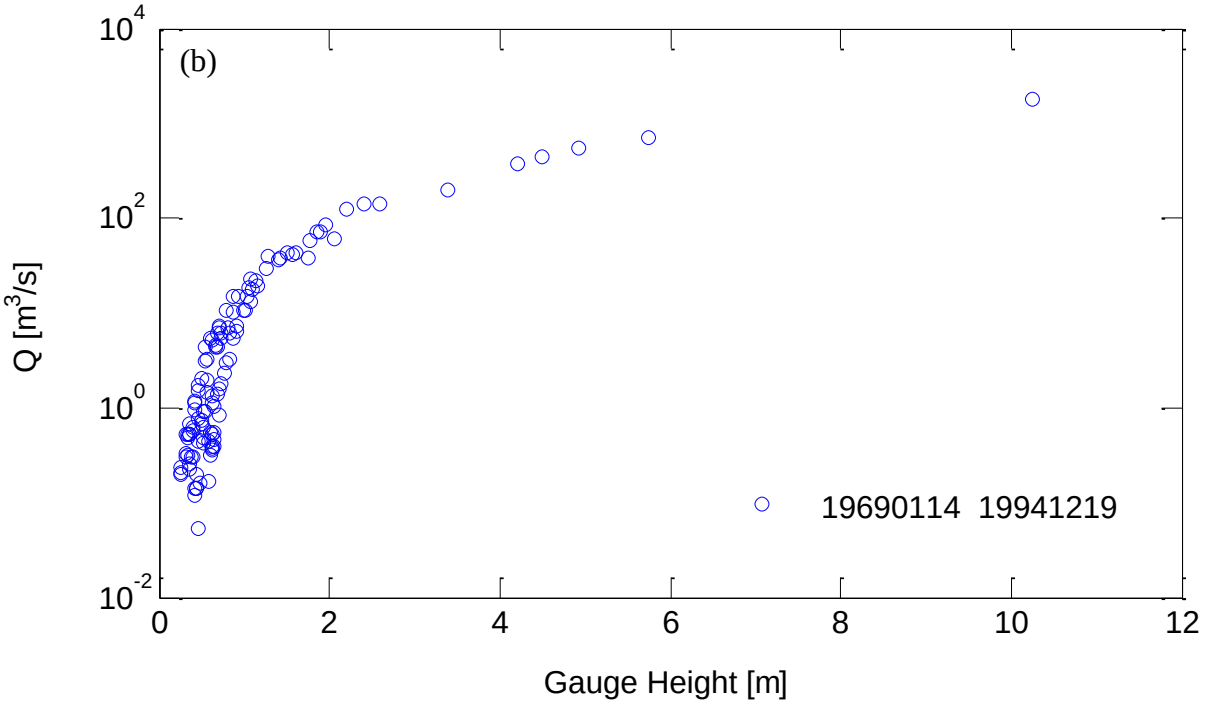

Figure A.15. (a) Q_s vs Q relationship from 1966 to 1977, (b) Q vs Gauge Height, (c) stream flow, and (d) bed material. Photos were taken from field investigation at Eel River near Dos Rios, CA.

16. Outlet Creek near Longvale, CA. (USGS site number 11472200)

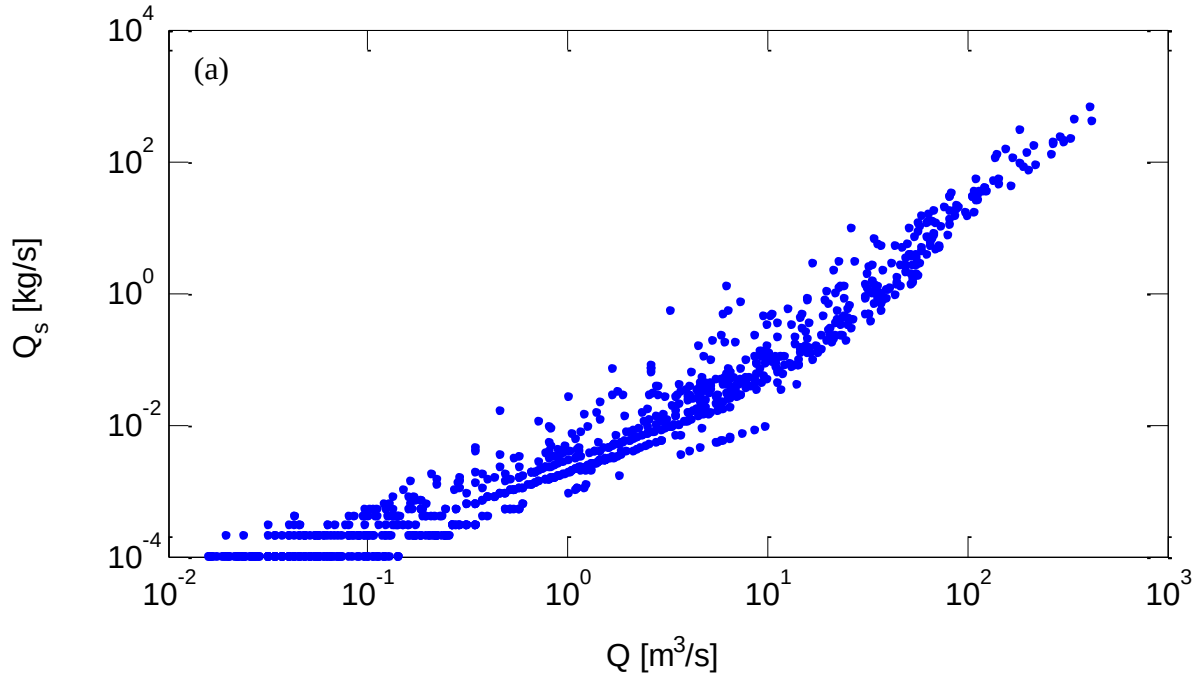

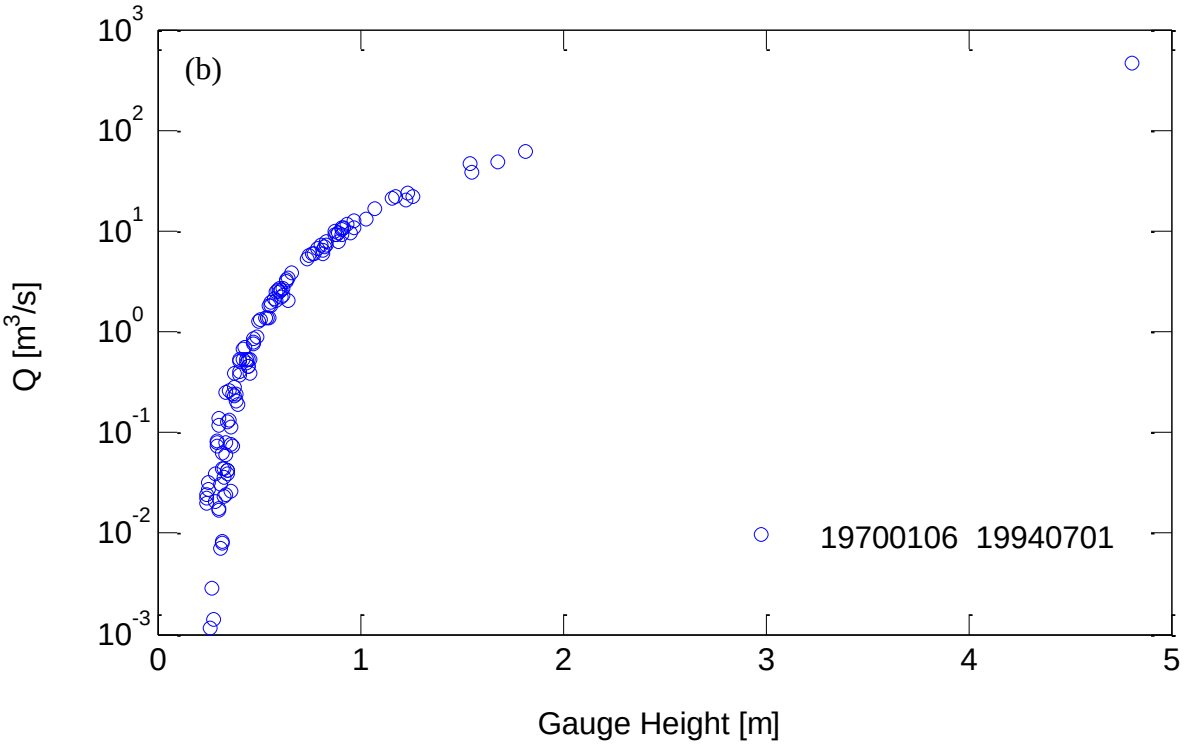

Figure A.16. (a) Q_s vs Q relationship from 1967 to 1970, (b) Q vs Gauge Height, (c) stream flow and (d) bed material. Photos were taken from field investigation at Outlet Creek near Longvale, CA.

17. MF Eel R above Black Butte River near Covelo, CA. (USGS site number 11472800)

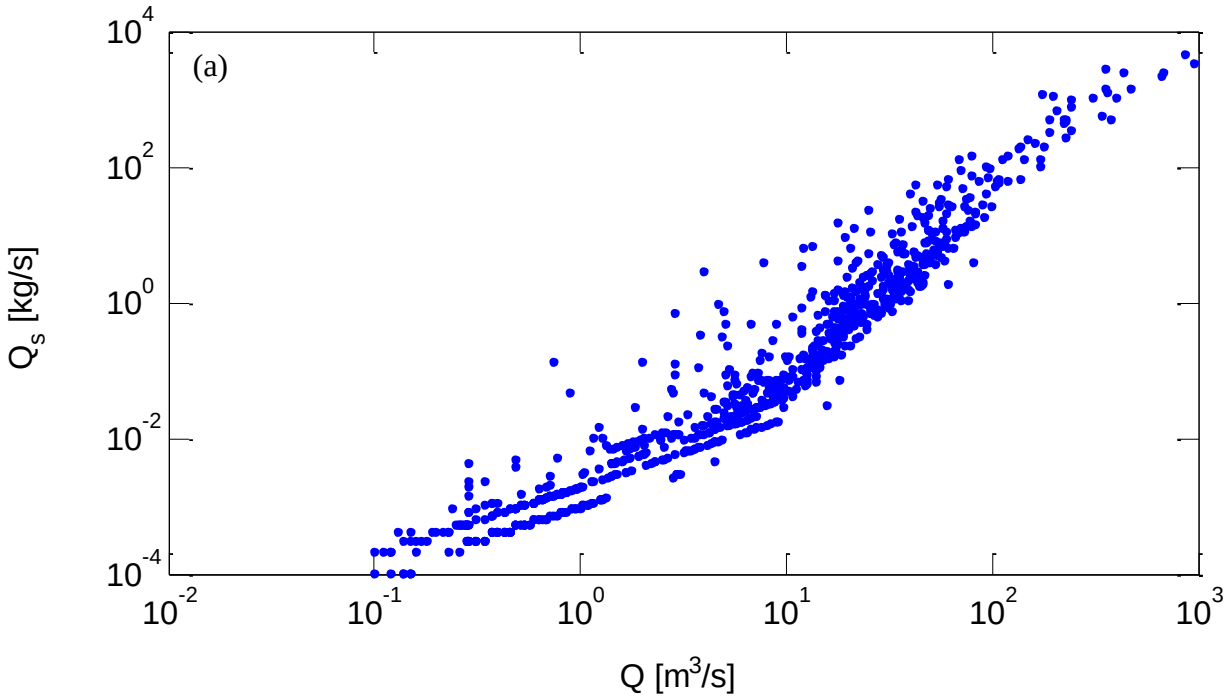

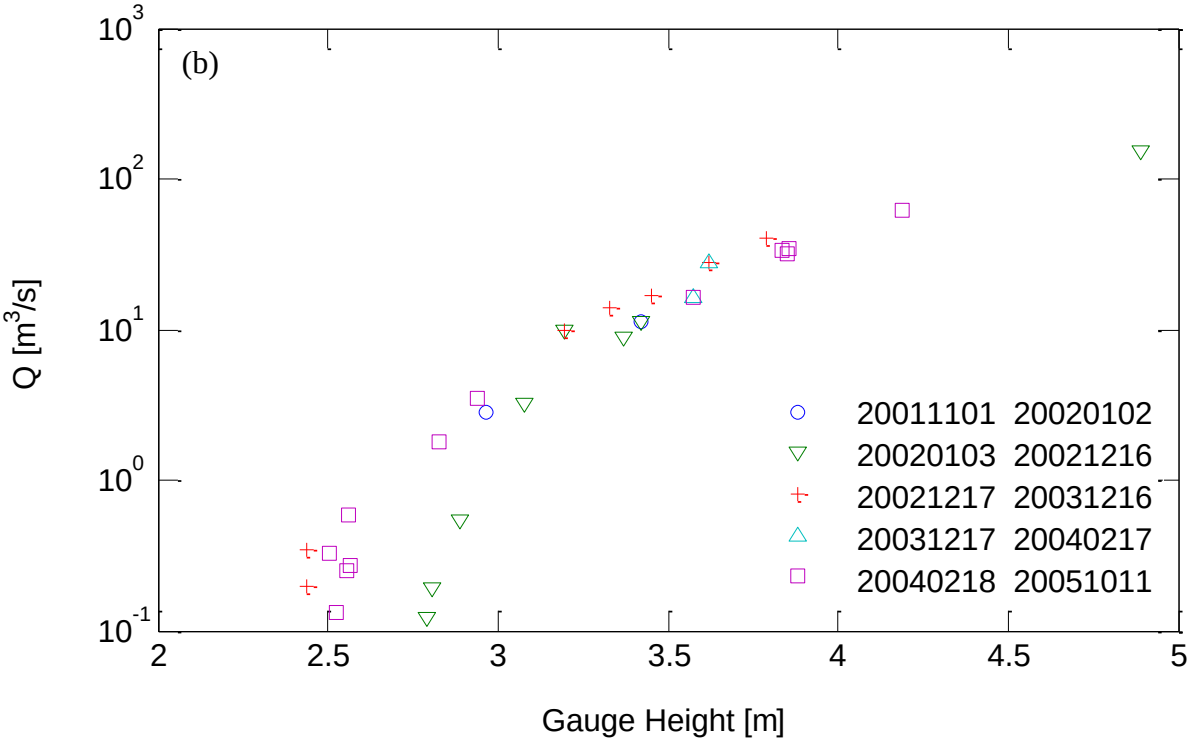

(c)

Figure A.17. (a) Q_s vs Q relationship from 1967 to 1970, (b) Q vs Gauge Height, (c) stream flow and (d) bed material. Photos were taken from field investigation at MF Eel River above Black Butte R near Covelo, CA.

18. Black Butte River near Covelo, CA. (USGS site number 11472900)

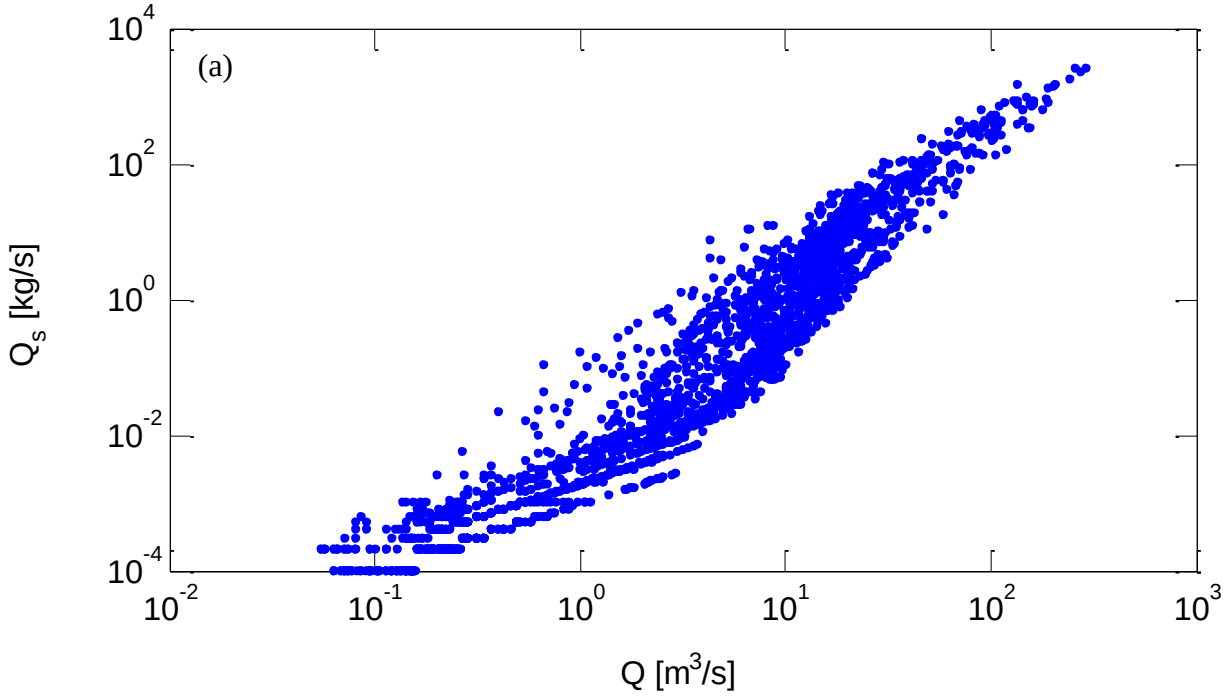

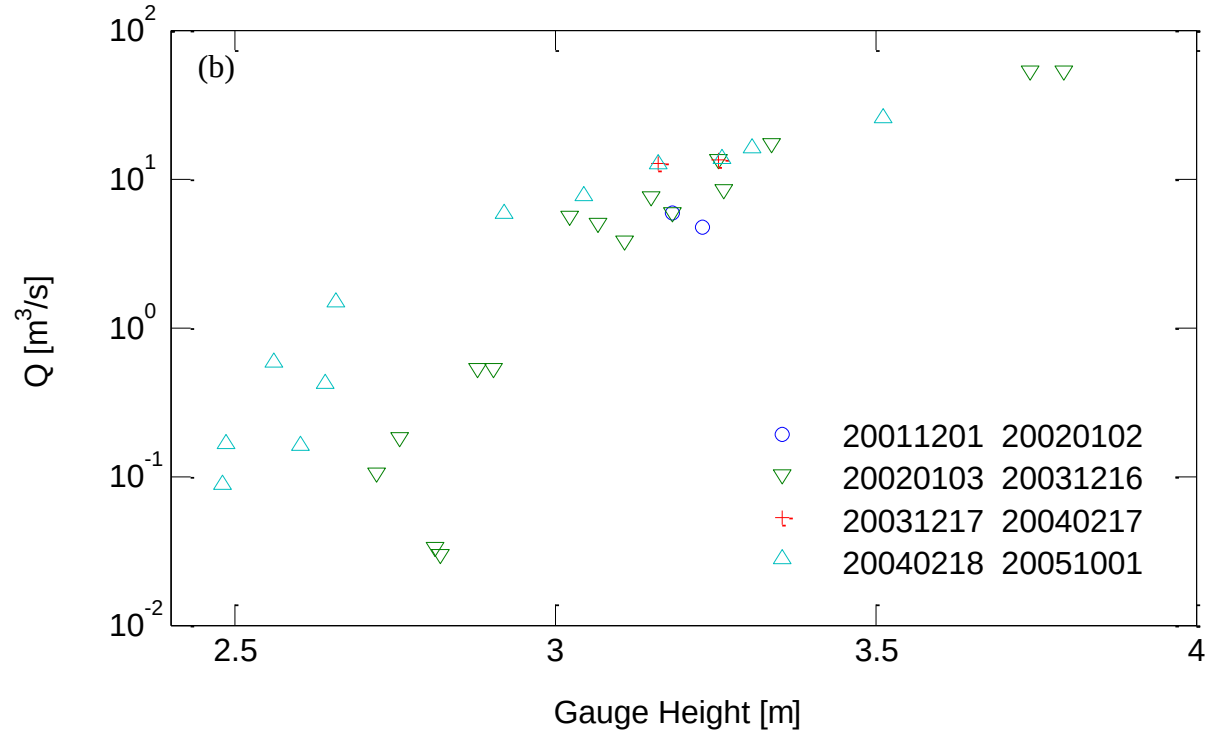

Figure A.18. (a) Q_s vs Q relationship from 1965 to 1973, (b) Q vs Gauge Height, (c) stream flow and (d) bed material. Photos were taken from field investigation at Black Butte River near Covelo, CA.

19. MF Eel River near Dos Rios, CA. (USGS site number 11473900)

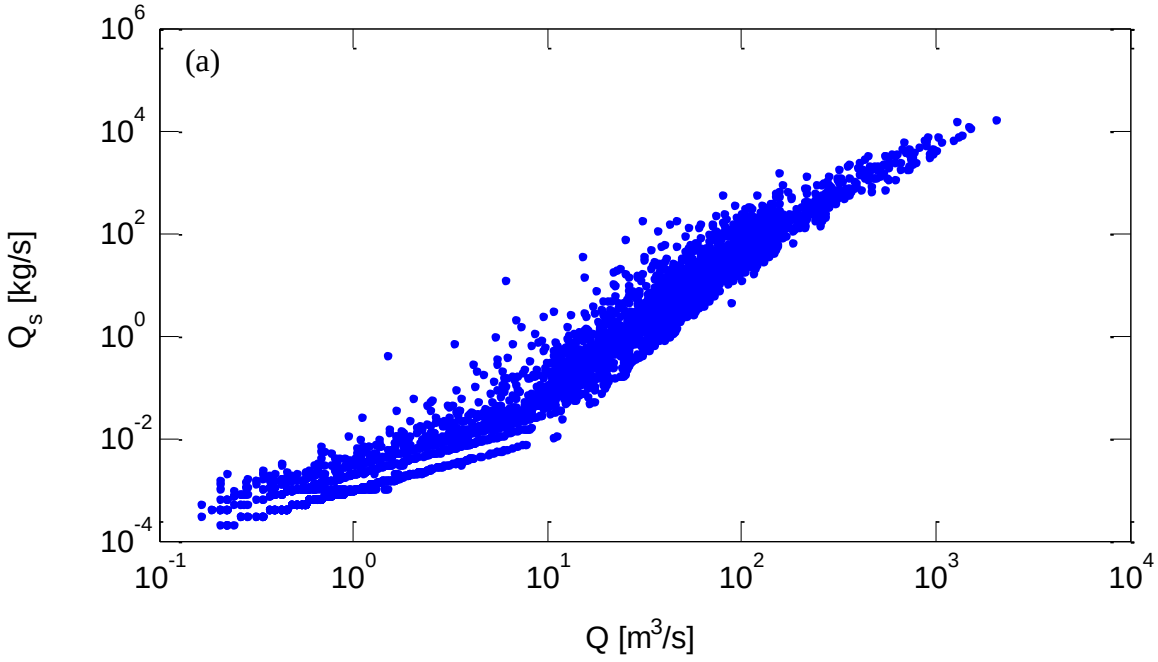

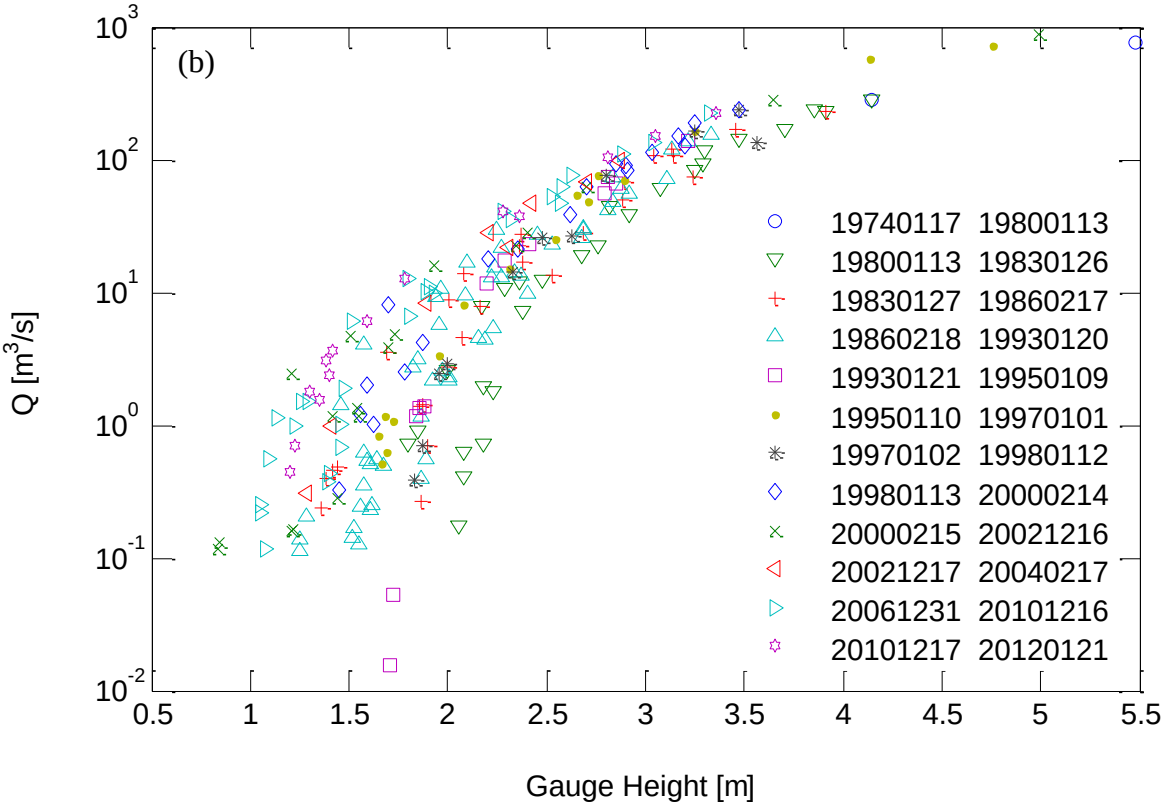

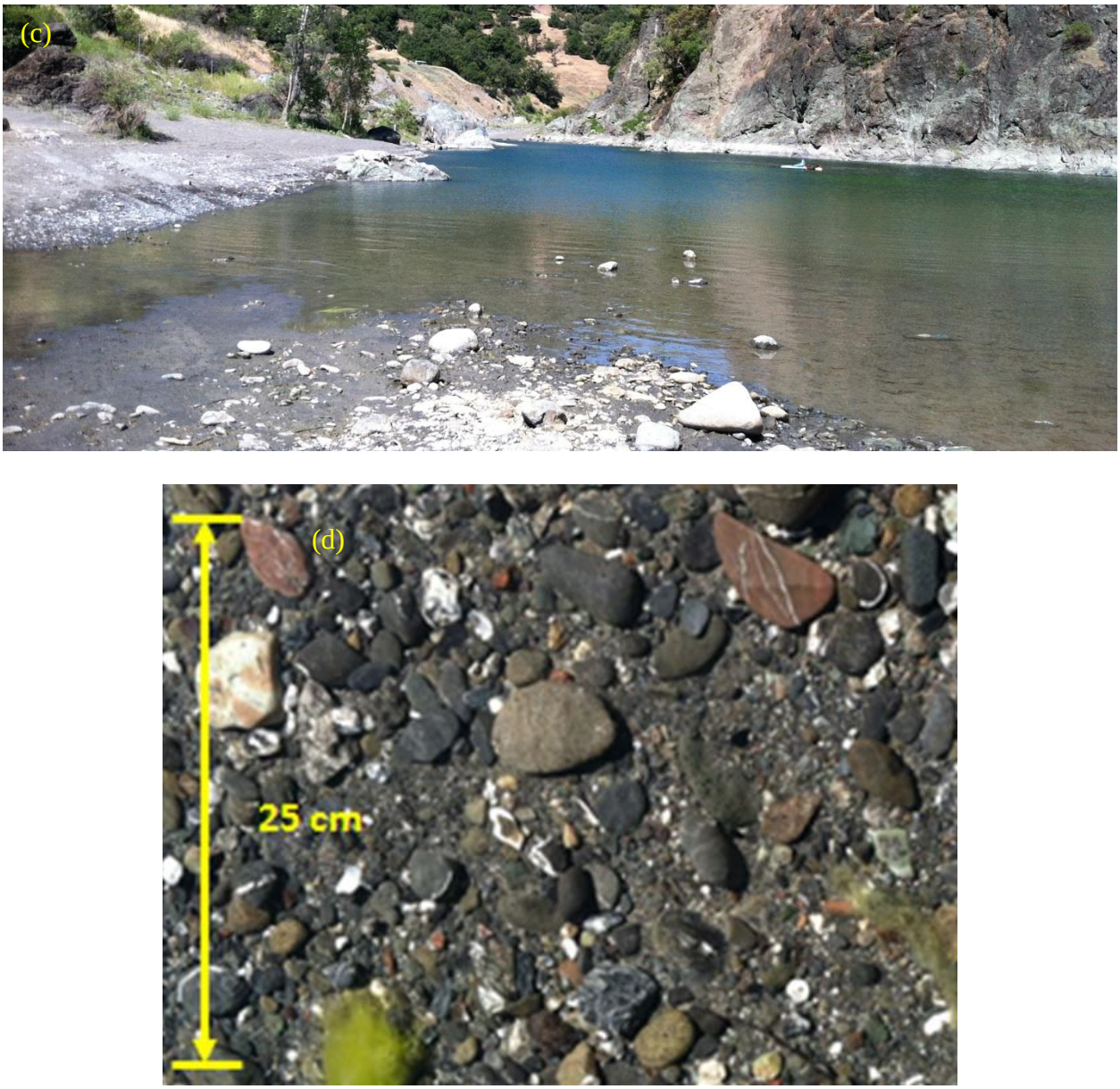

Figure A.19. (a) Q_s vs Q relationship from 1965 to 1976, (b) Q vs Gauge Height, (c) stream flow and (d) bed material. Photos were taken from field investigation at MF Eel River near Dos Rios, CA.

20. NF Eel River near Mina, CA. (USGS site number 11474500)

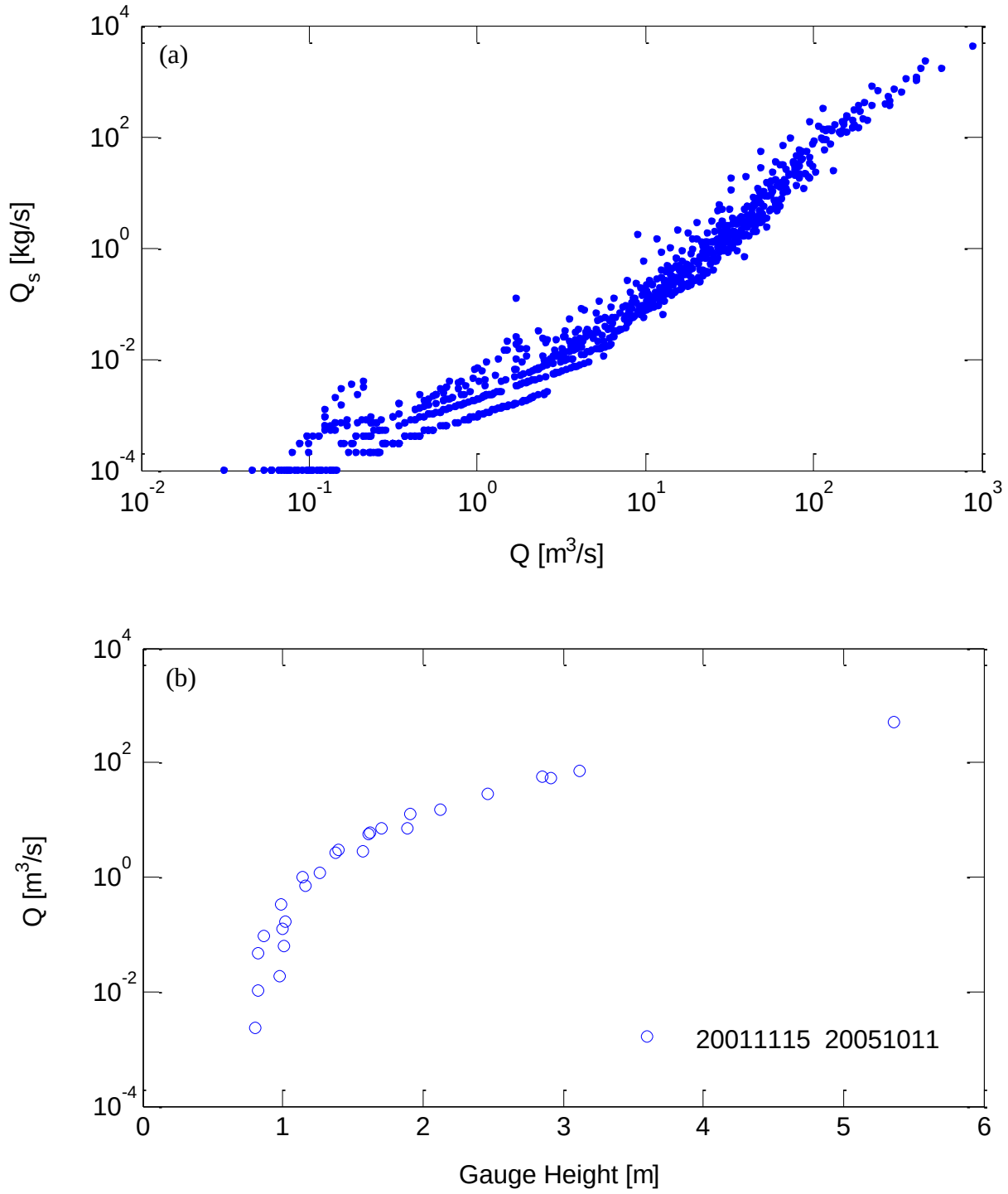

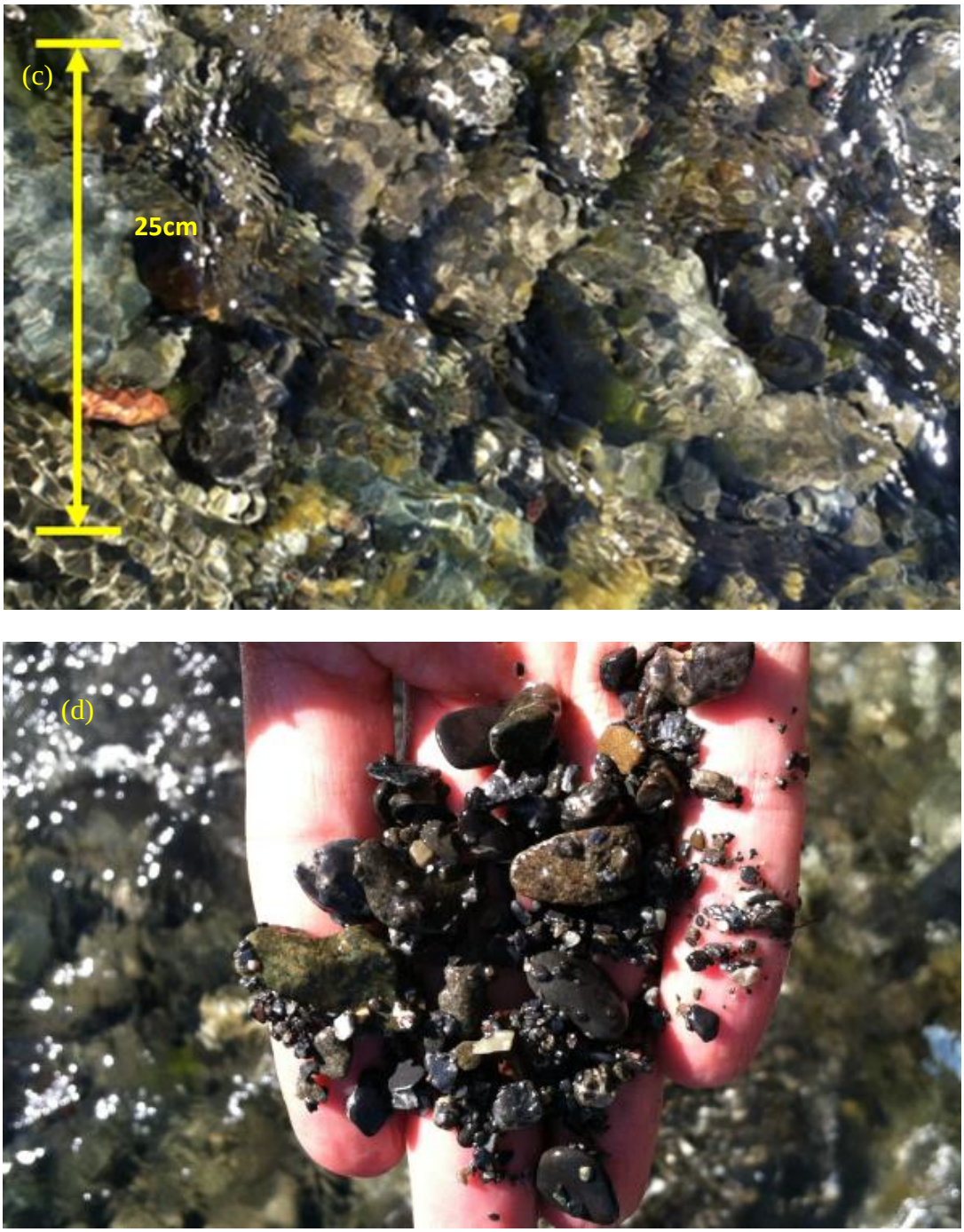

Figure A.20. (a) Q_s vs Q relationship from 1972 to 1975, (b) Q vs Gauge Height, (c) armored stream surface, and (d) bed materials below armor layer with fine gravels. Photos were taken from field investigation at NF Eel River near Mina, CA.

21. Eel River at Fort Seward, CA. (USGS site number 11475000)

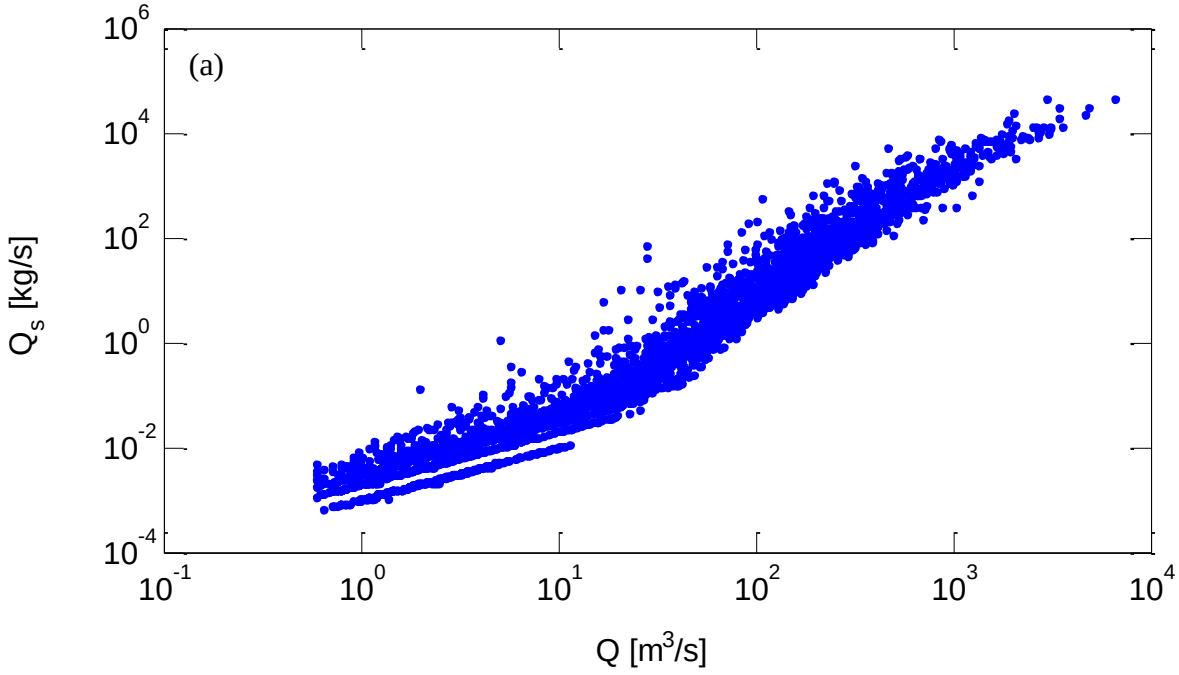

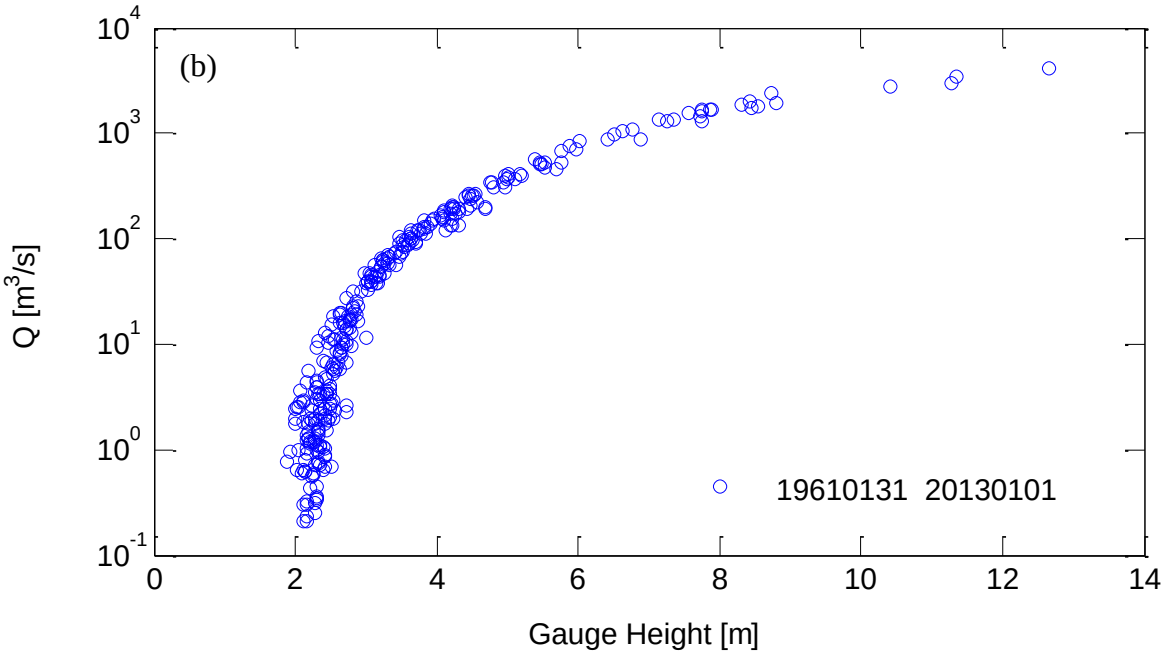

Figure A.21. (a) Q_s vs Q relationship from 1965 to 1991, (b) Q vs Gauge Height, (c) stream flow, and (d) bed materials at the surface of channel bed. Photos were taken from field investigation at Eel River at Fort Seward, CA.

22. Bull Creek near Weott, CA. (USGS site number 11476600)

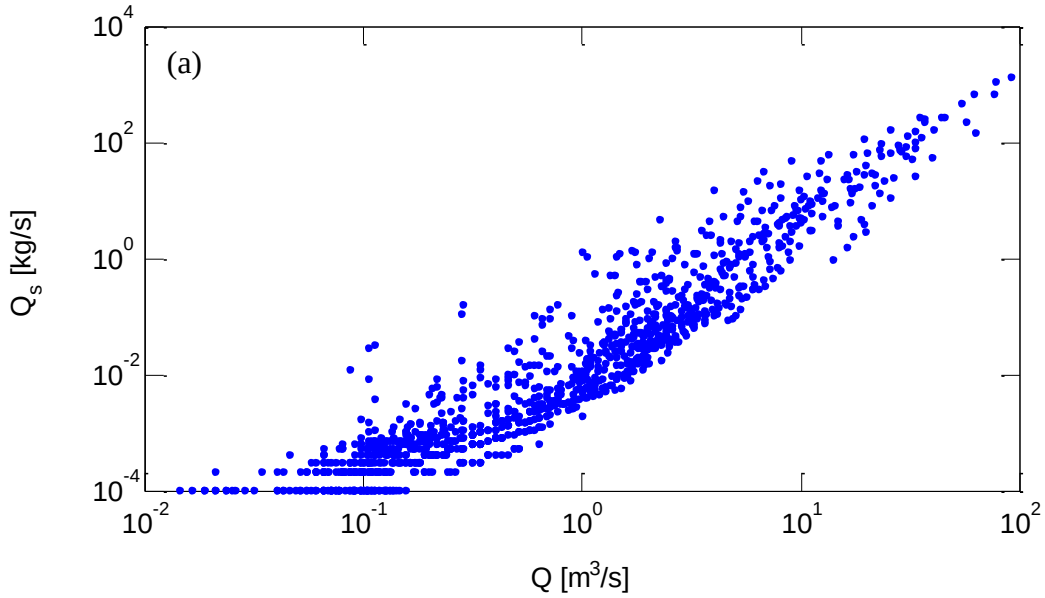

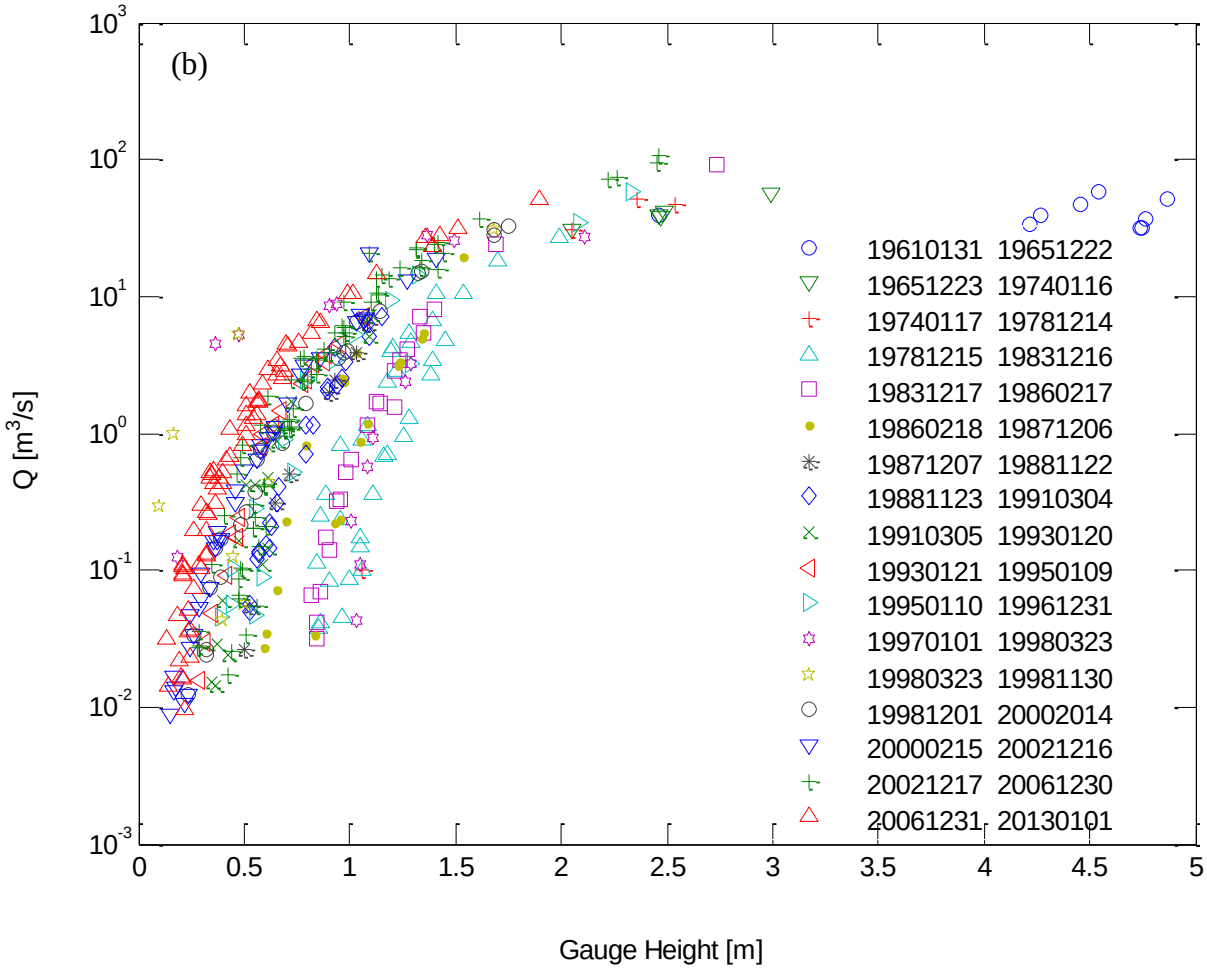

Figure A.22. (a) Q_s vs Q relationship from 1975 to 1979, (b) Q vs Gauge Height, (c) stream flow, and (d) channel bed. Photos were taken from field investigation at Bull Creek near Weott, CA.

23. Eel River at Scotia, CA. (USGS site number 11477000)

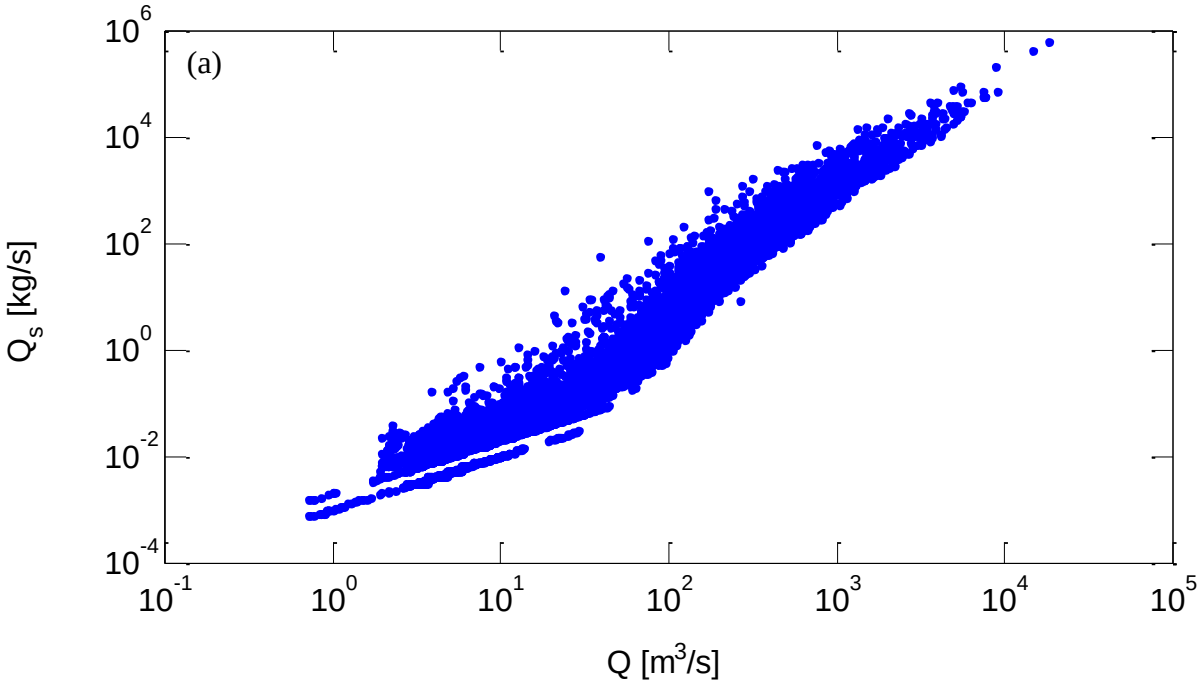

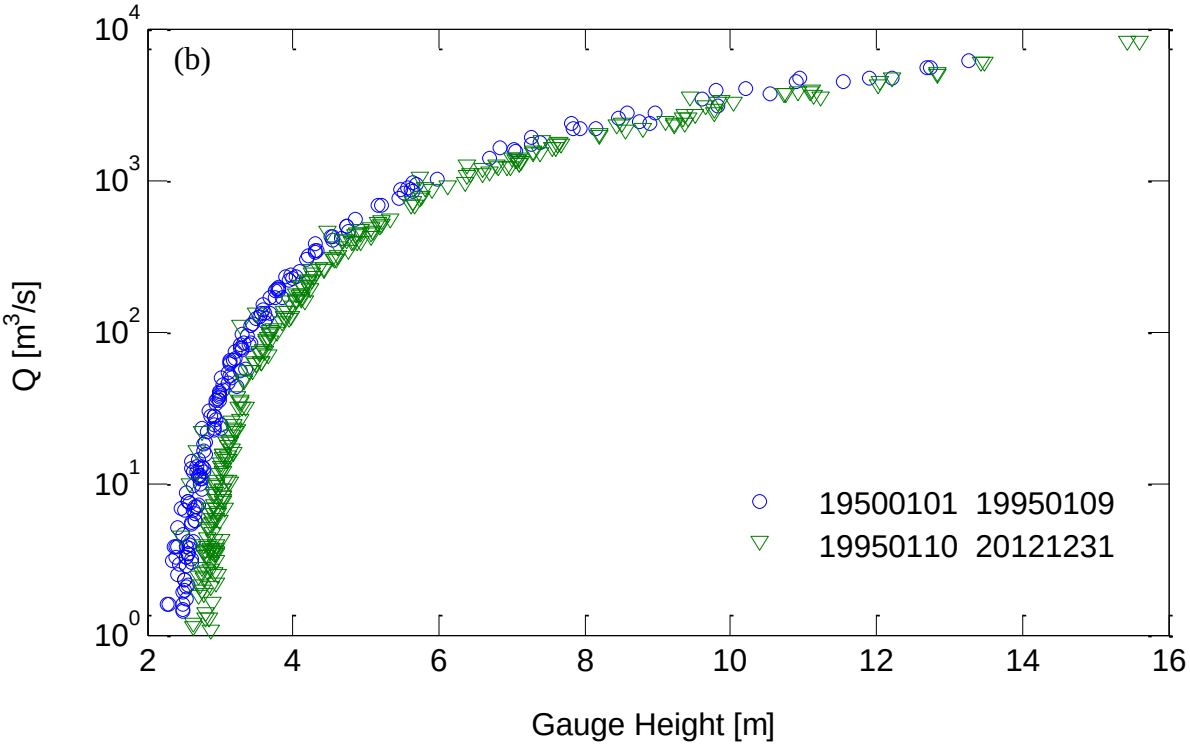

Figure A.23. (a) Q_s vs Q relationship from 1959 to 1980, (b) Q vs Gauge Height, (c) stream flow, and (d) channel bed. Photos were taken from field investigation at Eel River at Scotia, CA.

24. Redwood Creek near Blue Lake, CA. (USGS site number 11481500)

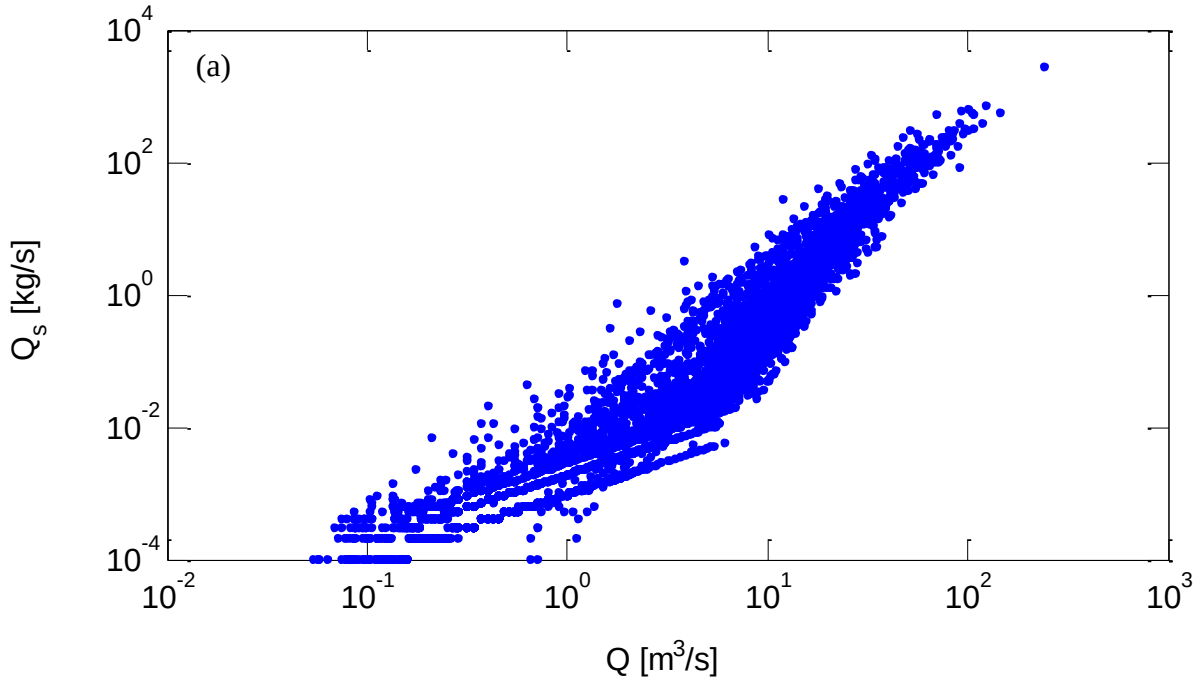

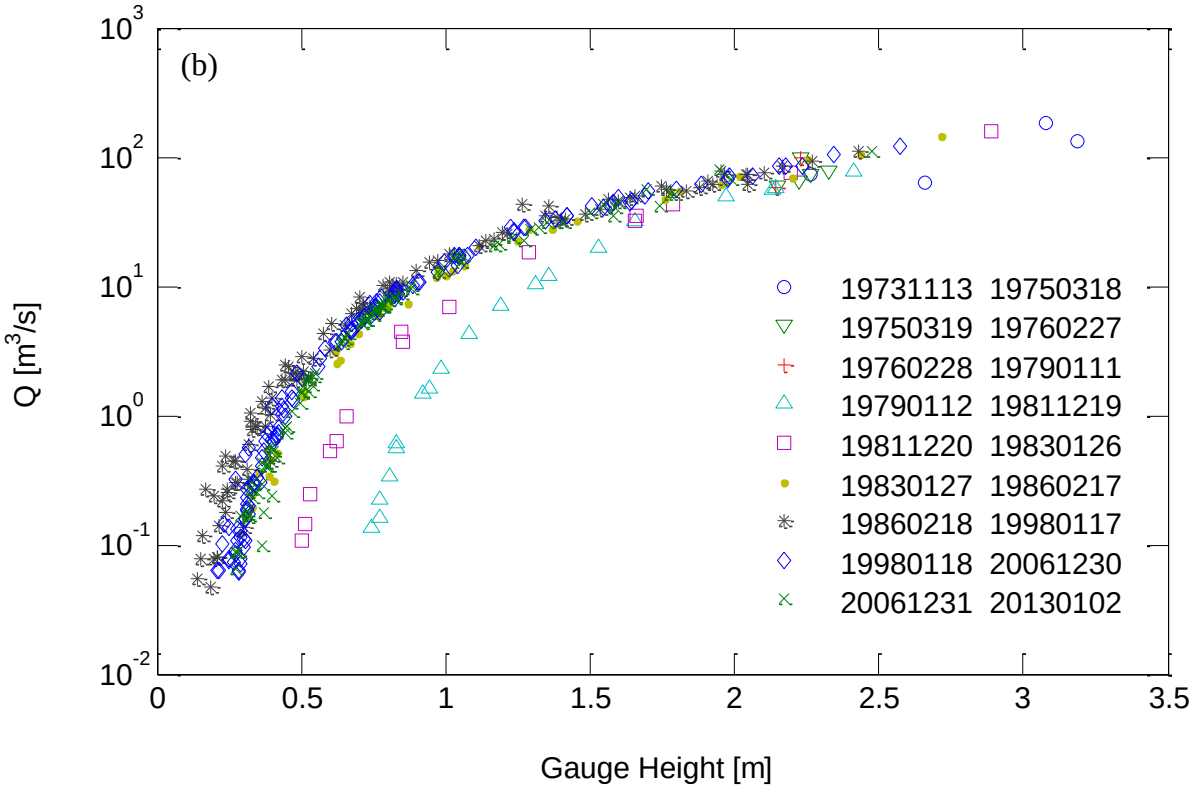

Figure A.24. (a) Q_s vs Q relationship from 1972 to 2002 (b) Q vs Gauge Height, and (c) gravelly channel bed at Redwood Creek near Blue Lake, CA. Photo provided by USGS field office.

25. Redwood Creek at Orick, CA. (USGS site number 11482500)

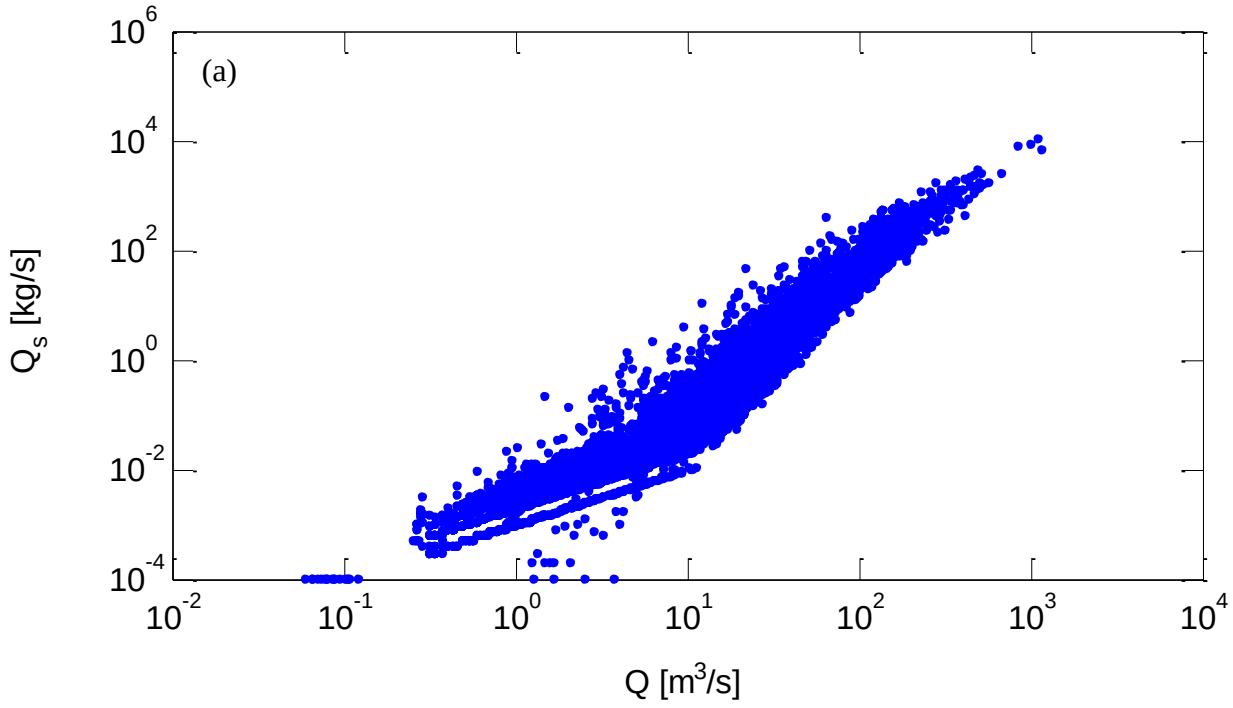

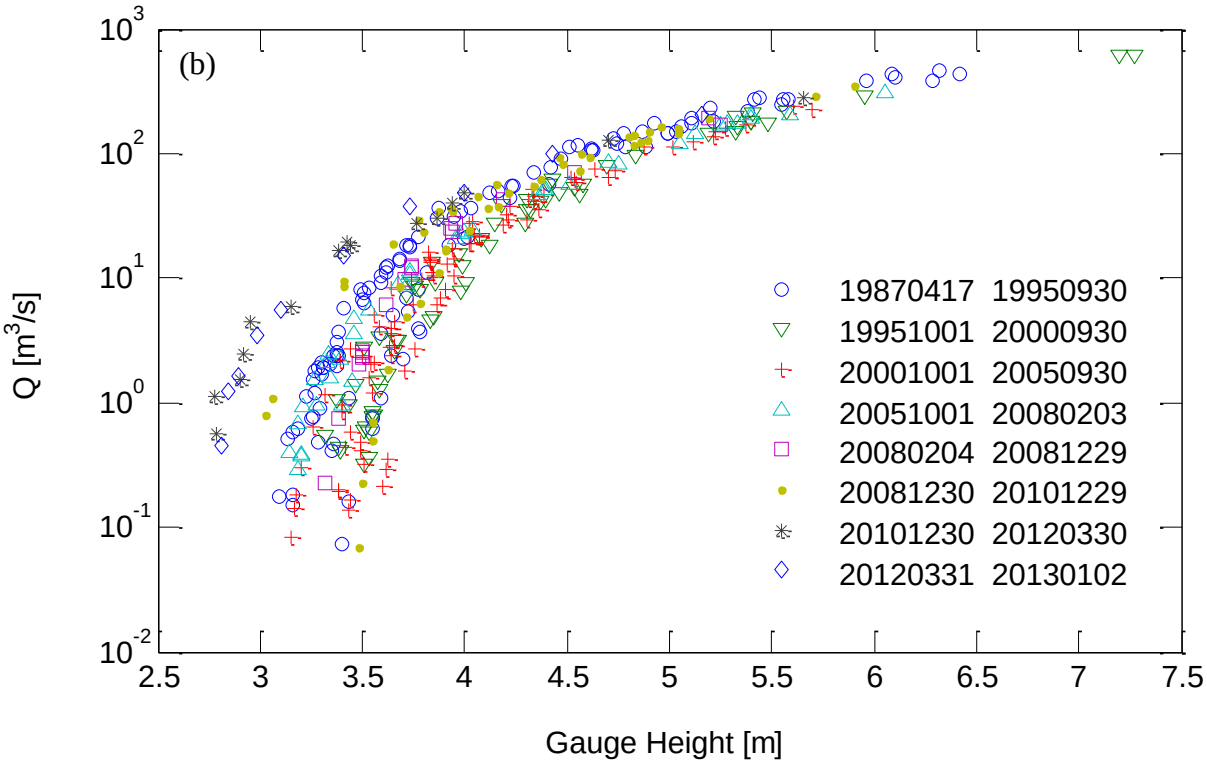
(b)
Q [m3/s]
Gauge Height [m]
19870417 19950930
19951001 20000930
20001001 20050930
20051001 20080203
20080204 20081229
20081230 20101229
20101230 20120330
20120331 20130102


(c)

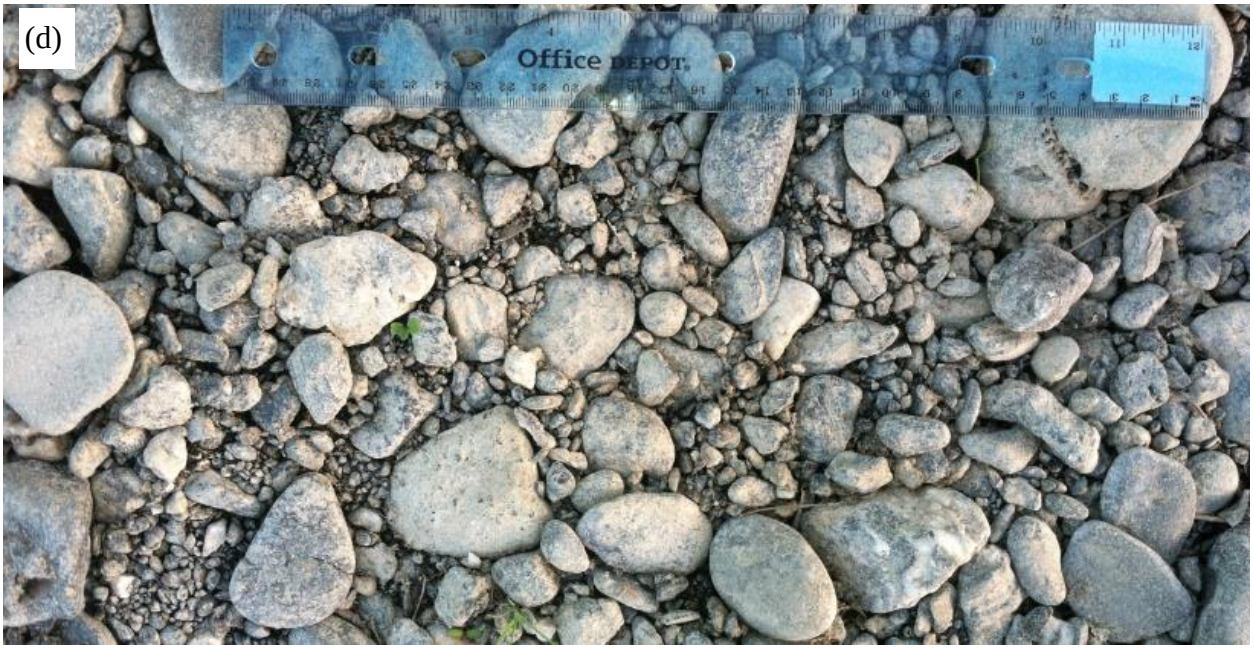

Figure A.25. (a) Q_s vs Q relationship from 1970 to 2001, (b) Q vs Gauge Height, (c) and (d) gravelly channel bed. Photos were taken from field investigation at Red Wood Creek at Orick, CA.

26. SF Trinity River below Hyampom, CA. (USGS site number 11528700)

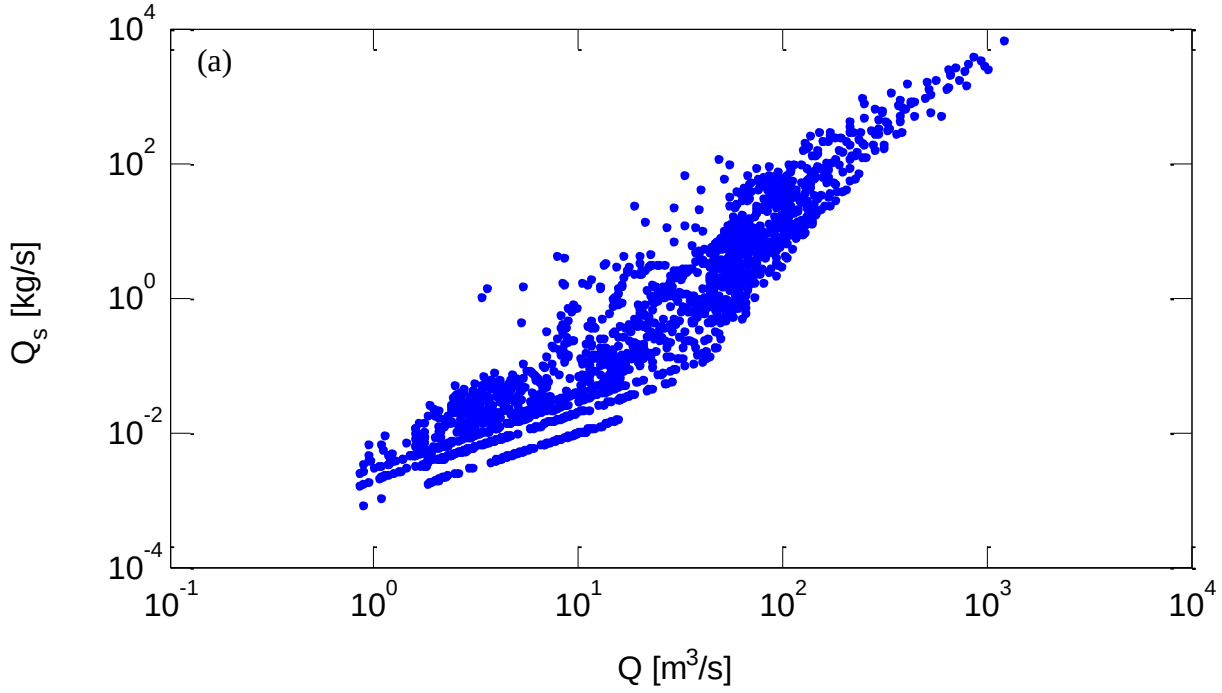

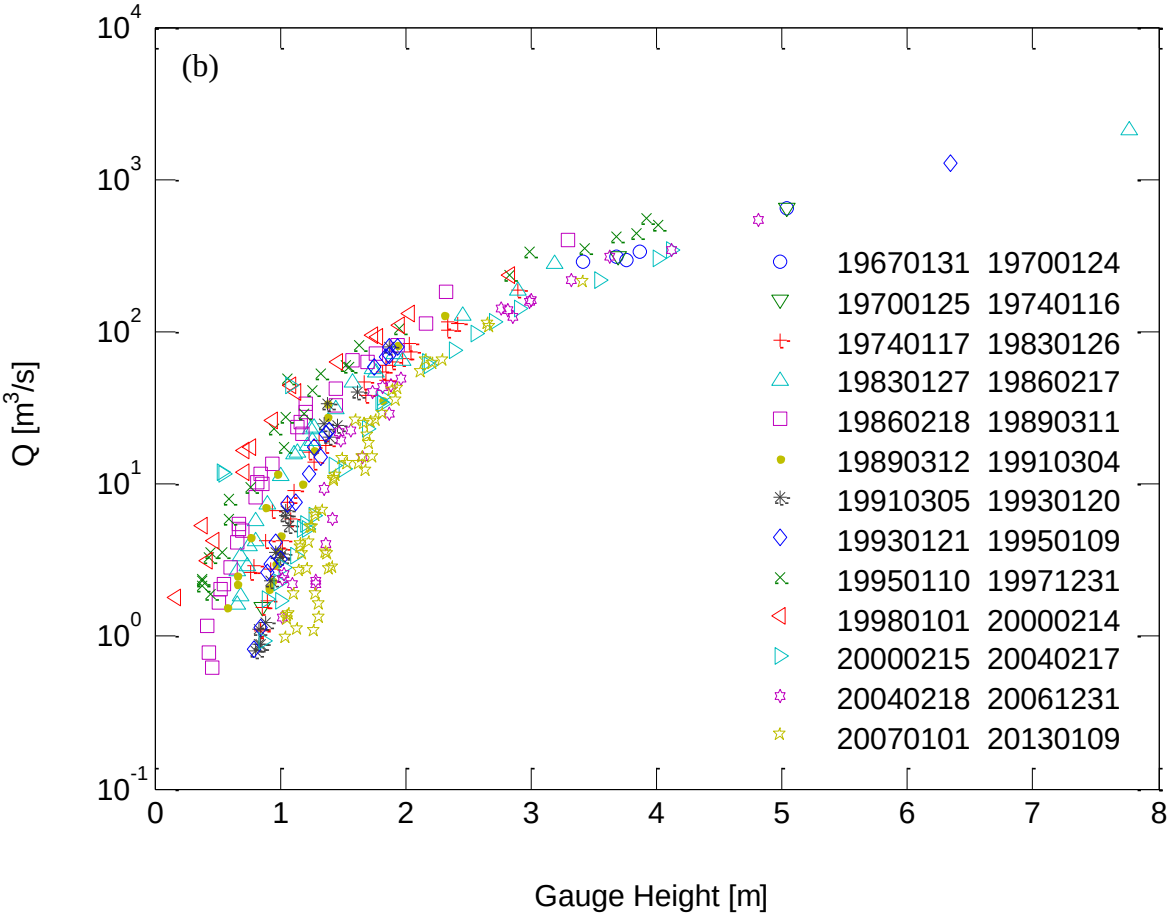
(b)
Q [m3/s]
Gauge Height [m]
19670131 19700124
19700125 19740116
19740117 19830126
19830127 19860217
19860218 19890311
19890312 19910304
19910305 19930120
19930121 19950109
19950110 19971231
19980101 20000214
20000215 20040217
20040218 20061231
20070101 20130109


(c)

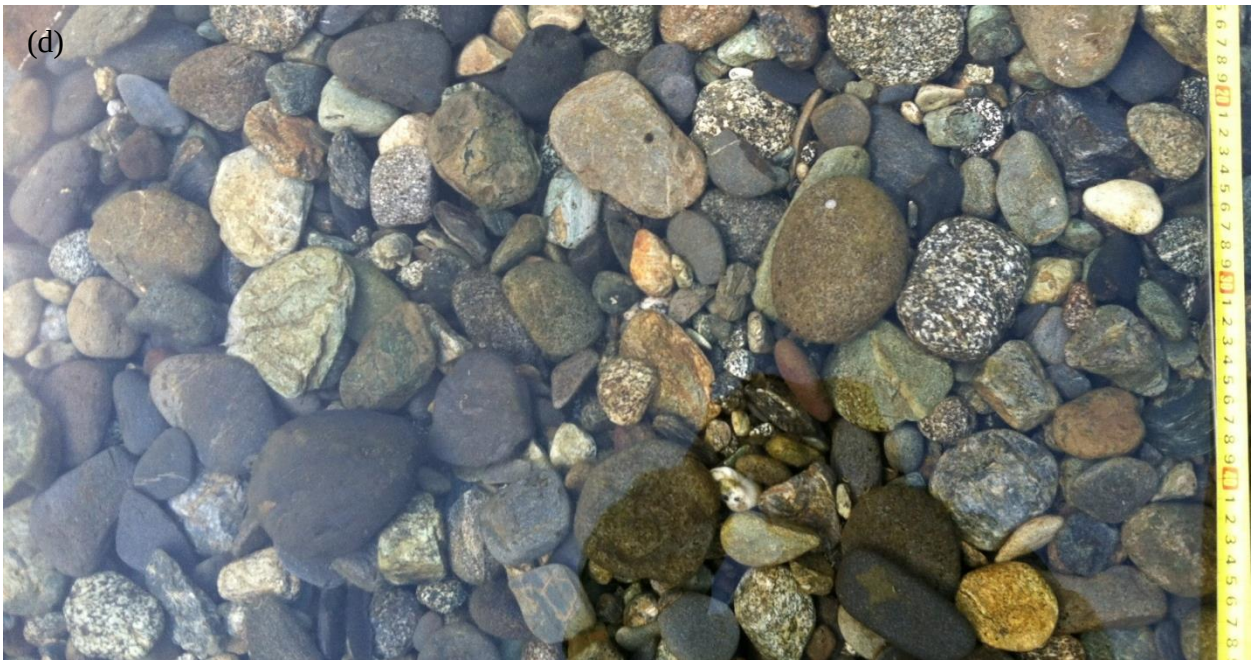

Figure A.26. (a) Q_s vs Q relationship from 1966 to 1982, (b) Q vs Gauge Height, (c) stream flow, and (d) gravelly bed materials. Photos were taken from field investigation at SF Trinity River below Hyampom, CA.

27. SF Trinity River near Salyer, CA. (USGS site number 11529000)

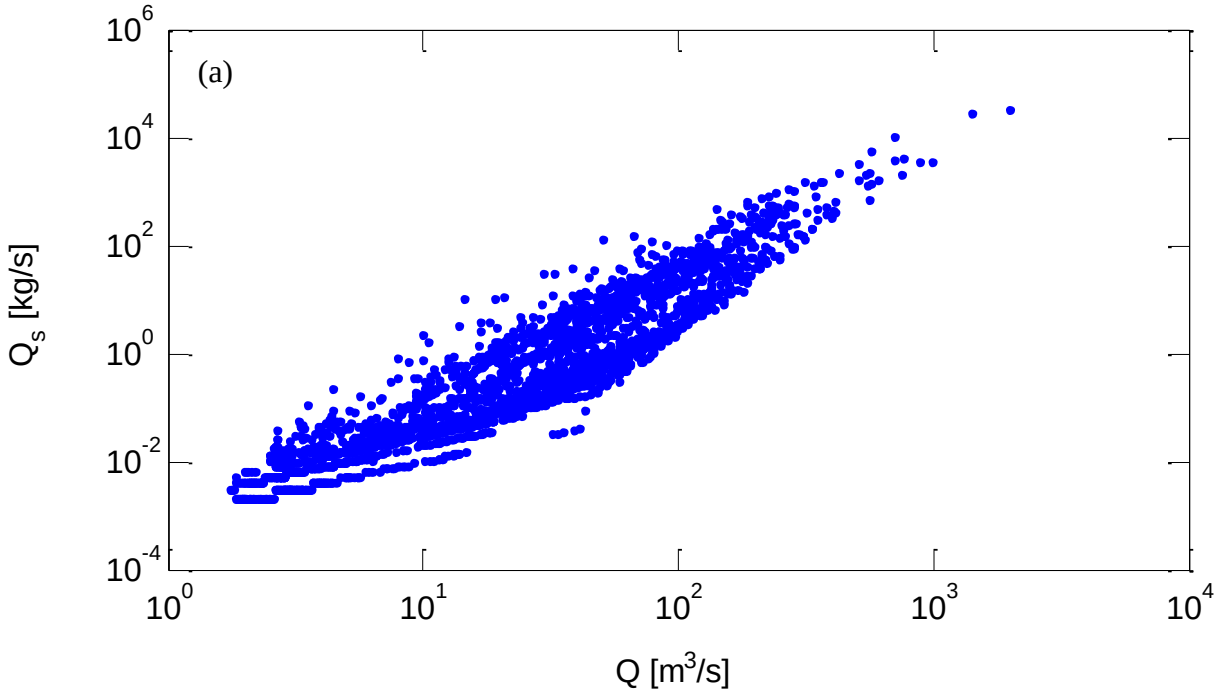

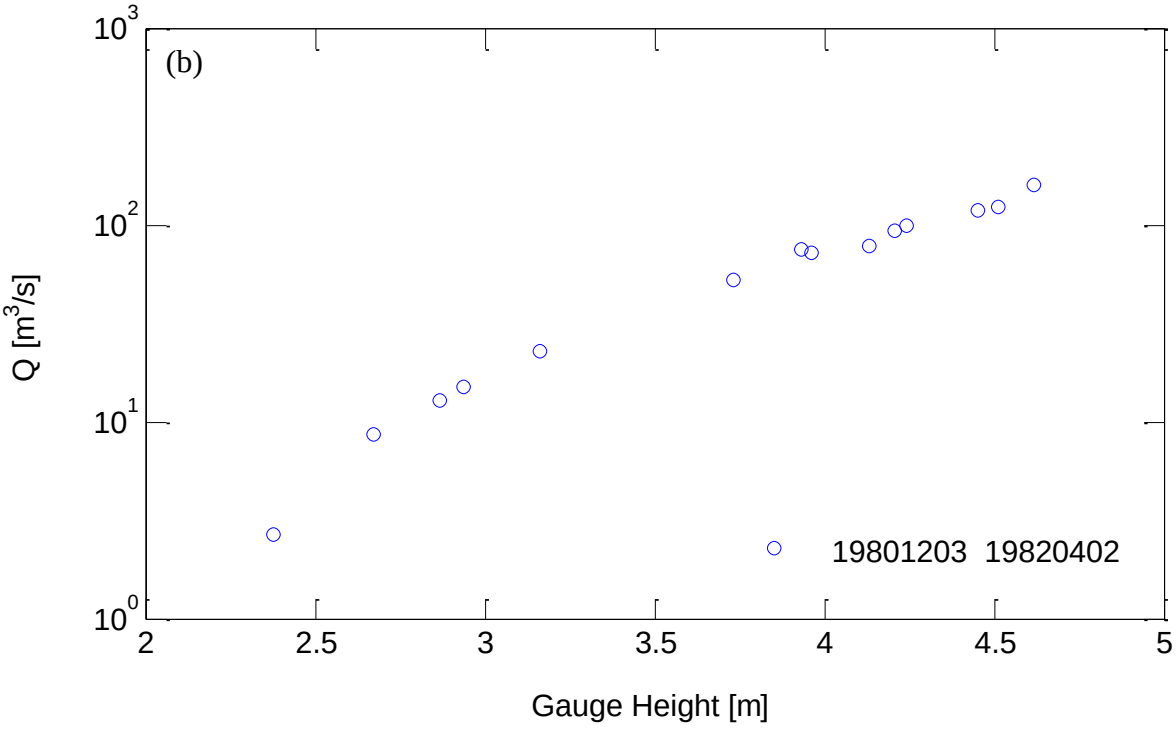
(b)
10^3
10^2
10^1
10^0
Q [m^3/s]
19801203 19820402
2
2.5
3
3.5
4
4.5
5
Gauge Height [m]


(c)

Figure A.27. (a) Q_s vs Q relationship from 1959 to 1967, (b) Q vs Gauge Height, (c) stream flow, and (d) gravelly bed materials. Photos were taken from field investigation at SF Trinity River near Salyer, CA.

28. Supply Creek at Hoopa, CA. (USGS site number 11530020)

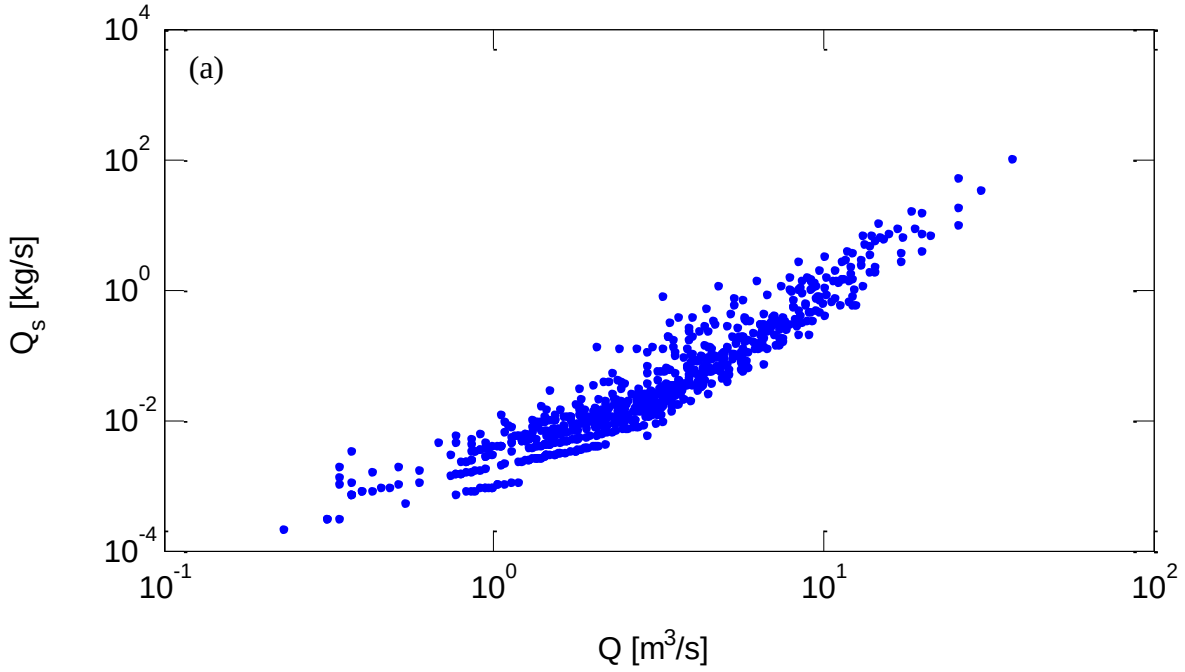

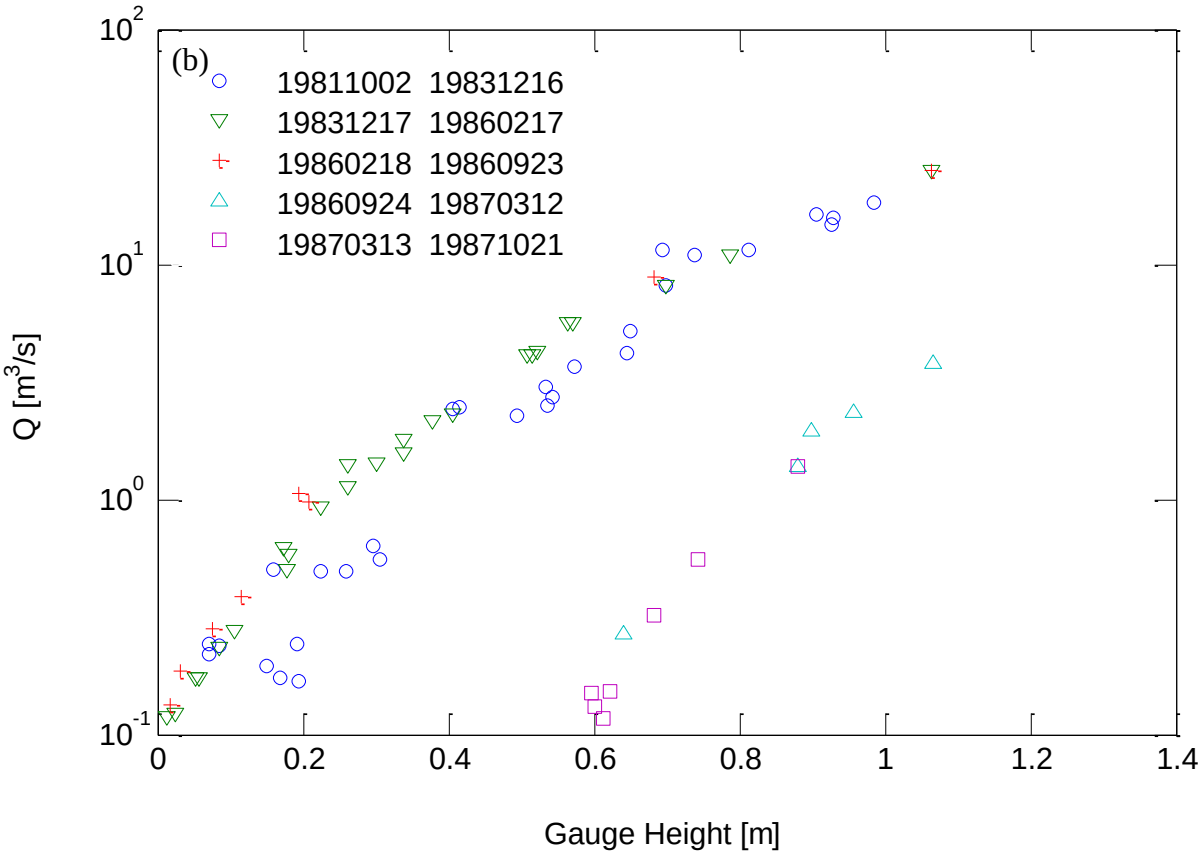
(b)
19811002 19831216
19831217 19860217
19860218 19860923
19860924 19870312
19870313 19871021
Q [m3/s]
Gauge Height [m]
10^2
10^1
10^0
10^-1
0
0.2
0.4
0.6
0.8
1
1.2
1.4


(c)

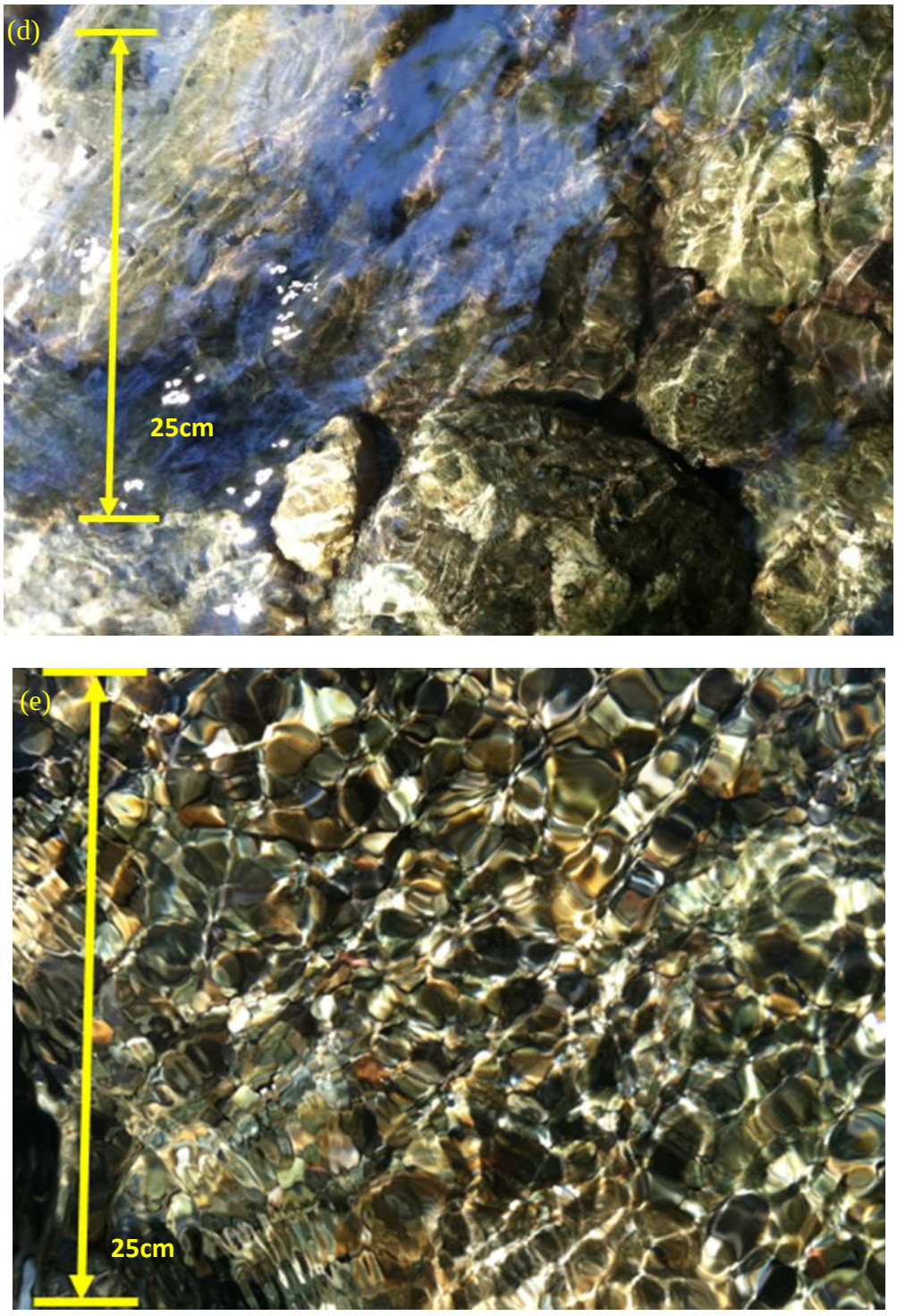

Figure A.28. (a) Q_s vs Q relationship from 1981 to 1985, (b) Q vs Gauge Height, (c) stream flow, (d) and (e) bed materials with cobbles and gravels. Photos were taken from field investigation at Supply Creek at Hoopa, CA.

29. Smith River near Cresent City, CA. (USGS site number 11532500)

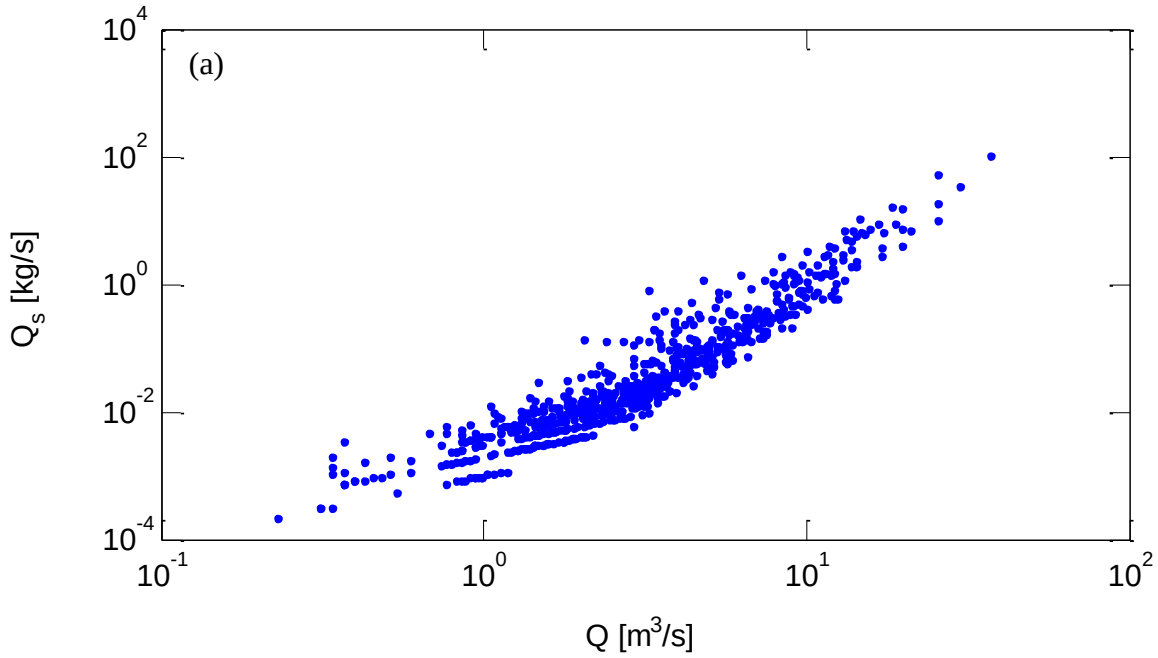

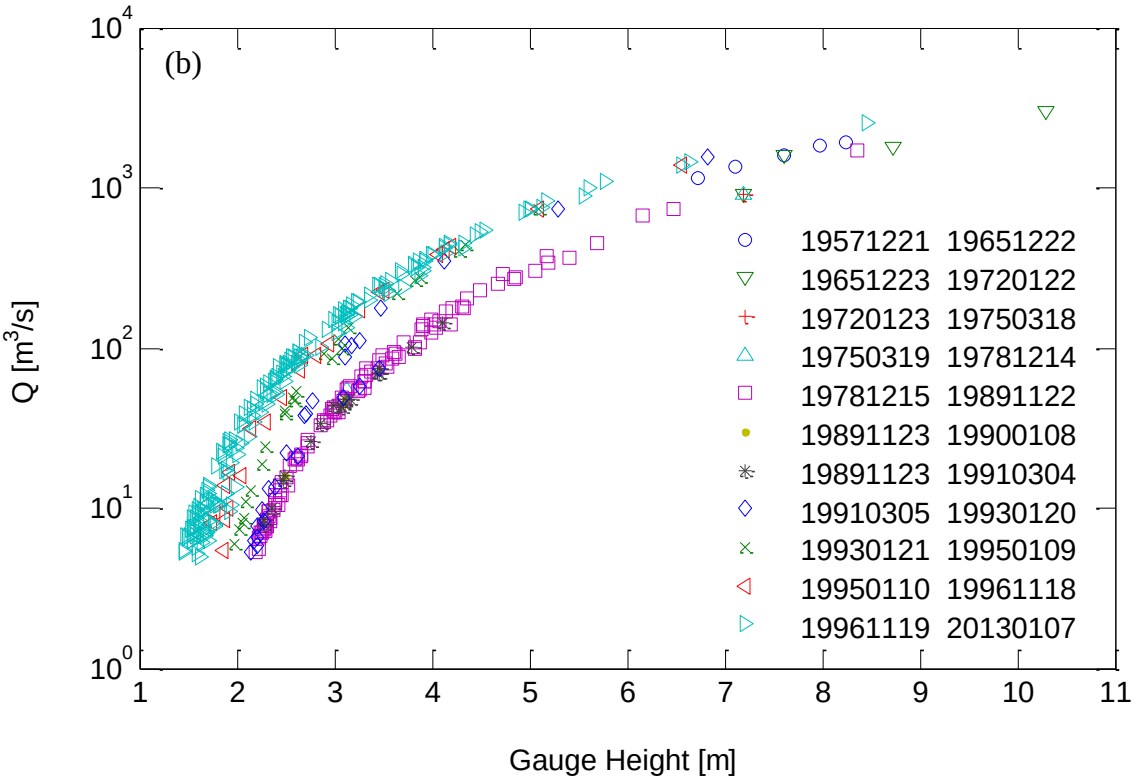

Figure A.29. (a) Q_s vs Q relationship from 1977 to 1981, (b) Q vs Gauge Height, (c) stream flow, and (d) bed materials with cobbles and gravels. Photos were taken from field investigation at Smith River near Crescent City, CA.

30. Elliott Creek near Copper, OREG. (USGS site number 14361600)

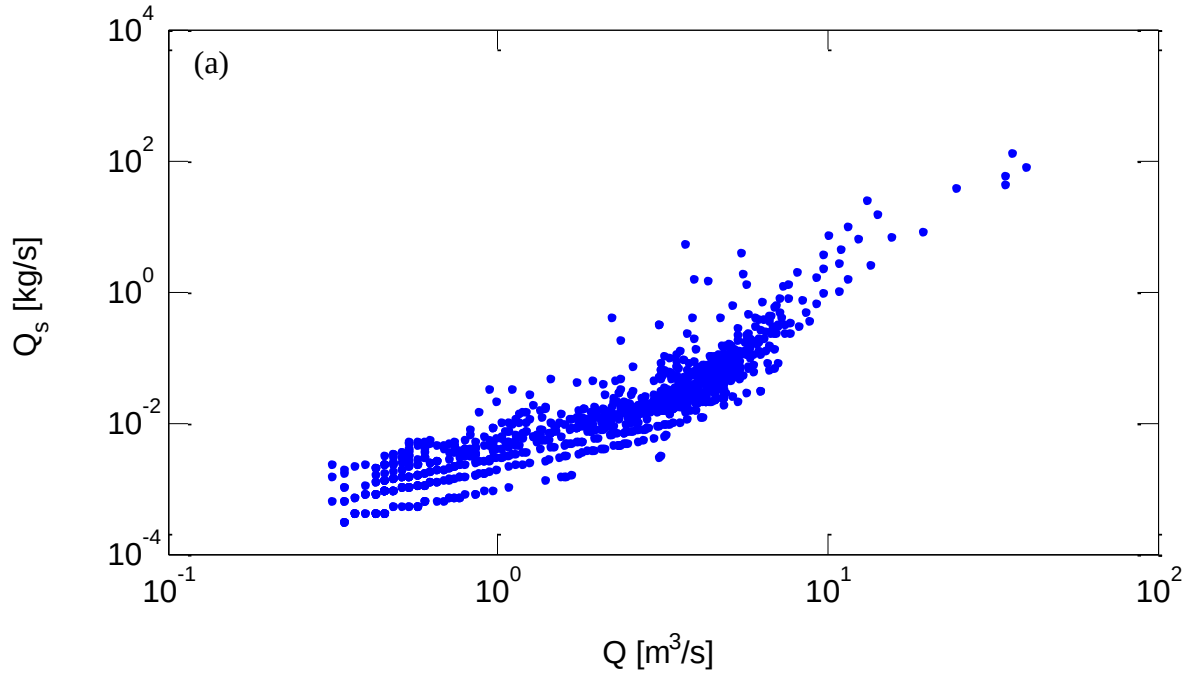

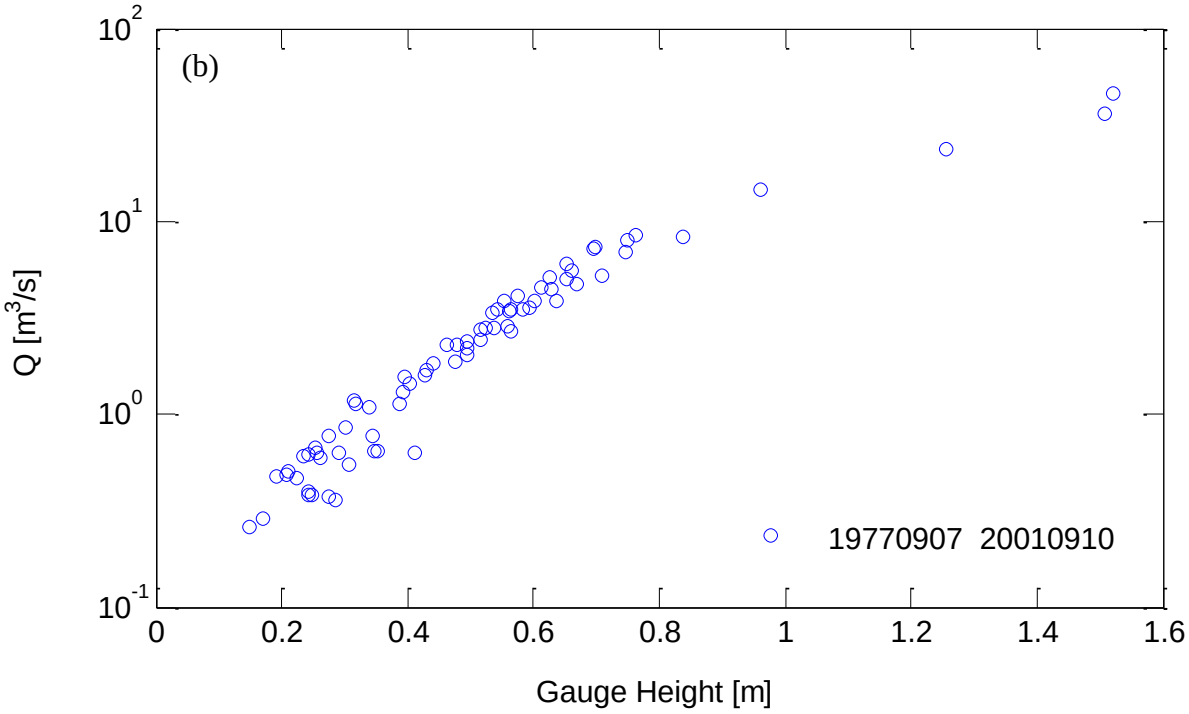

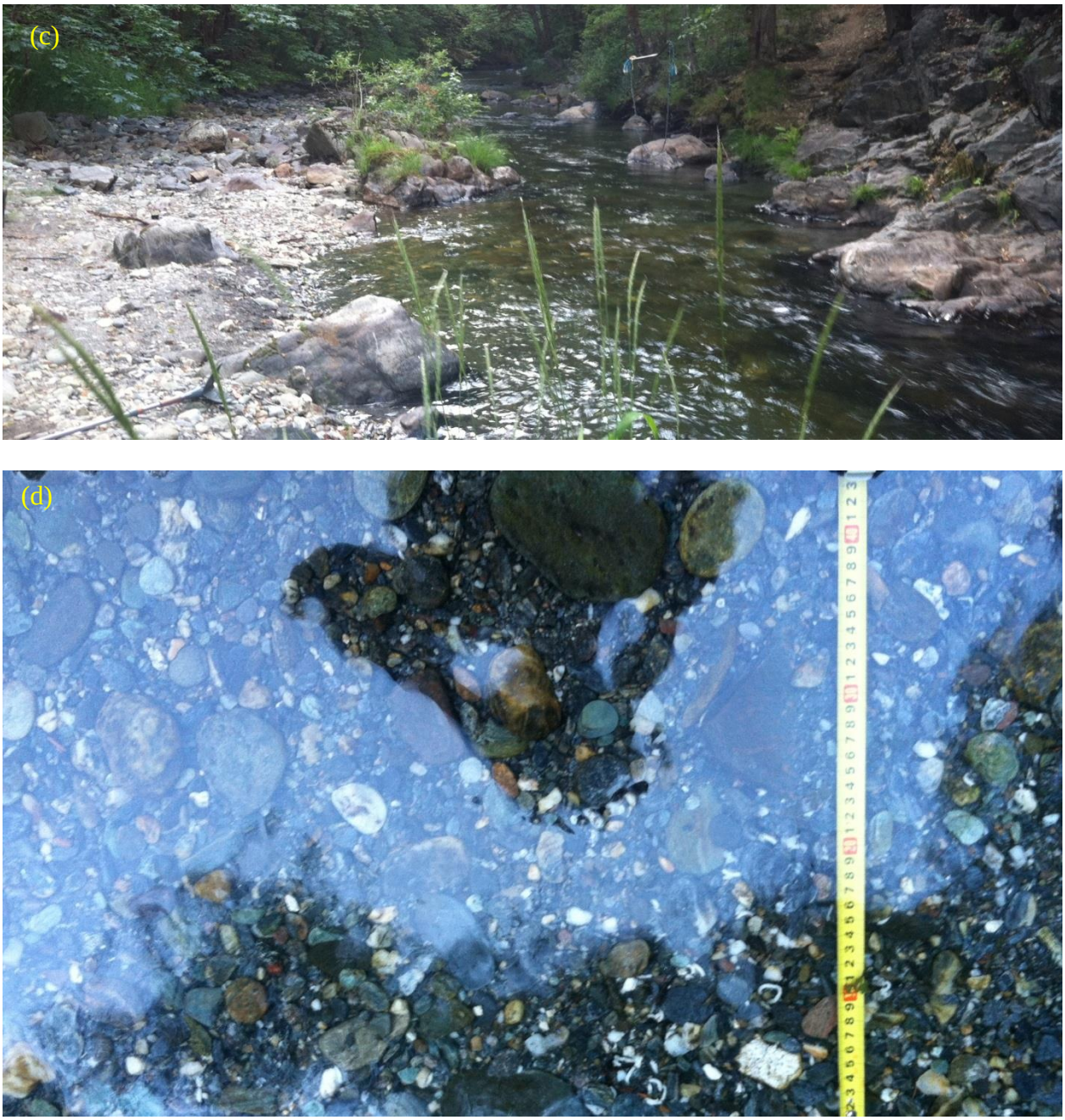

Figure A.30. (a) Q_s vs Q relationship from 1977 to 1987, (b) Q vs Gauge Height, (c) stream flow, and (d) gravelly bed materials. Photos were taken from field investigation at Elliott Creek near Copper, OREG.

B. Sites with no slope break in the relationship of Q_s to Q

1. Lopez Creek near Arroyo Grande, CA. (USGS site number 11141280)

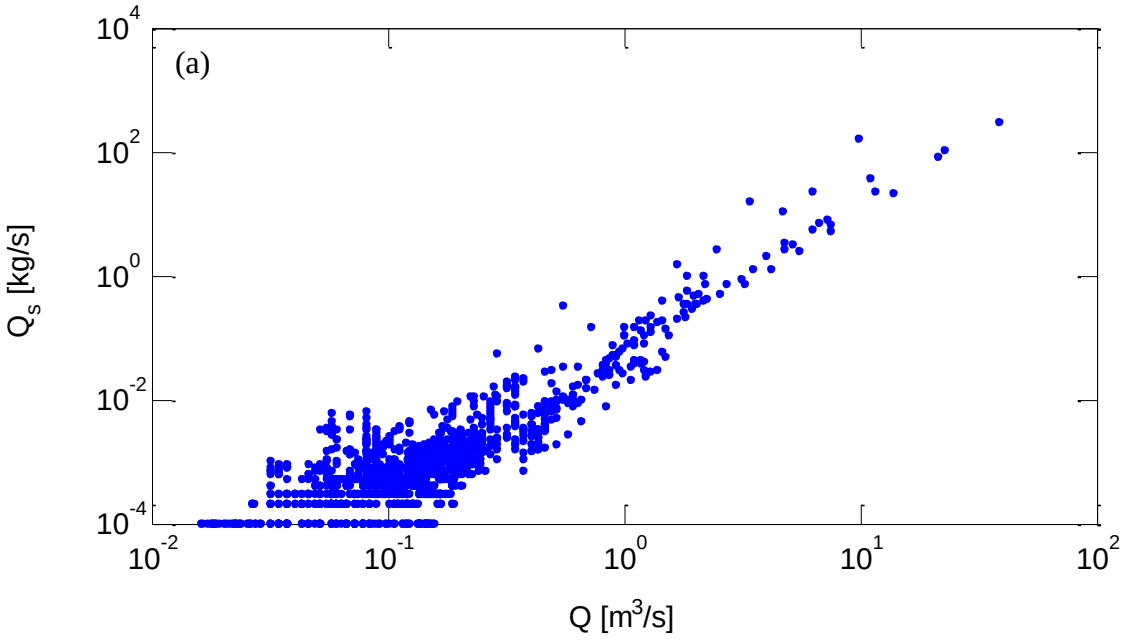

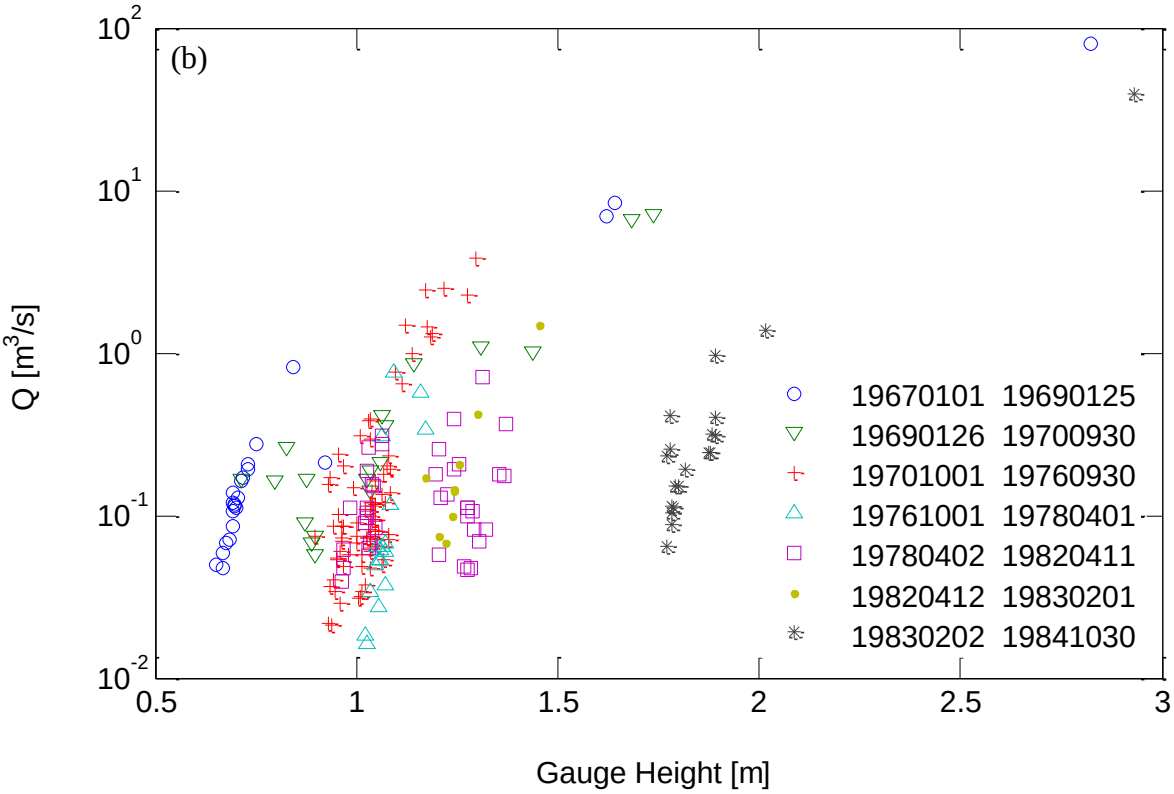

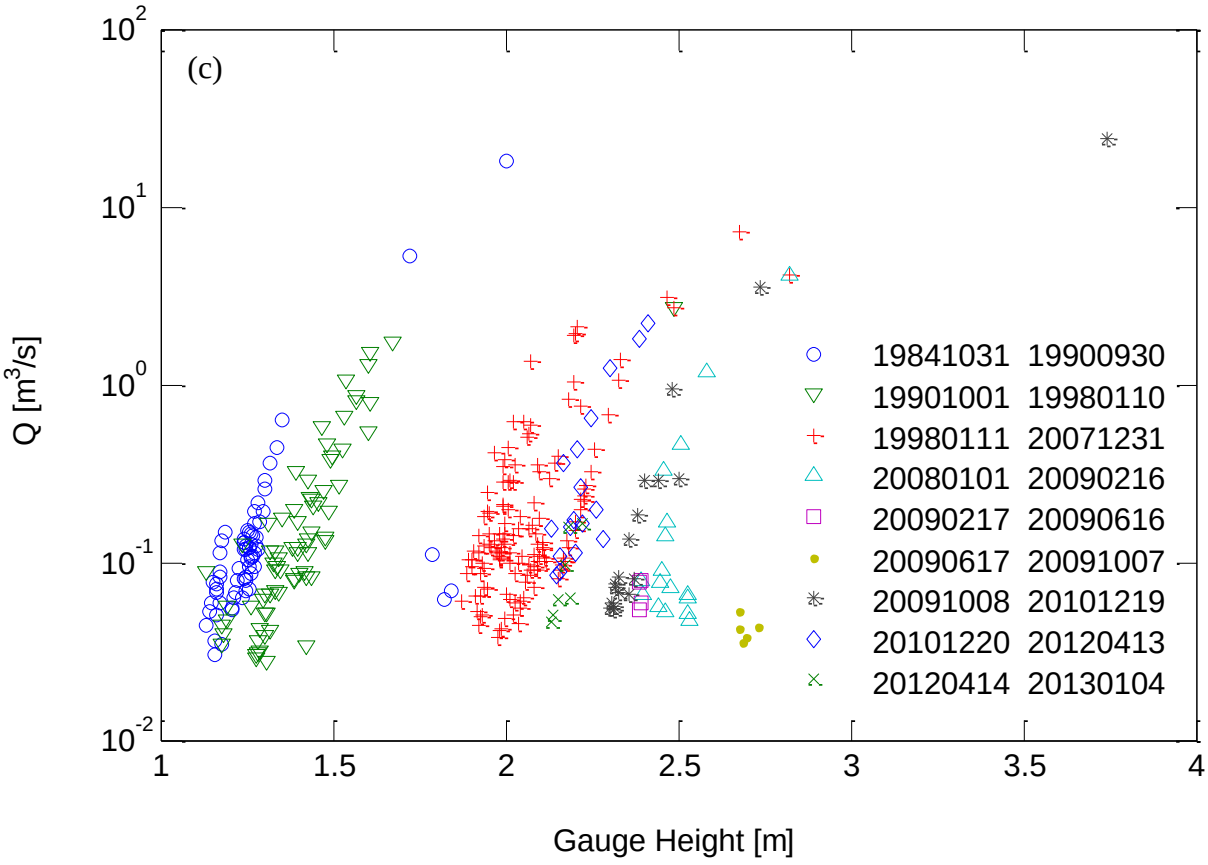
(c)
Q [m3/s]
Gauge Height [m]
19841031 19900930
19901001 19980110
19980111 20071231
20080101 20090216
20090217 20090616
20090617 20091007
20091008 20101219
20101220 20120413
20120414 20130104


(d)

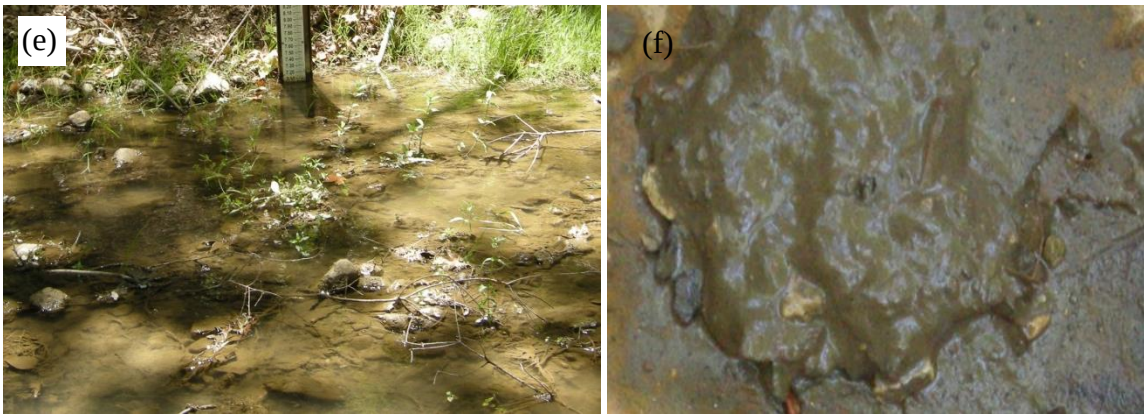

Figure A.31. (a) Q_s vs Q relationship from 1967 to 1972, (b) Q vs Gauge Height before 1984 when gauge station was re-located, (c) Q vs Gauge Height after 1984: gaging station was moved 0.4 mile upstream after October 31, 1984, (d) Channel bed at the previous gauge station operated before 1984. Photo was taken from field investigation in July 8, 2014. Channel bed surface is dominated by cobble/gravel where surface is covered by silt. Below cobble/gravel surface layer sand/fine gravel are observed, (e) Chanel bed at current gauge station and (f) deposited muddy sediment at the surface of current gauge station. Photos were also taken during field investigation at Lopez Creek near Arroyo Grande, CA in July 8, 2014.

2. Santa Rita Creek near Templeton, CA. (USGS site number 11147070)

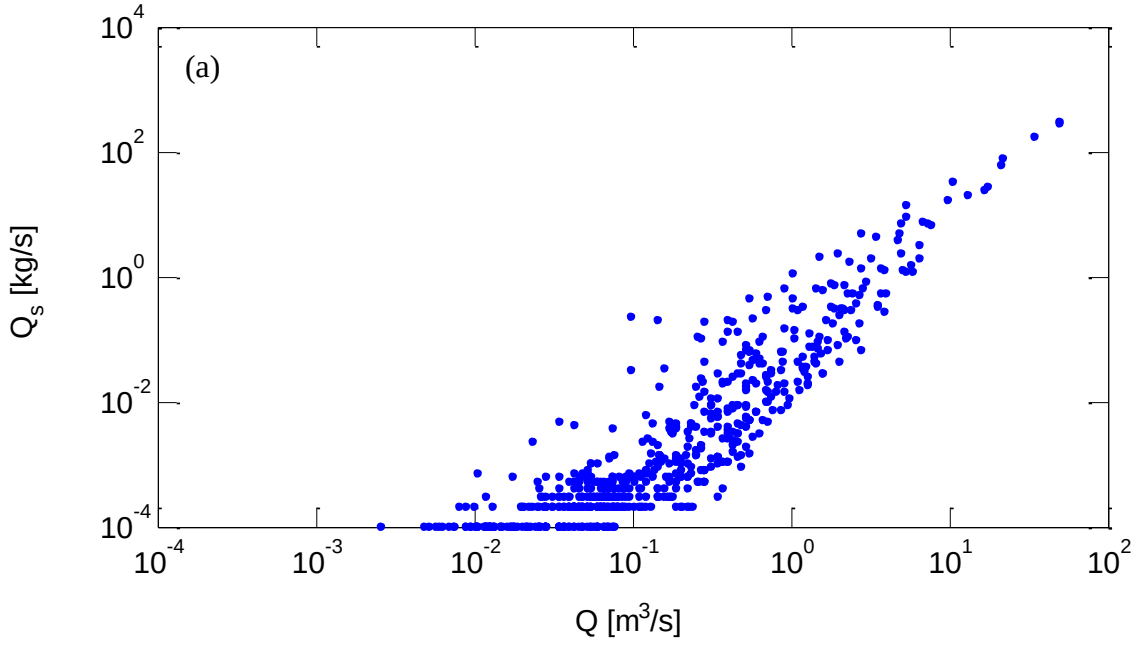

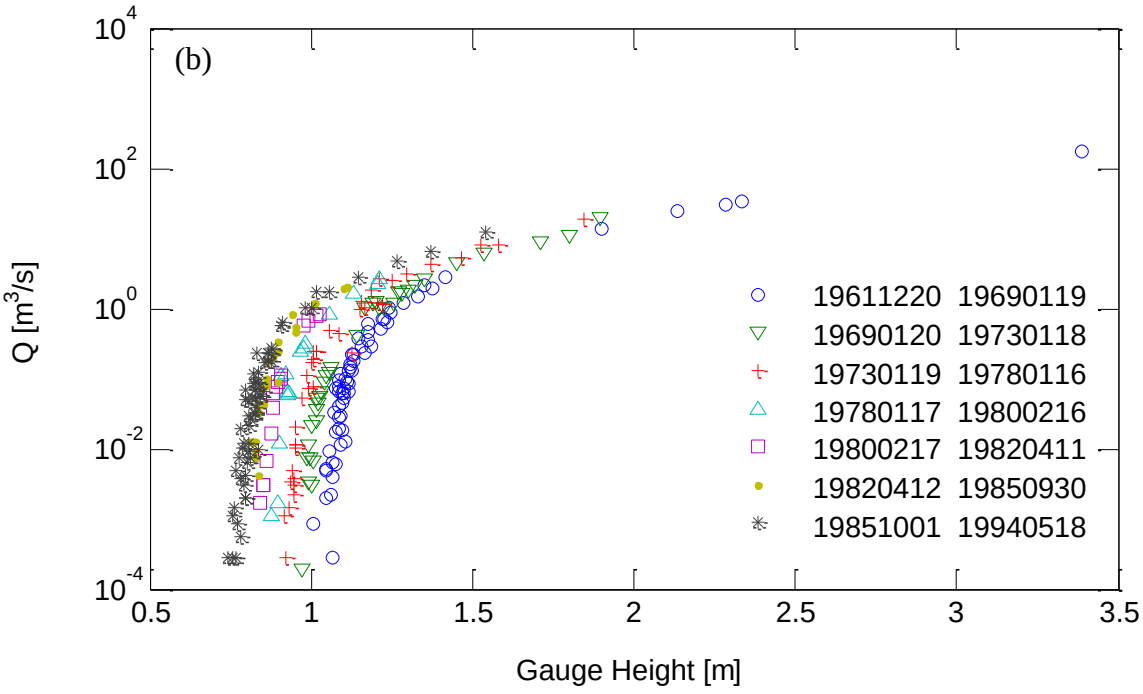

Figure A.32. (a) Q_s vs Q relationship from 1967 to 1972, (b) Q vs Gauge Height, and (c) channel bed. Photo was taken from field investigation at Santa Rita Creek near Templeton, CA.

3. San Antonio River near Lockwood, CA. (USGS site number 11149900)

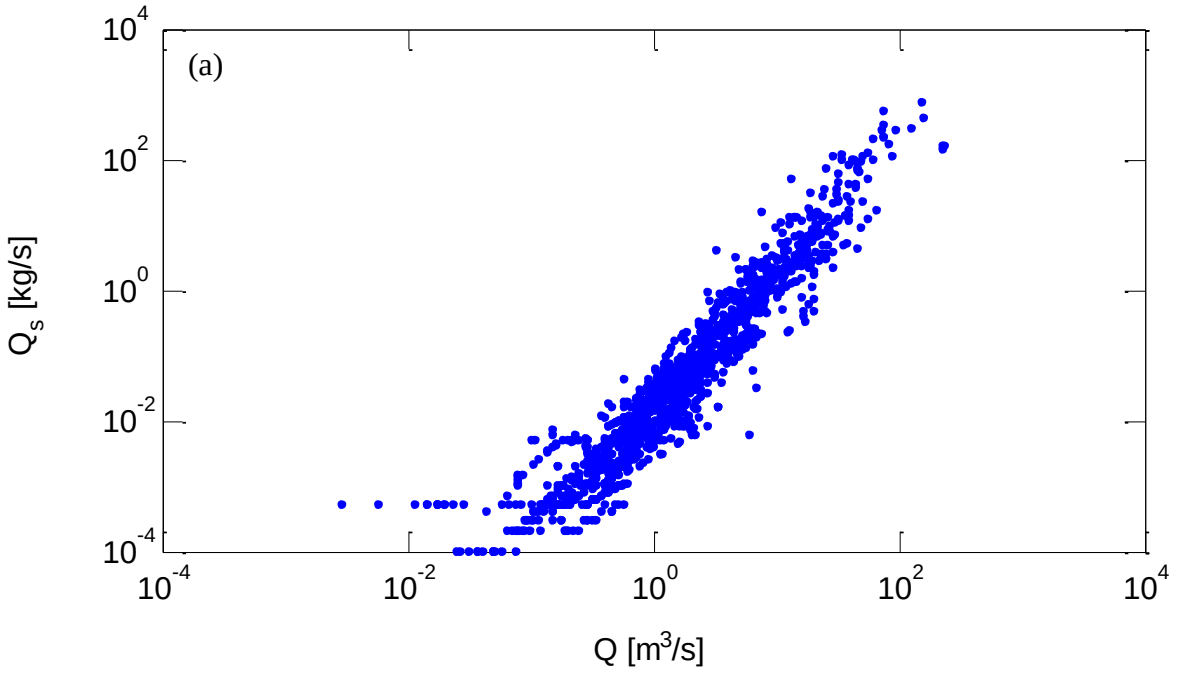

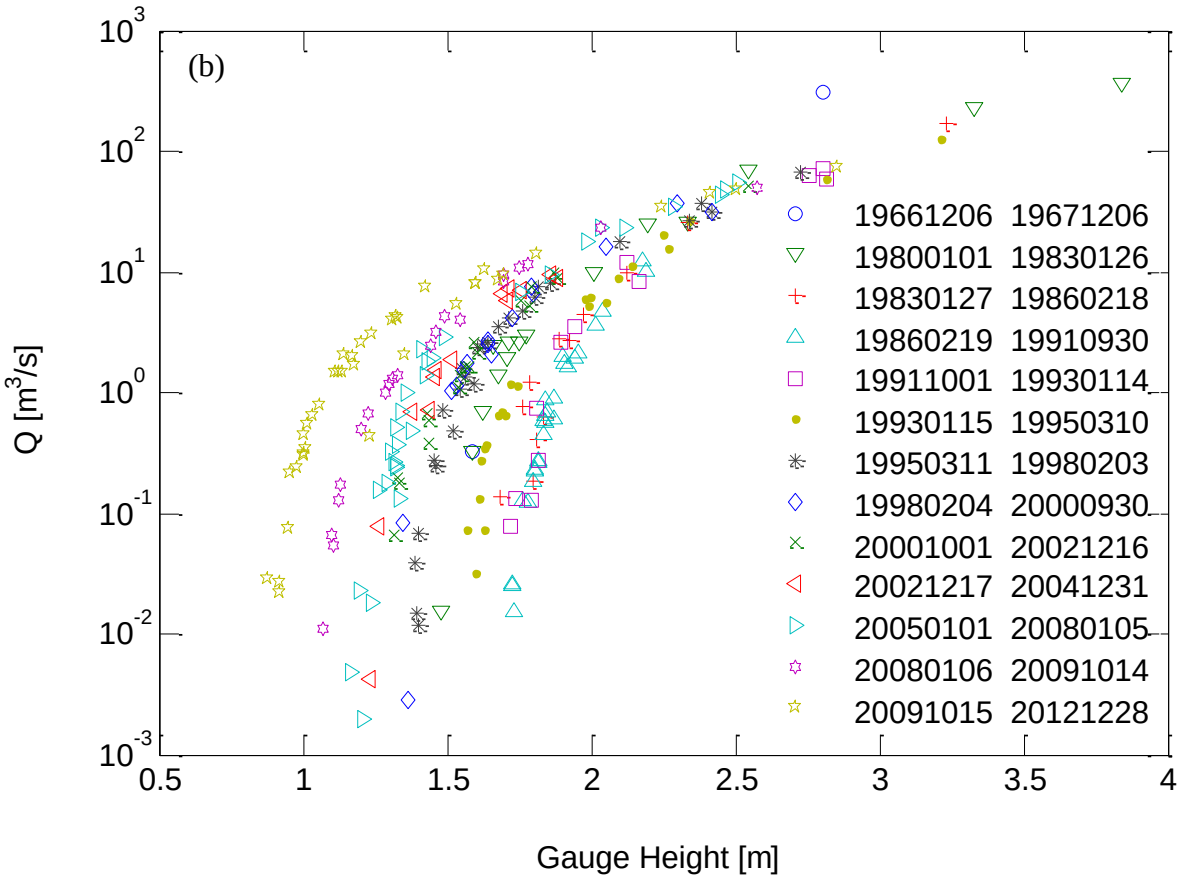

Figure A.33. (a) Q_s vs Q relationship from 1965 to 1973, (b) Q vs Gauge Height, (c) and (d) sandy channel bed. Photos were taken from field investigation at San Antonio River near Lockwood, CA.

4. Zayante Creek at Zayante, CA. (USGS site number 11160300)

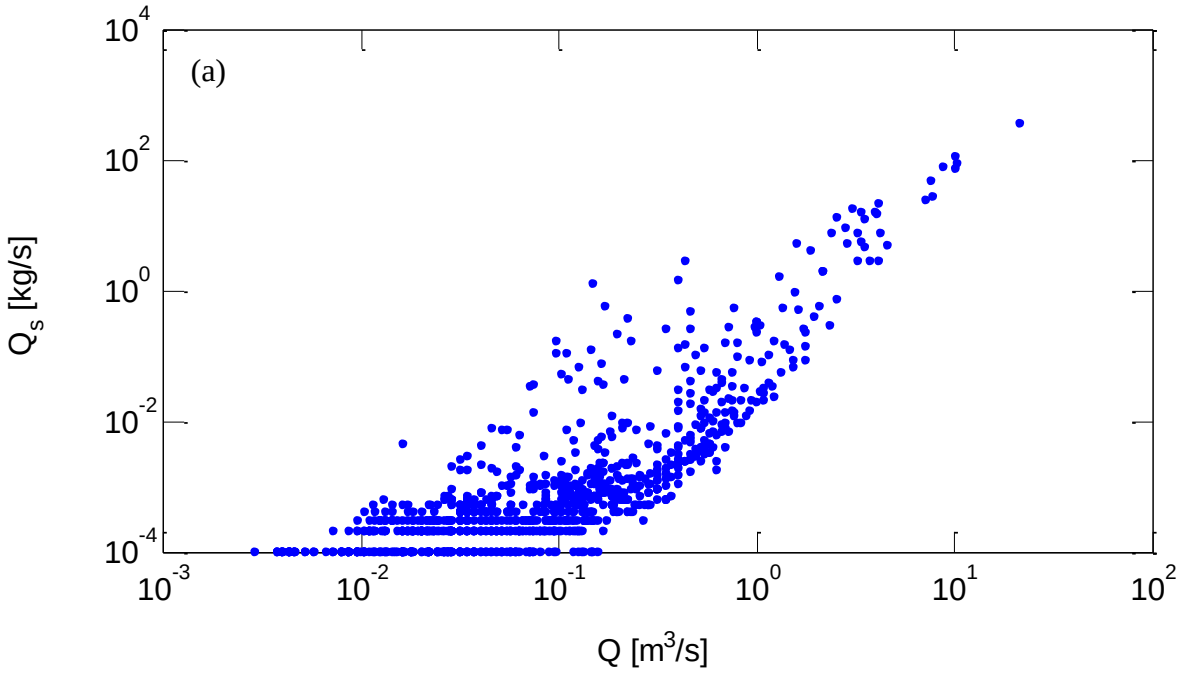

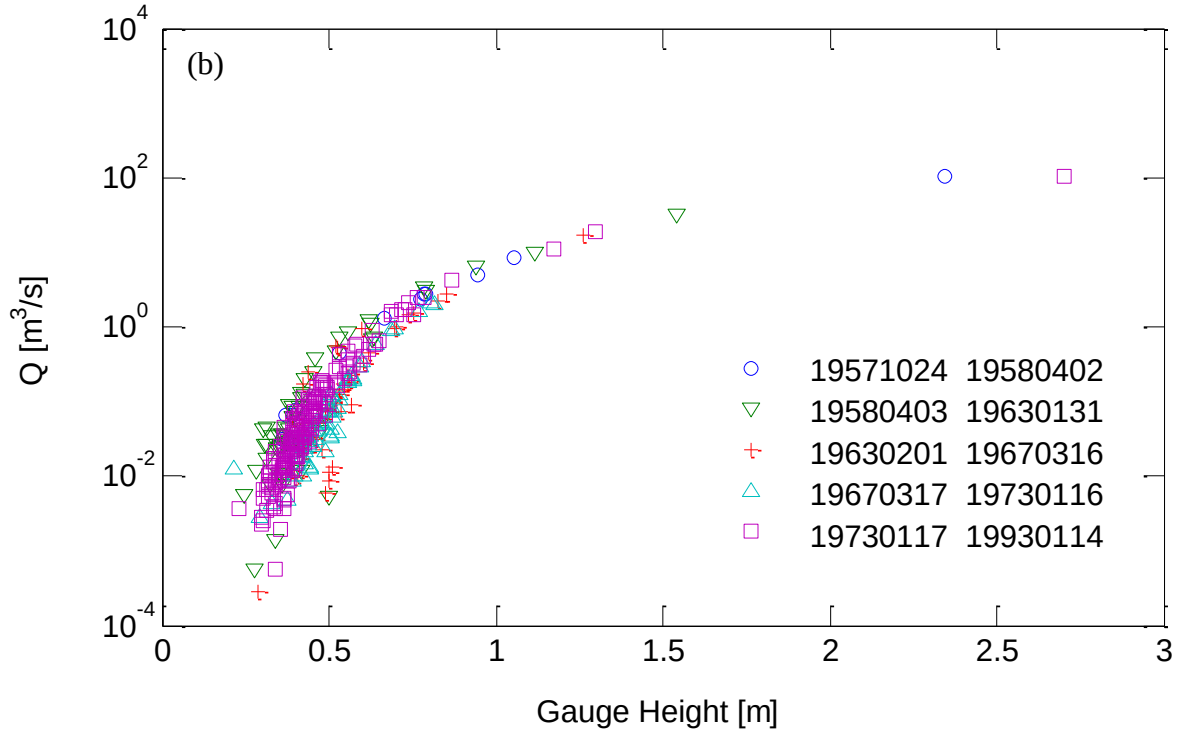

Figure A.34. (a) Q_s vs Q relationship from 1970 to 1973, (b) Q vs Gauge Height, and (c) bed rock dominated channel bed. Photo was taken from field investigation at Zayante Creek at Zayante, CA.

5. Arroyo Valle below Lang Canyon near Livermore, CA. (USGS site number 11176400)

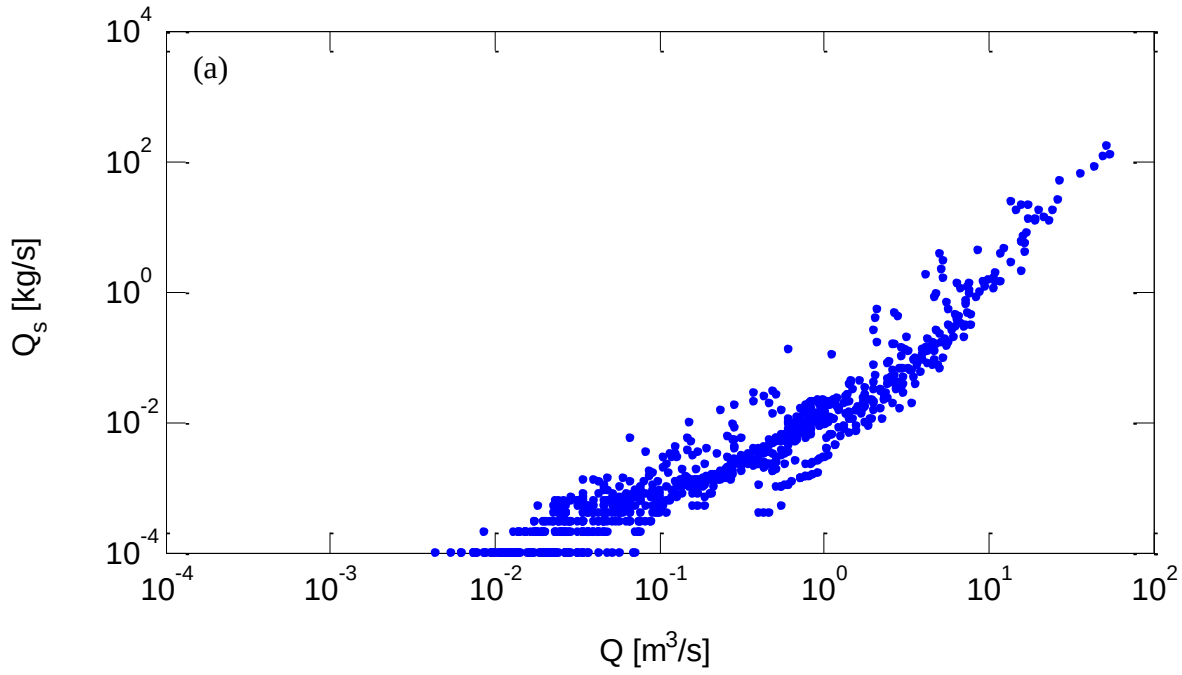

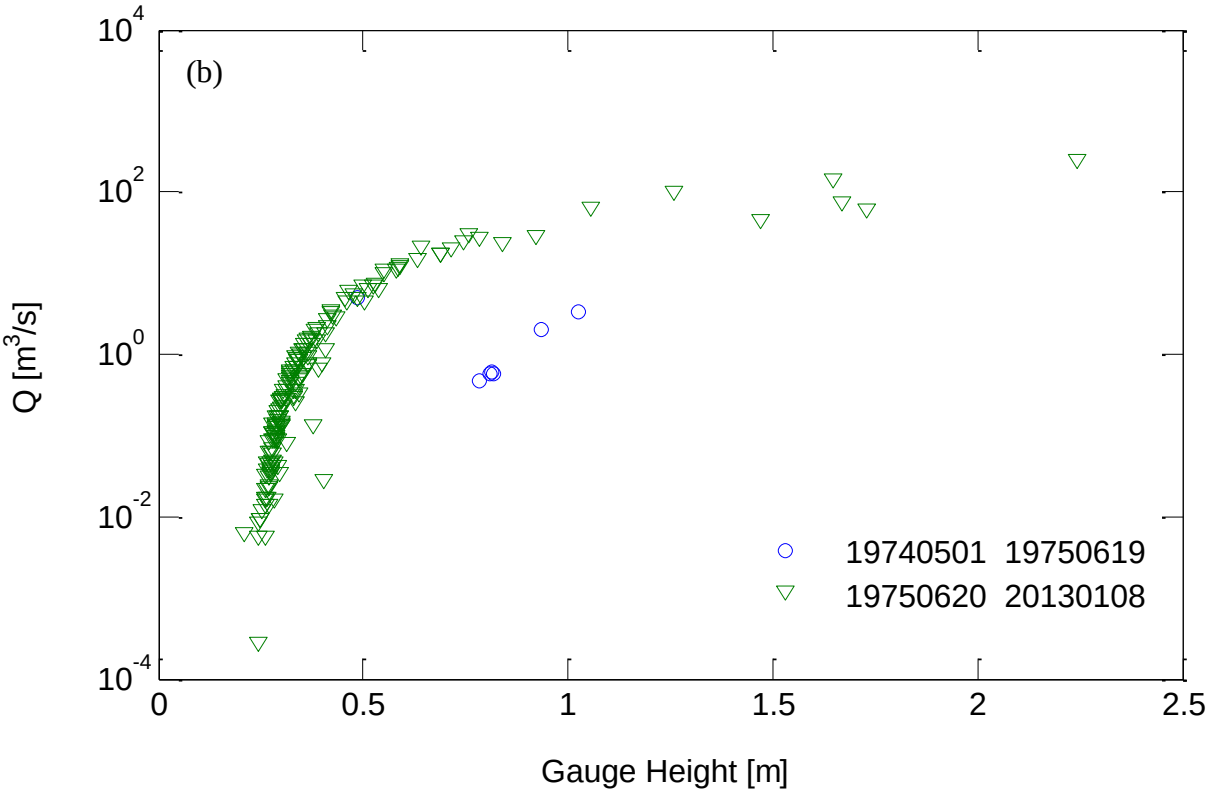
(b)
10^4
10^2
10^0
10^{-2}
10^{-4}
Q [m^3/s]
0
0.5
1
1.5
2
2.5
Gauge Height [m]
19740501 19750619
19750620 20130108


(c)

Figure A.35. (a) Q_s vs Q between 1973 to 1978, (b) Q vs Gauge Height, (c) and (d) dried channel bed with cobble/boulder and sand/fine gravel. Photos were taken from field investigation at Arroyo Valle below Lang Canyon near Livermore, CA. Note: There was a big change of Q_s vs Q rating curve by USGS after June, 1975 so gauge height to flow rate relationship is significantly different after June 1975 as shown in panel (b).

6. Cull Creek above Cull Creek Reservoir near Castro Valley, CA. (USGS site number 11180960)

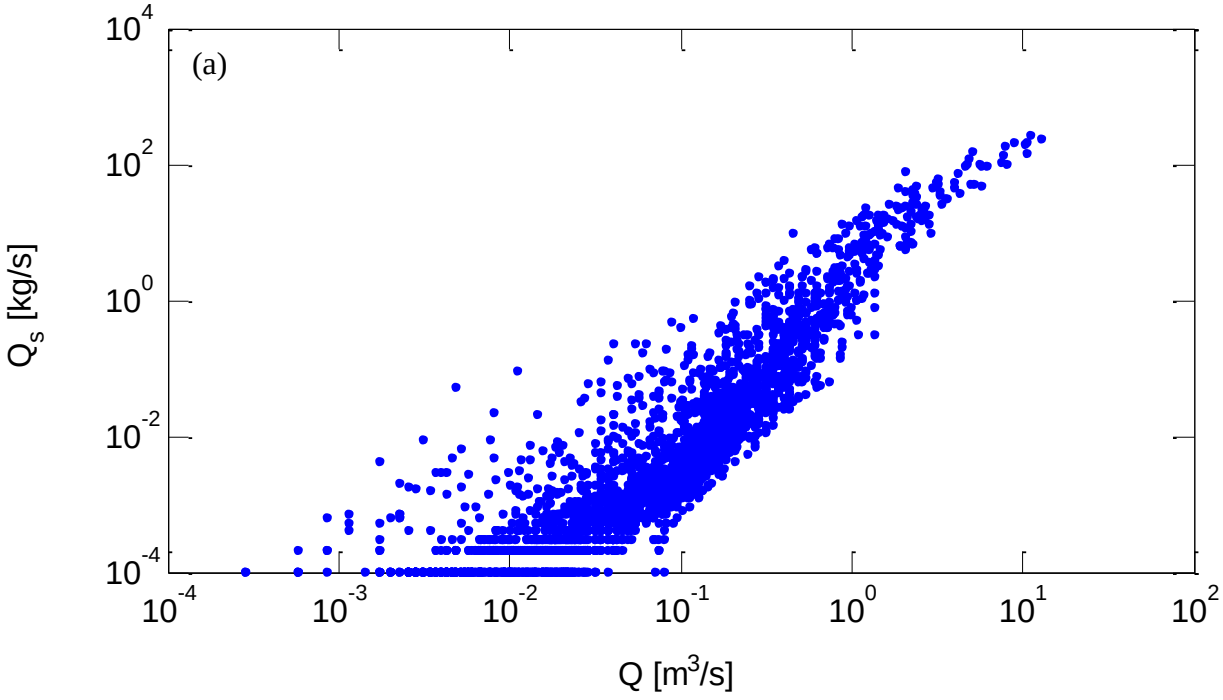

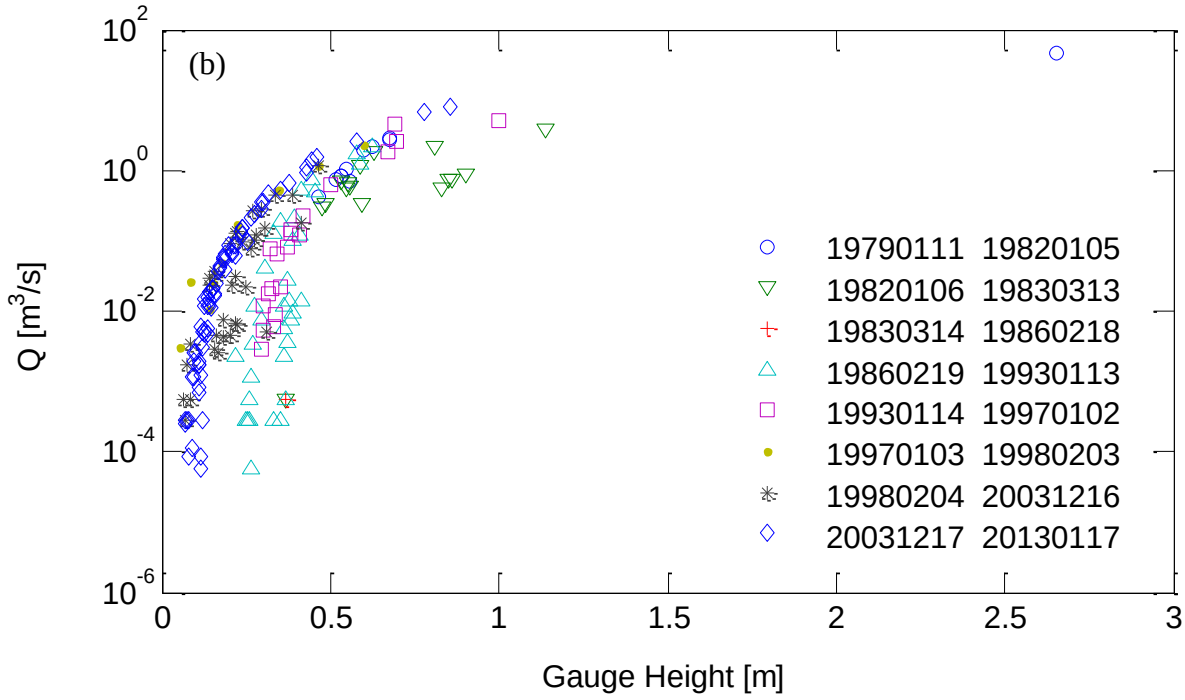

Figure A.36. (a) Q_s vs Q relationship from 1979 to 2002, (b) Q vs Gauge Height, and (c) bedrock dominated channel bed is partially covered by sand. Photo was taken from field investigation at Cull Creek above Cull Creek Reservoir near Castro Valley, CA.

7. Russian River near Ukiah, CA. (USGS site number 11461000)

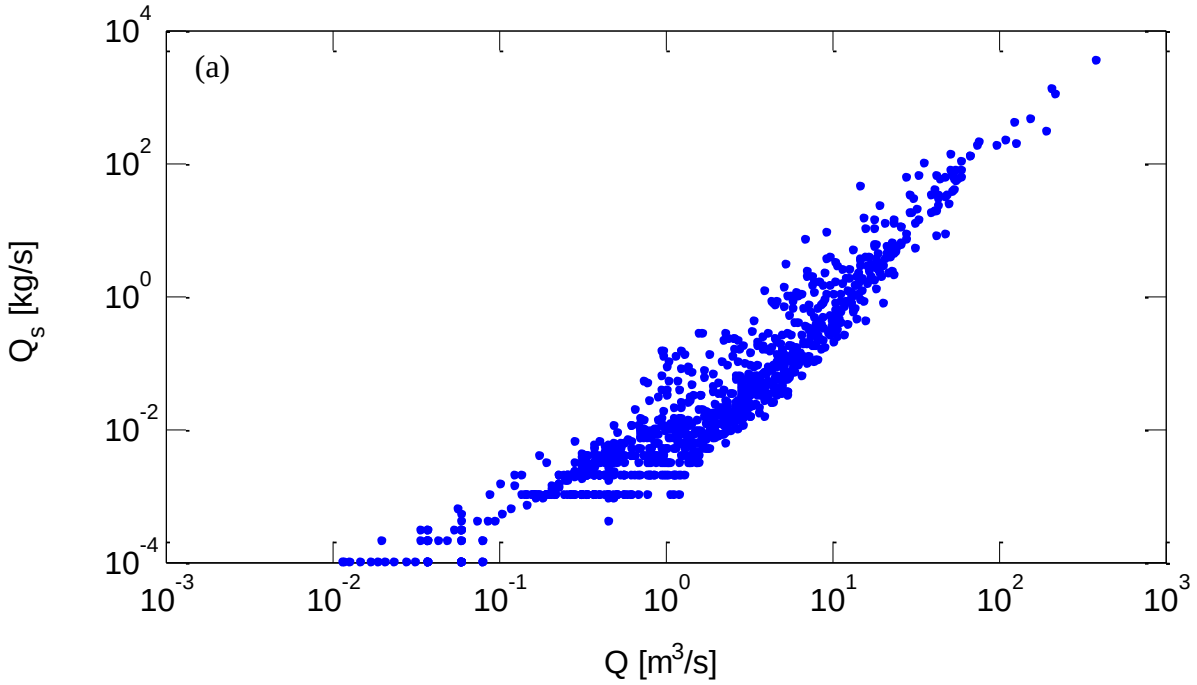

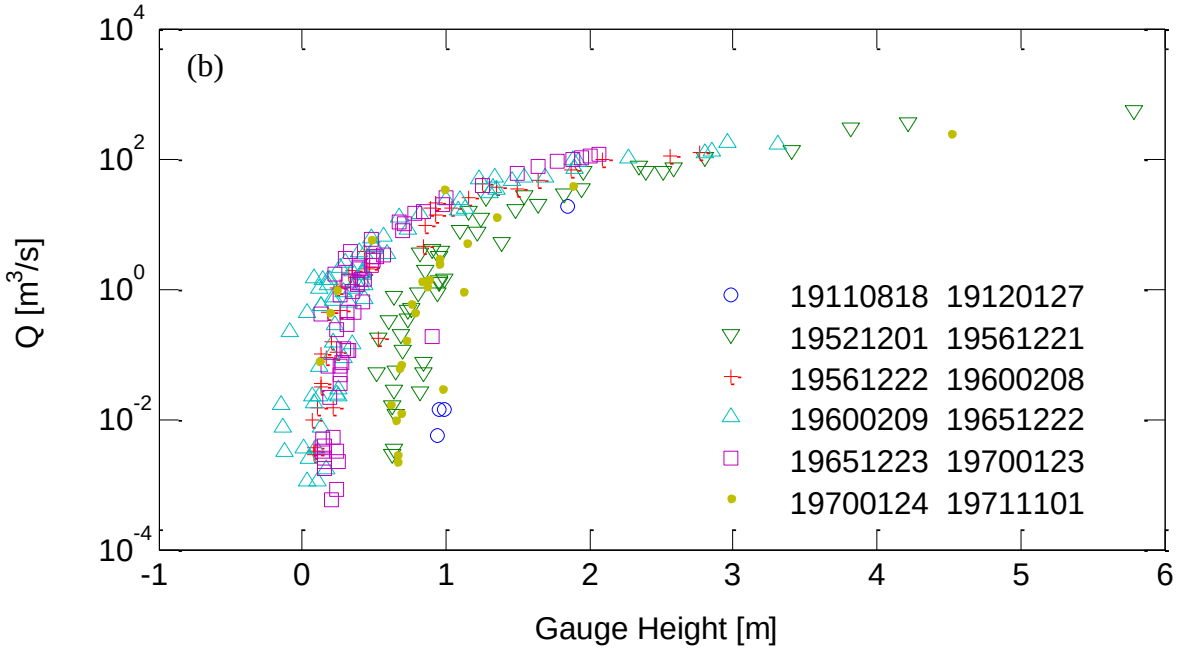

Figure A.37. (a) Q_s vs Q relationship from 1964 to 1968, (b) Q and Gauge Height relationship between 1911 and 1971, (d) and (e) channel bed is dominated by sand and gravel/cobbles. Photos were taken from field investigation at Russian River near Ukiah, CA. Note: Gauge station was moved 0.6 mile downstream after November 8, 1971.

8. Grass Valley Creek at Fawn Lodge near Lewiston, CA. (USGS site number 11525600)

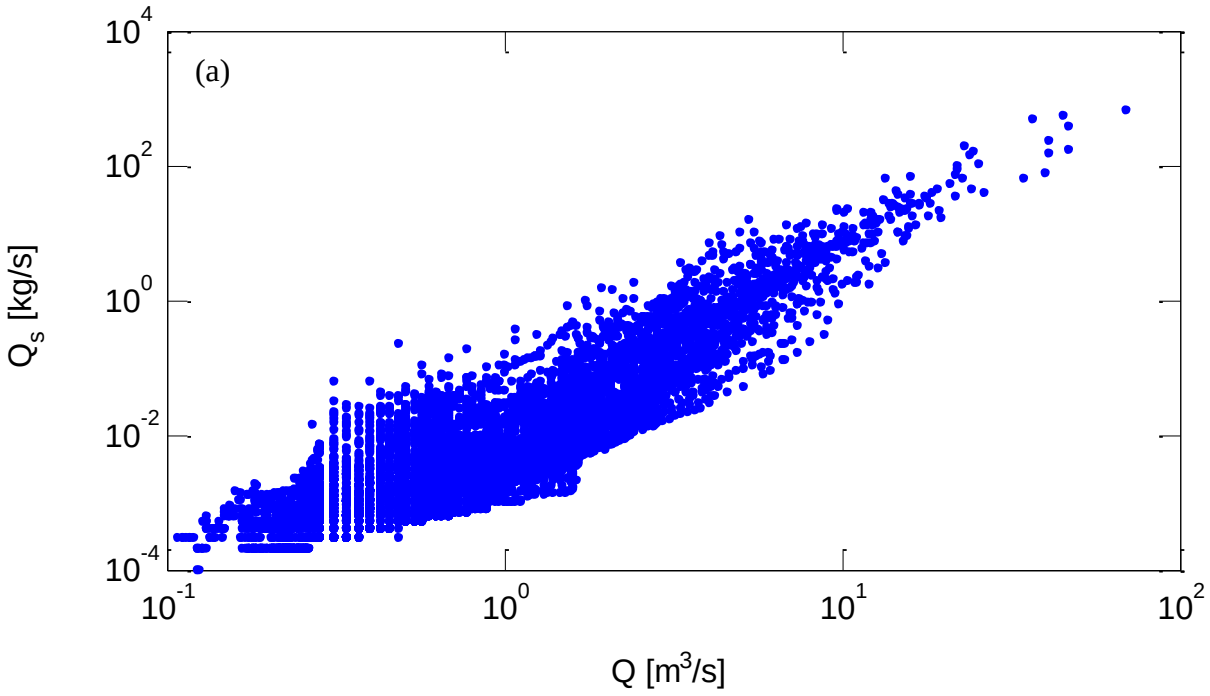

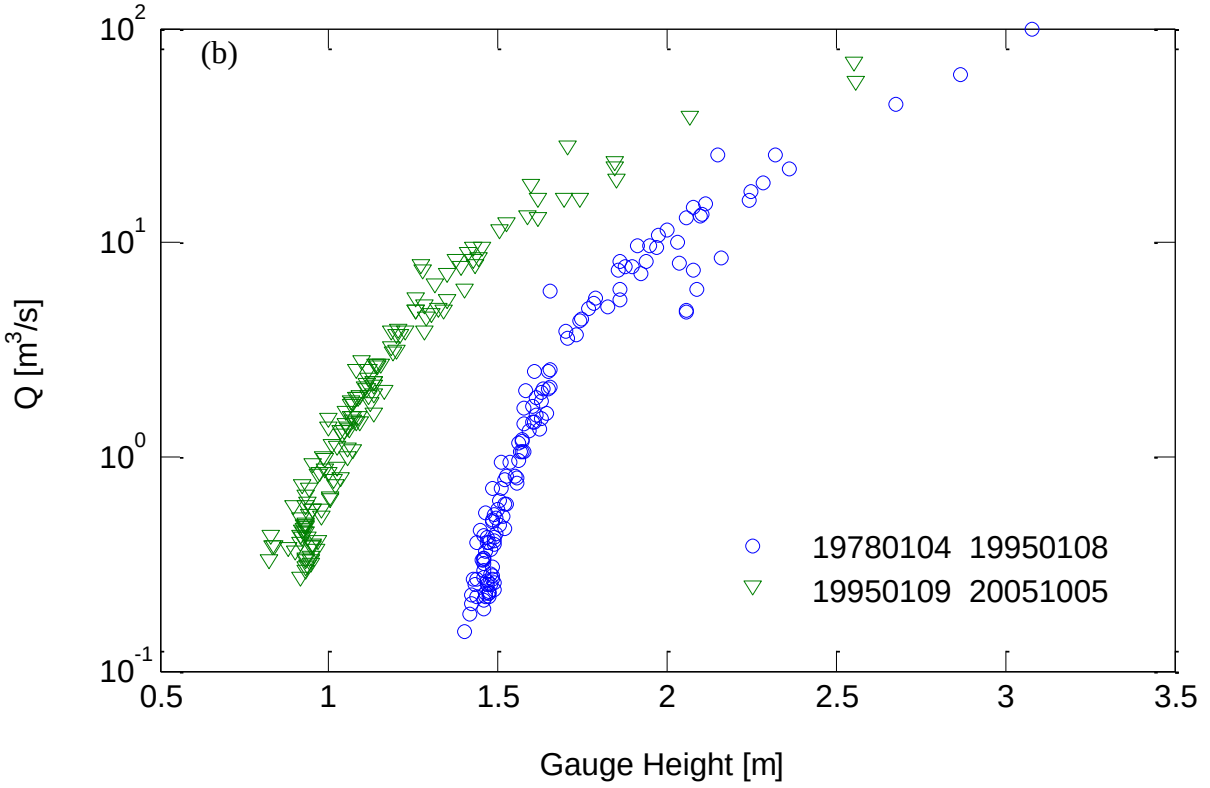

Figure A.38. (a) Q_s vs Q relationship from 1967 to 1986, (b) Q vs Gauge Height, and (c) channel bed is dominated by sand and cobbles. Photo was taken from field investigation at Grass Valley Creek at Fawn Lodge near Lewiston, CA.

Appendix B. Two Watersheds in the Russian River

1. Field measurements of USGS

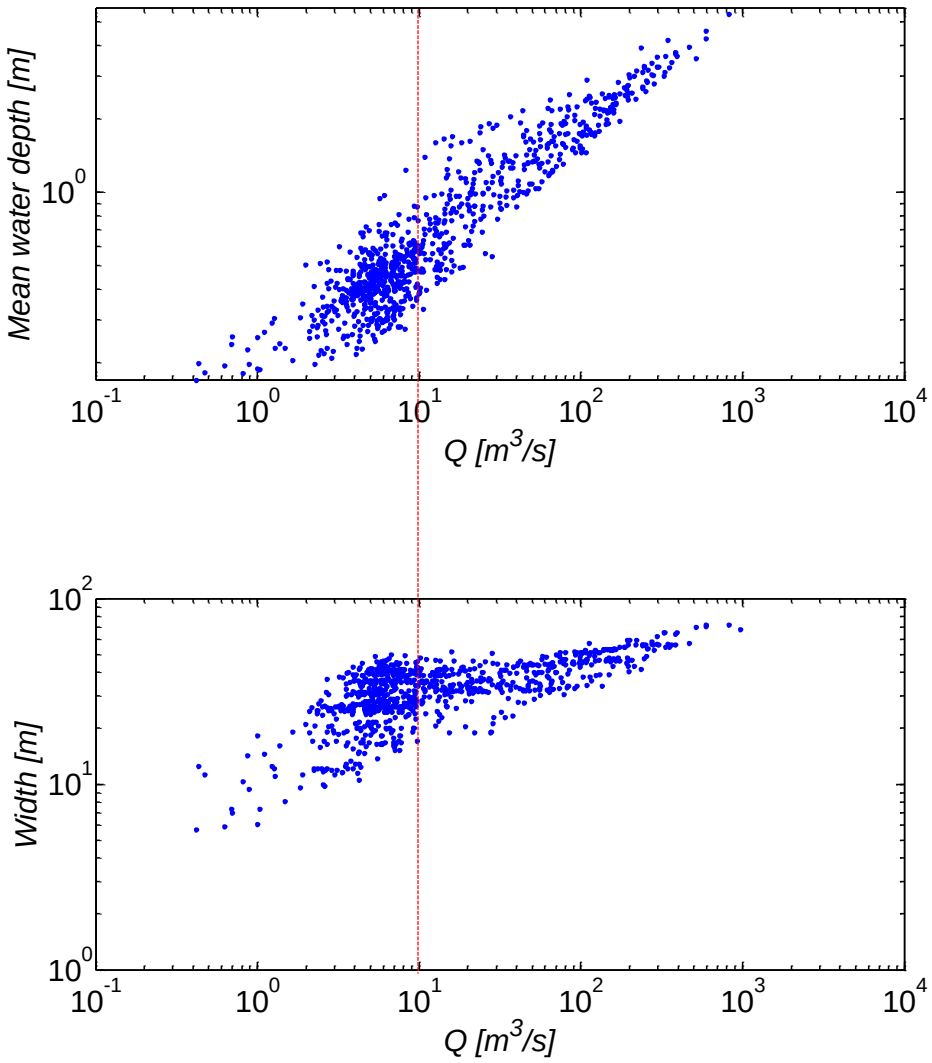

Figure B.1. Field measurements (between 1939 and 2013) reported by USGS in the Russian River at Hopland. The dotted vertical line represents a transition at Q ~ 10 m^3/s. There is no daily suspended sediment load data at Hopland.

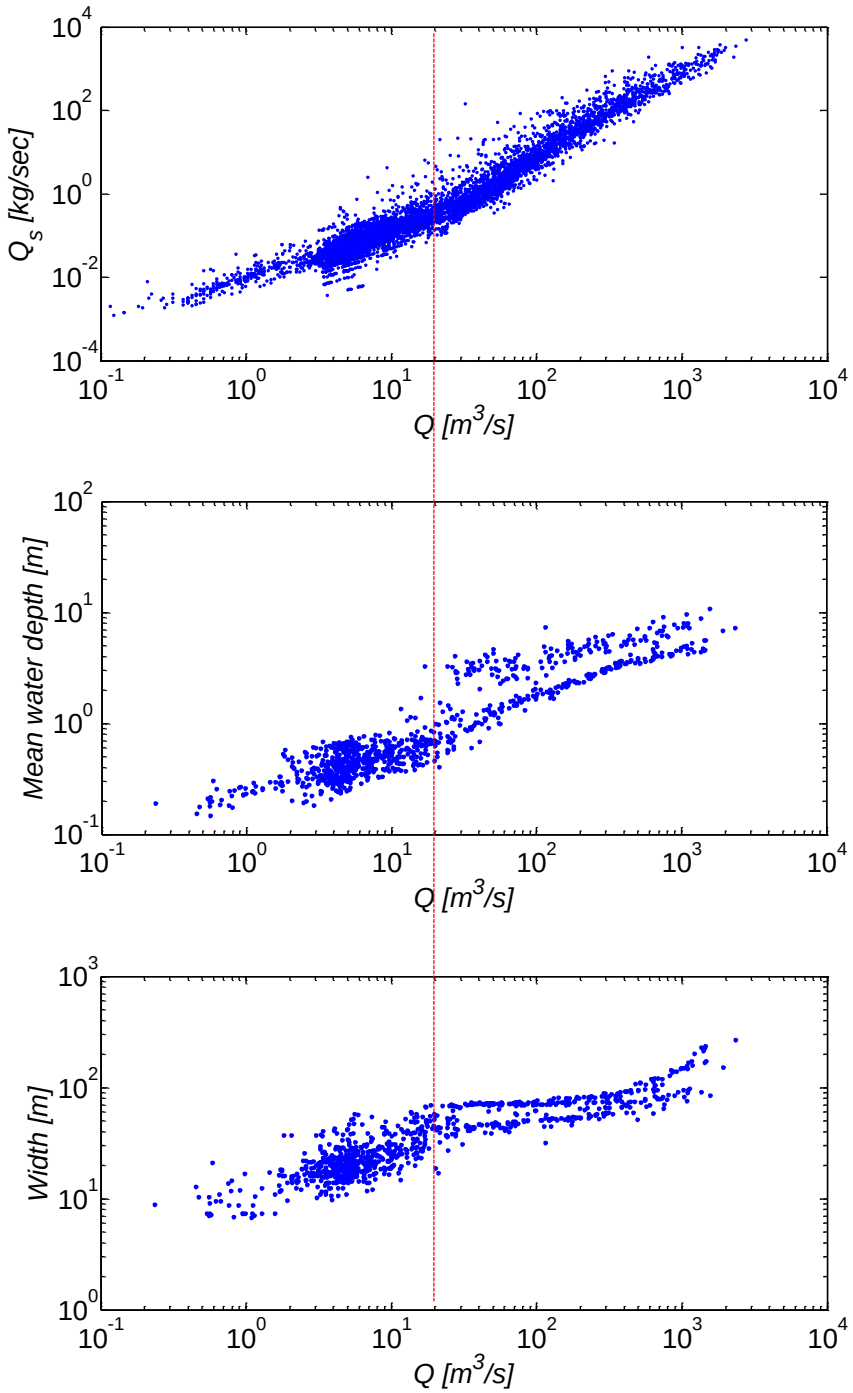

Figure B.1. Daily suspended load (between 1967 and 1986) and field measurements (between 1939 and 2013) reported by USGS in the Russian River at Guerneville. The dotted vertical line represents a transition at Q ~ 20 m^3/s.

2. Flow Rate and Gauge Height Relationship Reported by USGS

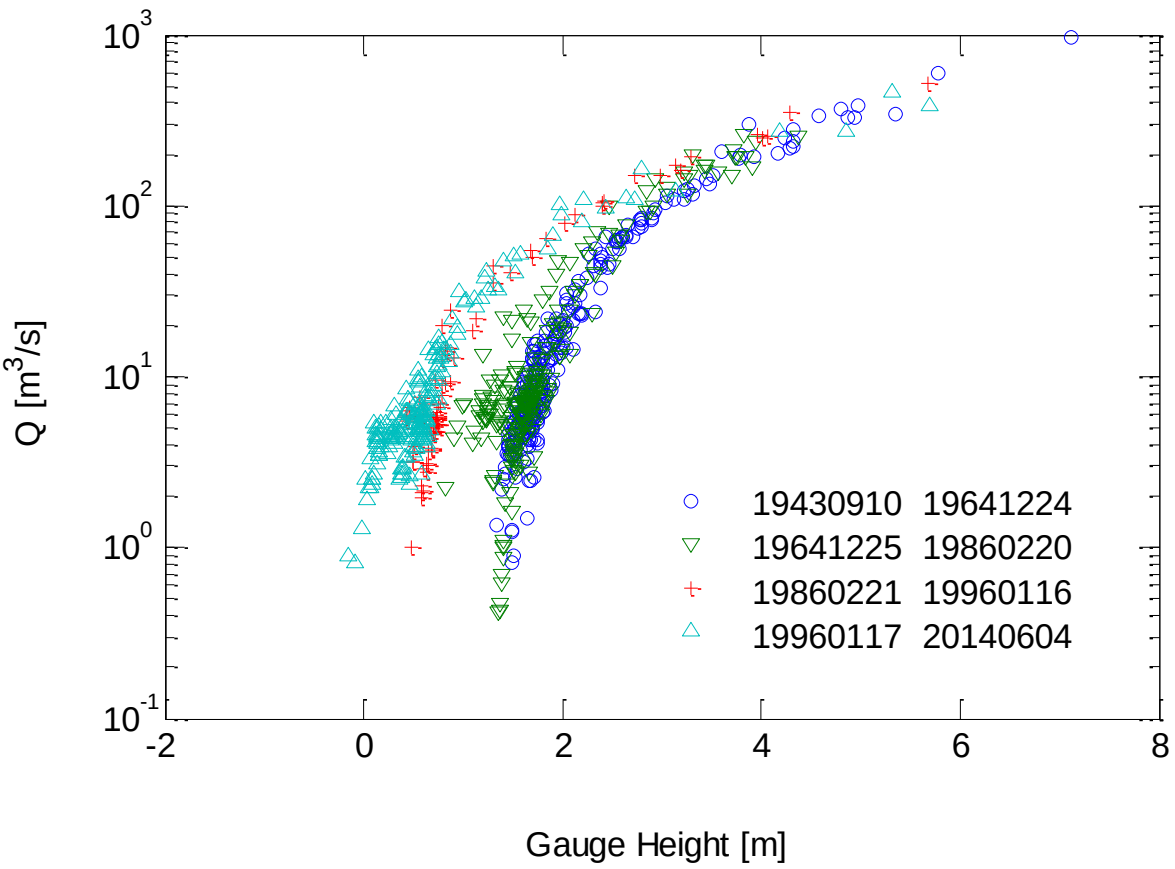

Figure B.3. Flow rate and Gauge Height relationship in the Russian River at Hopland reported by USGS.

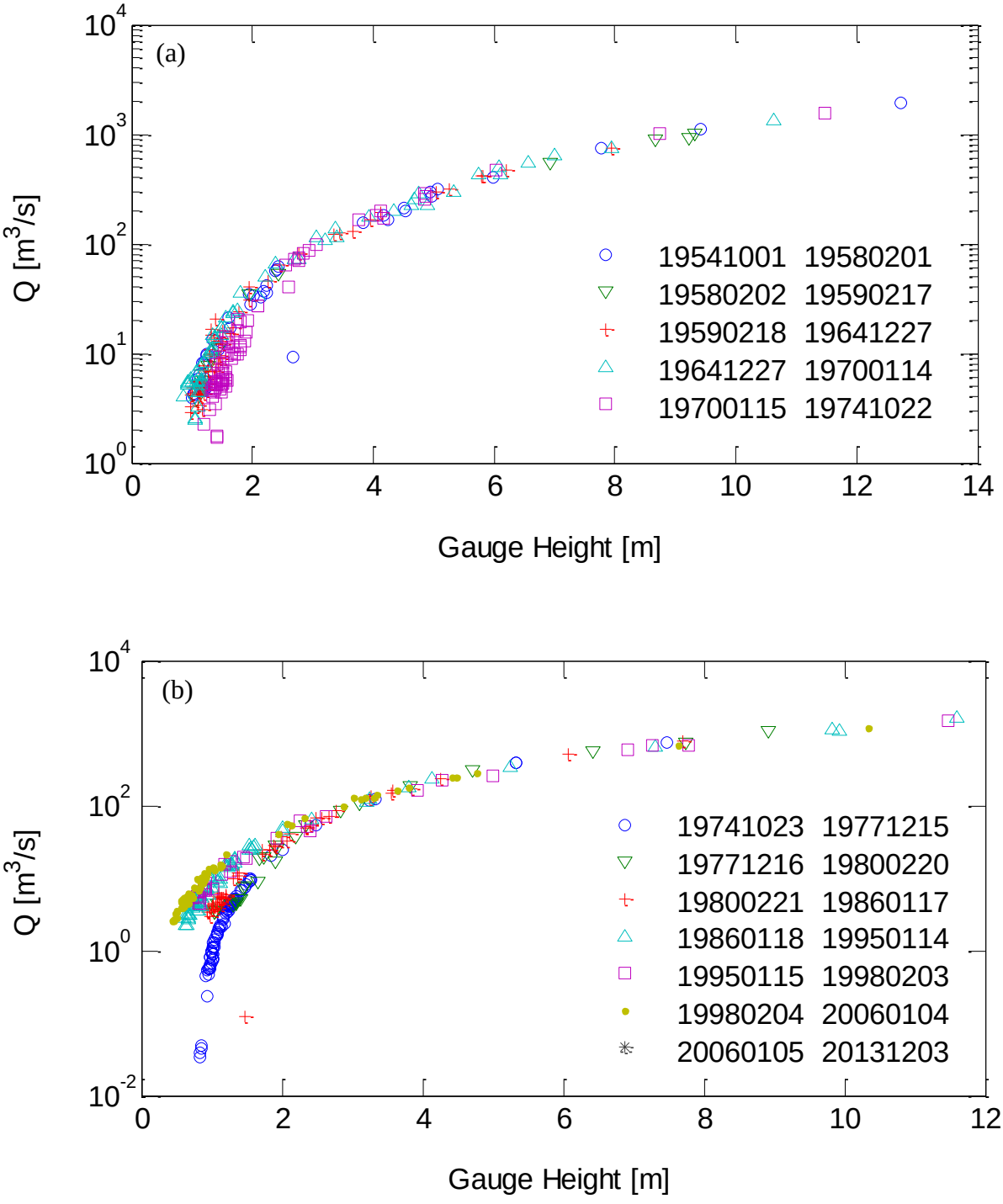

Figure B.4. Flow rate and Gauge Height relationship in the Russian River at Guerneville between 1954 and 2013. The gauge station was moved to 0.7 mile upstream after Oct 23, 1974. (a) Between Oct 1, 1954 and Oct 22, 1974 (b) Between Oct 23, 1974 and Dec 3, 2013.

3. Tables for Flood Events

Table B.1. Flood events at Guerneville in 2010 water year

No.	Date and time of flood (year, month, hour, minute)		Q peak [m^3/s]
	Start	at Q peak	
1	200912131800	200912132245	23
2	200912152200	200912161315	30
3	200912162000	200912170930	29
4	201001021615	201001030530	23
5	201001120745	201001131815	124
6	201001171515	201001210645	1073
7	201001250115	201001261145	1028
8	201002041400	201002051300	294
9	201002230700	201002241145	199
10	201002261145	201002270845	241
11	201003011615	201003040315	351
12	201003120815	201003131400	163
13	201003282330	201004011115	87
14	201004021000	201004031830	135
15	201004041300	201004051100	294
16	201004110645	201004130400	501
17	201004262315	201004281700	74
18	201005242115	201005290000	49

Table B.2. Flood events at Guerneville in 2013 water year

No.	Date and time of flood (year, month, hour, minute)		Q peak [m^3/s]
	Start	at Q peak	
1	201211281415	201211302130	674
2	201212020400	201212030445	889
3	201212042345	201212060045	297
4	201212161200	201212181045	86
5	201212201745	201212220700	736
6	201212230730	201212240645	1087

Table B.3. Flood events at Hopland between 2011 and 2013 water year

No.	2011 water year			2012 water year			2013 water year		
	Date and time (year, month, hour, minute)		Q_{peak}	Date and time (year, month, hour, minute)		Q_{peak}	Date and time (year, month, hour, minute)		Q_{peak}
	Start	at Q peak	[m3/s]	Start	at Q peak	[m3/s]	Start	at Q peak	[m3/s]
1	201010111100	201010130645	36	201201200245	201201200545	23	201211202045	201211210400	22
2	201010240015	201010241930	135	201201201815	201201210500	202	201211281730	201211282200	24
3	201010272215	201010281745	63	201201221215	201201231045	134	201211291630	201211301015	267
4	201010290100	201010291100	60	201202131330	201202131615	24	201212012045	201212021715	425
5	201011040545	201011041845	30	201203011330	201203011600	28	201212041500	201212050815	132
6	201011060145	201011071500	50	201203131215	201203131800	85	201212140530	201212141245	57
7	201011210415	201011211245	21	201203160130	201203170145	87	201212151145	201212171115	58
8	201011220400	201011221215	21	201203270415	201203272230	294	201212201415	201212211115	303
9	201011230415	201011231445	49	201203291830	201203300900	76	201212220330	201212221030	173
10	201011270700	201011271930	34	201203310600	201203311545	115	201212230415	201212231915	343
11	201011301215	201012030945	26	201203312215	201204010500	106	201212251200	201212261245	153
12	201012051130	201012060915	81	201204120145	201204121300	22	201212270415	201212271145	130
13	201012071415	201012072200	49	201204122200	201204131015	46	201301051000	201301060515	34
14	201012080330	201012081430	59				201303060700	201303061600	15
15	201012090130	201012090515	48						
16	201012132200	201012141115	72						
17	201012171745	201012180945	34						
18	201012190030	201012191815	132						
19	201012201400	201012210115	115						
20	201012212130	201012220800	171						
21	201012251045	201012252330	88						
22	201012261530	201012262215	84						
23	201012271200	201012271645	67						
24	201012280800	201012290530	331						
25	201012301415	201012302315	112						
26	201101130230	201101131845	44						
27	201101272315	201101301015	19						
28	201102140845	201102152230	218						
29	201102170915	201102180000	79						
30	201102231315	201102251015	37						
31	201102281730	201103031145	81						
32	201103052130	201103061200	40						
33	201103130915	201103140230	39						
34	201103150645	201103152330	174						
35	201103172030	201103181530	232						
36	201103191700	201103200800	273						
37	201103211400	201103220130	157						
38	201103230300	201103231200	153						
39	201103232145	201103241630	314						
40	201103250515	201103250845	233						
41	201103260315	201103261245	192						
42	201103270845	201103280000	200						

4. Data Correction and M_{max} at Hopland

Turbidity data from Hopland for one flood event was corrected when it became apparent that the turbidity sensor reached a maximum reading. During the Dec 2, 2012 flood event, there was a 4 hour period where the turbidity was reported as 1000 NTU, which is illustrated as black dotted line in Figure B.5. The turbidity in this period was corrected by interpolating turbidity values within the hysteresis relationship between flow rate and turbidity as indicated in Figure B.6. The Dec 2, 2012 flood event was the largest in the calibration period and the interpolated turbidity readings slightly changed M_{max} from 20,500 Mg before correction to 20,800 after correction. This slightly larger M_{max} is used for the model simulations of Hopland.

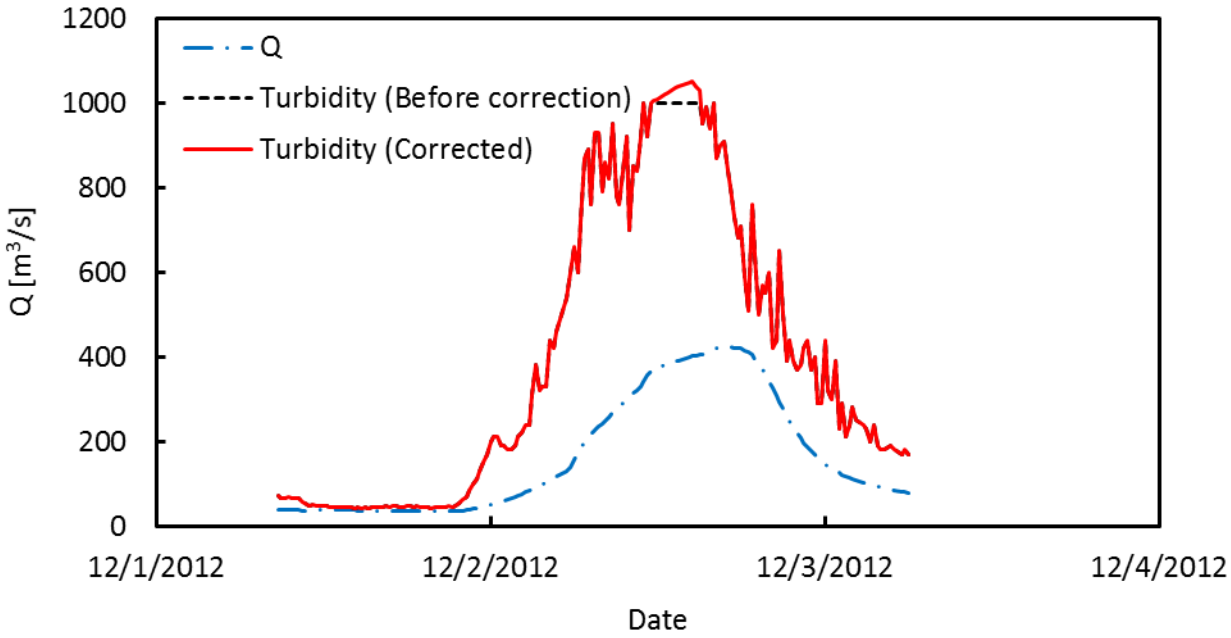

Figure B.5. Hydrograph at Hopland in Dec 2, 2012 flood.

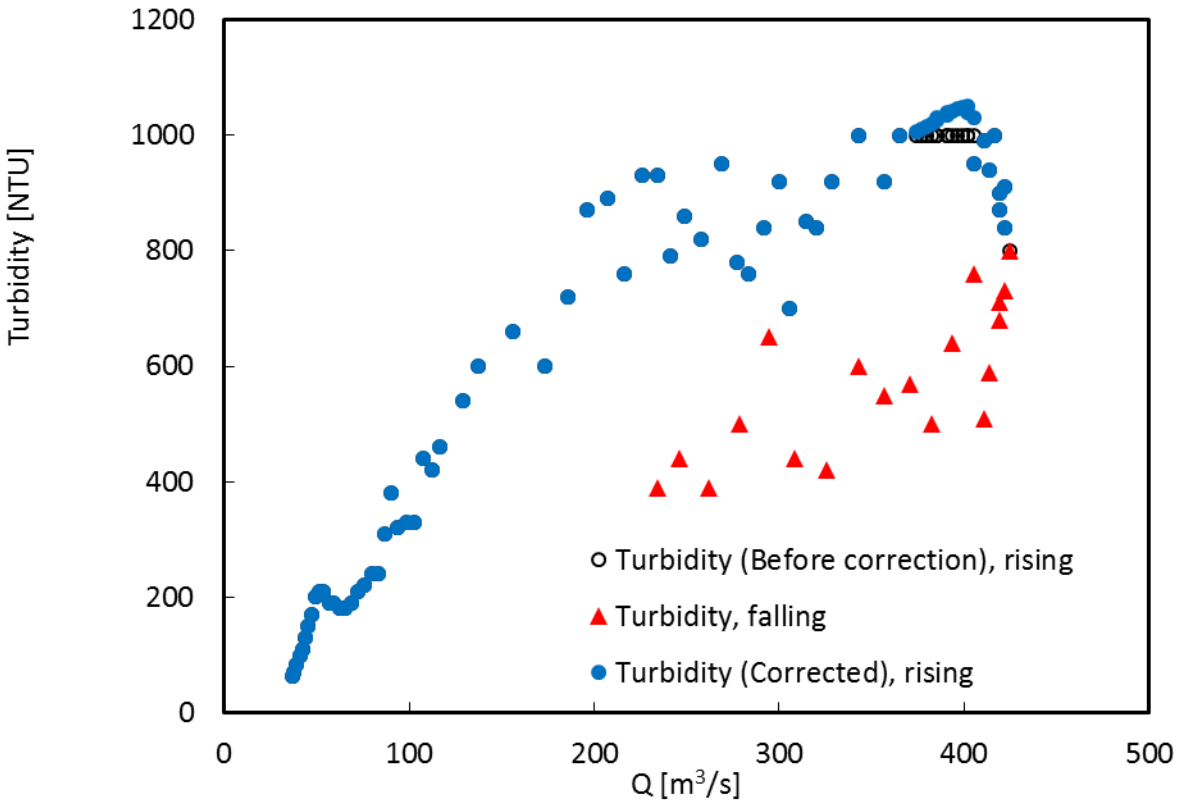

Figure B.6. The hysteresis between *Q* and turbidity at Hopland in Dec 2, 2012 flood.

5. Hysteresis and Hydrograph at Hopland between December 20 and 25, 2012

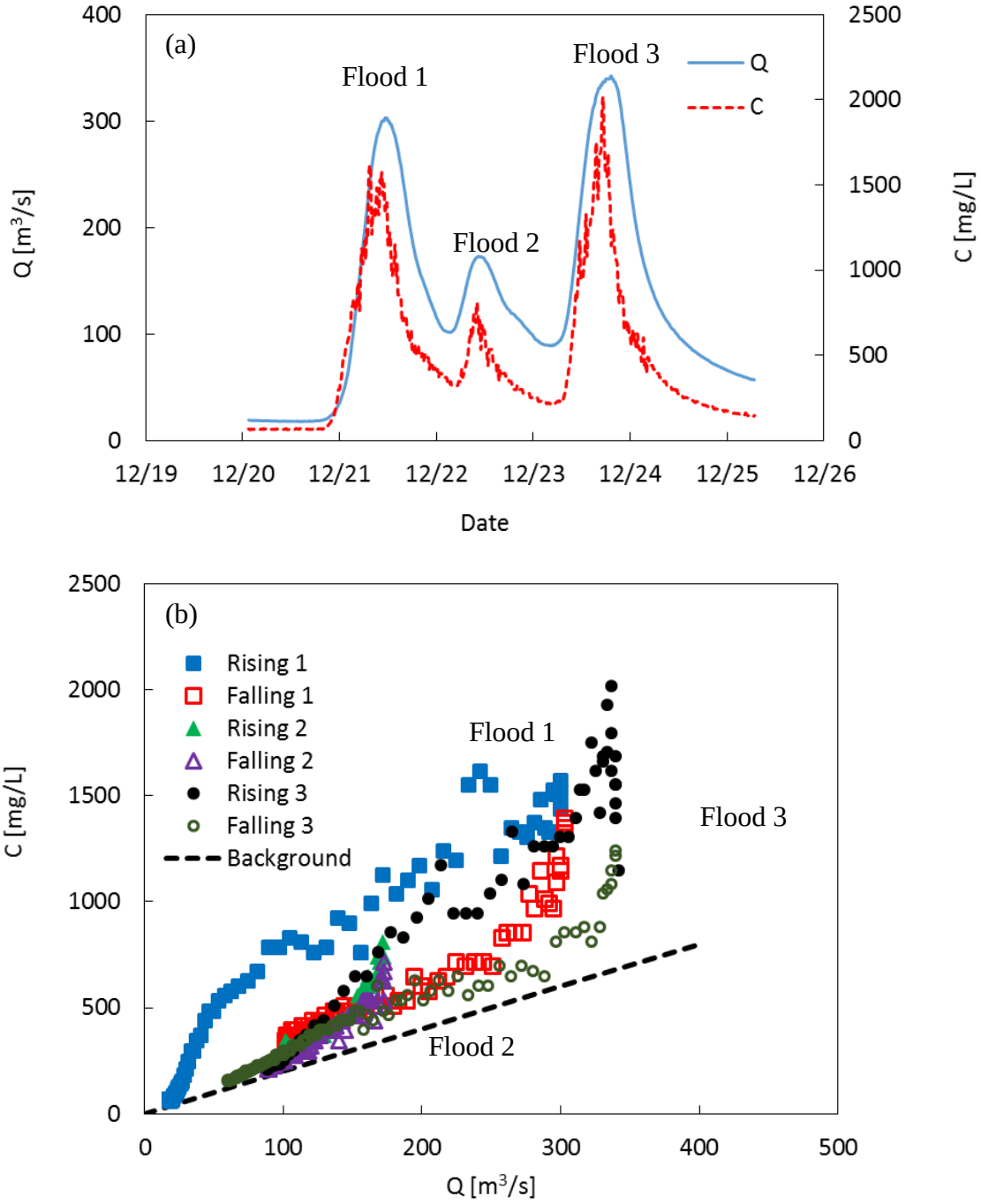

Figure B.7. The (a) hydrograph and (b) hysteresis of Q and C for three continuous floods at Hopland between December 20 and 25, 2012. The largest flood 3 shows smaller hysteresis than flood 1 during flow rate is less than about 300 m^3/s but shows additional release of fine particles when flow rate is larger than 300 m^3/s. All three floods shows good fit with background suspended particle concentration, $C_b=2Q$, as shown in black dotted line.

Appendix C. Two Watersheds in Ireland

1. Flow Rate vs Suspended Load

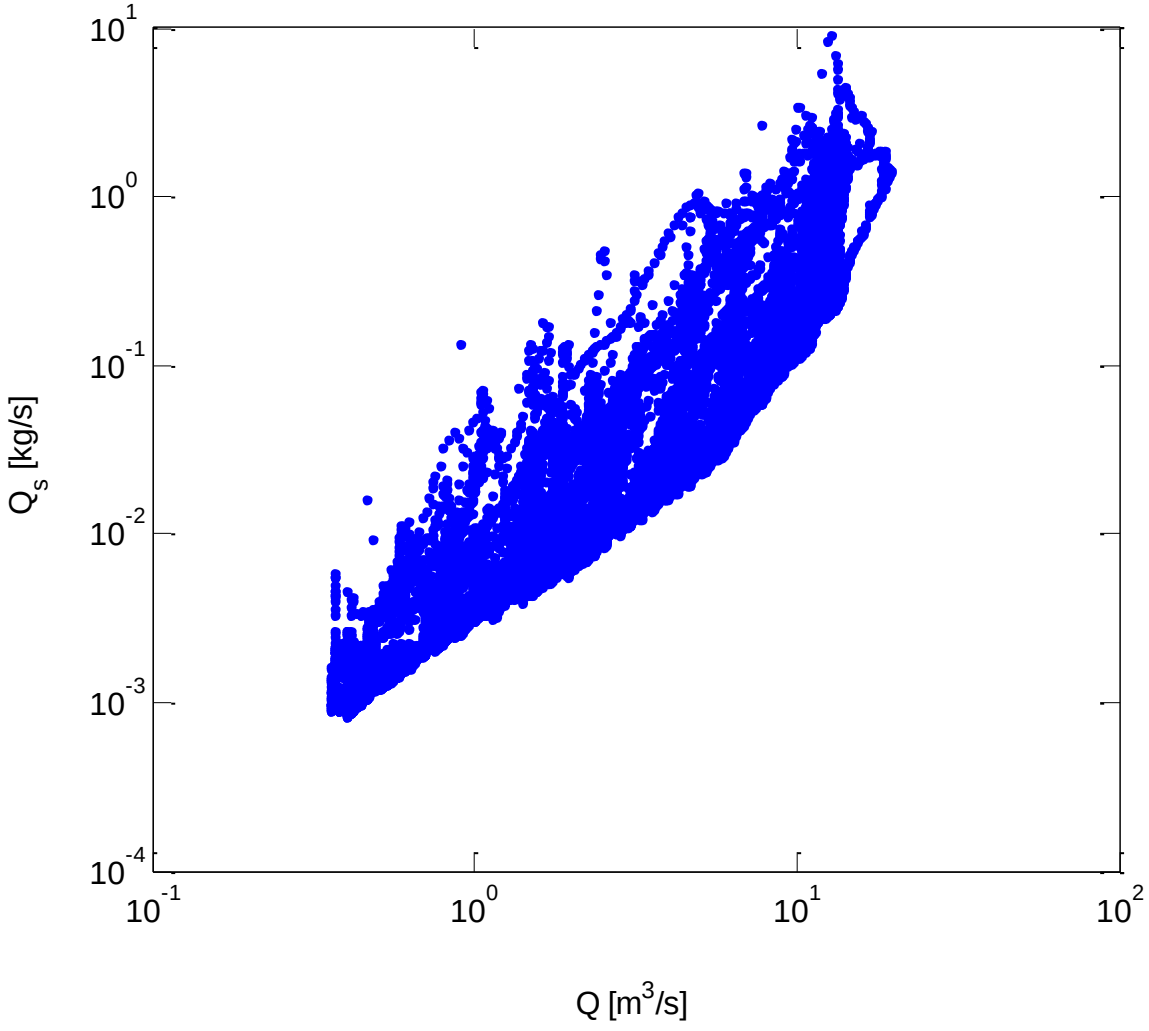

Figure C.1. The sediment loading curve for the Owenabue watershed over the period September 2009 to September 2010.

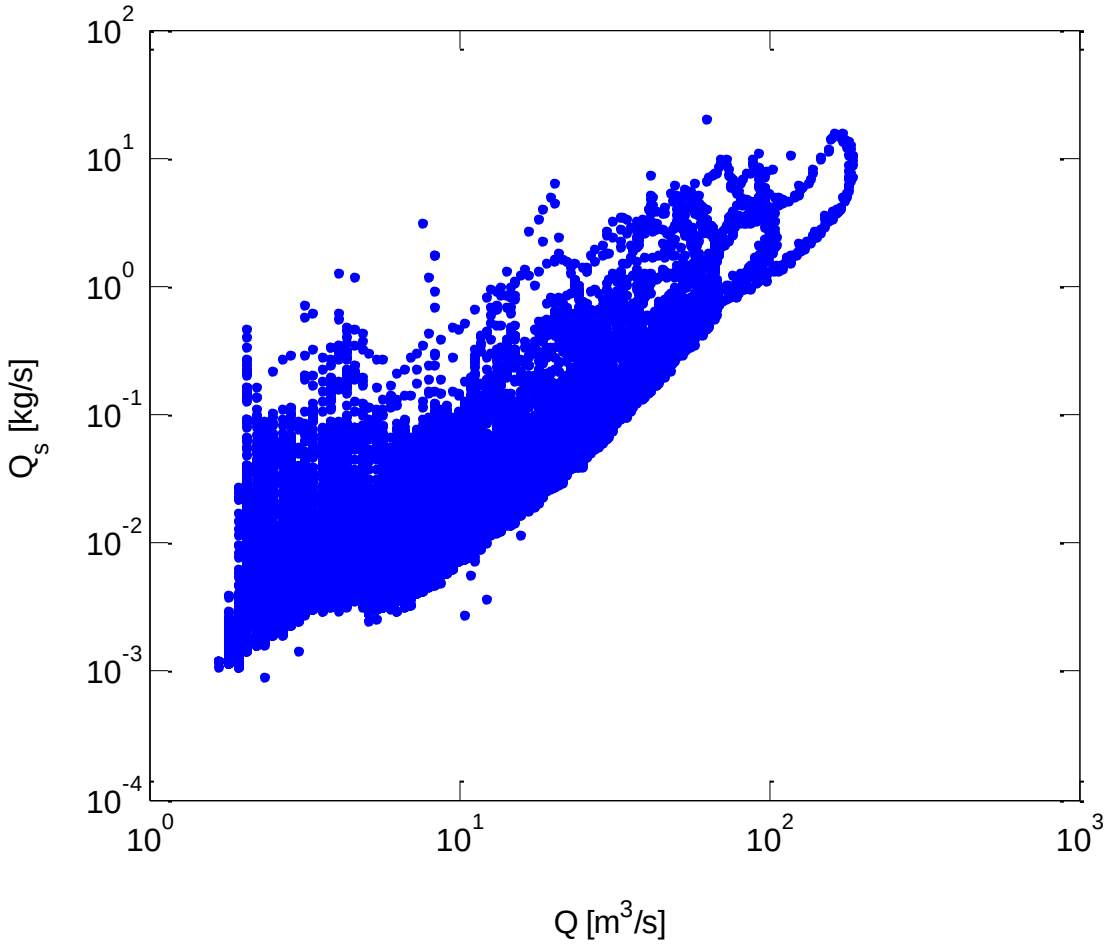

Figure C.2. The sediment loading curve for the Bandon watershed over the period February 2010 to February 2011.

2. Hysteresis and Hydrograph

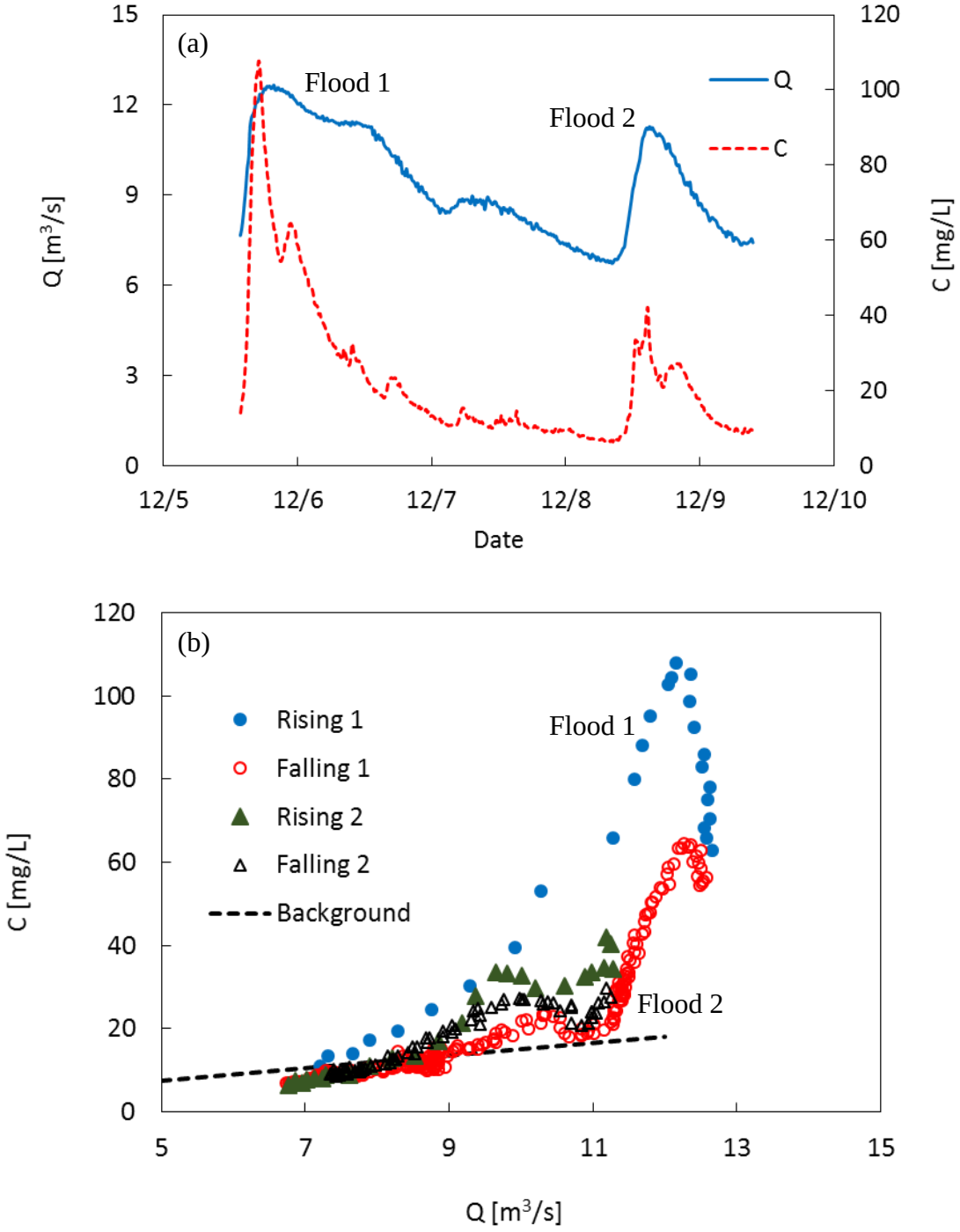

Figure C.3. The (a) hydrograph and (b) hysteresis of Q and C for sequential floods at Owenabue between December 5 and 10, 2009. No hysteresis is observed in the second flood which represents the depletion of fine sediment storage in the channel bed. Background suspended particle concentration, C_b=1.5Q, is represented as black dotted line.

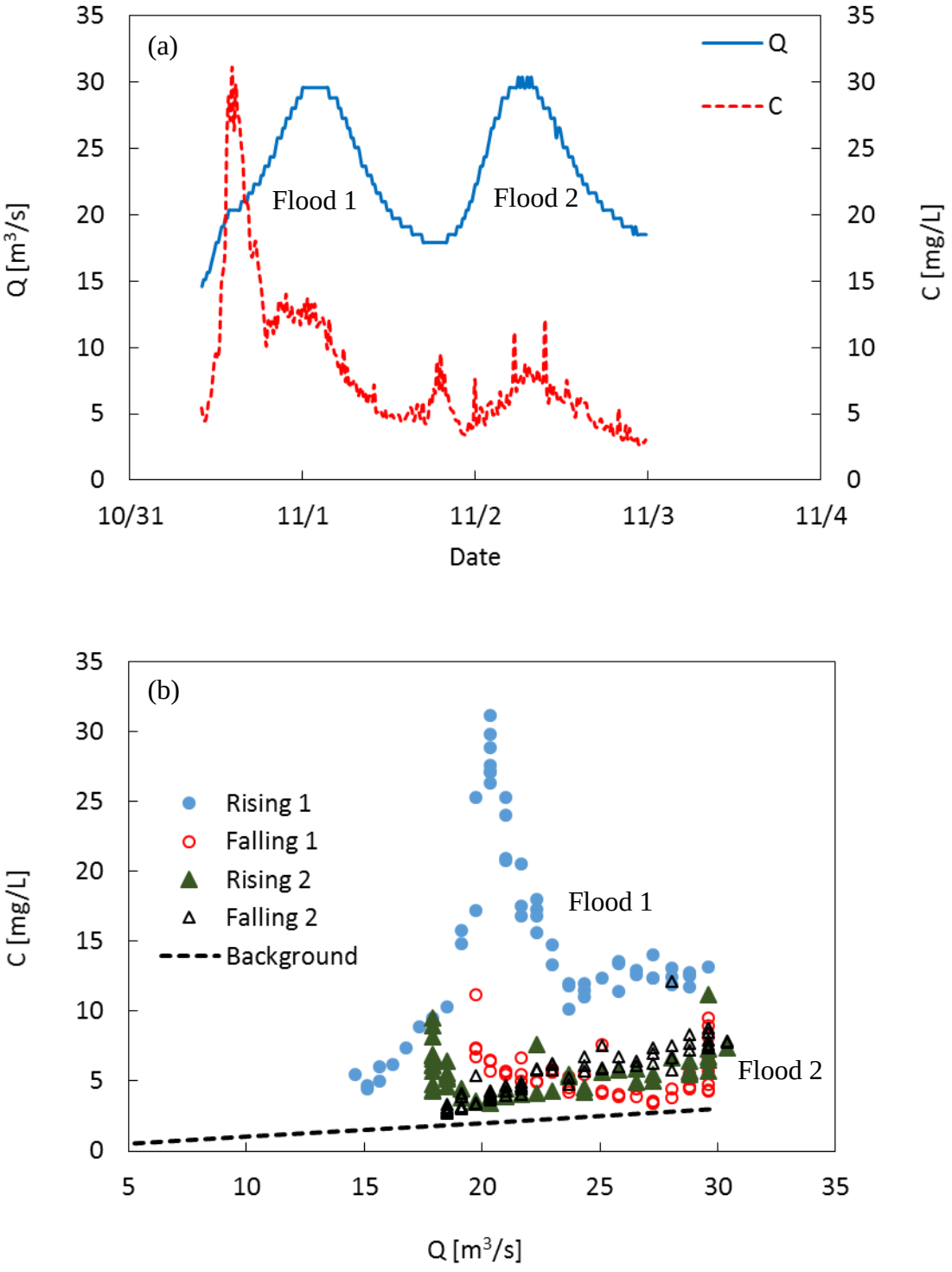

Figure C.4. The (a) hydrograph and (b) hysteresis of Q and C for sequential floods at Bandon between October 31 and November 2, 2010. No hysteresis is observed in the second flood which represents the depletion of fine sediment storage in the channel bed. Background suspended particle concentration, C_b=0.1Q, is represented as black dotted line.

Appendix D. Two Watersheds in France

1. Flow Rate vs Suspended Load

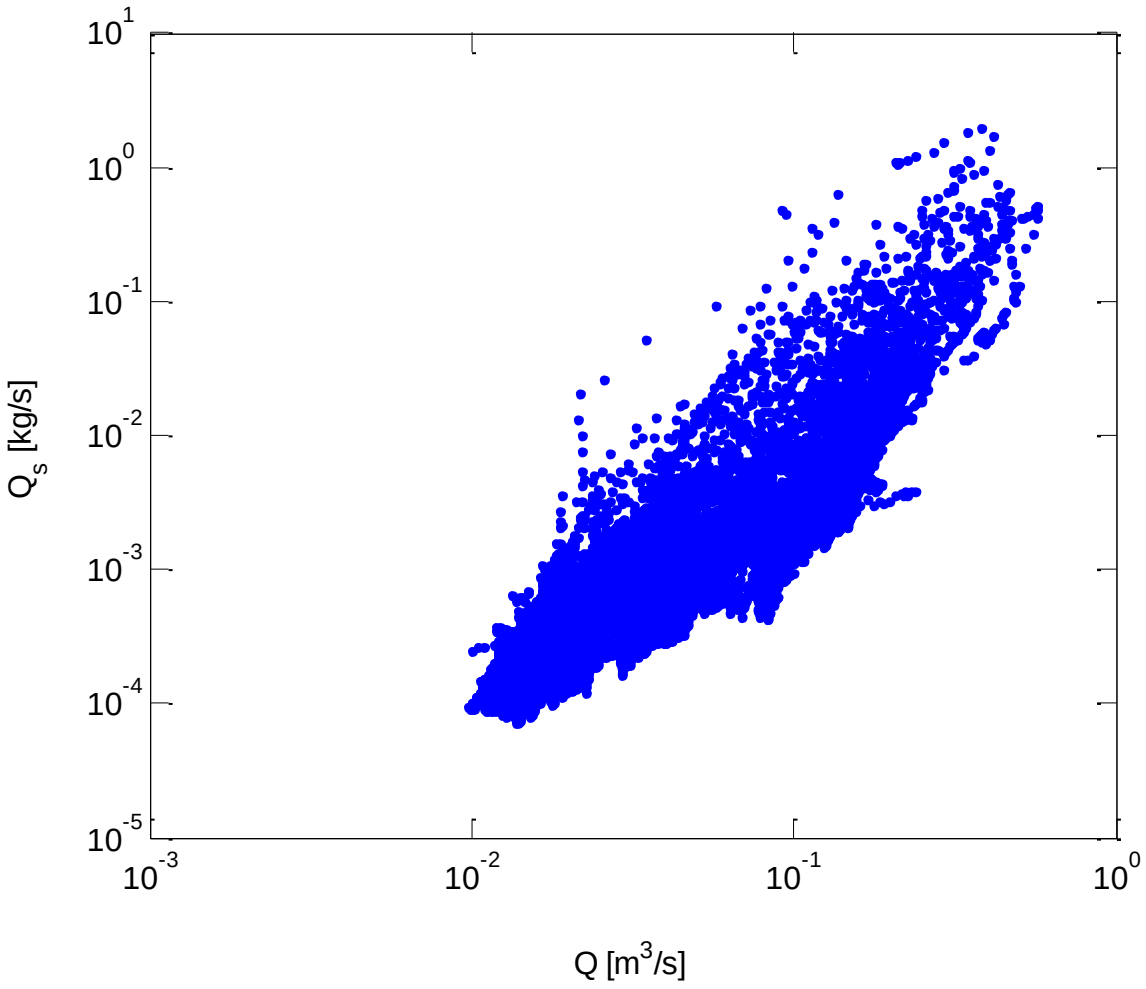

Figure D.1. The sediment loading curve for the Moulinet watershed over the period July 2002 to June 2003.

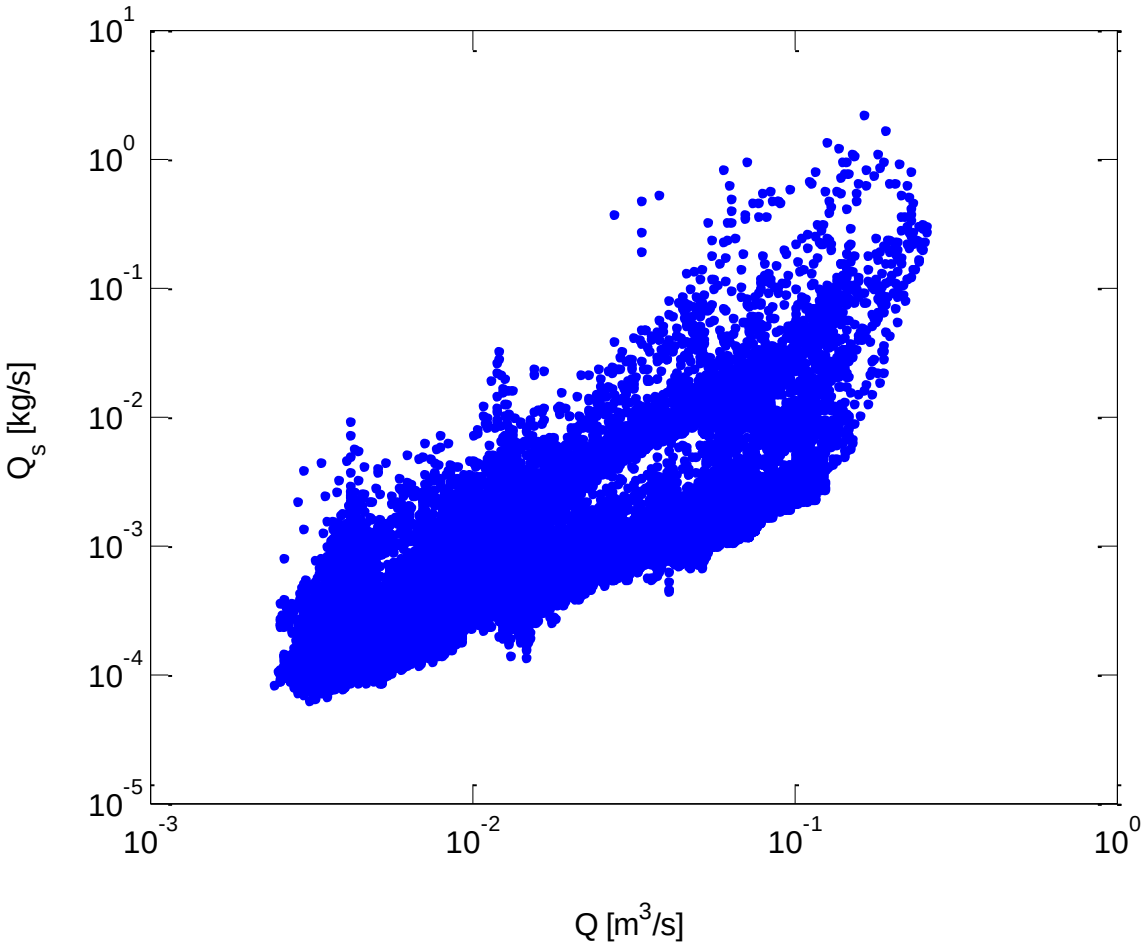

Figure D.2. The sediment loading curve for the Violettes watershed over the period June 2002 to May 2003.

2. Hydrograph and Hysteresis

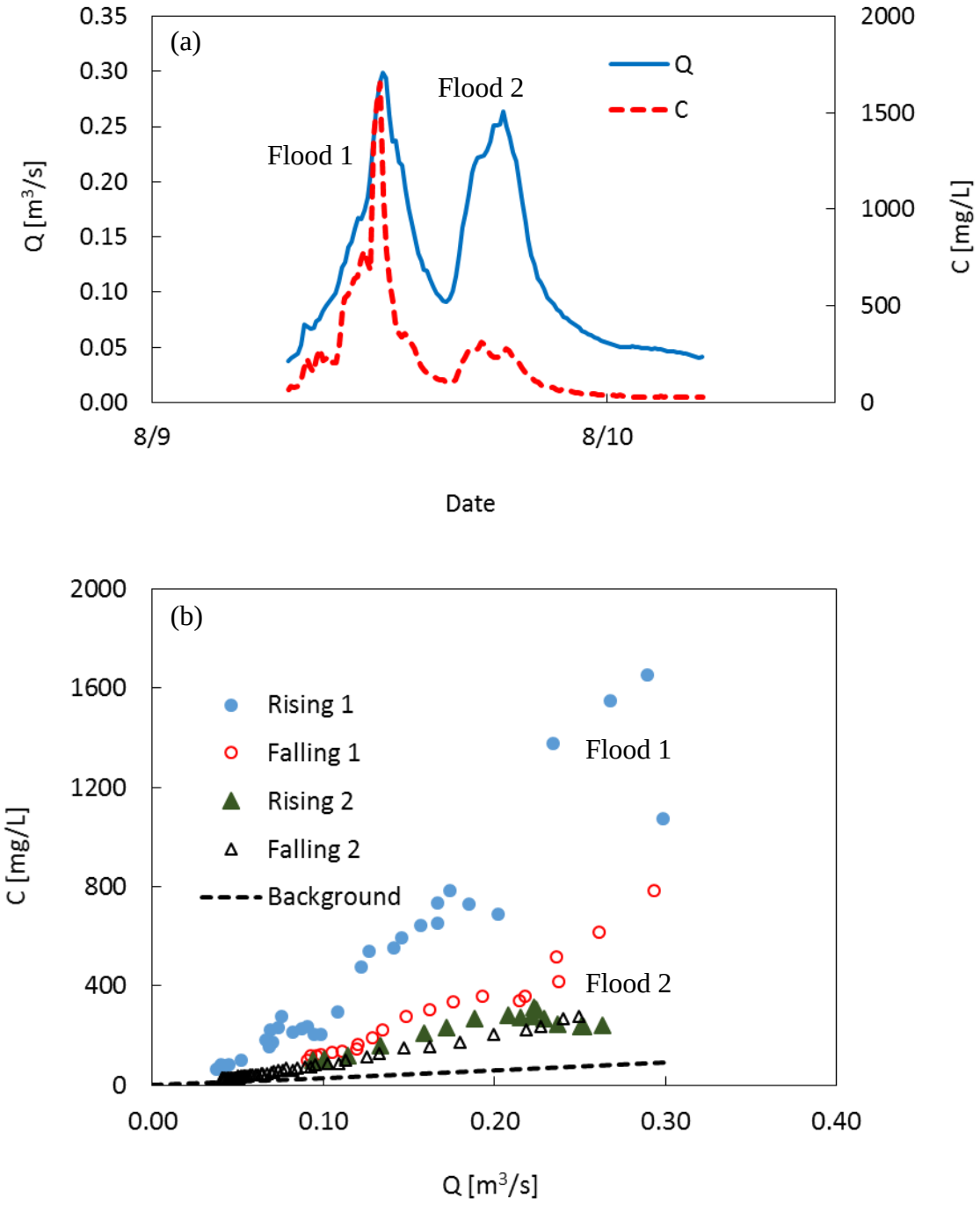

Figure D.3. The (a) hydrograph and (b) hysteresis of Q and C for sequential floods at Moulinet between August 9 and 10, 2002. Much less hysteresis is observed in flood 2 which demonstrates the depletion of fine sediment storage in the channel bed and only a contribution from watershed background. The background suspended particle concentration relationship, C_b=300Q, is represented as the black dotted line.

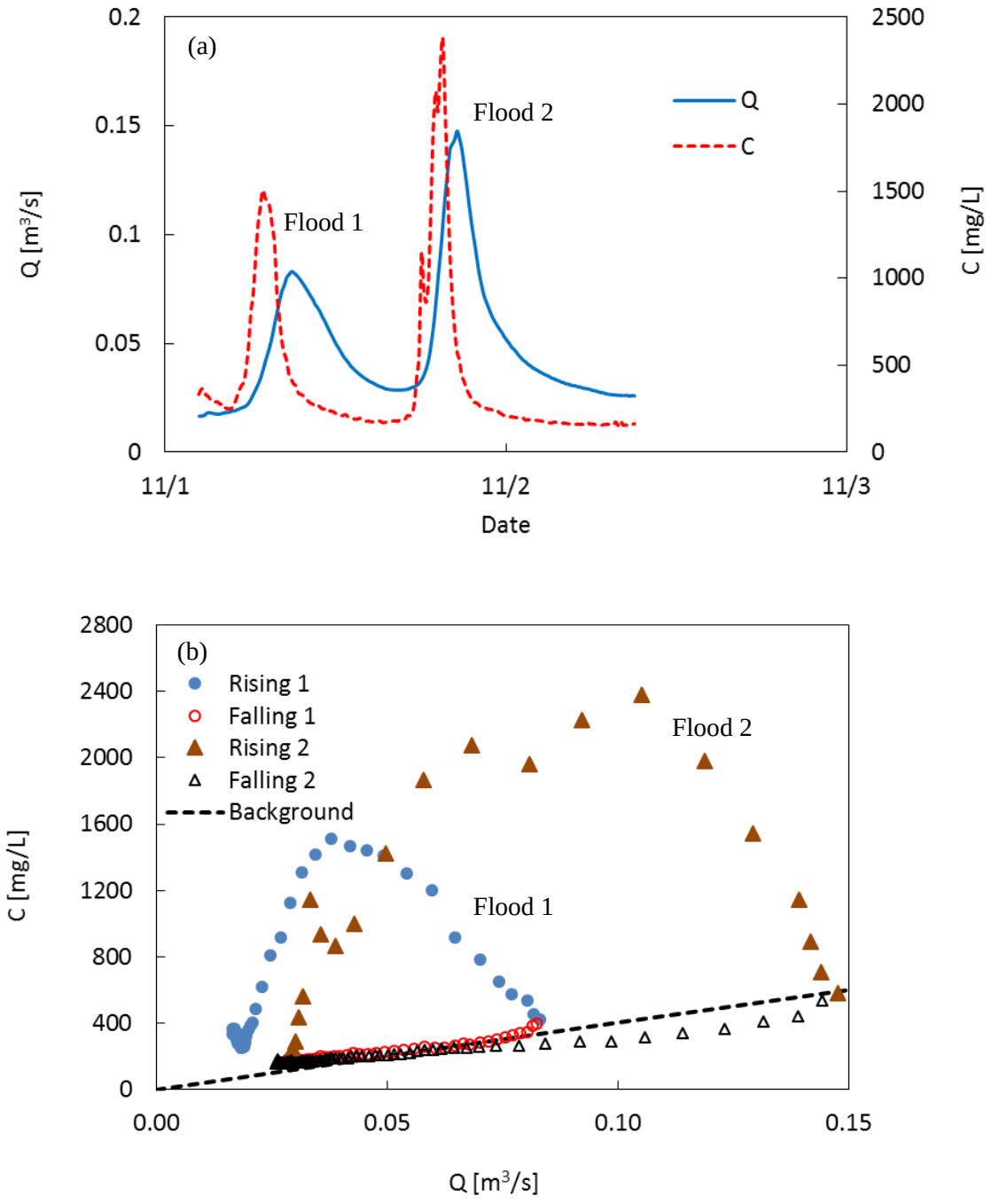

Figure D.4. The (a) hydrograph and (b) hysteresis of Q and C for sequential floods at Violettes between November 1 and 3, 2002. The higher peak flow rate in flood 2 gave additional fine particle removal from the sediment bed since the sediment bed fluidization depth was greater. Background suspended particle concentration, C_b=4000Q, is represented as black dotted line.

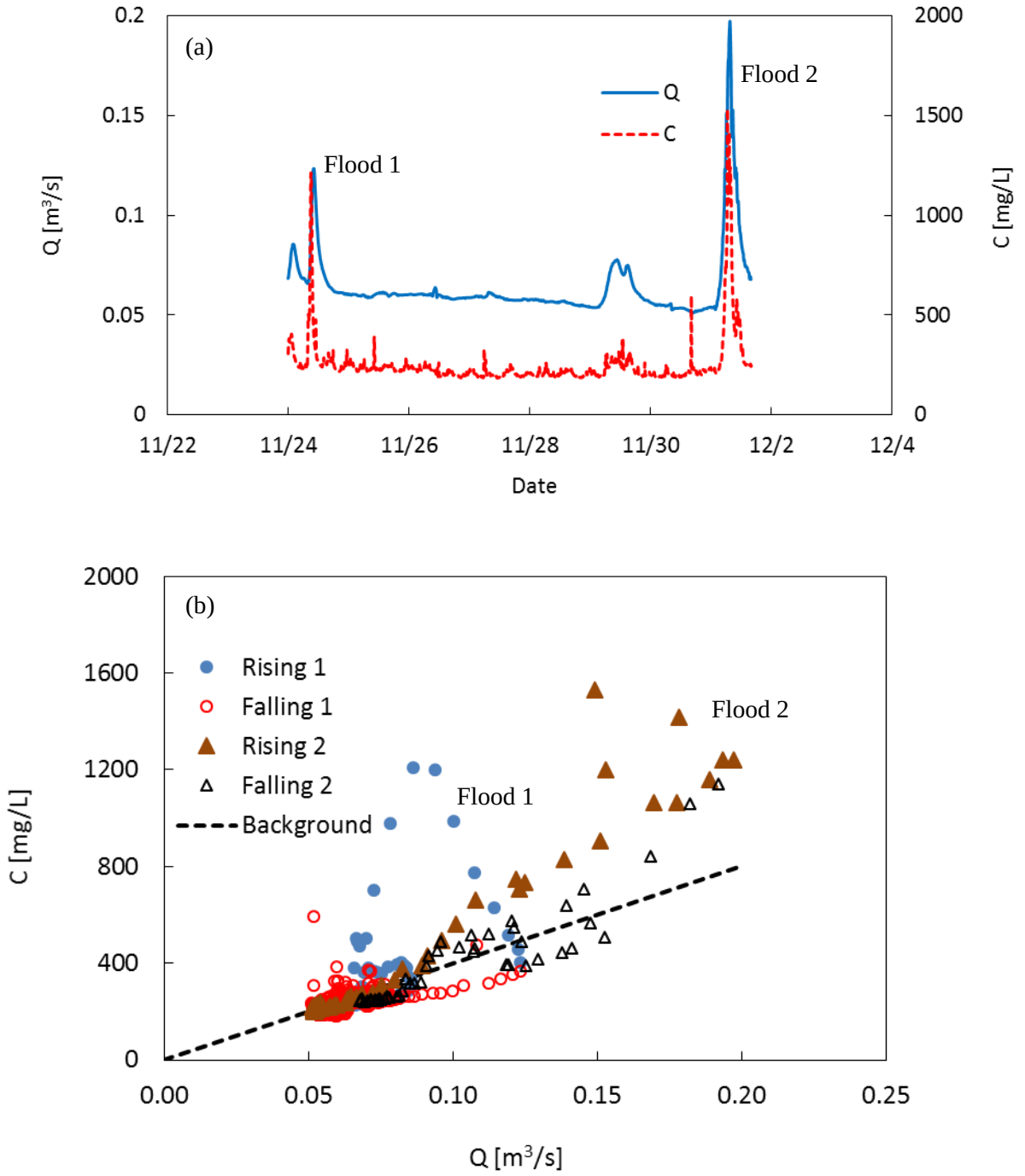

Figure D.5. The (a) hydrograph and (b) hysteresis of Q and C for sequential floods at Violettes between November 24 and December 2, 2002. Flood 2 shows considerable scatter in fine particle concentration and less hysteresis is observed. There was limited opportunity to accumulate fine particles within the sediment bed between the two floods events because partial bed fluidization is initated at flows of 0.05 m^3/s (Q_c). Background suspended particle concentration, C_b=4000Q, is represented as black dotted line.

3. Background Suspended Sediment Concentration

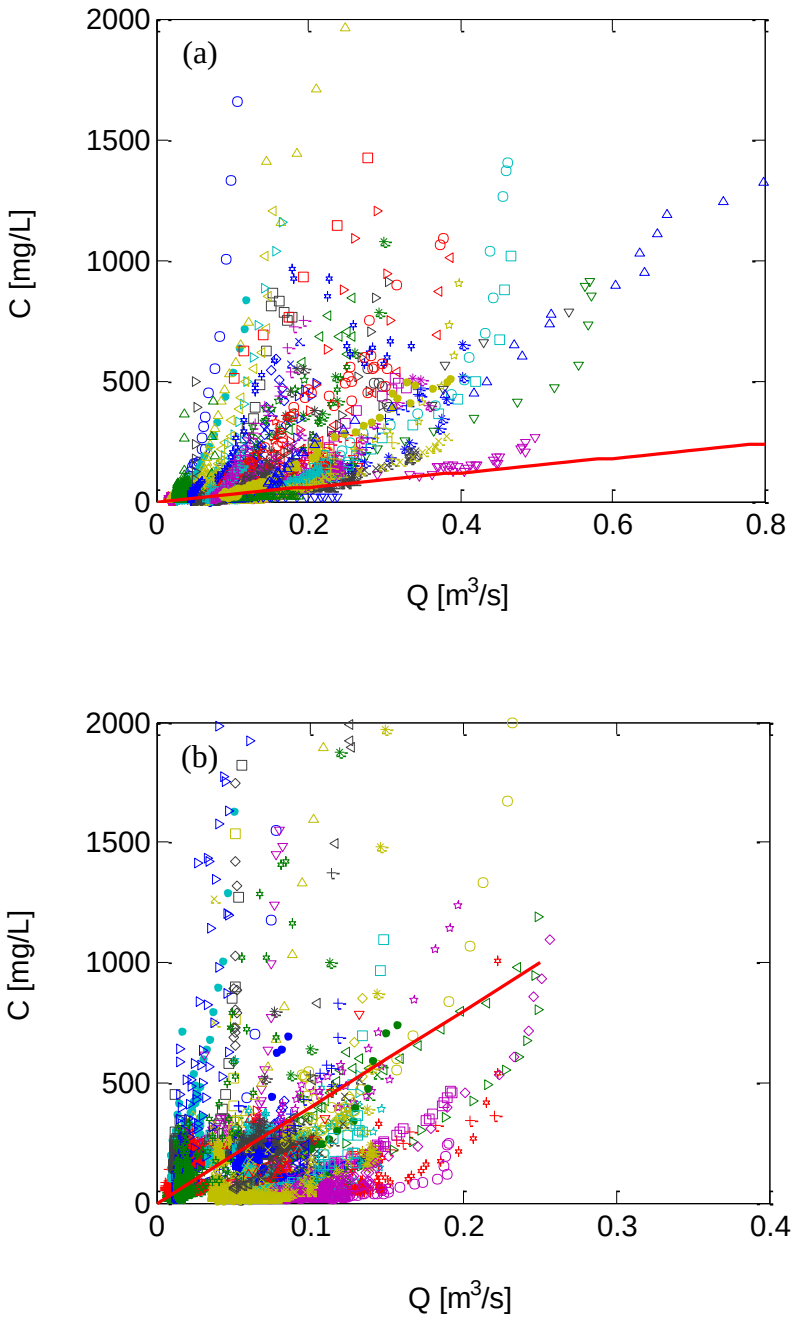

Figure D.4. Fine particle concentration during falling limb recession in the French watersheds for the range of suspended particle concentration less than 2000 mg/L at (a) Moulinet and (b) Violettes. The plotting symbols represent different flood events. The red lines are the assumed background suspended particle concentration dependence on flow rate given by equations (5.4).

4. Scatter of Background suspended sediment concentration at Violettes

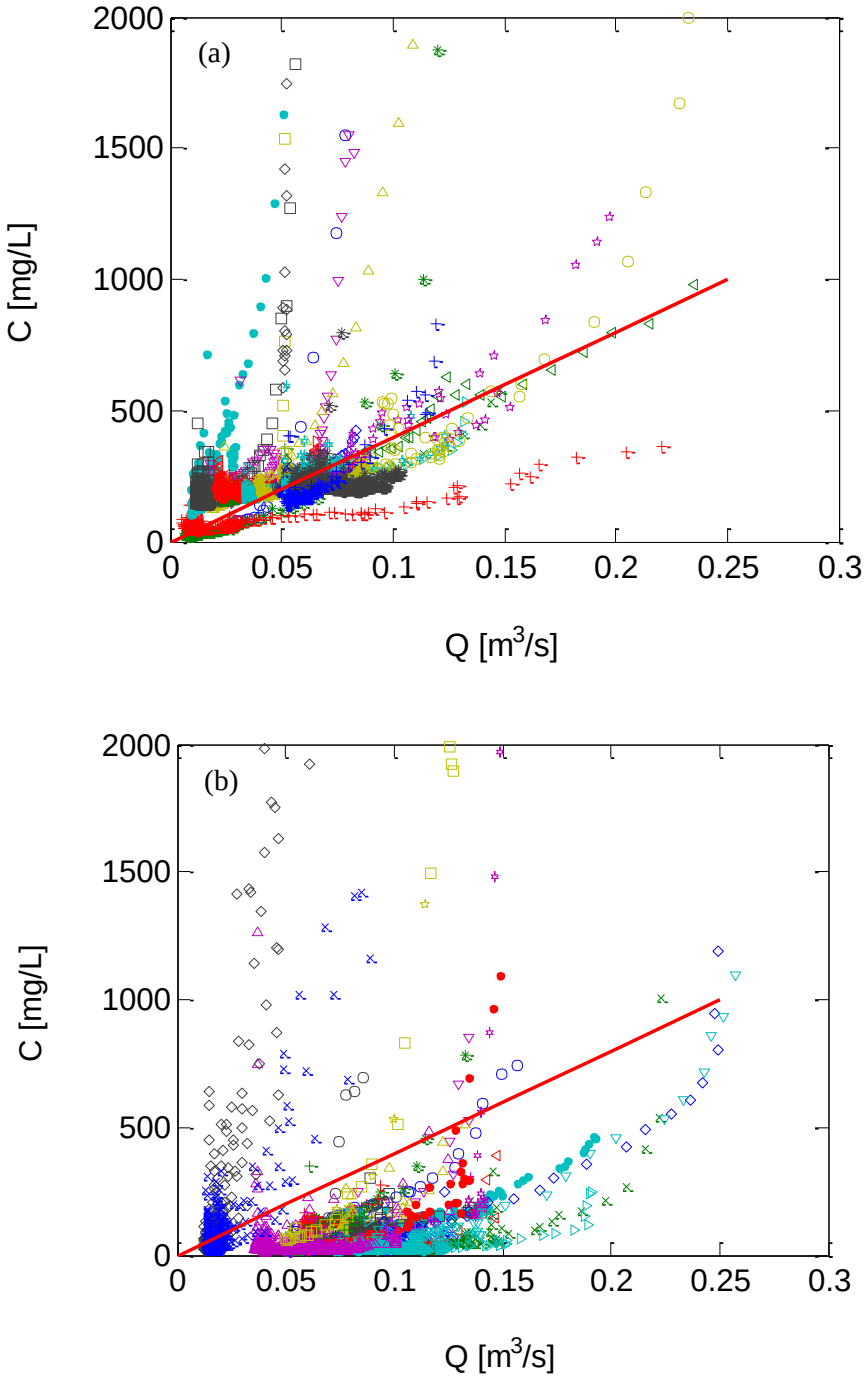

Figure D.5. Fine particle concentration during falling limb recession in the French watershed at Violettes for suspended particle concentrations less than 2000 mg/L (a) from Oct 9, 2002 to Dec 14, 2002 (b) from Dec 15, 2002 to May 21, 2003. The red lines are the assumed background suspended particle concentration dependence on flow rate as C_b=4000Q.

There is more scatter of fine particle concentration during falling limb recession at Violettes than Moulinet. It is noticeable that background fine particle concentration is much higher in earlier period of observation from October to December 14, 2002 than from December 15, 2002 to May, 2003 as shown in Figure D.5. The background concentration relationship at Violettes is determined as C_b=4000Q which is the most representative relationship that shows good fit with most of flood recessions.

Appendix E. Incline Creek in Lake Tahoe Basin

1. Flow Rate vs Suspended Load

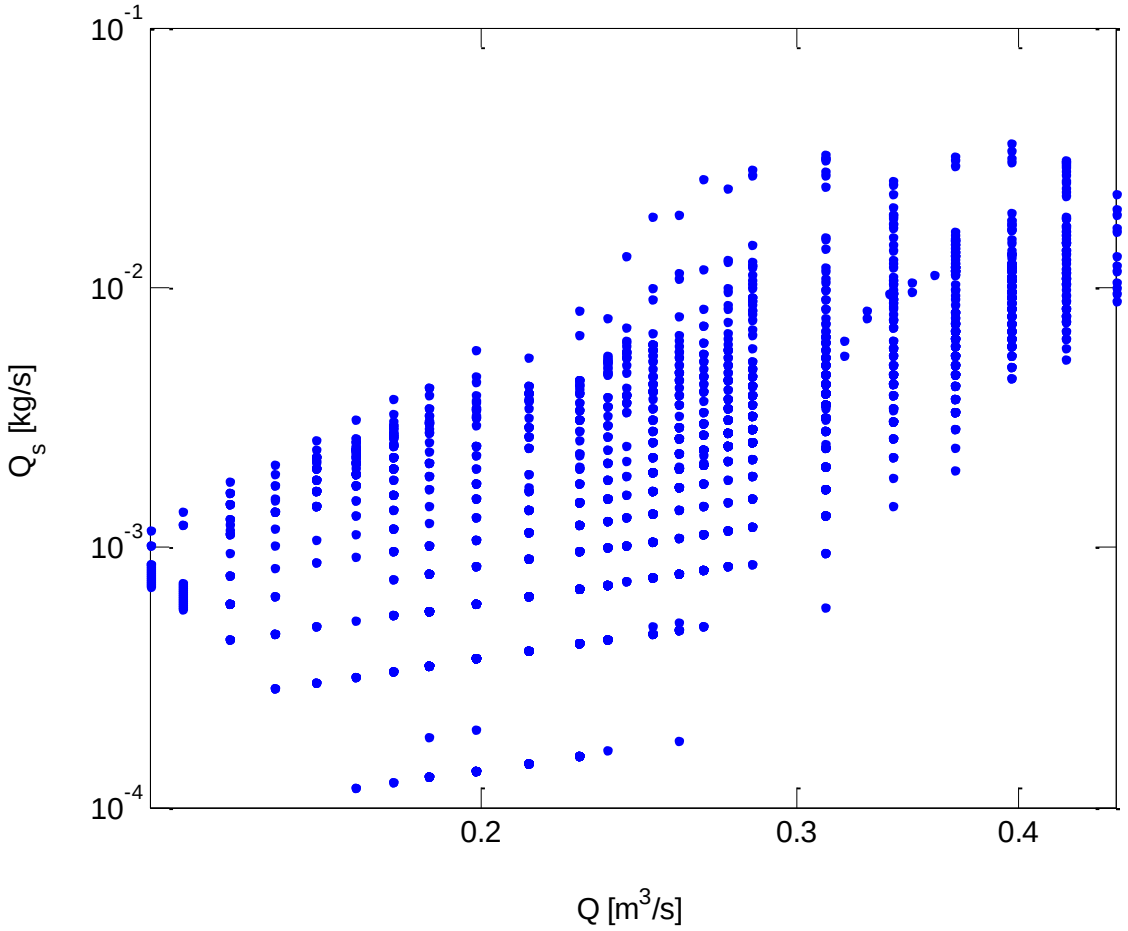

Figure E.1. Q_s to Q relationship at Incline Creek, Nevada in Lake Tahoe basin.

2. Hysteresis and Hydrograph

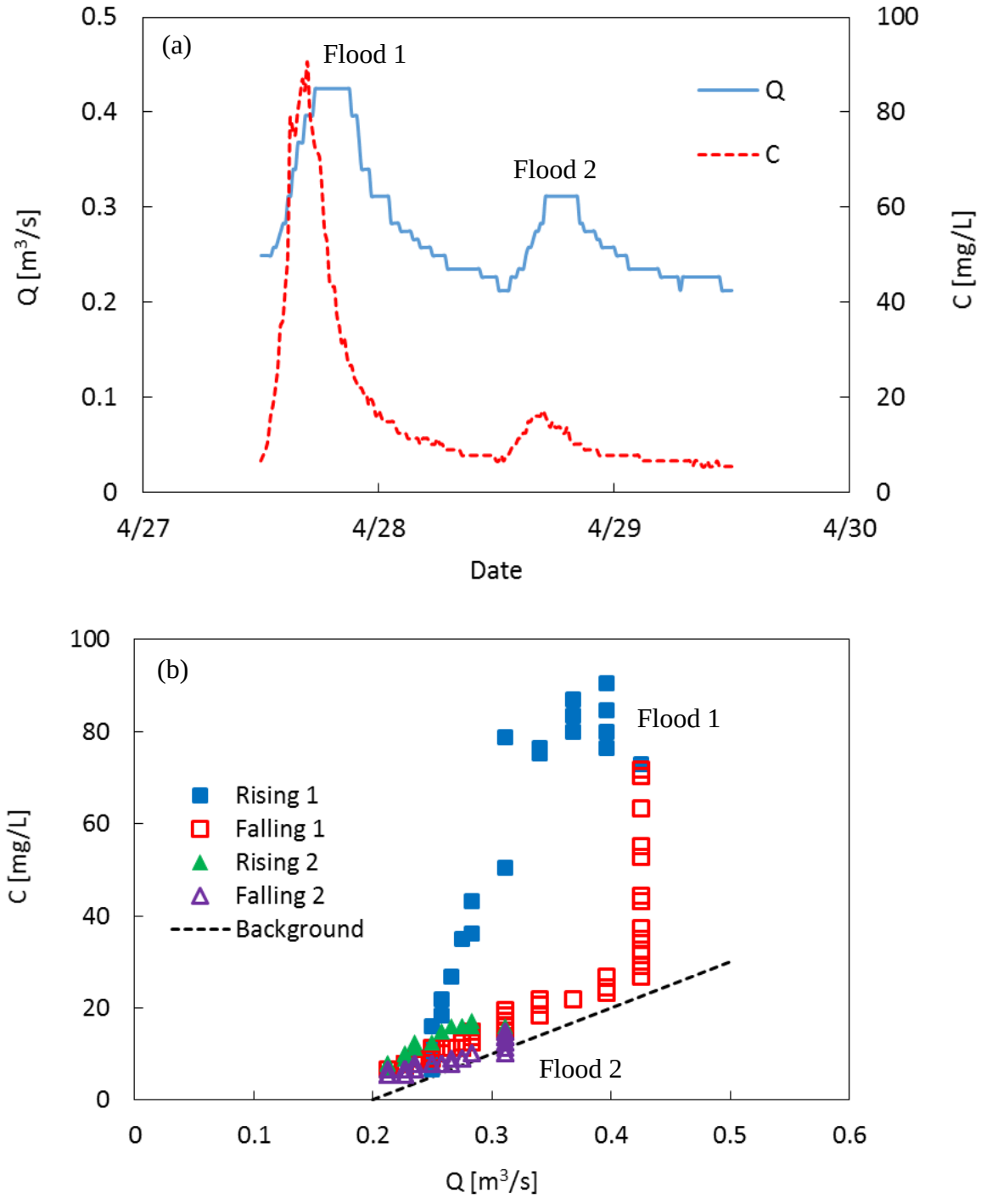

Figure E.2. The (a) hydrograph and (b) hysteresis of *Q* and *C* for continuous floods at Incline Creek between April 27 and 29, 2000. The second flood with far lower peak flow rate erodes few particles and the particle concentrations closely follow the assume background suspended particle concentration relationship, C_b=100(*Q*-0.2).

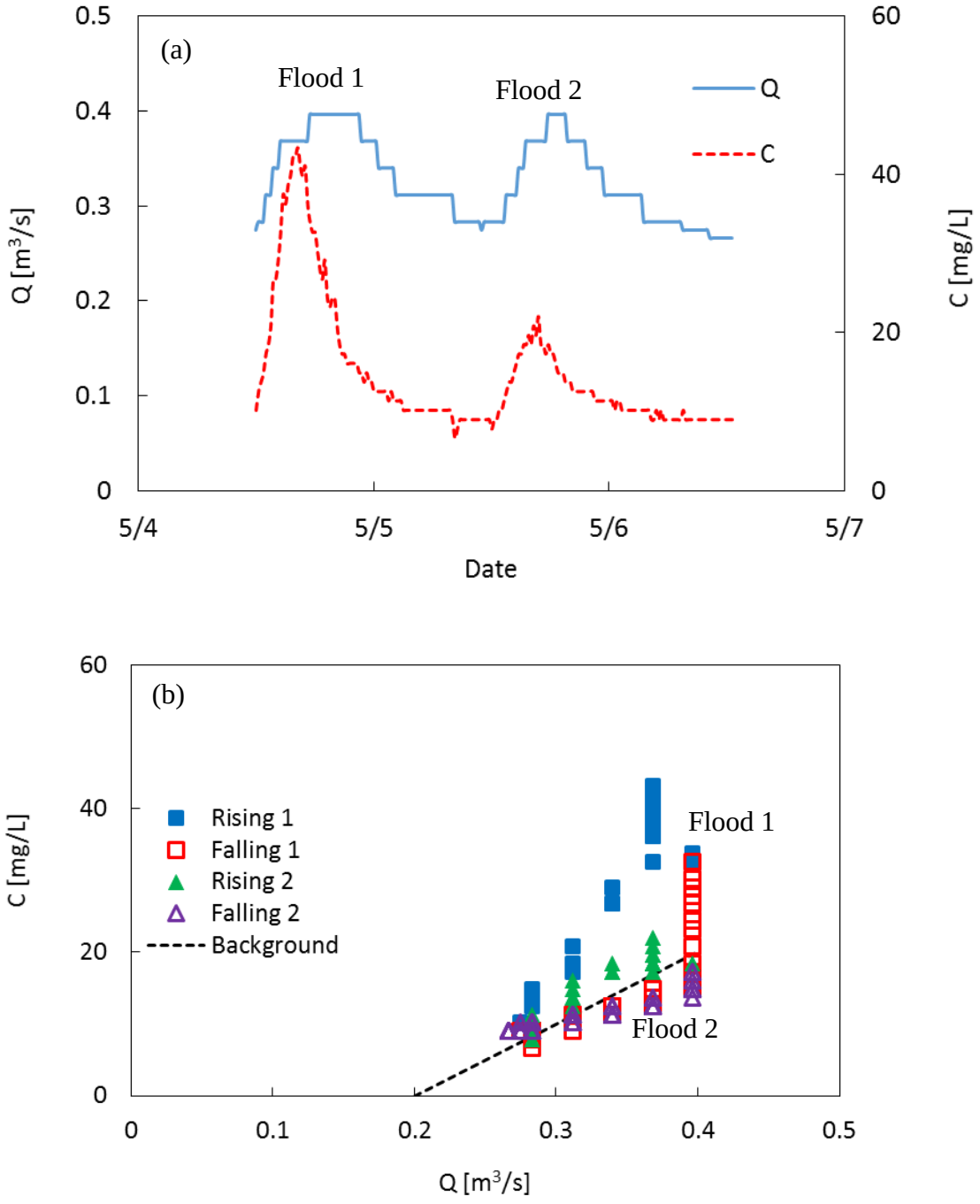

Figure E.3. The (a) hydrograph and (b) hysteresis of Q and C for continuous floods at Incline Creek between May 4 and 6, 2000. The first and second peak flow rates are similar while the first flood event has much greater hysteresis and greater fine particle release from the sediment bed. Background suspended particle concentration, C_b=100(Q-0.2), is represented as black dotted line and is a reasonable fit to the flow recession data.

Appendix F. Meuse River in Belgian-Dutch border

1. Flow Rate vs Suspended Load

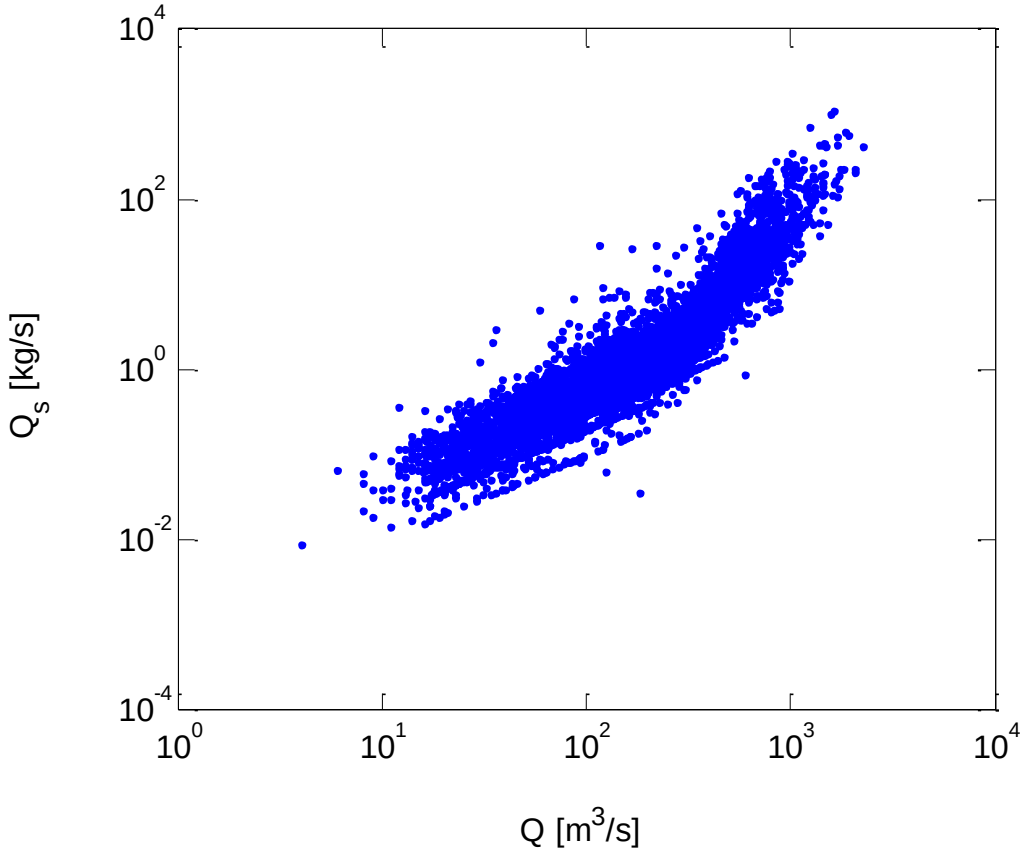

Figure F.1. Q_s to Q relationship at Eijsden gauging station in Meuse River from 1995 to 2010.

2. Hysteresis and Hydrograph

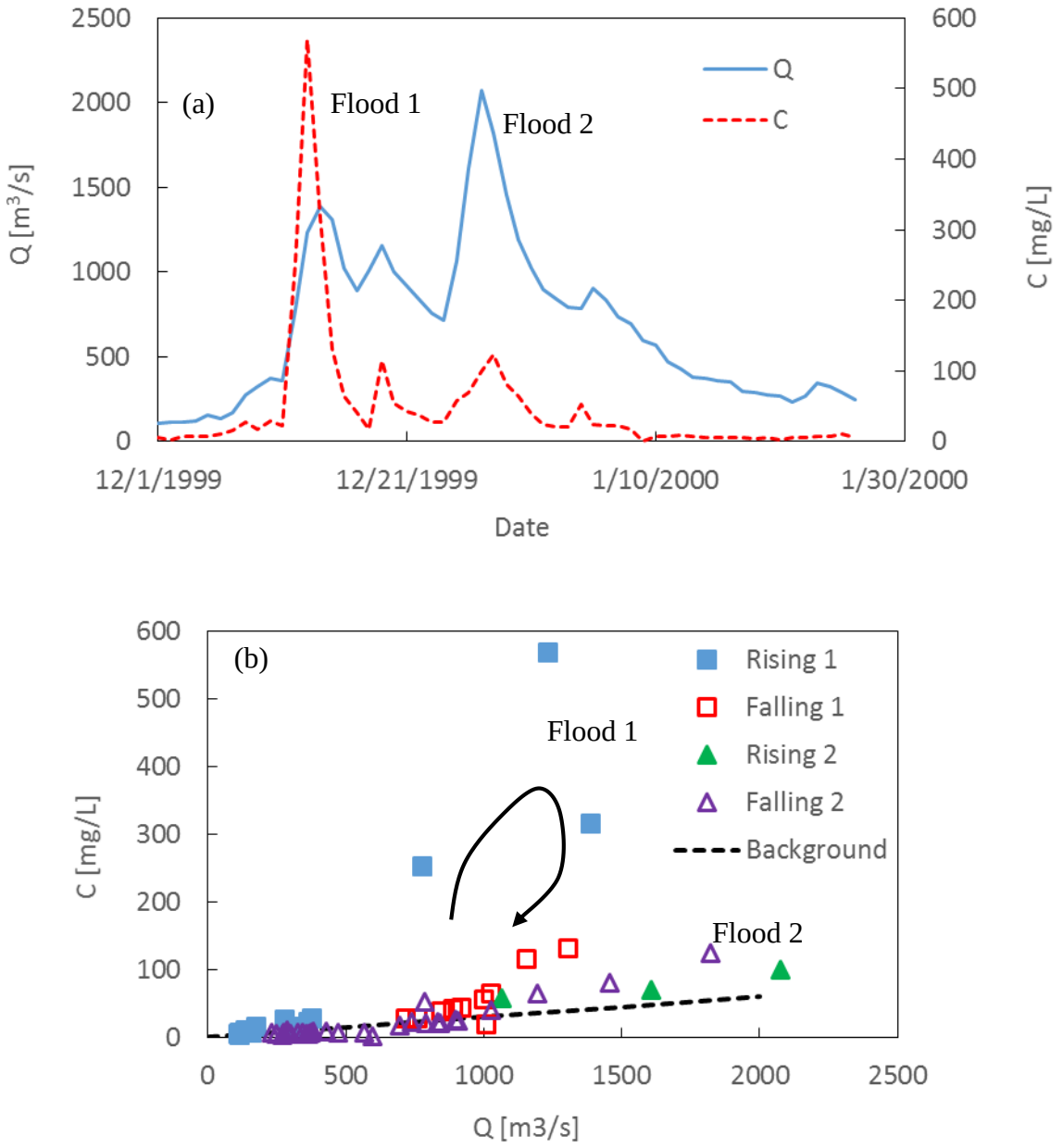

Figure E.2. The (a) hydrograph and (b) hysteresis of Q and C for sequential floods at Eijsden gauging station in Meuse River between December 1, 1999 and January 26, 2000. The first smaller flood releases fine particles from channel bed and has clockwise hysteresis. No hysteresis is observed in second larger flood as fine particle storage in channel bed is depleted by the previous flood. Background suspended particle concentration, C_b=0.03 Q, is represented as black dotted line and is a reasonable fit to the flood flow recession data.

Appendix G. Statistical analysis for a slope break in the relationship of Q_s to Q

A slope break in the relationship between log scaled Q_s and log scaled Q is consistently observed from the 30 minimally developed sites in California and eight sites utilized for model development and testing. In this appendix statistical analysis evaluates the likelihood of a slope break in the relationship of log scaled Q_s to log scaled Q.

1. Methods

A segmented (broken stick) regression line is calculated to statistically determine a slope break which minimizes residuals between observations and linear regression lines in log scaled Q_s to log scaled Q plot. The background on segmented regression lines is explained at the website (http://en.wikipedia.org/wiki/Segmented_regression). The two segmented regression lines for the higher flow regime ($Q>Q_c$) and the lower flow regime ($Q<Q_c$) are compared with a single regression line over the whole flow regime to test if the estimation is improved by using segmented regression.

The segmented regression lines with daily data in Meuse River between 1995 and 2000 are shown as an example in Figure G.1. The two broken lines (Dotted red line and solid magenta line) are plotted from segmented (broken stick) regression. The dashed black line represents single linear regression which minimized residuals for the whole data set. The breaking point is determined by minimizing residuals and is referred to as the critical flow rate where the slope break occurs. Calculations are performed by Matlab using function calls "BrokenStickRegression.m". The calculated flow rate for the slope break is Q_c=265 m^3/s which is close to the visually determined value of 280 m^3/s.

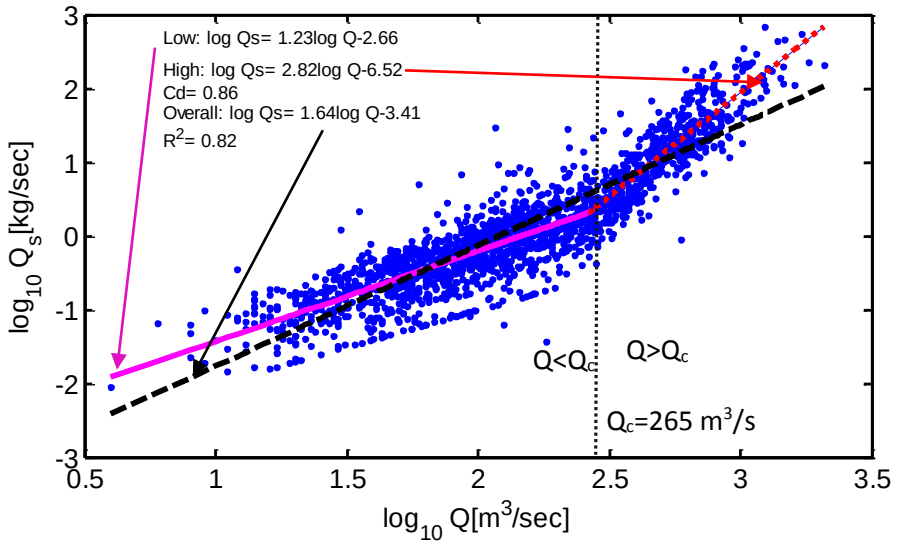

Figure G.1. The relationship of $\log_{10}Q_s$ to $\log_{10}Q$ for the Meuse River. Segmented regression lines are compared with a single regression line.

There are a number of tests that can be conducted to determine if the regression lines provide an improvement over a single linear regression. One comparison is based on a coefficient of determination C_d for segmented regression versus R^2 for the linear regression (dashed black line, $\log_{10}Q_s$=1.64[$\log_{10}Q$]-3.41). The coefficient of determination is calculated from

$$C_d = 1 - \frac{\sum(y-y_r)^2}{\sum(y-y_a)^2}$$

Where, y_r is separately determined by the two segments

$y_{r=A_1x+B_1 \ when\ Q<Q_C}$ (Solid magenta line, A_1=1.23, B_1=-2.66)

$y_{r=A_2x+B_2 \ when\ Q>Q_C}$ (Dotted red line, A_2=2.82, B_2=-6.52)

$x = log_{10}\,Q, y = log_{10}\,Q_S \ and \ y_a \ is \ average \ of \ y = log_{10}Q_s \ for \ all \ observations$

For an un-segmented regression, the values of C_d and R^2 are equal. In a segmented regression, C_d should be significantly larger than R^2 to justify the segmentation. R^2 is easily obtained by using Matlab or Excel. For the Meuse River C_d = 0.86 which is greater than R^2 = 0.82. This analysis says segmented regression is an improvement over single regression and the existence of a slope break is supported.

Since the data are not normally distributed, the Mann Whitney U test is used to determine if segmented regression lines and the single regression line are significantly different. The segmented regression line in the low flow regime (Solid magenta line for $Q<Q_c$) is compared with lower part of single regression line (Dashed black line for $Q<Q_c$) and similarly the segmented regression line in high flow regime (Dotted red line for $Q>Q_c$) is compared with higher part of single regression line (Dashed black line for $Q>Q_c$). For the Meuse River the p value is 0.0006 so the difference is significant when $Q<Q_c$. On the other hand the p value is 0.06 when $Q>Q_c$ so the difference is not significant.

The same method is applied in 7 other sites used for model development and 38 California sites with daily observation reported by USGS and utilized in Chapter 2. Within the 38 California sites, 30 sites have a visual slope break in the relationship between flow rate (Q) and suspended load (Q_s) while no slope break is observed in the other 8 sites. The 38 sites with daily data were not directly used for the model development in Chapter 4 because the temporal resolution of the data was not sufficient for model development and testing.

In 8 sites used for the model development, breaking points calculated from segmented regression are similar to visual identifications except for Moulinet and the two sites in Russian River watershed. The difference between segmented regression and single regression is significant in most sites except for the high flow regime ($Q>Q_c$) in Meuse River as summarized in Table G.1 below.

Table G.1. Summary of segmented regression in 8 sties used for model development

Sites	Visual identification	Segmented Regression			Mann Whitney U test				Number of data			
					$Q<Q_c$		$Q>Q_c$					
	Q_c [m^3/s]	Q_c [m^3/s]	C_d	R_a^2	P-value	h	P-value	h	Total	$Q<Q_c$	$Q>Q_c$	% Less than Q_c
Meuse	280	265	0.86	0.82	0.000566	1	0.061279	0	1823	1291	532	71
Owenabue	5	6	0.90	0.88	0.028251	1	2.23E-55	1	35040	29112	5928	83
Bandon	10	12	0.76	0.70	0.00082	1	1.37E-12	1	35040	25263	9777	72
Moulinet	0.10	0.02	0.81	0.81	1.52E-31	1	8.04E-05	1	52560	17377	35183	33
Violettes	0.05	0.03	0.66	0.65	0.009406	1	7.65E-15	1	52558	33109	19449	63
Hopland	10	22	0.94	0.93	7.30E-13	1	7.29E-06	1	105149	91505	13644	87
Guerneville	20	11	0.97	0.96	1.23E-98	1	1.73E-65	1	69978	36827	33151	53
Incline Creek	0.2	0.2	0.53	0.41	1.50E-19	1	8.69E-19	1	4896	1617	3279	33

Note) h=1 represent that the difference is significant with 95% confidence interval.

In the 38 California sites with daily data reported by USGS, the results are more complicated. The analysis forced a slope break even for the eight sites where no slope break was observed. Within the eight sites without a visually identified slope break, four sites had the segmented regression lines that were statistically different from single regression line in both high and low flow regimes. Within the 30 sites with visual slope breaks, the segmented regression tended to under estimate the breaking points (Q_c) compared to visual identifications (see Figure G.2 below). In the low flow regime the segmented regression lines are significantly different from a single regression line in 16 sites but only 7 sites show a significant difference in the high flow regime.

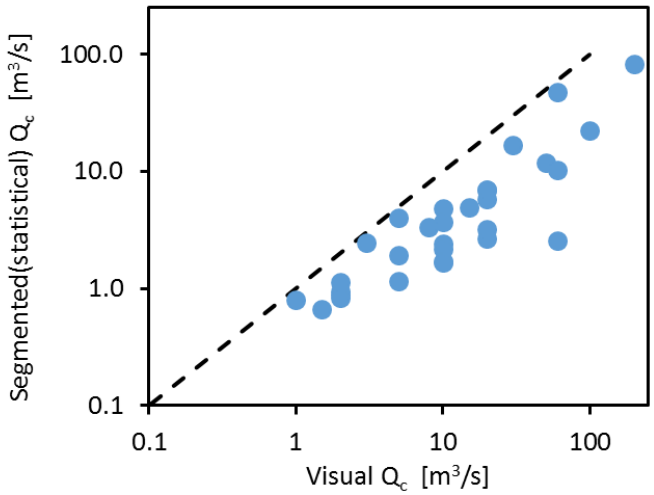

Figure G.2. Comparison of visually and statistically determined breaking points for 30 California sites with a slope break in the relationship of Q_s to Q. The dashed line is a 1:1 line.

This result suggests that segmented regression might be useful for the identification of a slope break in the relationship of log scaled Q_s to log scaled Q but the result would not always be reliable. The uncertainly is likely caused by the data density distribution. I used density distribution plots which shows the number of data within defined grids. The density plot methodology was obtained from my lab mate, Thomas Moran.

For example in the Meuse River the segmented regression calculated the breaking point close to Q_c identified visually. The density of data shows that the regression line passes through the region where data density is higher (yellow and red color regions).

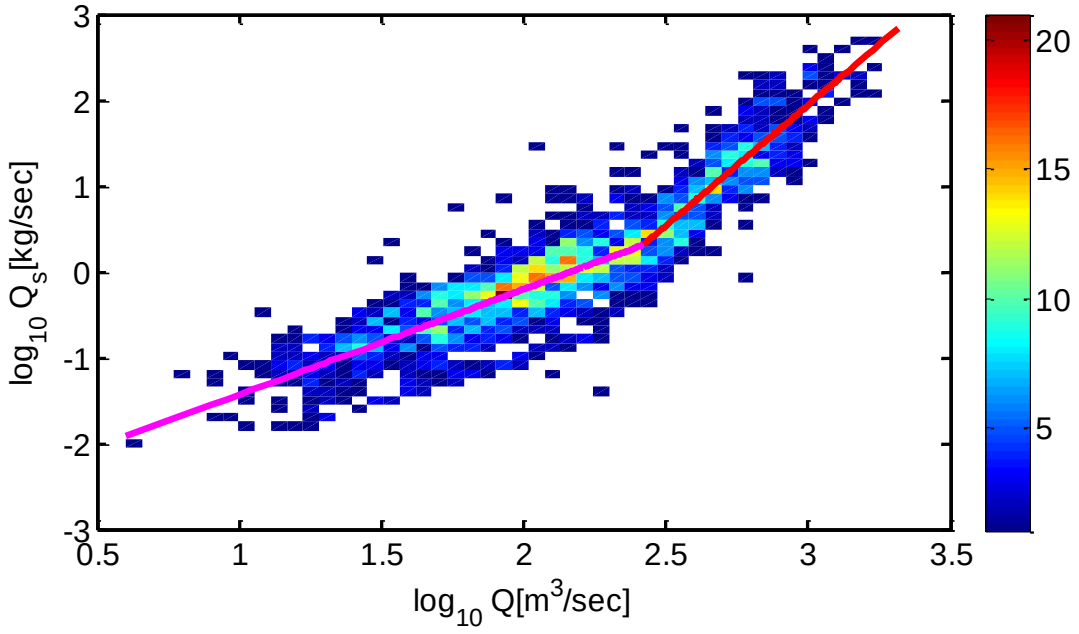

Figure G.3. Density plot of $\log_{10}Q_s$ to $\log_{10}Q$ in Meuse River. The color bar represent the number of data within a grid.

However in Moulinet, segmented regression calculates a breaking point at a much lower flow rate (Q=$10^{-1.68}$=0.02 m^3/s) than a visual observation (Q is about 0.1 m^3/s, log Q=-1). In addition to a lower value of the slope break, the segmented regression approach arrived at a decreased slope in the upper flow regime as shown in Figure G.4. This mis-match can be explained by this density plot which suggests that the regression line is dominated by the region with high data density (red and yellow regions).

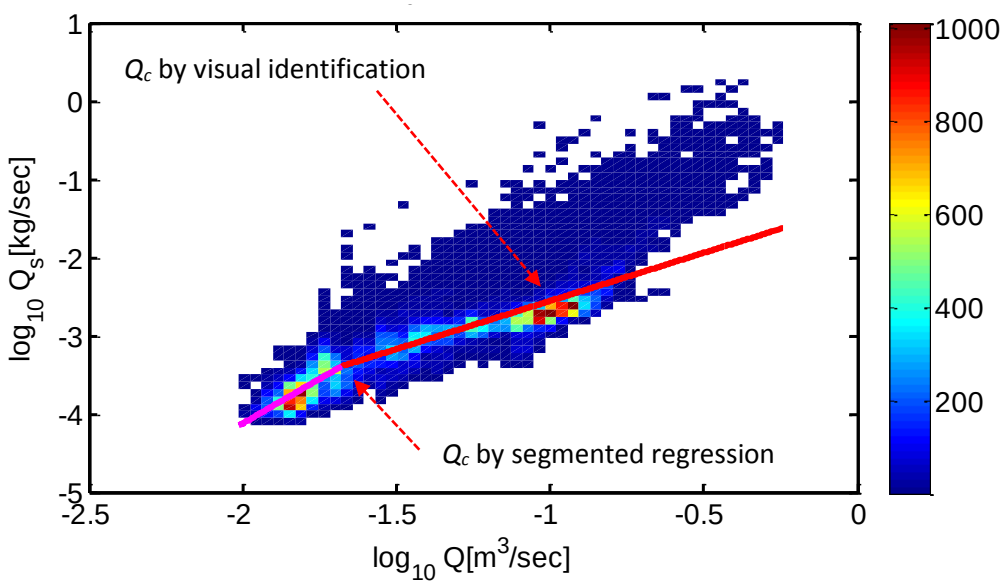

Figure G.4. Density plot of $\log_{10}Q_s$ to $\log_{10}Q$ in Moulinet with segmented regression lines.

Similarly in the 30 California sites with a visual slope break the segmented regression lines are dominated by the density of the data. The USGS usually reported more data in the lower flow regime, and the segmented regressions tend to underestimate breaking points compared to visual identifications. For example in Arroyo Seco near Greenfield, CA (USGS site number 11151870) a slope break is visually observed when flow rate is about 20 m^3/s ($\log_{10}$ 20=1.3). Segmented linear regression calculates a break point at about Q=5.8 m^3/s (log 10 5.8=0.76). This mis-match also can be explained by the density plot in Figure G.5. The high density data in the lower flow regime tend to dominate the shape of the regression line. This also may be related to the USGS practice of reporting a lower range suspended sediment concentration.

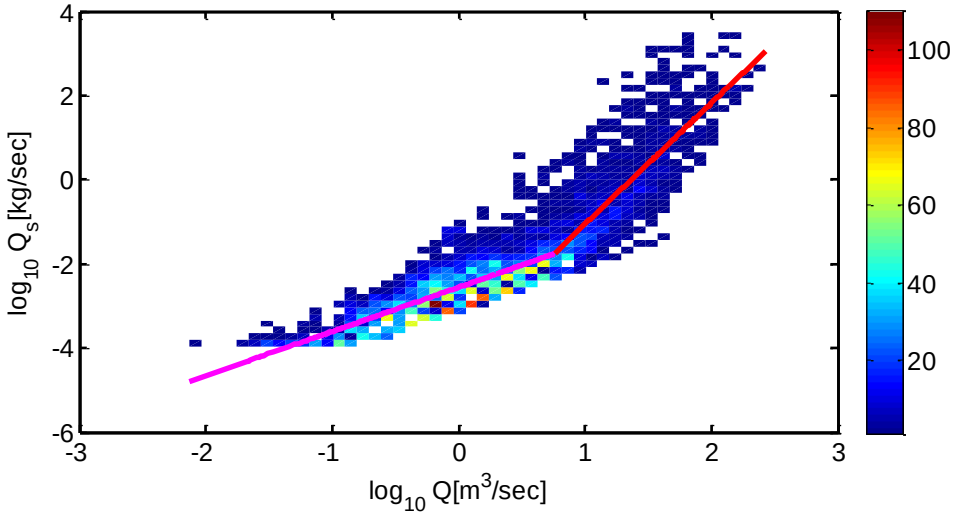

Figure G.5. Density plot of $\log_{10}Q_s$ to $\log_{10}Q$ in Arroyo Seco near Greenfield CA with calculated segmented linear regression lines.

Unlike the USGS reported data the Meuse data are relatively evenly distributed through both flow regimes. Thus the segmented regression and visual identification provide a similar estimation of the breaking point (Q_c).

In the sites where no slope break is observed the segmented regression determines a breaking point which is dominated by the high density data in the low flow regime. For example the segmented regression and density plot at Zayante Creek at Zayante, CA is shown in Figure G.6 where the channel bed is dominated by bed rock. The segmented regression line in the low flow regime is dominated by high density data.

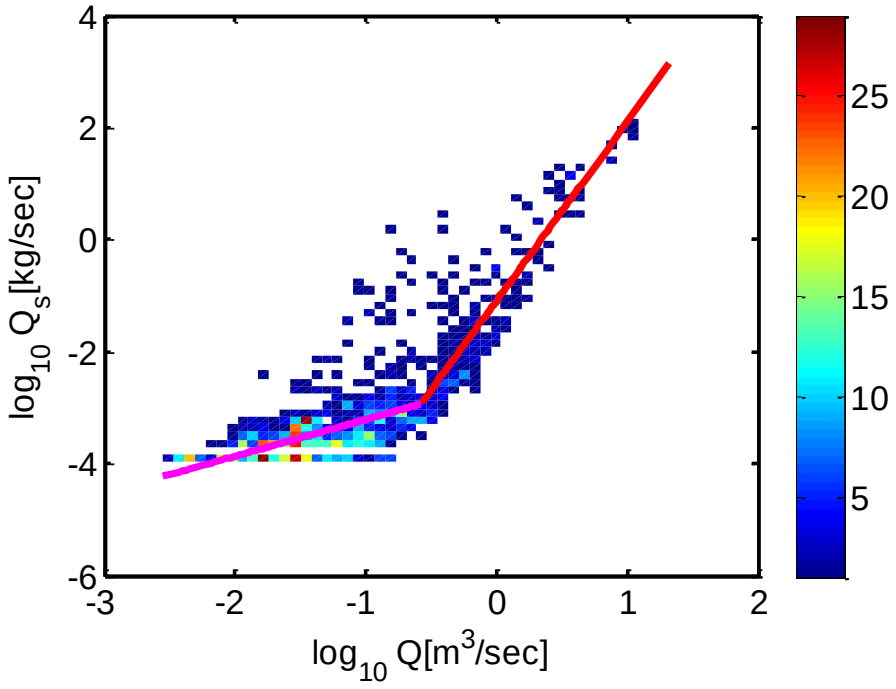

Figure G.6. Density plot of $\log_{10}Q_s$ to $\log_{10}Q$ in Zayant Creek at Zayante CA.

3 Conclusion

The above analysis suggests that statistical approach such as segmented regression may be helpful for the more consistent determination of a slope break in the relationship of Q_s to Q as shown in the Meuse River example. However the analysis of results at other sites also argues that the segmented regression result could be distorted by data distribution. This shows the limitation of a strict statistical approach and supports the visual identification of slope breaks for these hydrologic data.